Tectonics of the Western Betics: From mantle extensional exhumation to westward thrusting

Gianluca Frasca

ANNÉE 2014-2015

THÈSE / UNIVERSITÉ DE RENNES 1
sous le sceau de l'Université Européenne de Bretagne

pour le grade de

DOCTEUR DE L'UNIVERSITÉ DE RENNES 1

Mention : Géosciences

École doctorale Sciences de la Matière (SDLM)

présentée par

Gianluca Frasca

Préparée à l'unité de recherche Géosciences Rennes - UMR6118

Tectonics of the Western Betics: From mantle extensional exhumation to westward thrusting

Thèse soutenue à Montpellier
le 15 juillet 2015

devant le jury composé de :

Jean-Pierre BURG
Professeur - ETH Zürich / *Rapporteur*
Dominique FRIZON DE LAMOTTE
Professeur - Université de Cergy-Pontoise / *Rapporteur*
José-Miguel AZAÑON
Professeur - Universidad de Granada / *Examinateur*
Federico ROSSETTI
Professeur - Università Roma 3 / *Examinateur*
Stéphane MAZZOTTI
Professeur - Université Montpellier / *Examinateur*
Frédéric GUEYDAN
Professeur - Université Montpellier / *Directeur de thèse*
Jean-Pierre BRUN
Professeur - Université Rennes 1 / *Co-directeur de thèse*

Tectonics of the Western Betics:
From mantle extensional exhumation to westward thrusting

Tectonique de l'Ouest des Bétiques:
de l'exhumation du manteau en context extensif au chevauchement vers l'ouest

Gianluca Frasca

UNIVERSITÉ DE RENNES 1

Abstract

In the frame of the Africa-Europe convergence, the Mediterranean tectonic system presents a complex interaction between subduction rollback and upper-plate deformation during the Tertiary. The western Mediterranean is characterized by the *exhumation* of the largest *subcontinental mantle* massif worldwide (the *Ronda Peridotite*) and a narrow *arcuate geometry* across the Gibraltar arc within the Betic-Rif belt, where the relationship between slab dynamics and surface tectonics is not well understood. The thesis focuses on the Western Betics, which is characterized by two major thrusts: 1/ the *Internal/External Zone Boundary* limits the internal metamorphic domain (Alboran Domain) from the fold-and-thrust belts in the External Zone, and 2/ the *Ronda Peridotites Thrust* allows the juxtaposition of a hyper-stretched lithosphere with large bodies of sub-continental mantle rocks on top of upper crustal rocks.

First part: New structural data are presented and used to argue for two Lower Miocene E-W-trending strike-slip corridors played a major role in the deformation pattern of the Alboran Domain, in which E-W dextral strike-slip faults, N60°-trending thrusts and N140°-trending normal faults developed simultaneously during dextral strike-slip simple shear. The inferred continuous westward translation of the Alboran Domain is accommodated by a major E-W-trending lateral ramp (strike-slip) and a N60°-trending frontal thrust. At lithosphere-scale, we interpret the observed deformation pattern as the upper-plate expression of a lateral slab tear and of its westward propagation since Lower Miocene. The crustal emplacement of the Ronda Peridotites occurred at the onset of this westward motion.

Second part: New structural data together with Ar-Ar ages serve to document the changes in deformation processes that accommodate the progressive necking of a continental lithosphere. We identify three main successive steps. First, a mid-crustal shear zone and a crust-mantle shear zone accommodate ductile crust thinning and ascent of the sub-continental mantle. The shear zones act synchronously but with opposite senses of shear, top-to-W and top-to-E respectively in the crust-mantle extensional shear zone, and at the brittle-ductile transition in the crust. Second, hyper-stretching localizes in the neck, leading to an almost disappearance of the ductile crust and to crustal stretching values larger than 2000%, and bringing the upper crust into contact with the subcontinental mantle, each of them with their already acquired opposite senses of shear. Finally, high-angle normal faulting, dated by ^{40}Ar-^{39}Ar step-heating method on muscovite at ca. 21 Ma, cut through the Moho, where the ductile crust almost disappear and related block tilting ends the full exhumation of mantle in the zone of localized stretching.

Third part: New geochronological data precisely constrain the transition from rifting to thrusting. Using U-Pb LA-ICP-MS dating, we identify two distinct episodes of crustal melting associated with two large-scale tectonic contacts that bound the Ronda Peridotites. The first episode of partial melting within the HT foliation at ca. 22.5 Ma is related to the extreme thinning of the continental crust and to mantle exhumation. The second episode of crustal melting at ca. 20 Ma, marked by leucocratic granite dikes that intrude both the peridotites and the overlying thinned crustal envelope, is related to the thrust emplacement of the section of thinned and hot continental lithosphere on top of crustal rocks.

In summary, the Miocene tectonics of the western Betics is marked by the inversion of a continental rift, triggered by shortening of the upper continental plate and accommodated by E-W dextral strike-slip corridors. During thrusting and westward displacement of the Alboran domain with respect to Iberia, the hot upper plate, which involved the previously exhumed sub-continental mantle, underwent fast cooling.

Résumé

Une brève introduction

Les Bétiques et le Rif font partie de la chaine Alpes-Himalaya et affleurent dans l'ouest de la Méditerranée. Elles résultent de la convergence entre la plaque Ibérique et Africaine à partir du Crétacé Supérieur. Dans cette région, les données de tomographie sismique mettent en évidence un panneau de lithosphère verticale sous l'arc de Gibraltar. Le lien entre dynamique du panneau plongeant et formation de l'arc de Gibraltar est sujet à débat.

La chaine des Bétiques est composée d'une zone interne (Domaine d'Alborán), formée de roches métamorphiques, avec les plus importants affleurements mondiaux de manteau sous-continental (péridotites de Ronda) et d'une zone externe, formée par une chaine plissée des sediments des marges Iberiques et Africaines. L'ouest de la Cordillère Bétique (Sud-ouest de l'Espagne) est donc un terrain idéal pour l'étude de l'exhumation du manteau sous-continental et des processus tectoniques responsables de la formation des chaines arquées.

Cette thèse vise à établir un modèle tectonique accompagné d'un calendrier cinématique intégrant structures fragiles et ductiles. La thèse repose sur l'analyse des structures responsables de la forme arquée de la chaine et de l'exhumation du manteau sous-continental. Le but est, d'une part, de répondre à une problématique régionale, avec l'analyse géométrique et cinématique des zones de déplacement majeur, et d'autre part, de proposer des modèles simples et solides qui justifient les caractéristiques observées.

La Cordillère Bétique occidentale est une partie privilégiée du système Betico-rifain car la tectonique extensive oligo-miocene y est bien remarquablement bien conservée malgré les effets ultérieurs de la compression. C'est aussi une région idéale pour étudier l'empilement de nappe a échelle lithosphérique (domaine d'Alboran sur la marge ibérique). Cette superposition des déformations liées a l'extension (amincissement) et de celles liées a la compression (épaississement) dans un seul système géologique donne à l'ouest des bétiques une signature particulière dans l'évolution du système de l'ouest de la Méditerranée, très favorable pour l'étude de l'expression dans la plaque supérieure des phénomènes liées au recul du panneau plongeant et à l'extension arrière-arc.

Contexte Géologique

La **Zone Interne**, ou domaine d'Alboran, est caractérisée dans la Cordillère Bétique par un empilement de trois nappes métamorphiques, qui sont, de bas en haut: le Nevado-Filabride, l'Alpujarrides et Malaguides.

Le ***Nevado-Filabride*** affleure seulement dans la partie centrale et orientale des Bétiques et est principalement composé d'orthogneiss Paléozoïque et schistes graphiteux avec une mince couverture Permo-Trias avec des écailles mafiques et ultramafiques de roches ophiolitiques jurassique qui ont enregistrées un événement métamorphique de haute pression.

L'***Alpujarrides*** se compose principalement de Paléozoïque et du début du Mésozoïque ; avec de grands corps de péridotites sous-continental (Ronda). Le grade métamorphique alpin augmente généralement vers l'ouest. L'Alpujarrides est caractérisé par une forte déformation en extension Oligo-Miocène et par un grade métamorphique élévé, entrainant un évènement Miocène de haute-température.

Le ***Malaguide*** est composé de roches du Paléozoïque non-metamorphiques. Dans la partie la plus occidentale du système Bétique-Rif, la limite entre zone interne et zone externe est marquée par les unités de la ***Dorsale*****,** composées des sédiments Trias-Jurassique déformés et localement métamorphisés en haute température.

La **Zone Externe** est caractérisée par un prisme d'accrétion Miocène (Burdigalien-Langhien) qui touche deux domaines, appelés Subbetics et "Flysch Trough". Les ***Subbetics*** sont des sédiments mésozoïques partiellement détachés du socle de la marge ibérique, et sont divisés en plusieurs unités tectoniques (Subbetics externes, médian et interne), principalement basée sur leur position paléogéographique au cours du Jurassique. Le long de l'arc de Gibraltar, les sédiments marins profonds clastiques, le "Flysch Trough" est structurellement dessus les Subbetics. Les sédiments du ***Flysch Trough*** ont été déposés au cours du Crétacé inférieur dans une dépression structurelle de croûte continentale amincie ou océanique, probablement liée à une faille transformant. La sédimentation se termine dans le Miocène inférieur, marquant le début du raccourcissement dans le Flysch Trough.

Problématiques

L'ouest de la Cordillère Bétique a été largement étudié, mais encore toujours extrêmement débattu. La grand partie du travail présenté ici est dédié à la cinématique des zones de déformations majeures observées dans la région. Les questions majeures abordées durant cette thèse sont résumées ci-dessous :

1/ Quelle est la direction du déplacement du domaine d'Alboran ?

La question est quelles structures ont accommodé le mouvement du domaine d'Alboran à la terminaison du system bétique. Trois types de failles sont communément décrites dans la littérature géologique (avec direction N140, N50 et EW) et peuvent jouer un rôle dans le déplacement, mais avec des directions et amplitudes radicalement différentes. Il convient également de déterminer les âges relatifs du mouvement sur ces failles.

2/ Quel est l'ampleur de l'amincissement lithosphérique accompagnant l'exhumation du manteau sous-continental?

L'amincissement de la lithosphère continentale avec exhumation de manteau sous-continental et intrusions de gabbro a été récemment décrite. Aucune etude cependant ne permet de quantifier l'ampleur de l'amincissement crustal associé. De plus, l'âge des structures extensives signalées dans les roches de la croûte amincie est classiquement décrit comme tardif (Miocène supérieur) et donc non relié au rifting continental oligo-miocène.

3/ Quel est la séquence temporelle exacte entre extension/amincissement lithosphérique et compression/chevauchement du domaine d'Alboran sur la marge ibérique?

La littérature géologique montre deux structures associées au sommet et à la base du manteau de Ronda. La plupart des auteurs indiquent que le chevauchement à la base de la péridotite de Ronda est plus jeune que la zone de cisaillement extensive au haut de la péridotite de Ronda ; ce qui pose un problème tectonique. Les contraintes géochronologiques sont cependant rares car le métamorphisme de haute-température à ouvert l'ensemble des geo-chronomètres, ce qui explique les âges jeunes observées dans l'ouest des bétiques.

Méthodes - Structure de la thèse

Cette étude couple une cartographie intensive dans l'ouest des Bétiques et la géochronologie de haute température (U-Pb sur zircons) et moyenne température (^{40}Ar-^{39}Ar sur micas) pour contraindre les grandes zones de déformations caractéristiques du système et leurs âges.

Une **Introduction** générale à la géologie de la chaine, aux modèles proposés pour le système d'Alboran est tout d'abord présentée dans le **Chapitre 1** et permet de poser les problématiques de cette thèse.

Le **Chapitre 2** présente alors un article accepté à ***Tectonophysics***. Des nouvelles données structurales sur la limite zones internes/zones externes ont permis de proposer une nouvelle carte tectonique et d'identifier deux couloirs décrochants ayant joué un rôle majeur pendant la déformation du domaine d'Alboran. Dans ces couloirs, décrochements dextre orientés E-W, chevauchement N60º et failles normales orienté N140° se sont développés simultanément pendant un cisaillement simple dextre d'échelle régionale. Le mouvement progressif vers l'ouest du domaine Alboran est accommodé par une rampe latérale (décrochement) et un chevauchement frontal N60°. A l'échelle de la lithosphère, nous interprétons la déformation comme l'expression superficielle dans la plaque supérieure d'une déchirure latérale du panneau plongeant et de sa propagation vers l'ouest depuis le Miocène inférieur.

Le **Chapitre 3** présente un article soumis à ***Marine and Petroleum Geology.*** De nouvelles données structurales, couplées à des datations ^{40}Ar-^{39}Ar sur les micas dans les gouges de failles, ont permis de décrire les changements de modes de déformations dans la croute et le manteau durant une phase d'amincissement lithosphérique intense. Une succession progressive de trois stades de déformation est reconnue. Tout d'abord, deux zones de cisaillement, dans la croûte moyen et à la limite croûte-manteau, accommodent l'amincissement ductile de la croûte et l'exhumation du manteau sous-continental. Les zones de cisaillement agissent de façon synchrone, mais avec des sens opposés de cisaillement, vers l'ouest ou vers l'est respectivement dans la zone de cisaillement croûte-manteau, avec fusion partielle localisée dans la croûte profonde, et à proximité de la transition fragile-ductile dans la croûte. Deuxièmement, l'amincissement extrême (hyper-stretching) se localise dans le neck,

conduisant à une disparition quasi totale de la croûte ductile et à des valeurs d'étirement supérieures à 2000% de la croûte. La croûte supérieure devient en contact avec le manteau sous-continental, chacun d'eux préservant leurs sens de cisaillement opposés déjà acquis pendant la déformation antérieure. Enfin, des failles normales à fort pendage, datée à ca. 21 Ma, coupent l'ensemble de la lithosphère continentale hyper-étirée, entrainant la formation de blocs basculées lithosphériques

Le **Chapitre 4** présente un article soumis à ***Geology.*** De nouvelles données géochronologiques permettent de préciser le calendrier du modèle tectonique proposé. Il s'agit de datations par LA-ICP-MS des zircons dans des leuco-granites échantillonnés en fonction de leurs positions structurales et de leurs compositions chimiques. Il est donc possible de dater les différents stades de l'évolution tectonique de la région: 1/ l'exhumation du manteau, accompagné par de la fusion partielle dans la croute profonde avant 22.5 Ma et 2/ le chevauchement du manteau chaud sur des roches de croute continentale à 20 Ma.

Dans la **Conclusion**, les principaux résultats de ce travail sont résumés et nous permettent de proposer des perspectives de recherche, à la fois pour de futures études de terrain mais également pour des travaux de modélisation des processus.

Acknowledgements

First of all, I wish to express my thanks to Frédéric Gueydan for proposing the research questions of this thesis and for his guidance along these years. I am also indebted to Jean-Pierre Brun for welcoming me in Rennes and for kindly sharing his expertise during many pleasant discussions.

My deep thanks also go to Jean-Pierre Burg and Dominique Frizon de Lamotte for accepting to act as Referees of this work, as well as to José-Miguel Azañon, Federico Rossetti and Stéphane Mazzotti for their availability to take part in the jury.

Furthermore, I'd like to acknowledge the insightful discussions with Marc Poujol, Pavel Pitra, Bernard Célérier, Patrick Monié, Fleurice Parrat and Philippe Münch.

I am indebted to Géosciences Montpellier for generously hosting my activities, in particular thanks to Cyprien Astoury, Christophe Nevado and the rest of the lab staff who help me in the lab work. Special thanks go to the European Union that funded this work in the framework of the Marie Curie training network TOPOMOD and provided me with the unique opportunity to team up with a wonderful crew.

I want to thank all my fellow PhD students: all the officemates, from Marina, Elsa, Sabrina, Benjamin, Lise and Lucie to Kostas (see you back in our Ithacas!). Thanks to the past and next generation, from Camille, Robé, Théo, Fatna, Stéphanie, Antoine, Yannick, ...Laure, Manon, Romain... to Carlotta and Sofia. Thanks Mushegh for your help and Nori for all the fun moments. Thanks to Dino and Sergio: "quanto sa di sale lo pane altrui"! Thanks to Antonio "Falco" and Alicía for their logistic help and the evening talks making the fieldwork not a "feria sin músicas". My thoughts also go to those which I forgot to explicitly mention, but took part in this venture.

Finally, I also thank my brother and my parents for their support and Constanze for her encouragement "und du wartest, erwartest das...".

TABLE OF CONTENTS

Introduction

The objective of this thesis is identifying in the **field** the structures related to two main tectonic features commonly observed in subduction environments:

1- The **arc shape** of the boundary between subduction lower and upper plates;
2- The exhumation of **mantle** rocks to the surface on the concave side of the arcs; and related heating recorded in the crustal rocks of the upper plate.

We choose to concentrate on the western Betics in southern Spain. This area indeed hosts the Ronda Peridotite, the largest exhumed body of subcontinental mantle in the world, and is located where the Betic-Rif Cordillera curves to define one of the tightest arcs worldwide (Fig. I.1). The **geological study** of this region can furnish new insights on the origins of the features listed above. It is clear from the map that the size of the studied region is small compared to the size of the mountain belts. Consequently, the results of the present study will have in the future to be integrated together with other studies in order to provide definite answers to the questions at the scale of the whole Mediterranean system.

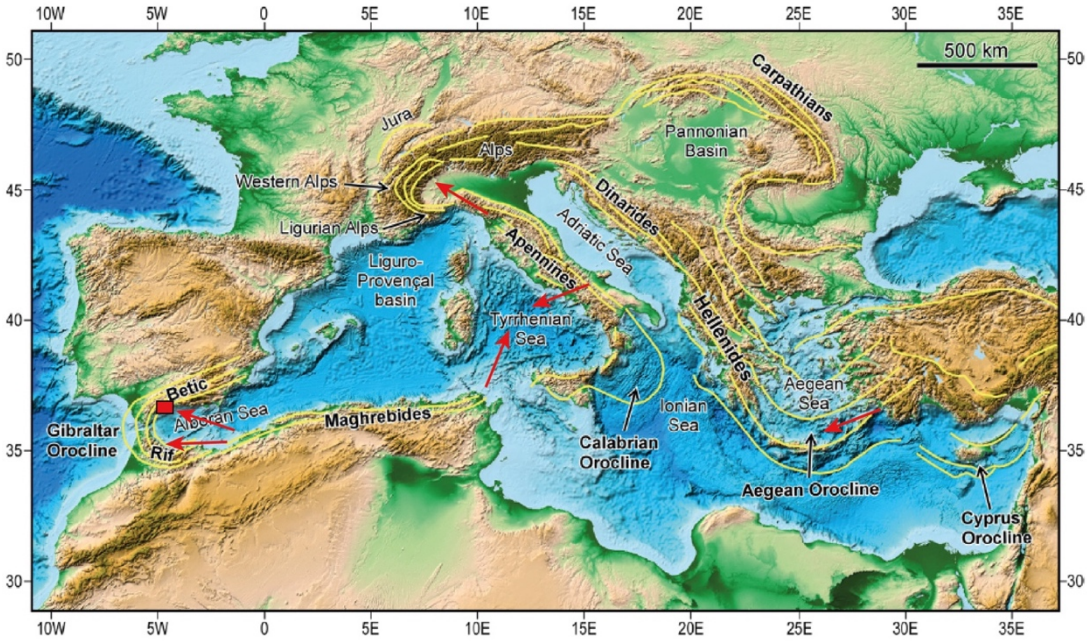

Figure I.1. Relief map of the Mediterranean area with the location of the arcs composing the Alpine-Mediterranean orogenic system (from Rosenbaum, 2014). The red box indicates the study area: the red arrows show some of the subcontinental mantle bodies cropping out in the upper plate of the subduction-related arc-systems.

The whole Mediterranean region has been classically recognized as a case study for the processes occurring on the upper plate of a subduction system (Le Pichon and Angelier, 1981; Malinverno and Ryan, 1986; Rehault et al., 1985). The Tyrrhenian and the Aegean system, in particular, have the biggest dimensions and are clearly associated with subducting oceanic lithosphere (Fig. I.2) (Faccenna et al., 1997; Jolivet and Brun, 2008; Wortel and Spakman, 2000). A similar origin has been proposed for the Betic-Rif Cordillera motivated by analogies with the rest of the Mediterranean subduction system (Faccenna et al., 2004; Lonergan and White, 1997; Rosenbaum and Lister, 2004; Royden, 1993). However, the soundness of this interpretation is debated due to the local complexity.

Figure I.2. Map of the Mediterranean area with the plate boundary evolution of the Mediterranean-Carpathian region (from Wortel and Spakman, 2000). The large black arrows indicate the inferred directions of lateral migration of slab detachment along the Apennines - Calabria arc, the Hellenic arc and the Carpathian arc. Blue: deeper than 2.5 km; intermediate blue: 2.5 to 1.0 km; light blue: shallower than 1.0 km. In green, the onshore areas. The darkest blue color corresponds approximately with the presence of oceanic lithosphere. The sawteeth point are in the direction of subduction. Black sawteeth indicate where the subducting slab is considered to be continuous. White sawteeth indicate plate boundary segments where slab detachment is assumed to have occurred. Red sawteeth (Calabria) indicate that slab detachment may have taken place recently. For the western Mediterranean region, three stages in the migration of the plate boundary are displayed. Black and white sawteeth have the same meaning as above, but now refer to the situation at the indicated times in the evolution. Adr, Adriatic Sea; Aeg, Aegean Sea; Alb, Alboran Sea; Ap, Apennines; Cr, Crete; A-P, Algero-Provencual Basin; Bet, Betics; Cal, Calabria; Car, Carpathians; Co, Corsica; Cr, Crete; Din, Dinarids; Hel, Hellenic Arc/Trench; Ion, Ionian Sea; Lev, Levantine Basin; Mag, Maghrebides (from the Rif to Sicily); NAF, North Anatolian Fault; Pan, Pannonian Basin; Rif, Rif; Sa, Sardinia; Si, Sicily; Tur, Turkey; and Tyr, Tyrrhenian Sea.

The Betic-Rif is indeed situated in a region of diffuse present-day deformation at the boundary between Nubia and Iberia plates, even if a broad band of shallow earthquakes makes the plate boundary difficult to locate (Fig. I.3). In fact, several different solution for the position of the plate boundary have been proposed and will be reviewed in chapter 1, section 3. The plate boundary location is not obvious to locate even using field geological observations: this difficulty was actually one of the reasons of skepticism on the plate tectonics model manifested by some field-oriented geologists in the 60's (Trümpy, 2001). Moreover, the presence of intermediate and deep seismicity, strike-slip motion and local extensional features make difficult the attribution of the Gibraltar deformation to one of the classical plate boundaries.

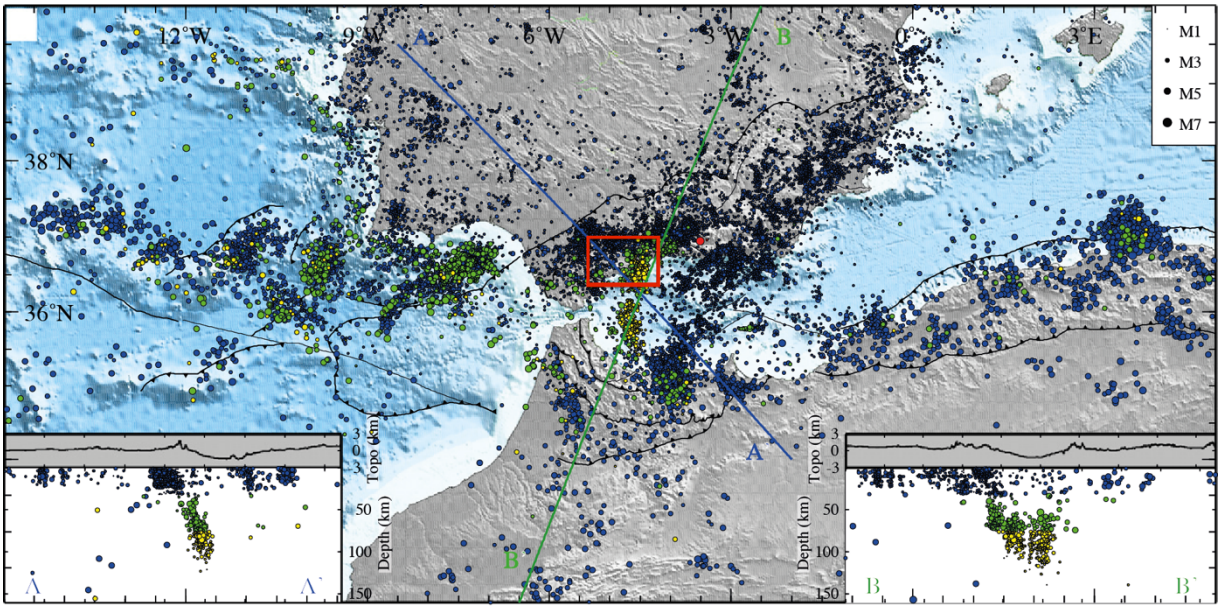

Figure I.3. Instrumental seismicity occurring in the Alboran region and nearby since 2000. Earthquakes are sized as a function of magnitude and classified with different colors as a function of the focus depth. Vertical cross sections of seismicity are reported in the lower left (A–A′) and lower right (B–B′) panels (from Palano et al., 2013).

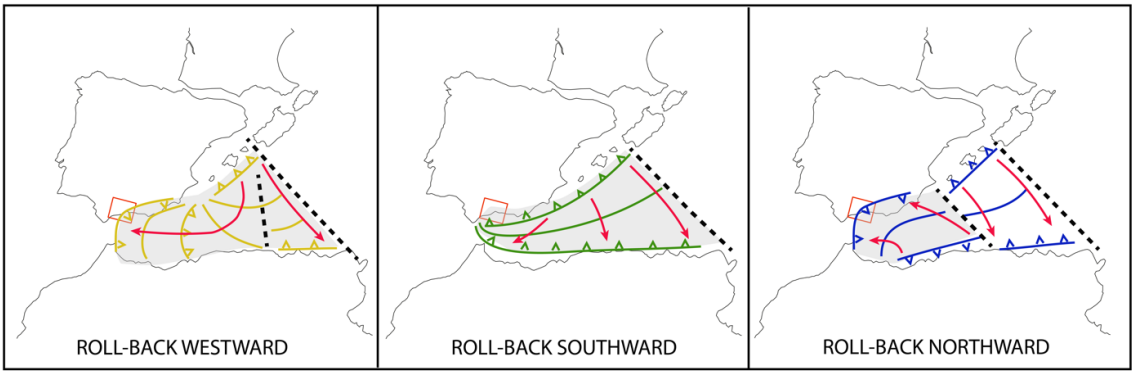

Figure I.4. Three different reconstruction scenarios for the western Mediterranean oligo-miocene evolution (shown in the paleogeography at ~35Ma, redrawn after Chertova et al., 2014). On the left, the scenario starts from an initial short subduction zone near the Baleares (e.g., Frizon de Lamotte et al., 2009; Lonergan and White, 1997; Rosenbaum et al., 2004). The scenario in the middle involves a long initial trench along the entire Gibraltar-Baleares margin (e.g., Faccenna et al., 2004; Jolivet et al., 2006; Wortel and Spakman, 2000). The scenario on the right starts from a S-SE dipping initial subduction zone under the African margin (Vergés and Fernández, 2012). Dashed lines represent proposed transform fault regions.

The difficulties in the interpretation do not derive from lack of data. On the contrary, the Betic-Rif Cordillera has been extensively studied (e.g. see reviews Crespo-Blanc and Frizon de Lamotte, 2006; Chalouan et al., 2008; Platt et al., 2013), producing a plethora of contrasting data and radically different interpretations. This situation has produced a scientific debate not only within the local community devoted to the geology of the Betics but also between those who investigate the geodynamics of the western Mediterranean: see figure I.4 for a quick summary of the main reconstructions proposed.

In order to contribute to the debate and in relationship with the two main goals mentioned at the beginning, we pose two main questions concerning the tectonics of the western Betics (Fig. I.5):

1- Timing, direction and amount of the **displacement** of the structures that are characterized by an arcuate trend;
2- Timing and structures responsible for the **exhumation** and for the crustal emplacement of the **mantle** rocks, and their original location in the Mediterranean during the Lower Miocene.

Following this introduction, the thesis is organized in four chapters with a conclusion that summarizes the results and indicates some perspectives for future research. The relationships between mantle exhumation at crustal level and displacement along the arcuate structures will be investigated using new structural and geochronological data collected in the western Betics.

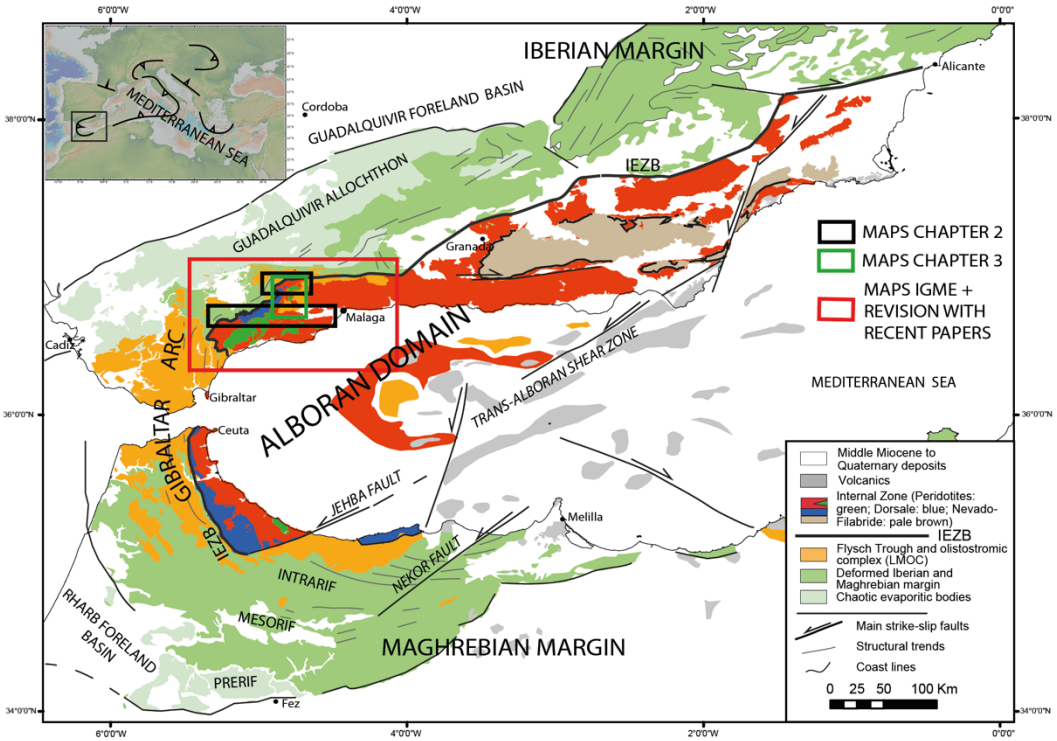

Figure I.5. Simplified tectonic map of the Betic-Rif belt (redrawn after IGME: http://info.igme.es/cartografia/magna50.asp?c=s and Crespo-Blanc and Frizon de Lamotte, 2006 for the Betics, Chalouan et al., 2008 for the Rif and Martínez-García et al., 2013 for the Alboran Domain). In the left-up corner the inset show the location of the area in the Mediterranean (from GeoMapApp, http://www.geomapapp.org). The maps shown in the chapters are indicated with different colors.

Chapter 1 contains the bibliographical and methodological preliminaries. First, the main geological features of the Betic-Rif are introduced. Then, the geodynamical and geophysical context is described. The different working hypotheses and models proposed in the past for the whole belt are analyzed highlighting the possible role of the western Betics in

the discrimination between them. At the end of the introduction, the GIS database built during this research is briefly presented and the geochronological methods used in the thesis are briefly summarized and explained.

The other chapters are the real contributions to the objectives of the study. These four chapters are presented in the form of focused reports, accepted or submitted for publication to international journals. In the annexes at the end of the thesis additional data, maps and pictures give further strength to the interpretations presented in the chapters. We focus on the period between the Oligocene and the Lower Messinian (33-8 Ma): the three central chapters are in particular focused on the periods 19-16 Ma (Chapter 2), 33-23 Ma (Chapter 3) and 23-20 Ma (Chapter 4).

Chapter 2 is devoted to the "**Lower Miocene structural record of the westward motion of the Alboran Domain in the Western Betics (southern Spain)**", and corresponds to a paper accepted for publication in ***Tectonophysics***. The chapter is a regional-scale study with new structural data and results derived from the synthesis of our field mapping campaign (15 weeks and 8734 structural measurements) and previous geological maps. A lateral-frontal ramp structure permits to justify the arcuate shape of the local structural trends and to accommodate about 60 km of displacement of the upper plate rocks relative to Iberia. The identification of a syn-tectonic Lower Miocene sedimentary basin defines the timing of the displacement. Its decrease towards the west suggests a relationship with the verticalization of the imaged slab below the western Betics.

Chapter 3 is entitled "**Hyper-stretching in a continental rift up to mantle exhumation (Western Betics, Spain)**", submitted for publication to ***Marine and Petroleum Geology***. It provides new structural and geochronological constraints to the 3D kinematics pattern associated with lithosphere necking process.

Chapter 4 aims to provide unequivocal constraints for the exact timing of rifting and subsequent rift-inversion that allows the final crustal emplacement of the Ronda peridotites: It is entitled "**Two successive events of crustal melting resulting from extensional exhumation and then thrusting of the Ronda Peridotites (South Spain)**", and corresponds to a paper submitted to ***Geology***.

In the final discussion we summarize our conclusions and provide some research lines for the future. The results hopefully will be used to extract parameters and boundary conditions for the modeling of the mechanical processes involved in the western Betics. All the models proposed in the past and summarized in section 1.2 involve of course the whole lithosphere and it will be thus not possible to choose between them in the conclusion of this thesis. The restricted dimension of the studied area cannot permit directly to use our results to constrain the geodynamics of the western Mediterranean system. Nevertheless, the vast exposure conditions of an entire large section of lithosphere in the western Betics and the multi-disciplinar approach carried out thanks to collaboration between Géosciences Montpellier and Géosciences Rennes can help to give a first order constraints and the data presented in the

thesis thus may have a great importance for the interpretation of the architecture of the Betic-Rif Cordillera and more generally for our understanding of the western termination of the Mediterranean realm.

The major outcomes of this work can be summarized as follows

1. The tectonics of the western Betics is characterized by a fast transition from upper plate extreme thinning up to mantle exhumation followed by thrusting of the Ronda peridotites. Both tectonic events are marked by crustal melting, at respectively 22.5 Ma and 20 Ma. This provides a simple and convincing tectonic framework that explains the entire set of geochronological data at regional scale.

2. The Alboran displacement relative to Iberia is initiated during Lower Miocene (20-16 Ma), propagates towards the west, and is accommodated by E-W lateral strike-slip corridors and frontal NE-trending thrusts, explaining the arcuate pattern of the western Betics. The thrusting of the Ronda peridotites likely occurs at the onset of such westward displacement.

3. The Alboran domain in the western Betics presents an exceptional exposure of a hyper-stretched portion of continental lithosphere, allowing a unique description of kinematics patterns associated with lithosphere necking process.

Chapter 1

Tectonic background, research questions and methods

This introductory chapter is meant to provide the reader with the instruments to appreciate the issues undertaken in the thesis and to describe the main investigation methods. The chapter is divided into six sections. The first section is a broad introduction to the Betic-Rif system and its exceptional geological features. The second section details the structures of a specific portion of the Betic-Rif, the Gibraltar arc, where our interest is concentrated. The third section summarize the research debate on the tectonic models for the formation of the Alboran system. The fourth section concentrates on possibly the most remarkable feature of the region, the Ronda Peridotites, describing their structures and relationships with the neighboring crustal rocks. Several models for their formation are also reviewed. Section 5 summarize the main questions arising from the previous four sections and briefly outlines our contributions, as well as the methods used to obtain them. Section 6 is entirely devoted to an extended description of the research methods used in the thesis, including the reconstruction of the state-of-the-art, the fieldwork and the geochronological analyses.

1.1 Betic-Rif system

The circum-mediterranean orogenic system stretches along southern Europe and has been formed since Late Mesozoic time in a tectonic environment controlled by the northward relative motion of Africa with respect to Eurasia (Dewey et al. 1989). During Late Tertiary, arcuate thrust belts started to develop around extensional basins floored by thinned continental or new oceanic crust (Fig. 1.1A) (Jolivet and Faccenna, 2000). Two of these arc-basin systems are coupled with well-defined subduction zones: the Calabrian-Tyrrhenian and the Aegean-Hellenic systems are unquestionably underlain by active subduction zones (Fig. 1.1B).

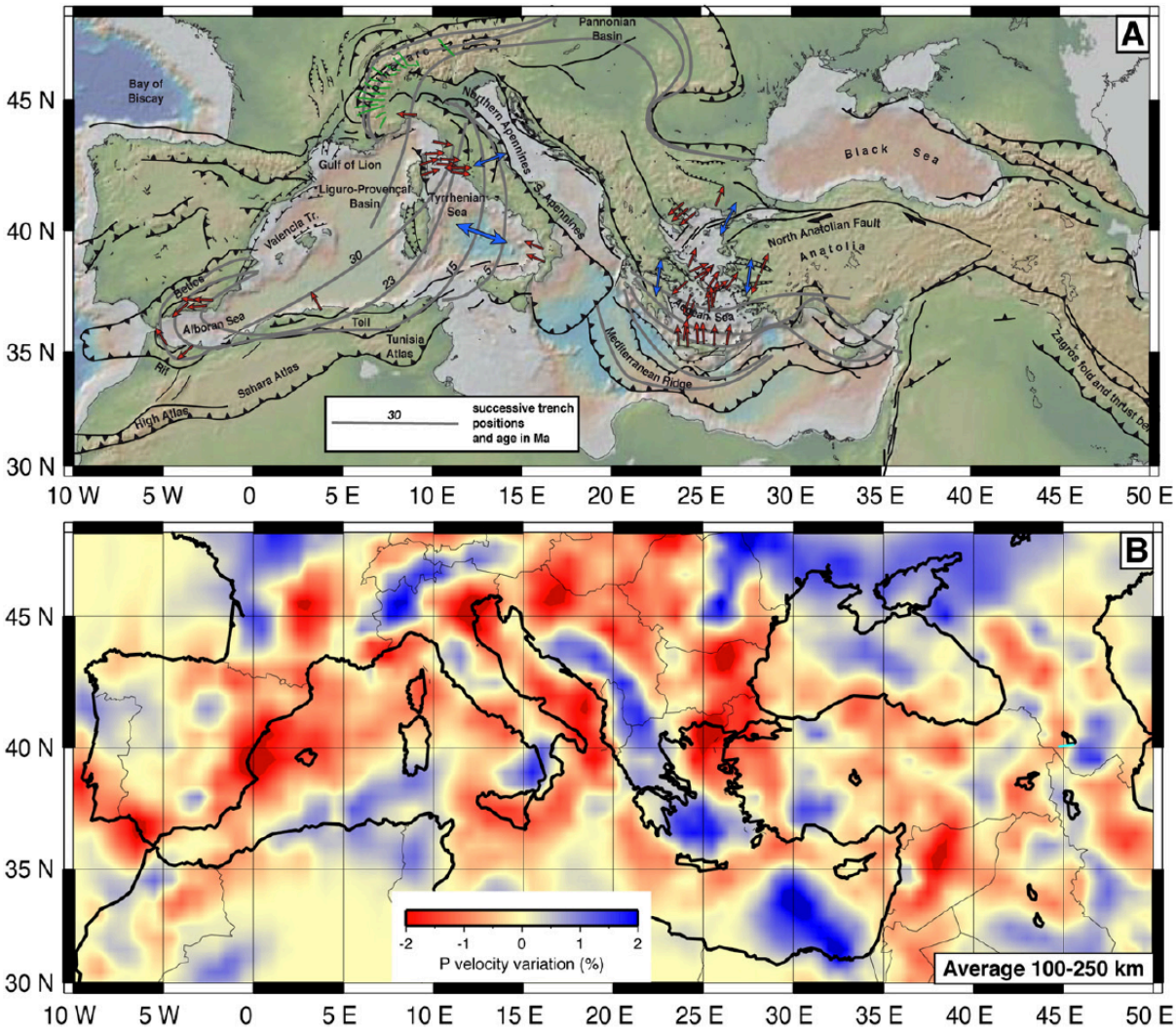

Figure 1.1. A: Topographic and bathymetric map of the Mediterranean region showing the position of the main structures: thrust fronts, subduction zones, main strike–slip and normal faults. Grey lines show the successive positions of the trenches. Red arrows show the directions of ductile stretching within metamorphic core complexes and blue arrows the directions of active extension in the back-arc domains. B: Tomographic model of Piromallo and Morelli (2003) shows the average V_P perturbation in the topmost mantle (vertical average of four model layers, between 100 and 250 km depth). (from Jolivet et al., 2009)

Conversely, as we can observe in Figure 1.1, the Carpathian-Pannonian, Appennine-northern Tyrrhenian, and Betic-Rif-Alboran systems reveal only fragmentary evidences for the subduction of an oceanic lithosphere (Platt, 2007). Moreover, tectonic analysis in the Mediterranean system is complicated by the existence of several micro-plates (e.g. Iberia and Adria) and numerous micro-continental fragments (e.g. Briançonnais and Alkapeca) with debated existance and kinematics poorly known (e.g. Handy et al., 2010). Lateral extrapolations of surface geology and of geophysical informations between the arcs are thus extremely debated. This leads in general to strongly different scenarios for the western Mediterranean, as we say in the introduction (Fig. I.4): for most authors nevertheless the Betic-Rif has an appenninic-related evolution, as shown in Figure 1.2.

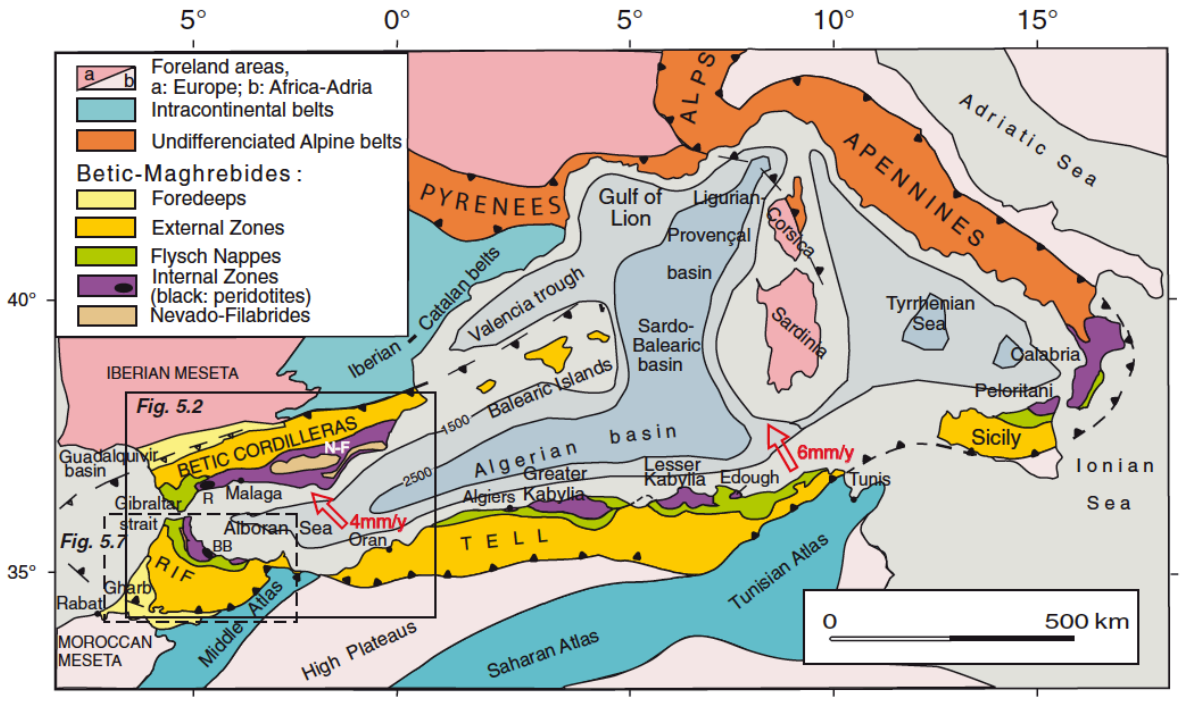

Figure 1.2. Tectonic sketch map of the Western Mediterranean from Chalouan et al. (2008). N-F = Nevado-Filábride; R = Ronda Peridotite; BB = Beni Bousera. Note that the metamorphic rocks in Calabria are considered an equivalent of the Betic-Rif metamorphic rocks in the reconstruction.

The Alboran region is the most remarkable example of the Mediterranean arc-basin couple and it is characterized by an Internal and an External Zone (Fig. 1.3). The Internal-External Boundary Zone (IEZB, Platt et al., 2013) marks the limit between the two Zones and will be studied in detail in the western Betics in Chapter 2.

The External Zone is a thrust belt that involves mainly the passive margin of the Iberia and Nubia plates and the Internal Zone, hereafter called Alboran Domain (violet and beige in Fig. 1.2, and violet in Fig. 1.3), is characterized by extension and subsidence. In the following we discuss the most important geological features and the problems that arise from the analyses of both of them.

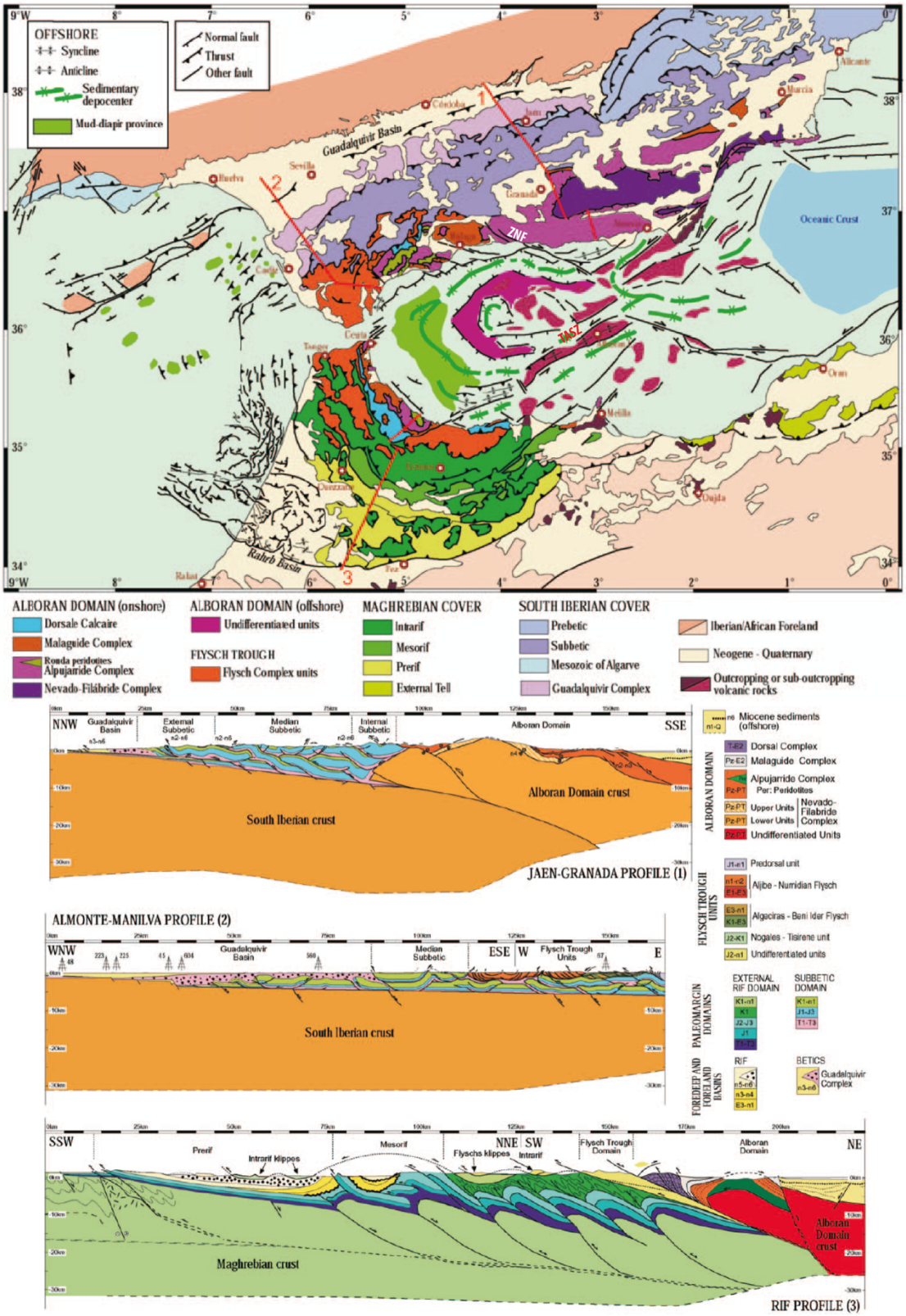

Figure 1.3. Top, structural map showing the main tectonic domains around the Gibraltar arc. Bottom, cross-sections along the Betics and the Rif (from Crespo-Blanc and Frizon de Lamotte, 2006). Location on on the map. Pz: Paleozoic; PT: Permo-Triassic; T: Triassic; J: Jurassic; K: Cretaceous; E: Eocene; M: Miocene; Q: Quaternary.

Since in the core of the thesis we will focus mainly on the Western Betics, we discuss hereafter the geology of the External Zone and of the Alboran Domain mainly in relationships with what we will observe in the Western Betics and to introduce the structural-geological setting of the Gibraltar arc and of the mantle rocks exhumation, with only few hints to the Rif belt. We will use as a guide the general map of the Betic-Rif, slightly modified from Frasca et al. (2015), to show the main units composing the westernmost Mediterranean system (Fig. 1.4). This map is based on compilations of the available data and the field mapping presented in this thesis (see section 1.6, Methods).

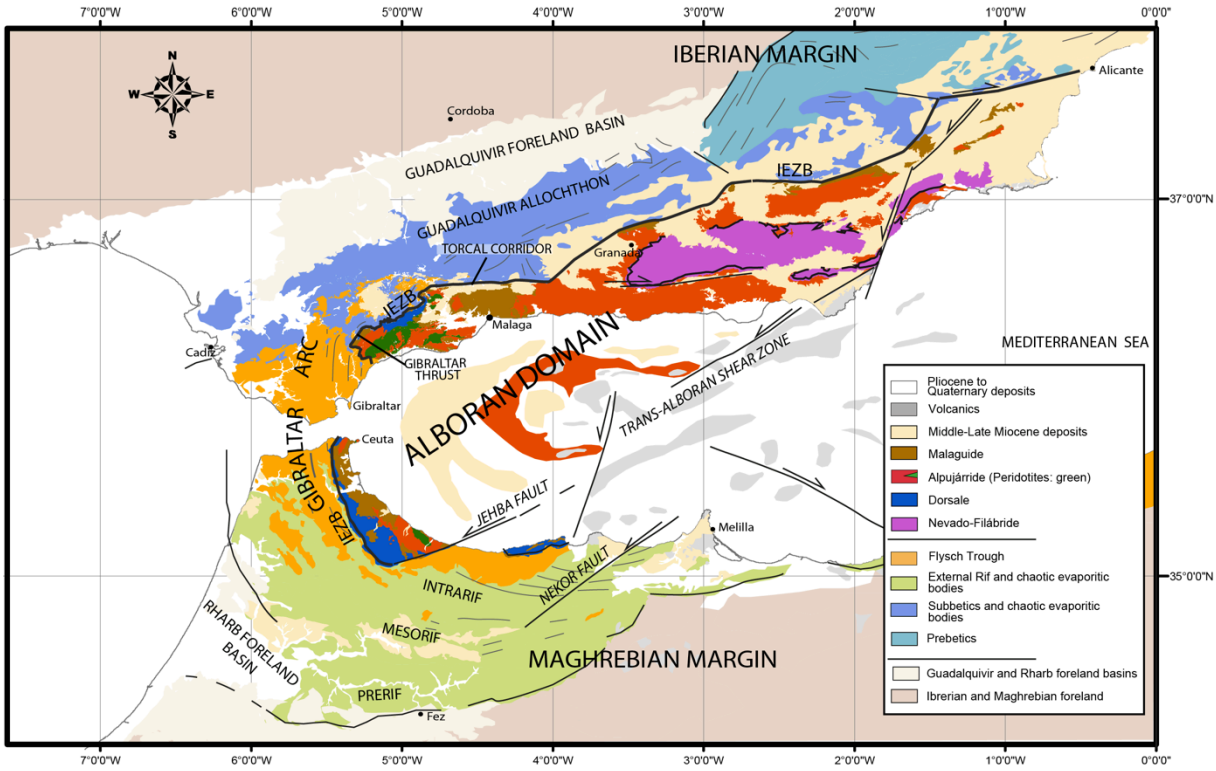

Figure 1.4. Tectonic map of the Alboran region (modified from Frasca et al., 2015).

1.1.1 External Zone

The thrust belt that crops out around the Alboran Domain in the Betic Cordillera is an accretionary wedge that involves three domains, called Prebetic, Subbetics and "Flysch Trough" (Fig. 1.5). The *Prebetic* is cropping out only in the Eastern Betics and is made of the deformed Iberian Mesozoic carbonatic platform (Allerton et al., 1994). The *Subbetics* are the Mesozoic to Tertiary sedimentary cover partly detached from the Iberian margin basement, and are equivalent to Infra and Meso-Rif for the Maghrebian margin, as described in Crespo-Blanc and Frizon de Lamotte (2006). The "*Flysch Trough* Complex" is composed mainly by Oligo-Lower Miocene terrigenous sediments detached from the original unknown basement and partly Cretaceous sediments (Lujàn et al., 2006). In the central and western Betics, the

Subbetic thrust belt progrades into the Guadalquivir flexural basin and the Prebetic disappears beneath the Subbetics.

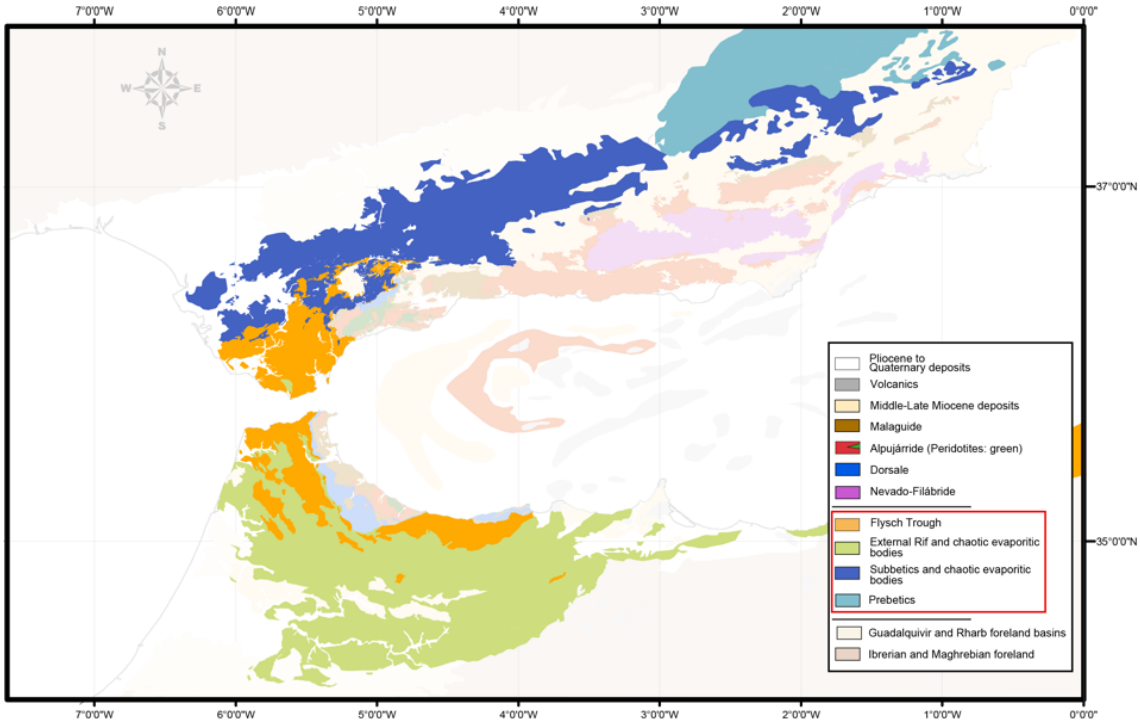

Figure 1.5. Tectonic map of the Alboran region (from Frasca et al., 2015). The tectonics units in the External Zone are without transparency.

Several problems, as underlined by Platt et al., 2013, arise during the study of the External Zone:

1. large volumes of rocks with a *chaotic* internal structure prevent good structural analysis in some regions (Sanz de Galdeano et al., 2008, Ruiz-Constán et al., 2012; Pedrera et al., 2012);
2. a *forethrust-backthrust* structure along the internal side of the Subbetic in the Eastern Betics, and also partly in the Western Betics (Allerton et al., 1994; Martín-Algarra, 1987; Luján et al., 2006) (see cross-section of Fig. 1.3);
3. polyphase deformation, including large-scale fold interference structures (Crespo-Blanc, 2007; Crespo-Blanc, 2012), that we will discuss partly in chapter 2;
4. uncertainties in the *paleogeographic position*, significance, and inter-relationships of some units, most notably the *Internal Subbetic* and the some units in the *Flysch Trough* that we will discuss a little bit further in this section;
5. evidence for *basement involvement* during thrusting (Fig. 1.3), mostly in the Rif side (cross-section, Fig. 1.3). Indeed, parts of the Mesorif show ductile strain and a well-developed slaty cleavage (Crespo-Blanc and Frizon, 2006), and in the Temsamane massif (Intrarif) the rocks show low greenschist facies metamorphism, probably of middle Miocene age (Negro et al. 2007). Conversely, thin-skinned folding and thrusting occurred during the Miocene in the Betic External Zone. However, Permian terrigenous sediments crop out at the boundary between Internal and Median Subbetics in the Western Betics (Bourgois, 1978; Martín-

Algarra, 1987; Martín-Algarra and Checa, 1990), indicating the involvement of rocks below the triassic evaporites that usually act as a *décollement* level during the thin-skinned thrusting.

Subbetics

The Subbetics (fig. 1.6) are divided into several tectonic units (External Subbetics, Median Subbetics and Internal Subbetics), mainly based on their paleogeographic position during the Jurassic and the observed differences in sedimentary facies of the Cretaceous deposits (García-Hernández et al., 1980; Vera et al., 2004, Martín-Algarra and Vera, 2004).

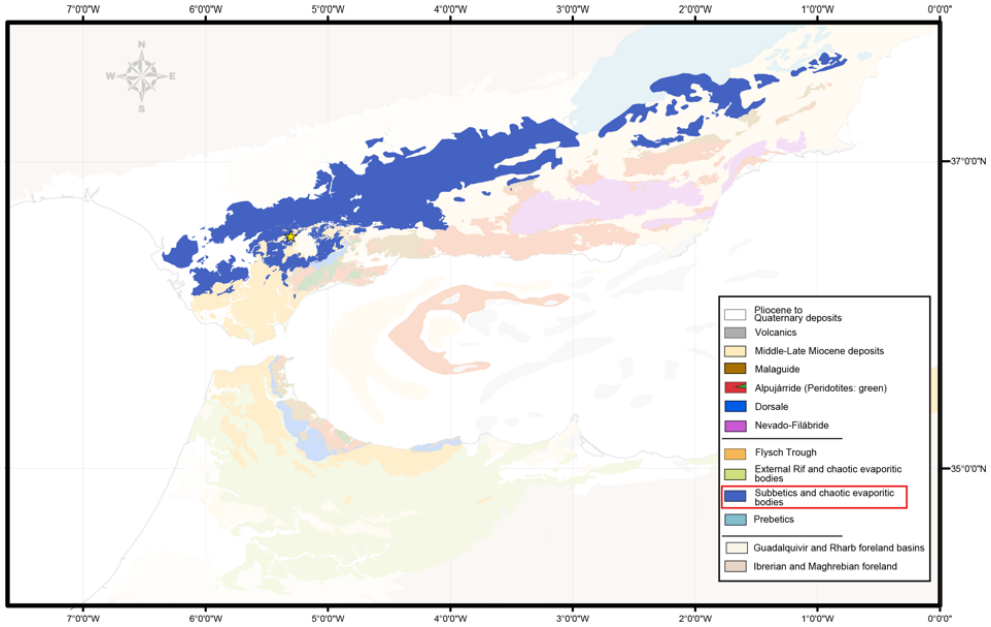

Figure 1.6. Tectonic map of the Alboran region (from Frasca et al., 2015). The Subbetics is without transparency. The star show the location of the Montecorto slice.

The stratigraphic sequence of the Internal Subbetic (also called Penibetic; Martín-Algarra, 1987) units, which are partly object of the study in chapter 2, includes, from bottom to top:

1. massive carbonates (Triassic, not chaotic) with on top evaporites (Hidalga group);
2. platform dolostones (Liassic), massive oolitic limestones, and pelagic limestones, which are nodular at the base and oolitic towards the top (Dogger and Malm) and at the top an unconformity marked by an hard-ground (Early Cretaceous) (Libar Group);
3. pelagic layered limestones (alternating white and pink pelagic marls and marly limestones of Upper Cretaceous to Paleogene age) and also oligo-miocene deposits (Espartina Group) (Martín-Algarra, 1987; Cano Medina, 1990; Martín-Algarra and Vera, 2004).

This subdivision clearly identifies a "mechanical stratigraphy" that controls the evolution of the thrust belt (Expósito et al., 2012; Vergés and Fernández, 2012).

In the western sector of the study area, the Subbetic rocks consist predominantly of Triassic evaporites (Figs. 1.7a and 1.7b), whose structural position and emplacement age are

largely controversial, but surely have a strong influence on the displacement of the Internal Subbetics. Flinch et al. (1996) proposed that the salt rocks were emplaced originally within Mesozoic sedimentary sequence in passive-margin setting. The diapiric allochthonous masses were then overthrusted as an accretionary wedge during the Miocene forming km-thick bodies. By contrast, Bourgois (1978) claimed that the Triassic rocks are polygenetic breccias, formed during the Burdigalian, of Subbetic rocks in a gypsum cement (Fig. 1.7a). The major part of these deposits is composed of sheared clays (Fig. 1.7c) and contain from centimetric clast (Fig. 1.7a) to kilometric blocks (Fig. 1.7b) of different origin, also with strong similarity of rocks of the Alboran Domain (Fig. 1.7d) (Montecorto sliver, see yellow star in Fig. 1.6., Bourgois, 1978; Martín-Algarra and Checa, 1990).

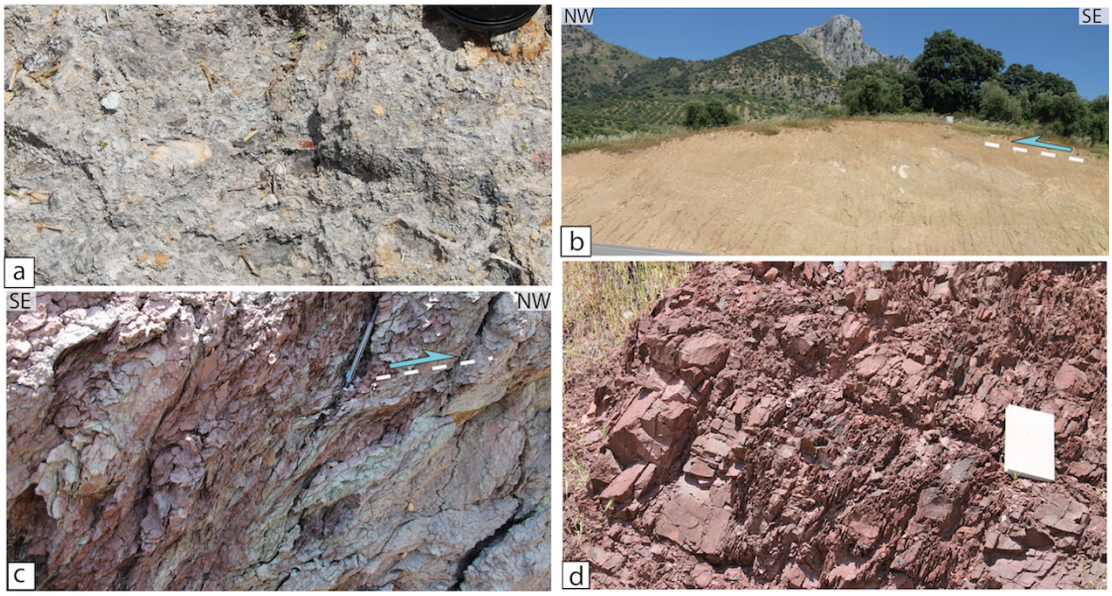

Figure 1.7. Chaotic deposits at the base of the Internal Subbetics in the Western Betics. (a) Breccia with gypsum matrix containing clasts of Subbetics carbonatic rocks. (b) Landscape view of the mélange. Foreground with sheared breccias and background with a km-scale carbonatic mesozoic block. (c) Deformed clays in the matrix of the deposits indicate a shear top-to-NW. (d) Permian reddish sandstones in the Montecorto slice (Photographs by G. Frasca).

Flysch Trough

The Flysch Trough is also subject of debate concerning the structures (Fig. 1.8). Deep marine clastic sediments, called hereafter the "*Flysch Trough*" lies structurally on top of the Subbetics in the External Zone (Martín-Algarra et al., 2004b; Luján et al., 2006; Kirker and Platt, 1998) (cross-section, Fig. 1.3). The Flysch Trough sediments started to deposit during the Lower Cretaceous in a structural depression floored by oceanic or thinned continental crust, most probably related to a transform setting (Biju-Duval et al., 1977; Dercourt et al., 1986; Thurow and Kuhnt, 1986). The "Flysch Trough" is mainly composed by Miocene terrigenous sediments and is organized in a coherent accretionary prism north of Gibraltar (Guerrera et al., 2012; Luján et al., 2006). Two main groups are individuated: 1) slivers of Cretaceous sediments at the base, considered as separated tectonic units (Martín-Algarra, 1987) and 2) large amounts of Paleogene to Miocene flysch-type deposits, considered as pre-compression and Aquitanian to Lower Burdigalian in age (Martín-Algarra et al., 2004b).

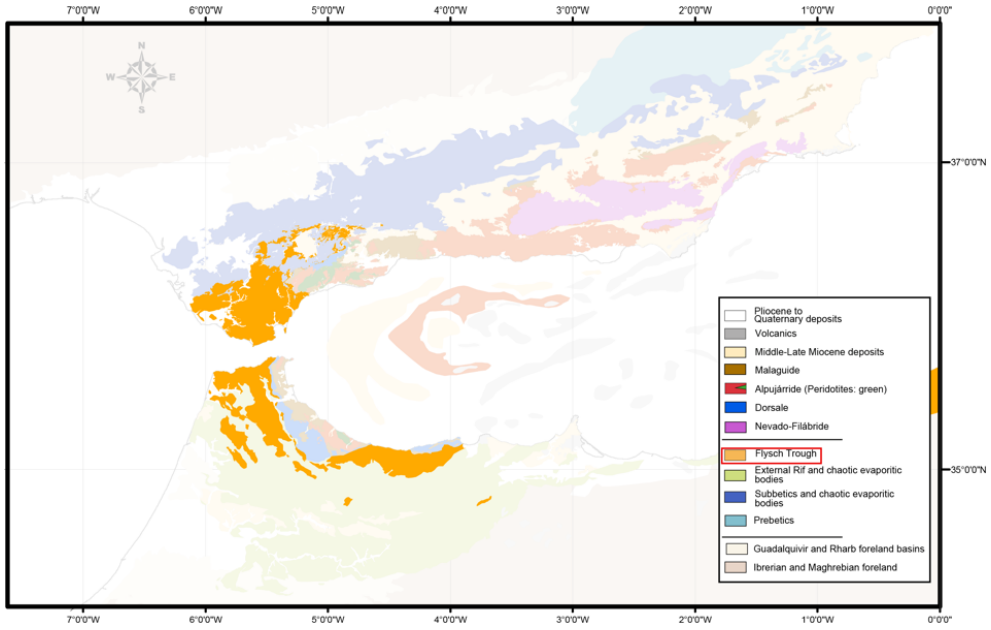

Figure 1.8. Tectonic map of the Alboran region (modified from Frasca et al., 2015). The Flysch is without transparency.

The sediments of the second group are usually separated in several units on the base of the relative abundance of quartz or lithic fraction in the terrigenous sediments composing them (Martín-Algarra and Vera, 2004). Lower Miocene quartz-arenites of the **Aljibe** Flysch (called Numidian in the Rif) are part of a widespread turbidite sandstone sequence deposited on the southern side of the basin (Fig. 1.9). These quartz-rich sandstones most probably have an African origin, given the predominance of Mesozoic carbonate shelves in Iberia, Adria, and the Alboran Domain. Immature micaceous sandstones of late Oligocene to early Miocene age of the **Algeciras** Flysch (the Beni Ider Flysch is the equivalent in the Rif) were probably deposited on the north side of the basin (Fig. 1.9). However, these terrigenous sediments appear to be trench or foreland basin deposits derived from the Alboran Domain which underwent active deformation, metamorphism, and uplift by the end of the Oligocene (Guerrera et al., 2012).

The youngest sediments are **Burdigalian mélange** deposits consisting of blocks of older sediment (particularly the Numidian Flysch and Dorsale) in a matrix of sheared brown shale (Fig. 1.10b) (Bourgois, 1978) are found at the top of the main flysch units in the Gibraltar area, but they also occur locally above the Internal Subbetic and below the Alboran Domain (Fig. 1.10a). The age of these chaotic sediments is most probably getting younger towards the west where the backthrusting of the Median Subbetics involve a *mélange* containing Serravallian to Langhian fossils (Bourgois, 1978). It is debated, when these sediments are observed on top of the Alboran Domain (Fig. 1.10d), whether this is relationship is depositional or due to backthrusting (Martín-Algarra et al., 2009; Suades and Crespo-Blanc, 2013) (Fig. 1.10c). The relationships between the Alboran Domain structures

and these deposits will be investigated in Chapter 2. However, bad outcropping conditions prevent from good structural analysis of these Miocene deposits.

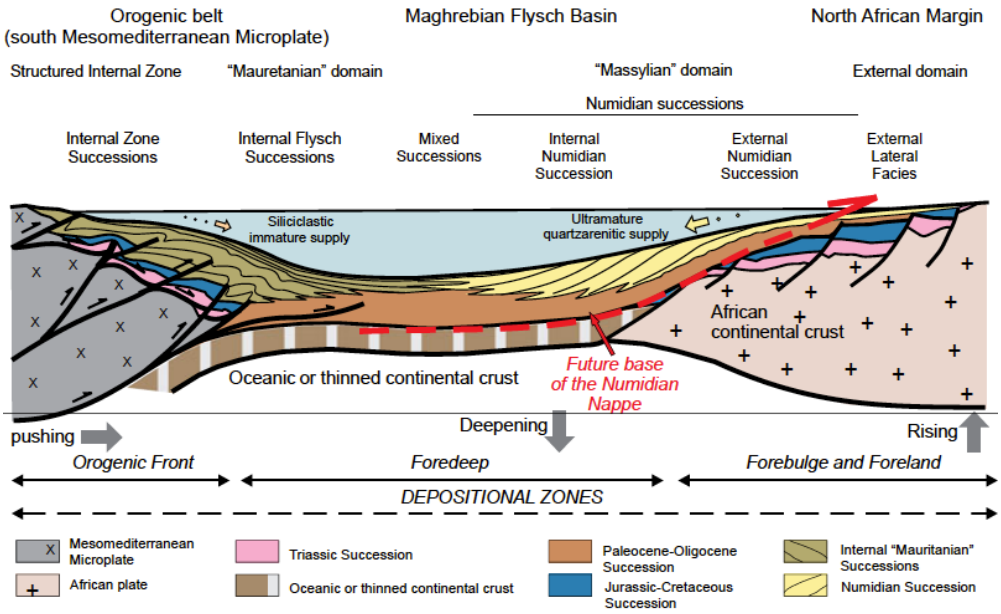

Figure 1.9. Synthetic section showing a tectono-sedimentary model across the Flysch Trough Basin with its internal and external margins during the Oligocene–Early Miocene (from Guerrera et al., 2012). On the left Mesomediterranean microplate is the upper plate of the subducting system.

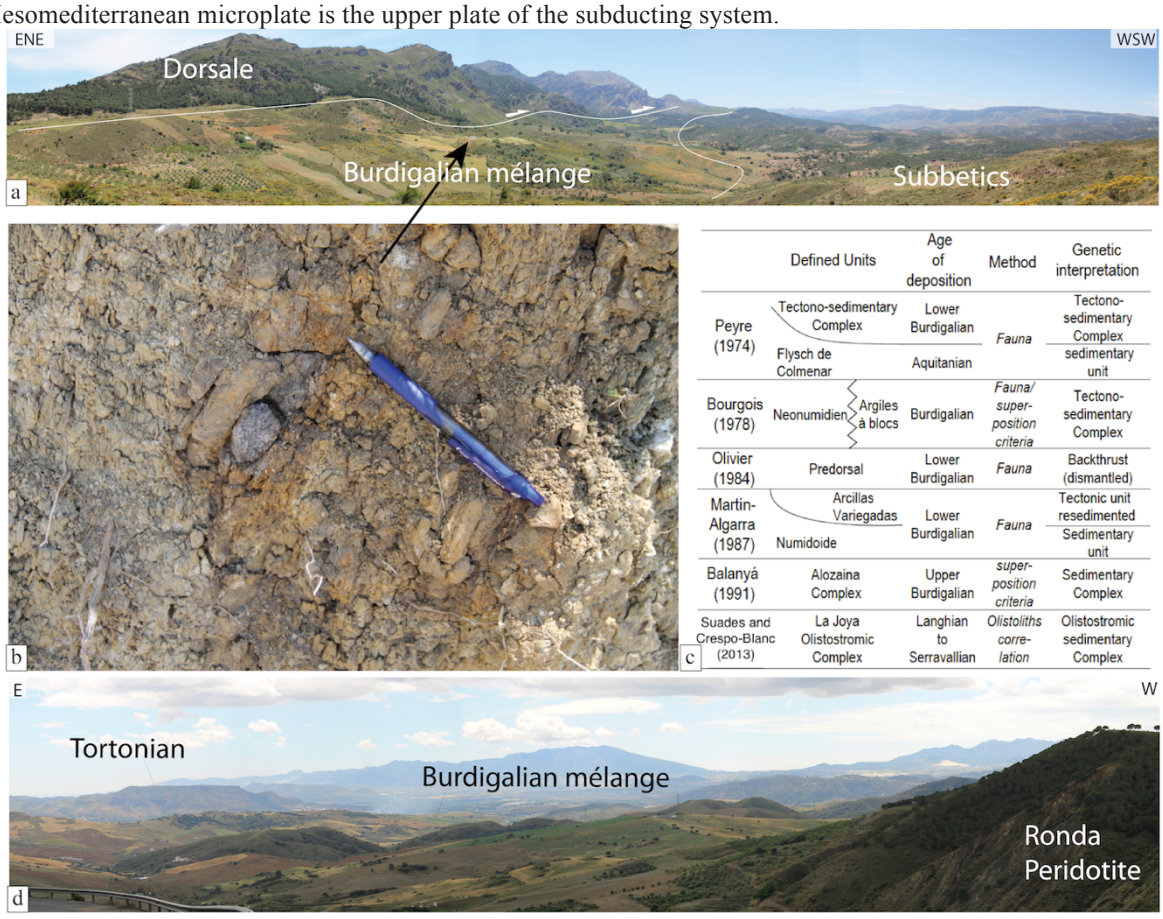

Figure 1.10. The Burdigalian mélange deposits in the Western Betics. (a) Landscape view of the mélange on top of the Subbetics and below the Alboran Domain. (b) A clast of Alboran rock in brownish claysh matrix. The position of the outcrop is shown with a black arrow in Figure 1.10a. (c) Summary of the names attributed to the

mélange (modified after Suades and Crespo-Blanc, 2013). (d) Burdigalian mélange on top of Alboran Domain rocks (Photographs by G. Frasca).

The sedimentation ends in the Lower Miocene, marking the onset of the main shortening event in the Flysch Trough (Luján et al., 2003). The westward motion dominates close to the Alboran Domain, while different patterns develop where evaporites and not subbetics rocks occur along the basal décollement of the thrust imbrications (Luján et al., 2006). The kinematic vector derived from thrust fault thus swings along the western Subbetics arc as reported in Fig. 1.11. Chapter 2 will provide some insights on this peculiar deformation pattern.

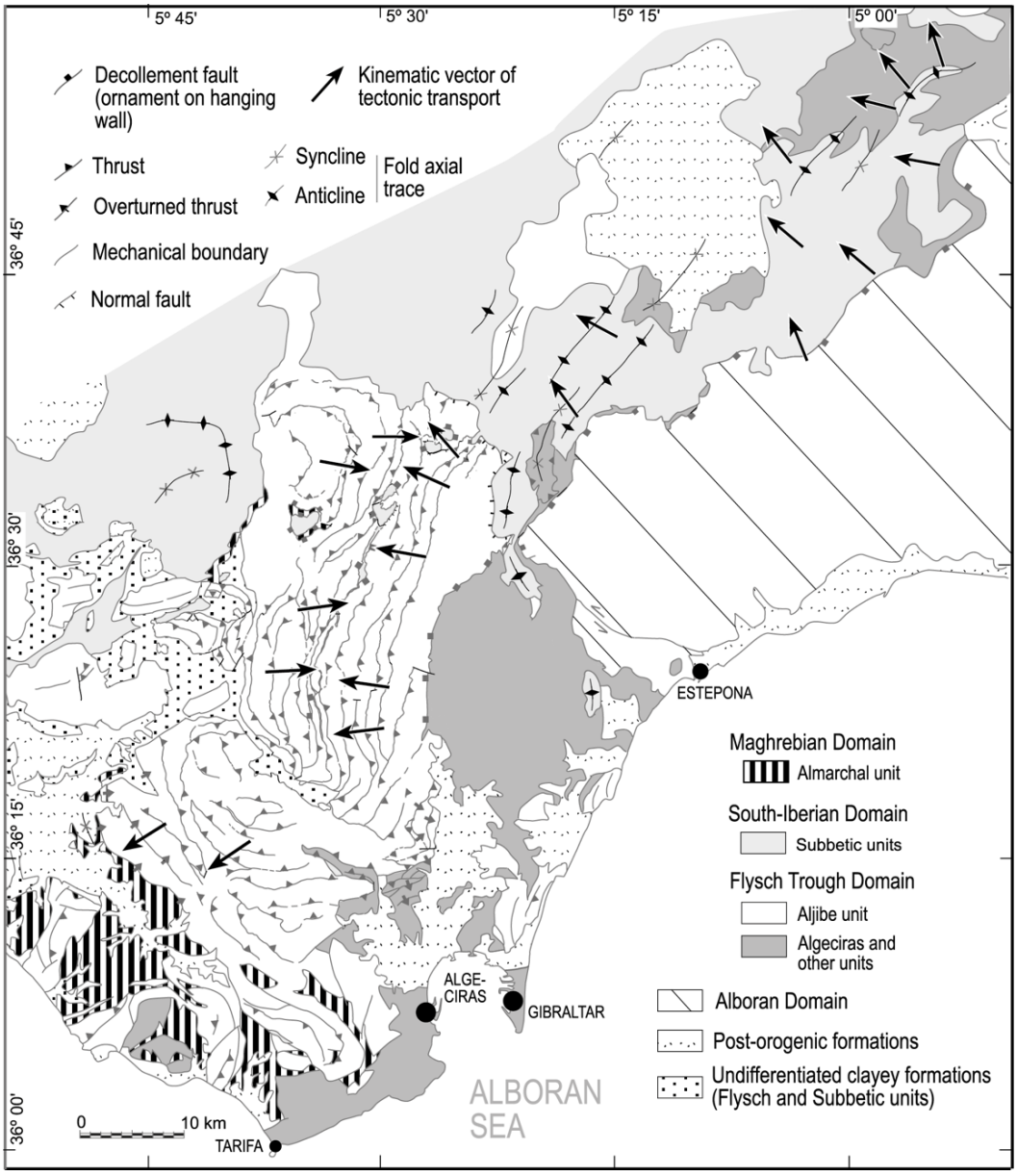

Figure 1.11. Present-day pattern of tectonic transport kinematic indicators around the northern branch of the Gibraltar Arc (from Lujan et al., 2006) according to data for the Flysch Trough in Lujan et al. (2006) and for the Subbetics units in Crespo-Blanc and Campos (2001).

1.1.2 Alboran Domain

The Internal Zone, or Alboran Domain, is made up of a large number of tectonic units classically grouped into three main tectonic groups, usually referred as *nappe* or tectono-metamorphic complex (e.g., Chalouan et al., 2008; Egeler and Simon, 1969; Torres-Roldán, 1979; Platt et al., 2013). The metamorphic tectonic groups are, in ascending order, the Nevado-Filábride, the Alpujarride (called Sebtide in the Rif) and the Malaguide (called Ghomaride in the Rif) and will be described in the following (Fig. 1.12). The distinction between them is done on the basis of many field criteria, mainly the lithological and metamorphic characteristics of the rocks. However, a strict definition is often difficult in the field, and also after further petrographic analyses, because of the similarities between the rocks of the different groups and because of the variations in the metamorphic grade inside each group (e.g. Tubía et al., 1992, and Platzman et al., 2004, for Malaguide and Alpujarride distinction in the Western Betics). The main feature used to discriminate between the groups is thus usually a jump in metamorphic grade associated with large-scale shear zones (Vissers, 2012).

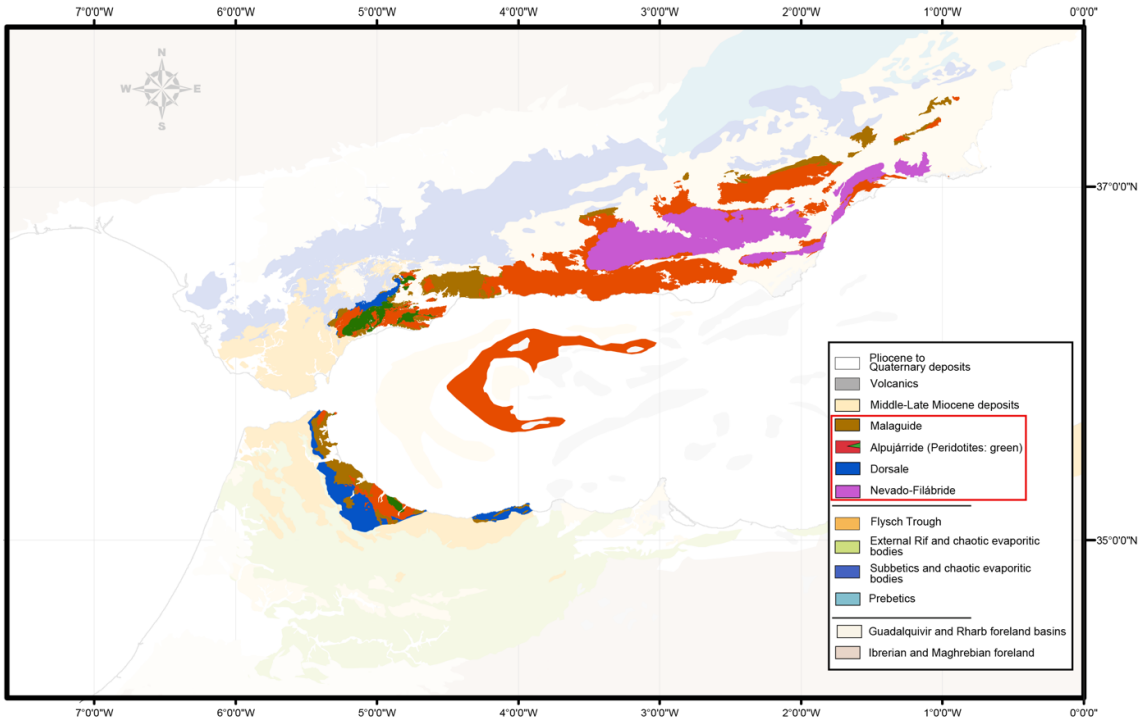

Figure 1.12. Tectonic map of the Alboran region (modified from Frasca et al., 2015). The Alboran Domain is without transparency.

The origin of the names Nevado-Filabride, Alpujarride and Malaguide in the old geological literature is nevertheless related to differences in the stratigraphic facies of the Mesozoic and early Tertiary cover sequences of these three groups. Unfortunately, in the Betic-Rif this classic criterion for the distinction of the *nappes* is difficult to apply, because only ante-Triassic rocks are involved in the deformation. In fact, the criterion is based on the hypothesis that sedimentary facies belts are associated to Mesozoic basins and the distribution

of the Mesozoic basins controls the later reactivation. The basins started to develop after the Triassic with a strike-slip kinematics (Dercourt et al. 1986, Biju-Duval et al., 1977) that implied strong lateral changes in the sedimentary facies along the pull-apart basins (Fig. 1.13). This deformation and the age of the sediments make the stratigraphic differences a problematic criterion. Furthermore, the deeper *nappes* were deformed and metamorphosed already during the Hercynian orogeny (e.g. Kornprobst, 1976; Gueydan et al., 2015). In the following thus we will not endow the terms Malaguide, Alpujarride and Nevado-Filabride with a paleogeographic significance, but we will use them in relationships with the Lower Miocene tectonic contacts that bound them.

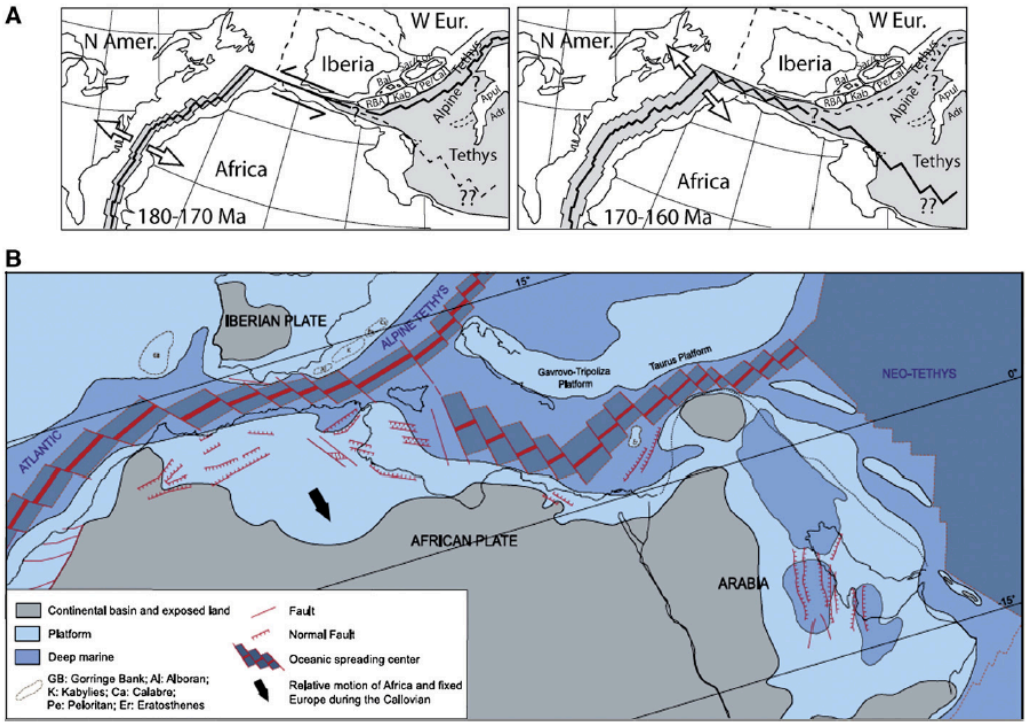

Figure 1.13. Paleogeographic reconstructions of the Atlantic–Tethyan oceanic realms in the Jurassic (from Gutscher et al., 2012). (A) Schematic reconstruction showing two-step rifting opening showing first pure strike–slip motion between the NW corner of Africa and the southern Grand Banks margin (transform margin), followed by a shift in plate motions leading to oblique and highly segmented seafloor spreading along the N margin of Africa (southwestern Tethyan margin). (B) Detailed reconstruction showing segmentation of the western Tethyan oceanic lithosphere formed at an oblique spreading center.

In the following we describe the most important characteristics of them in ascending structural order, from the Dorsale to the Malaguide. The Dorsale is composed of non-metamorphosed Mesozoic sediments. In the Nevado-Filabride rocks Tethysian oceanic remnants are affected by a high-pressure metamorphic event (Monié et al., 1991; Platt et al., 2006). In the Nevado-Filabride rocks Tethysian oceanic remnants are affected by a high-pressure metamorphic event (Platt et al., 2006). In the Alpujarride the metamorphic grade increases westward (Tubía et al., 1992), from high-pressure/low-temperature south of Granada (Azañón et al., 1998) to medium-pressure/high-temperature in the Western Betics

(Argles et al., 1999). The Malaguide is characterized by Hercynian low-grade metamorphism (Chalouan and Michard, 1990).

Dorsale

The "Dorsale Calcaire" units are associated with the Alboran domain and they are usually situated on top of the Flysch Units and below the metamorphic units of the Internal Zone (Fig. 1.3), and underline the Alboran Domain all across the Gibraltar arc (Fig. 1.14). The Dorsale units are composed of Triassic to Neogene carbonatic sediments essentially non-metamorphosed.

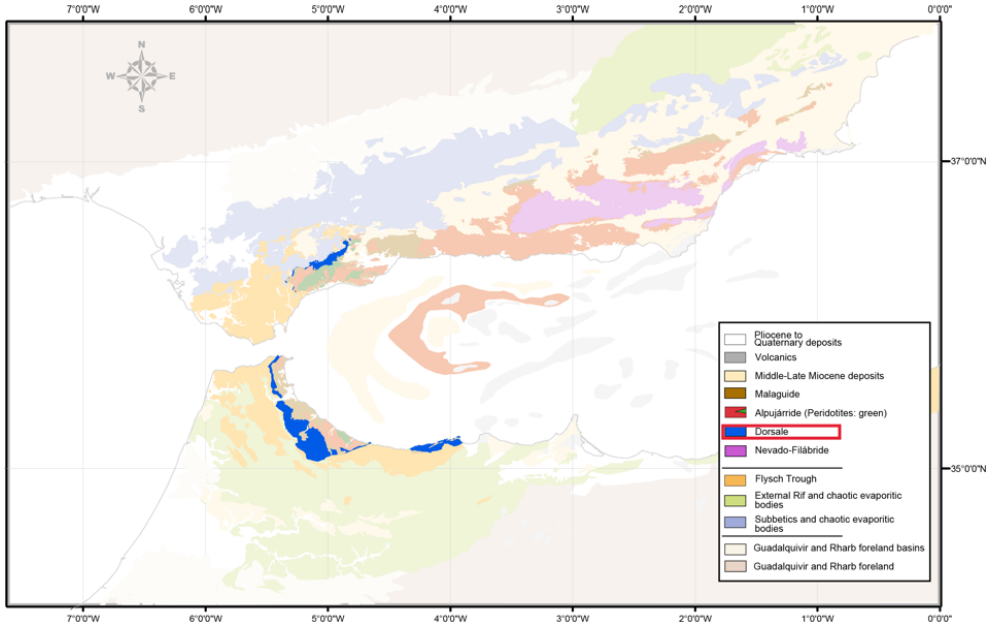

Figure 1.14. Tectonic map of the Alboran region (from Frasca et al., 2015). In blue the Dorsale rocks along the Gibraltar arc.

Figure 1.15. Dorsale in the Western Betics. (a) Landscape view of the position of the Dorsale above the Subbetics and below the metamorphic Alboran Domain. (b) Shearing with associated yellowish HT phlogopite-tremolite aggregates at the boundary with the Internal Zone between Casarabonela and Yunquera (on the left in Figure 1.15a) (Photographs by G. Frasca).

The relationship between the Dorsale and the other units of the Alboran Domain is still debated. The Dorsale belongs to the Alpujarride, according to Chalouan et al. (2008) and Wildi et al. (1977), or to the Malaguide, according to Didon et al. (1973), Balanyá and

García-Dueñas (1987) and Sanz de Galdeano et al. (2001b). In spite of the original basement, Triassic-Liassic massive carbonates characterize the Dorsale range in the Western Betics. In some cases these calcareous slivers overlie upper Carnian evaporites, which clearly correspond to levels of the Malaguide, and played a major role in the detachment of the Dorsale units from their original (and controversial) basement (Chalouan et al., 2008). The carbonate sequence itself begins with greyish dolomites. They represent mainly the Norian massive carbonates. Radiolarite appears during the Sinemurian (O'Dogherty et al., 2001).

The direction of emplacement is top to the WNW for Kirker and Platt (1998) and top to NW for Expósito et al. (2012) in the Western Betics, while is top-to-SW for Vitale et al. (2014b) in the Rif, although with common backthrusting (Fig. 1.16). The top-to-NW sense of shear is reported by Mazzoli et al. (2013) in the Western Betics and related to the high-temperature thrusting of the metamorphic units (Figs. 1.15b and 1.16). A swing at large scale around the arc is thus supposed by the Naples group for the emplacement of the Alboran Domain, and also, most probably, for the emplacement of the metamorphic unit onto the Dorsale rocks. Note that the age of the emplacement on the External Zone is slightly younger in the Rif where the emplacement is not Aquitanian-Burdigalian as in the Western Betics (Martín-Algarra, 1987), but Burdigalian-Langhian (Vitale et al., 2014a).

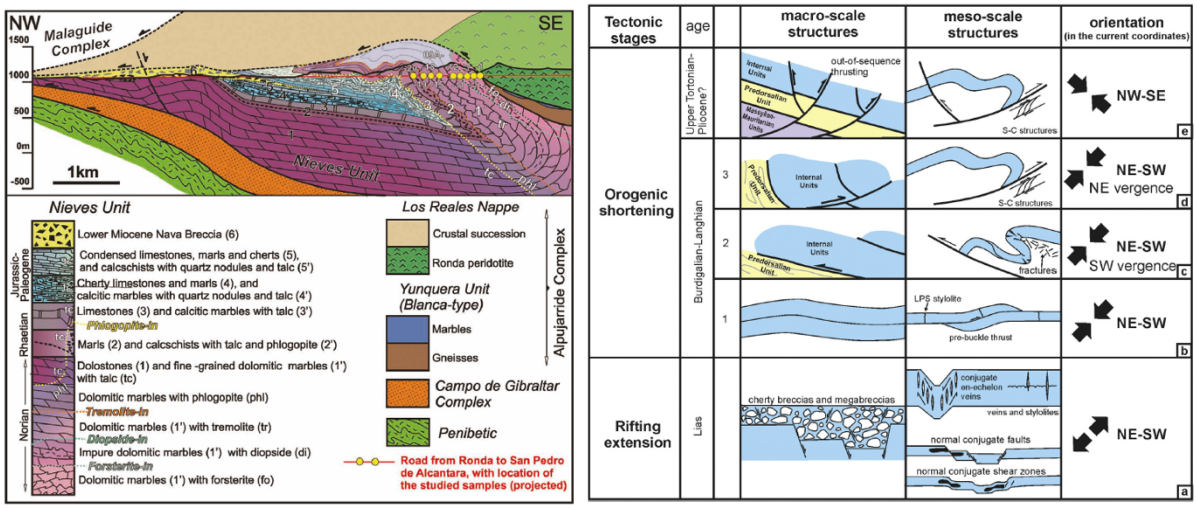

Figure 1.16. Deformation in the Dorsale Units. (left) Geological cross-section (roughly parallel to the Ronda–San Pedro de Alcantara road) through the edge of the Ronda peridotites at Sierra Bermeja (from Mazzoli et al., 2013). Metamorphic zoning of the aureole (shaded) in the Nieves Unit is shown by index minerals. For details see Mazzoli et al, 2013. (right) Cartoon showing deformation structures and related deformation orientation and ages (Vitale et al., 2014a).

Conglomerates whose age is debated, although generally considered post-Lower Aquitanian (Felder, 1980), are locally founded on top of the Dorsale Units (Nava Breccia, Bourgois, 1978; Martín-Algarra and Estévez, 1984). Independently on the paleogeogeographic position, the presence of these Lower Miocene sediments (Nava Breccia) (Fig. 1.16) involved in the high-temperaure deformation strongly suggests that the

emplacement of the metamorphic rocks onto the Dorsale Unit is Miocene and not older (Mazzoli and Martín-Algarra, 2011, and ref. therein).

Nevado-Filábride

The Nevado-Filábride group is cropping out only in central and eastern Betics in a tectonic window below the Alpujarride and the Malaguide (Fig. 1.17a), in a structural position broadly similar to the one of the Dorsale units, but far from the Internal-External Zone Boundary.

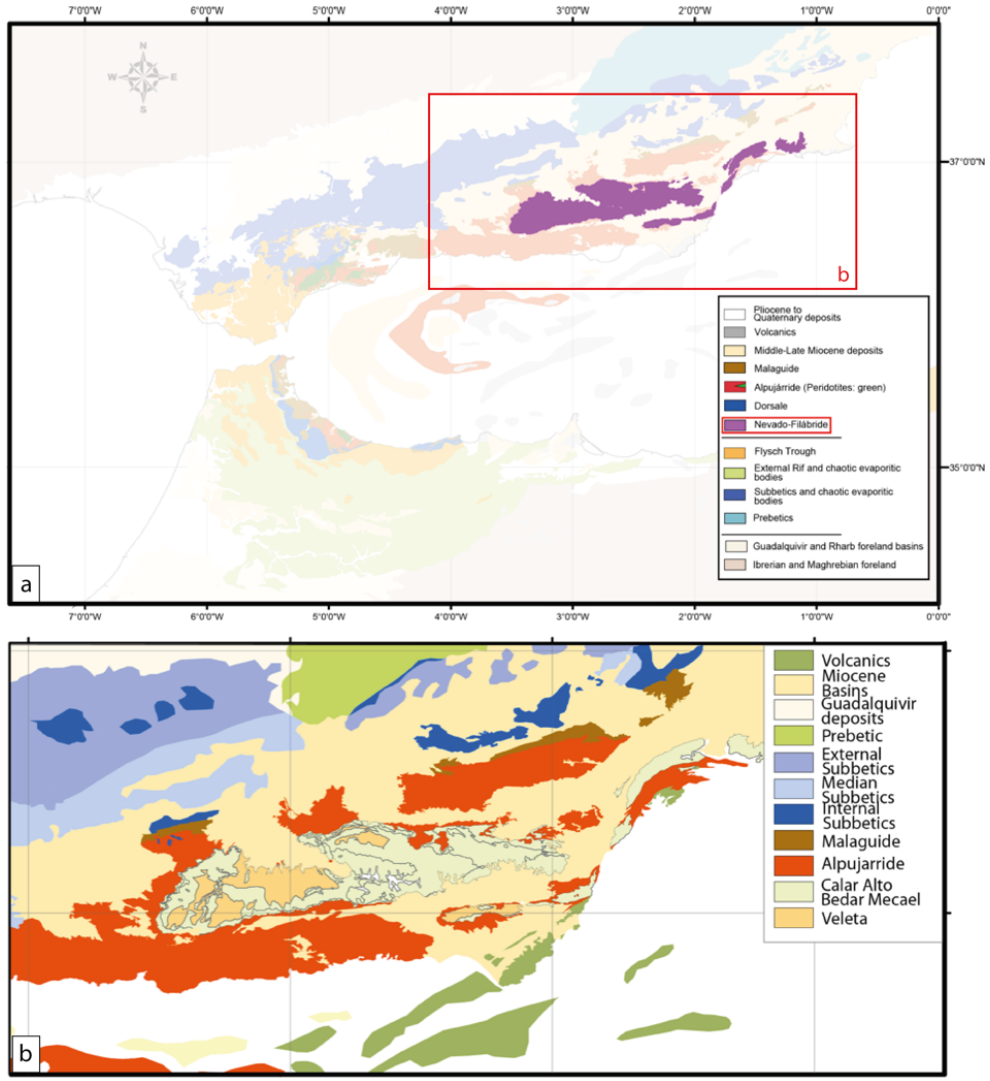

Figure 1.17. Tectonic map of the Alboran region (modified from Frasca et al., 2015). The Nevado-Filábride is without transparency. Schematic representation of the main tectonic groups and Miocene basins cropping out in Central and Eastern Betics (from Behr and Platt, 2012; Crespo-Blanc and Azañon, 2000).

The Nevado-Filábride is usually divided into three tectonic units, which are from base to top the Ragua (Veleta) Unit, the Calar Alto Unit and the Bedar Macael Unit (Martínez-Martínez et al., 2002, Martínez-Martínez et al., 2010; Behr and Platt, 2012) (Fig. 1.17b). Metamorphic terrigenous and evaporitic deposits and Paleocene calc-alkaline basaltic

andesite (K-Ar age; Puga et al., 1996) locally define the boundaries of the units (Puga et al., 2011) (Fig. 1.18a). Most authors consider the contacts between the units composing the Nevado-Filábride as zones of ductile shear, usually described as normal faults or extensional detachments (e.g. Augier et al., 2005c; García-Duenas et al., 1988; Martínez-Martínez et al., 2002; Platt et al., 1984), but also as thrusts (Frizon de Lamotte et al., 1991). The age of the Tertiary metamorphism is strongly debated (Augier et al. 2005a; Monié et al., 1991; Platt et al., 2006): the same is for the exhumation path of the different units (Fig. 1.18b), most probably starting during the Serravallian (~14-12 Ma). The exhumation is constrained by sedimentary basins (Augier et al., 2005c), quickly described in sub-section 1.1.3, and by low-T thermochronology (Clark and Dempster, 2009; Johnson et al., 1997; Vazquez et al., 2011) collected at different altitude and reported on Figure 1.18c.

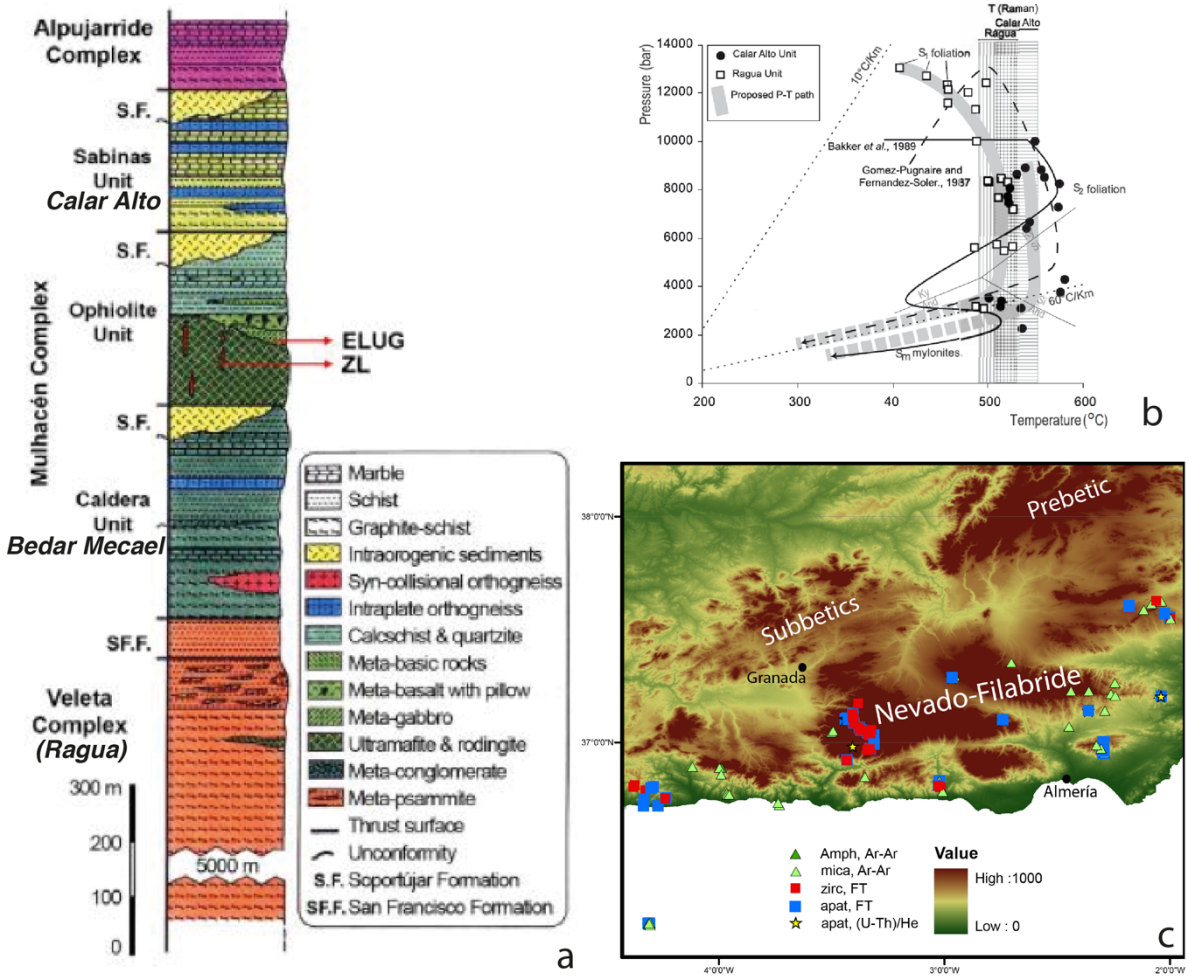

Figure 1.18. (a) Lithostratigraphic log showing the main rock-types that form the different units of Veleta and Mulhacén group. The metagabbros from the Ophiolite Unit indicated by the arrows are dated at 185 ± 3 Ma, an age similar to the one proposed by Tubía et al. (2009) for amphibolitised metagabbros in the Alpujarride of the Western Betics. (b) Different exhumation paths for the Nevado-Filábride units (Augier et al., 2005b). (c) Position of the samples dated in the past for Ar-Ar and LT-thermochronology (Behr and Platt, 2012; Clark and Dempster, 2009; Monié et al., 1991; Johnson et al., 1997; Platt et al., 2005; Vazquez et al., 2011) on a DEM of the central Betics.

Alpujárride-Sebtide

The Alpujárride-Sebtide group is distributed and characterizes the whole Alboran Domain and contains the Ronda Peridotite slivers (Fig. 1.19).

Four main groups of Alpujárride-Sebtide tectonic units can be distinguished in the Betics using structural and metamorphic criteria (Fig. 1.20), following partly Sánchez-Gómez et al. (1999), Tubía et al. (1992), Azañón et al. (1994), and Balanyá et al. (1997).

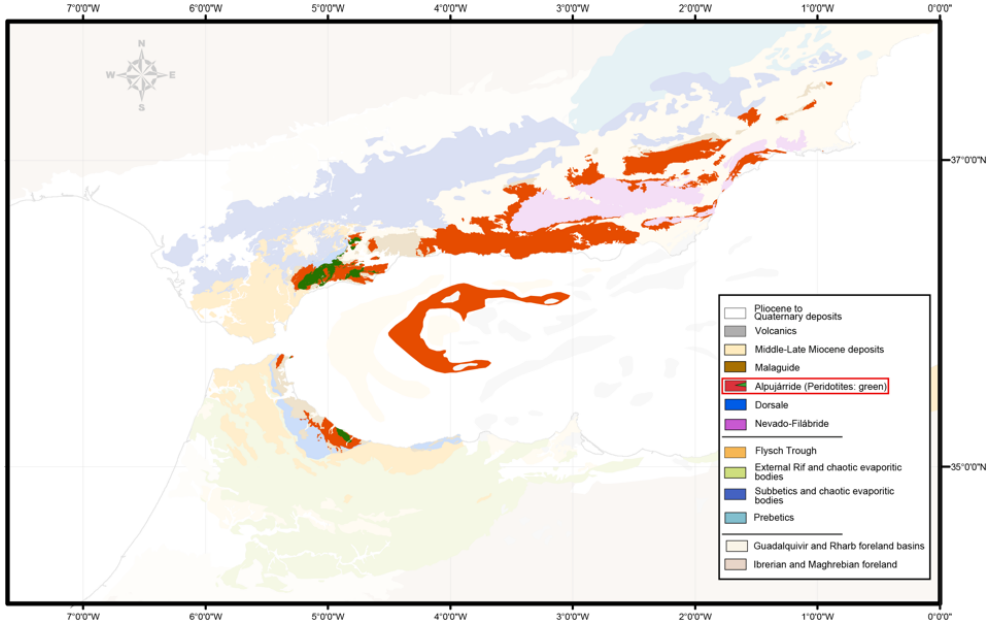

Figure 1.19. Tectonic map of the Alboran region (modified from Frasca et al., 2015). In red the Alpujárride-Sebtide rocks and in green peridotite slivers.

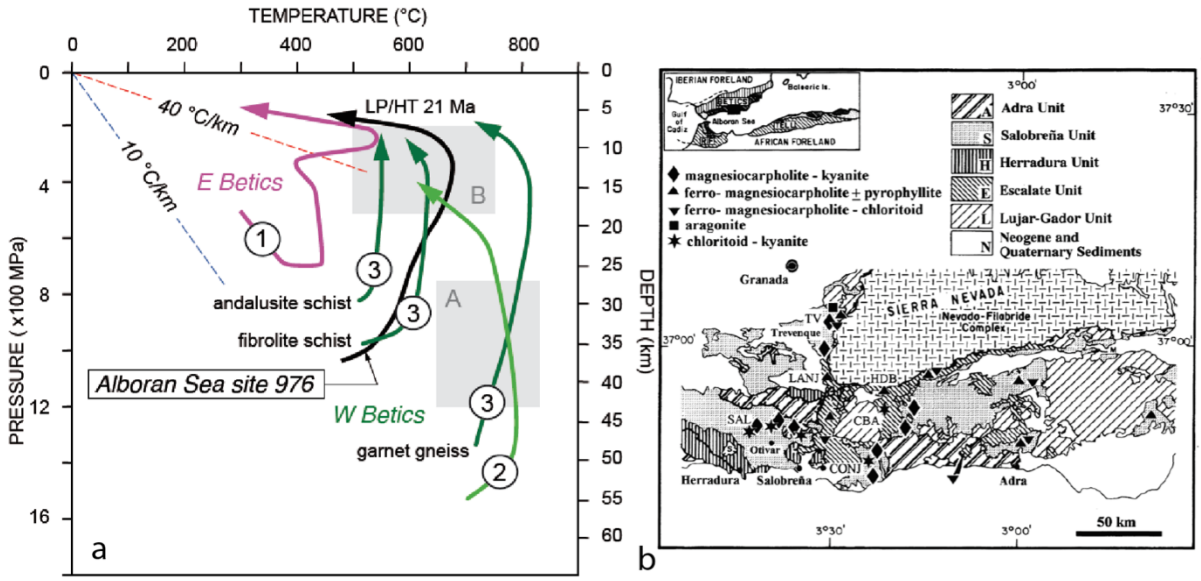

Figure 1.20. (a) P-T paths for rocks of the Alpujarride complex, after (1) Bakker et al. (1989) for the eastern Betics, and after (2) Tubía & Gil Ibarguchi (1991) and (3) Platt et al. (2003b) for the western Betics. PT path for site 976 in the Alboran Sea after Platt et al. (1998). P-T fields for the western Betics after (A) Torres-Roldán (1981) and (B) Westerhof (1977). Depth scale assumes average crustal density of 2800 kg/m3. (b) HP assemblages in the central part of the Betic Cordillera (Azañon and Goffé, 1997).

From bottom to top, summarizing, the groups of units are the following:

1. The Lujar-Gador-Escalate Group crops out only in the central and eastern Betics. The units contain Triassic carbonate rocks and Permian–Triassic metapelites, with low-pressure/low-temperature metamorphism. Only in the Escalate Unit the metapelites record high-pressure, low-temperature evolving to low-pressure, low-temperature metamorphism (Booth-Rea et al., 2005) (Fig. 1.20).
2. The Blanca Group is classicaly represented in the Ojen Unit in the western Betics (Fig. 1.21) and structurally correspond to the Herradura Unit in the Central Betics (Azañon et al., 1998). It is made of Triassic, Permian-Triassic, and Paleozoic protoliths, but in the upper part of the lithologic sequence (Triassic and Permian-Triassic protoliths), high-grade metamorphic conditions can be recognized (Westerhof, 1977; Azañon and Crespo-Blanc, 2000). Amphibolitised eclogites are locally reported (Tubía and Gil Ibarguchi, 1991).

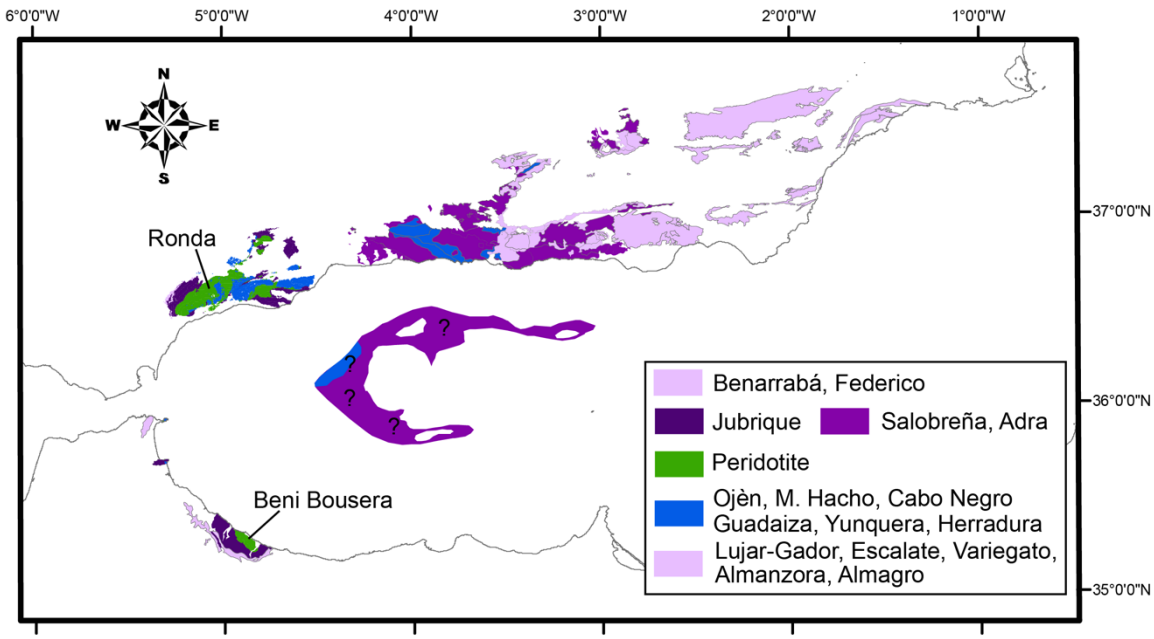

Figure 1.21. Map of the Betic-Rif with a distinction in four different groups. Migmatites and high grade rocks can occur sporadically also in the eastern Betics: the distinction between groups is not only related to the metamorphic grade.

3. The Jubrique Group is typified by the Jubrique Unit in the western Betics (Fig. 1.21). It lies in the same structural position of the Adra and Salobreña Unit in the Central Betics that contains as well a significant volume of migmatites (Azañon and Crespo-Blanc, 2000) (Azañon et al., 1996). The lithologic sequence of this unit is formed by Triassic and Permian-Triassic protoliths in lowgrade metamorphic conditions and from Paleozoic protoliths that reached medium- and high-grade metamorphic conditions in their upper and lower levels respectively (Torres-Roldán, 1979).
   The Ronda peridotite massifs and other minor-scale ultramafic slices discussed in section 1.4 are intercalated between the units of the Jubrique and Blanca Groups (Sánchez-Gómez et al., 1995) (Fig. 1.21).

4. The Federico Group is cropping out mainly in the Rifean side of the Gibraltar arc. It contains several slivers with Permian-Upper Triassic sediments (Chalouan et al., 2008, and ref. therein) (Fig. 1.21). Few relict mineral assemblages preserved suggest a Tertiary high-pressure metamorphic event of debated age (Balanyá et al., 1997).

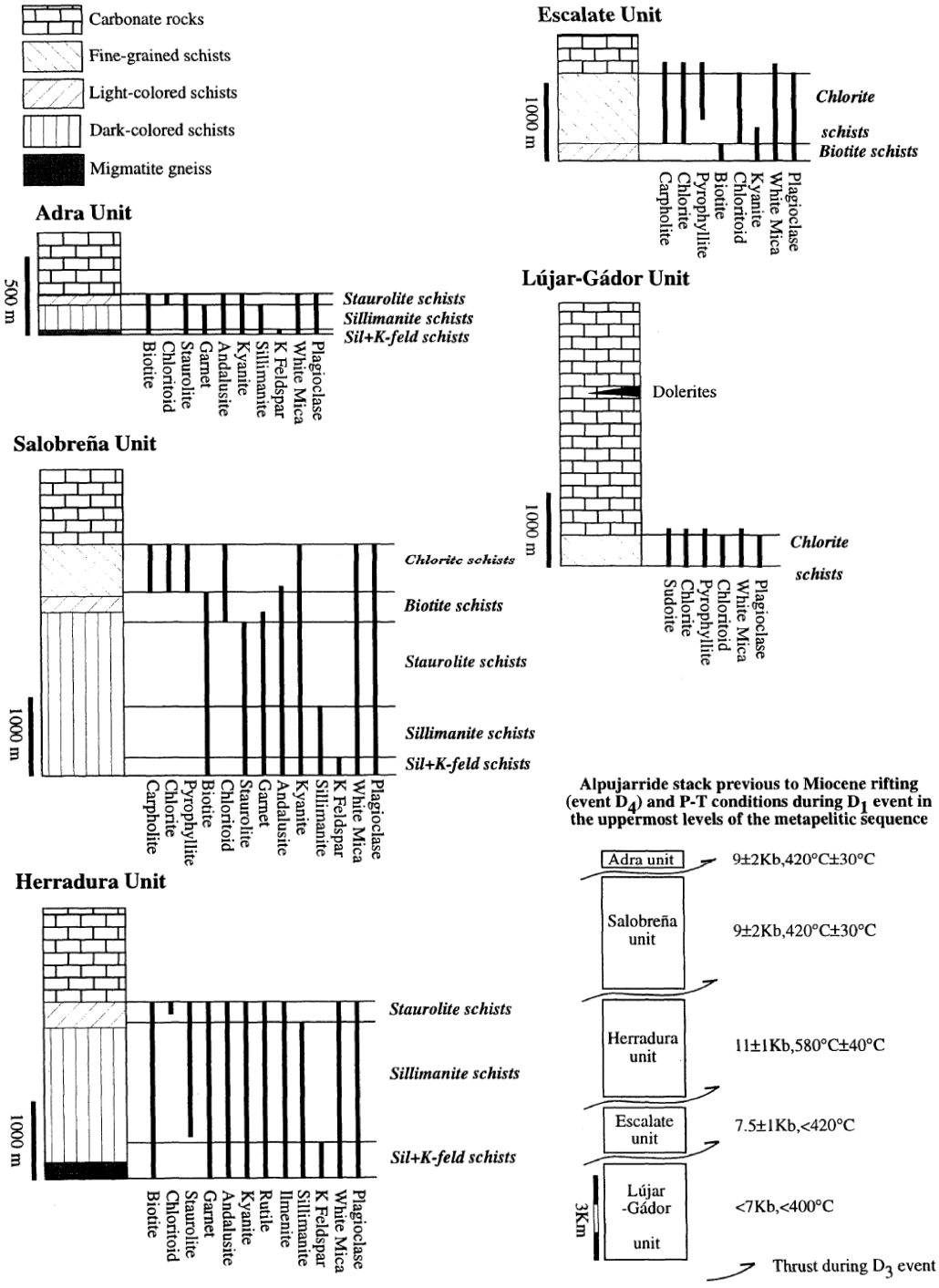

Figure 1.22. Lithological sequence, metamotphic mineral assemblages, and mineral zones of the Alpujarride Units outcropping in Fig. 1.20b (Azañon and Crespo-Blanc, 2000). Inset on the down-right corner shows the idealized column of Alpujarride stack previous to the excision due to the Alboran extension. The P-T conditions regarding the thickening event in the uppermost levels of the metapelitic sequence are indicated for each unit. For details see Azañon and Crespo-Blanc, 2000.

At first sight thus, the metamorphic grade is increasing towards the western Alboran domain (Fig. 1.21) and the tertiary HP metamorphism appear unambiguously only in the units that preserve a Mesozoic cover (Fig. 1.22), while in the deeper crust the HP can be related to the Hercynian orogeny (Gueydan et al., 2015; Zeck and Williams, 2002).

Malaguide-Ghomaride

The Malaguide-Ghomaride forms the uppermost units of the Alboran Domain and it is situated on top of the Alpujarride-Sebtide, systematically associated with it (Fig. 1.23).

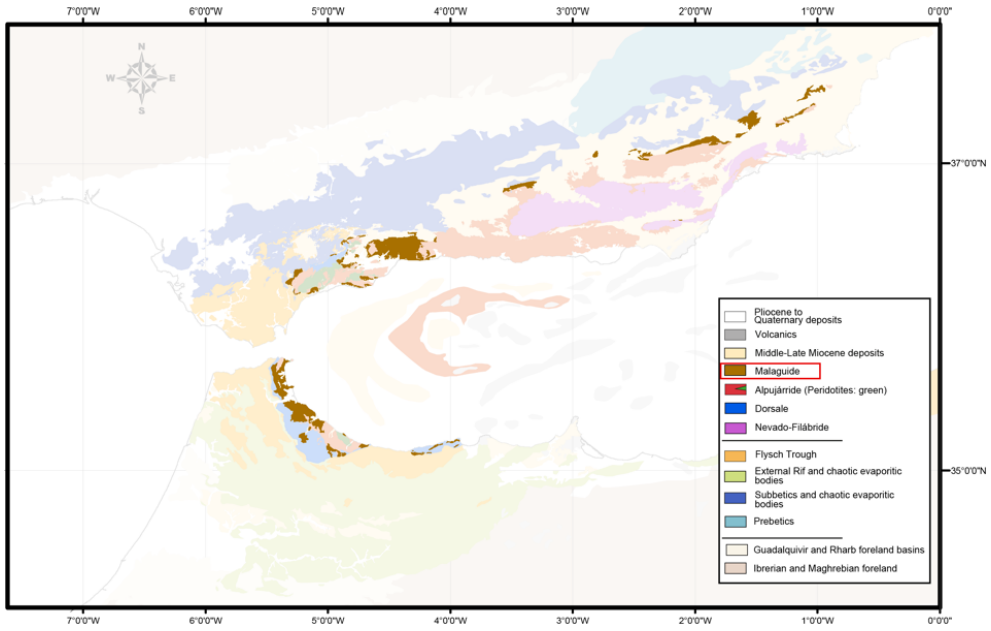

Figure 1.23. Tectonic map of the Alboran region (modified from Frasca et al., 2015). In beige the Malaguide-Ghomaride rocks.

The Malaguide (Ghomaride in the Rif; Durand-Delga, 1963, 1980) is essentially present in the western part of the Betic Cordillera but it also appears in the central and oriental parts of the Alboran Domain along the border between Alboran Domain and External Zone (Fig. 1.23). The contact between the Malaguide and Alpujarride units are described as detachments or low-angle normal faults (García-Dueñas et al., 1992; Lonergan and Platt, 1995; Balanyá et al., 1997; Booth-Rea et al., 2003), although if differences in sedimentary facies in the carbonate covers (Egeler and Simon, 1969; Sanz de Galdeano et al., 2001b) suggest an original thrust relationships with the Alpujarride, then obliterated by extension.

The Malaguide is composed mainly of Paleozoic rocks with Hercynian low-grade metamorphism (Chalouan and Michard, 1990). However, close to the Alpujarride, the Alpine metamorphic grade increases (Negro et al., 2006) with occurrence of andalusite (Cuevas et

al., 2001; Platzman et al., 2004) and reset of some Ar-Ar and FT ages at 25 Ma (Platt et al., 2003a), partly suggesting a common evolution for Malaguide and Alpujarride during the regional Alpine metamorphism (Torres-Roldán, 1979). The non-metamorphic cover is Mesozoic to Paleogene (Chalouan et al., 2008; Martín-Algarra et al., 2009; Perri et al., 2013). The metamorphic history and also the cooling history appear different from the Alpujarride, as it can be observed in Figure 1.24, where the Paleozoic FT ages reported are always from the Malaguide rocks.

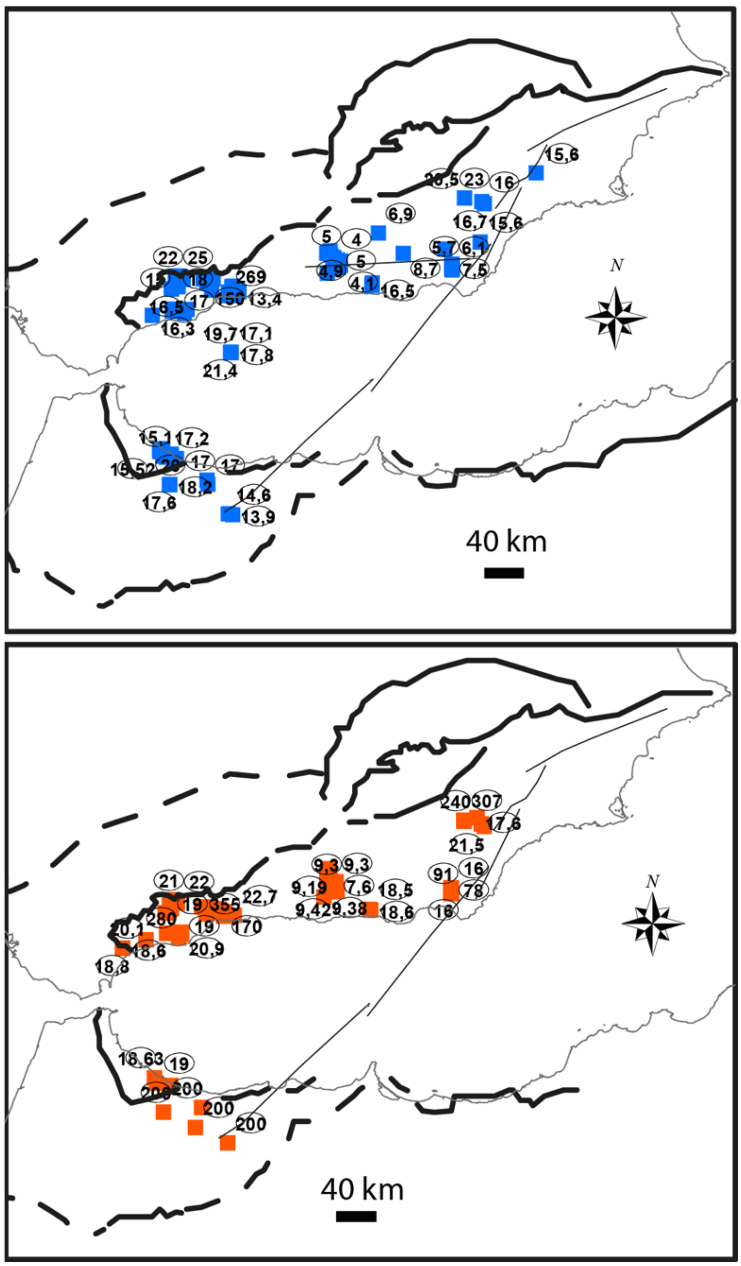

Figure 1.24. Apatite Fission track (from Esteban et al., 2004; Esteban et al., 2005; Esteban et al., 2004; Platt et al., 2003; Platt et al., 2005; Johnson, 1997; Behr and Platt, 2012; Hurford et al., 1999; Sosson et al., 1998; Clark and Dempster, 2009; Perri et al., 2013; Azdimousa et al., 2014; Romagny et al., 2014) and Zircon Fission track in red (from Behr and Platt, 2012; Esteban et al., 2004; Esteban et al., 2005; Platt et al., 2003; Platt et al., 2005; Johnson et al., 1997)

1.1.3 Tertiary basin

In the Betic-Rif Cordillera is possible to identify four different groups of Tertiary basins related to four different tectonic contexts. In this subsection we go quickly through them with a particular accent on the structures considered the cause of their deposition and following a chronological order that reflects the progression of the tectonic events. However, it must be stressed out that the four groups are interrelated because the sediments in them are in most case laterally and temporally continuous. The identification and the description of the Tertiary basins (Fig. 1.25) is important because they mark the timing of the formation of the arc and can give insights for the comprehension of the mantle exhumation and emplacement processes.

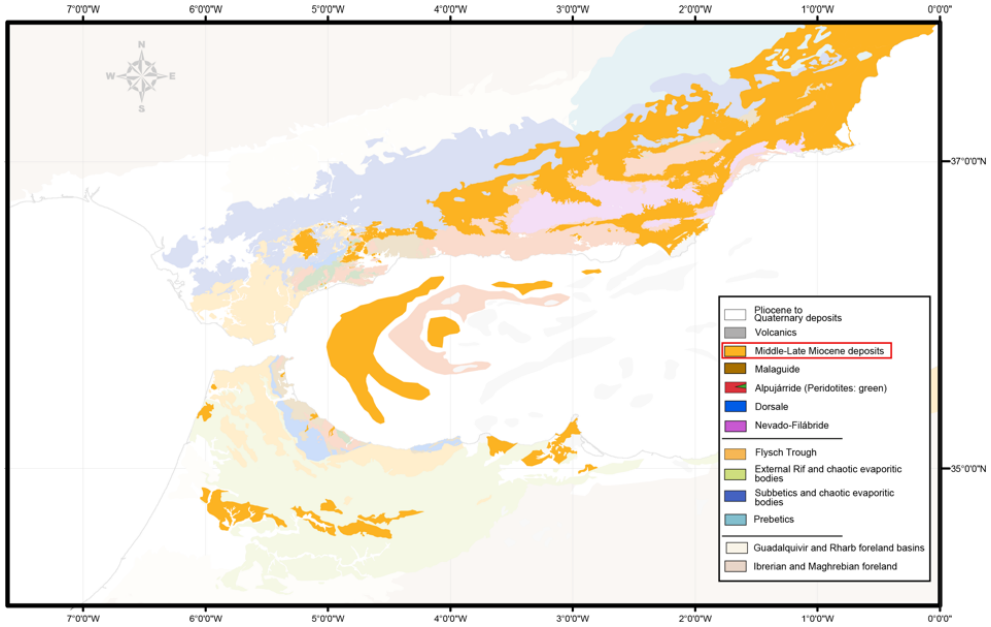

Figure 1.25. Tectonic map of the Alboran region (modified from Frasca et al., 2015). In orange without transparency the Miocene sediments, Flysch Trough excluded.

Transgressive cover of the Alboran Domain

In the first group the sediments are Oligocene to Lower Miocene in age, rest unconformably on rocks of the Alboran Domain and include clasts derived from them (Serrano et al., 2007). The base of the deposits is younger to the west, where the great part of these deposits crop out, suggesting a westward evolution of the system, and is systematically deposited on Malaguide rocks (Figs. 1.26 and 1.27).

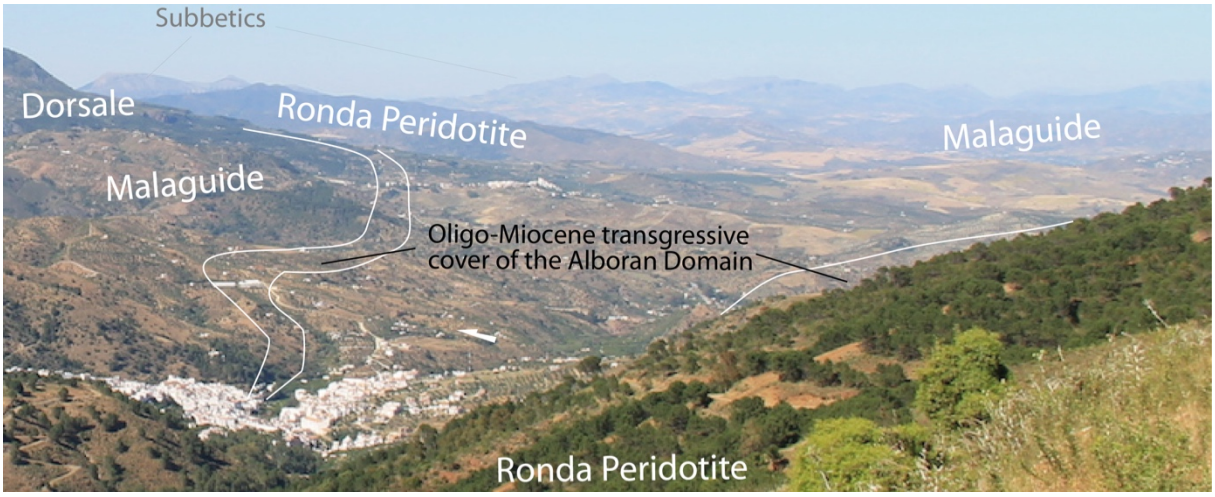

Figure 1.26. Landscape view of the Oligo-Miocene sediments lying on top of the Malaguide rocks in Tolox region (Photograph by G. Frasca).

This transgressive group is usually divided in two formations: Ciudad-Granada at the base and La Viñuela at the top (Fig. 1.27) (Serrano et al., 2007). The stratigraphic succession is characterized by a deepening trend upward with a change in sedimentation-type at around 20 Ma, corresponding to the temporal boundary between the two formations (Serrano et al., 2007). In the La Viñuela formation the deposition involves metamorphic rocks of the Alboran Domain with in few areas also peridotites and marbles (Aguado et al., 1990). The uppermost part of the Alboran terrigenous cover is composed of Lower to Mid-Miocene chaotic deposits with blocks of Alboran Domain (Malaguide and Dorsale; Martín-Algarra, 1987) and of Flysch Trough (Suades and Crespo-Blanc, 2013) (Fig. 1.26). These Oligo-Lower Miocene sediments do not rework Nevado-Filábride rocks that indeed has been exhumed later (Johnson, 1997). Moreover, the rapid lateral change in sedimentary facies suggests a deposition in a strike-slip dominated environment, as shown in Figure 1.27.

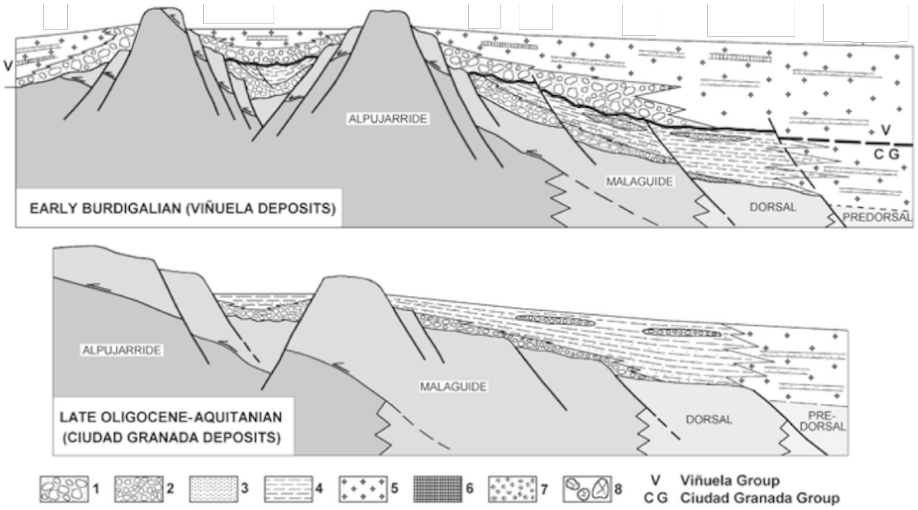

Figure 1.27. Tectono-sedimentary framework of the transgressive formations of the Oligocene-Lower Miocene sediments on top of the Alboran Domain. 1. Breccias; 2. Conglomerates; 3. Sandstones; 4. Reddish pelites; 5.Lightcoloured siliceous marls; 6. Silexites; 7. Dusty brown pelites with a nodular appearance; 8. Large blocks. Representative sequences presented in Serrano et al. (2007).

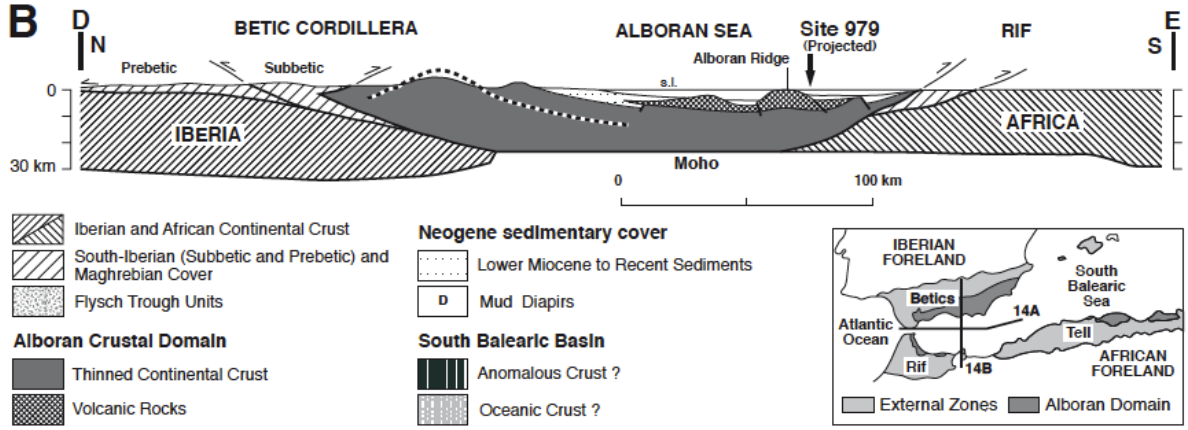

Figure 1.28. Schematic true-scale section to illustrate the north-south crustal structure of the Alboran Basin (from Comas et al., 1999) based on a synthesis of structural data from Spain and Morocco and *Conrad* seismic lines and on a density model obtained by comparing observed and calculated Bouguer anomaly data (Watts et al., 1993). Note that the crustal section shows the thinning of the continental crust beneath the Alboran Basin. The intracrustal reflectors (hatched white lines in the Alboran Domain), shown by the MCS *Conrad* profiles, are interpreted as extensional detachment faults or the top of the reflective lower crust.

West Alboran Basin

The Alboran Basin lies below the Alboran Sea (Fig. 1.28) and is divided in several subbasins (Watts et al., 1993). We focus on the westernmost, in red in Figure 1.29, that has been deposited most probably in continuity with the sediments described above and now lie in a trough that is deep almost 9 km (Comas et al., 1992; Comas et al., 1999; Iribarren et al., 2009) (Fig. 1.29). The western alboran basin is interpreted often as the back-arc (Suades et al., 2013): indeed the depocenters in the Alboran Sea and the faults that bound them appear to follow the curvature of the Gibraltar arc. In fact, an alternative interpretation is that the west Alboran basin is part of the forearc of the Alboran Subduction system (Booth-Rea et al., 2007).

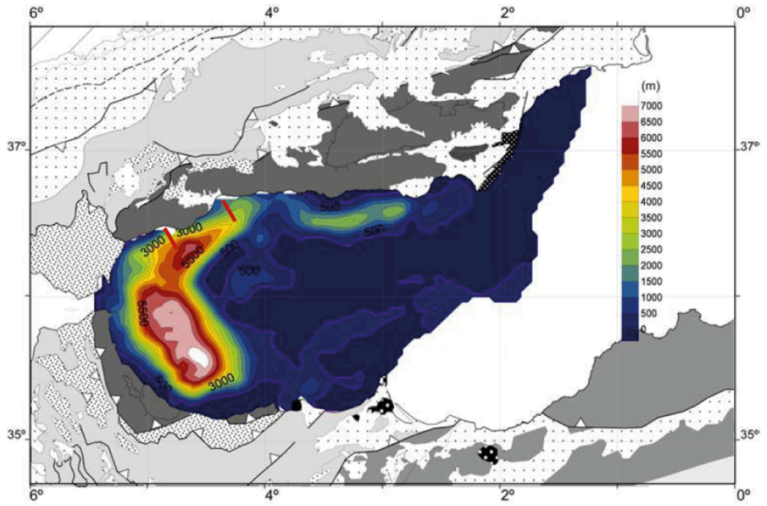

Figure 1.29. Isopachs for the Lower Miocene sediments in the Alboran Basin (from Iribarren et al., 2009). The two red segments indicate the locations of the seismic profiles in Figure 1.30.

The basin is an half-graben which shows a very complete Miocene to Holocene sedimentary sequence with strong differences in the structural style between the two flanks of the basin and along strike (Suades et al., 2013). The initial synrift fill is of Burdigalian or possibly older age (Comas et al., 1999). Tectonic subsidence analyses (Watts et al., 1993; Docherty and Banda, 1995) estimate that rapid extension continued during the early and middle Miocene. Two stages of extensional faulting are usually described: an earlier Burdigalian-Langhian (~ 17-15 Ma) and a Serravallian-early Tortonian (~ 14-9 Ma) stage (Comas et al., 1999; Suades et al., 2013).

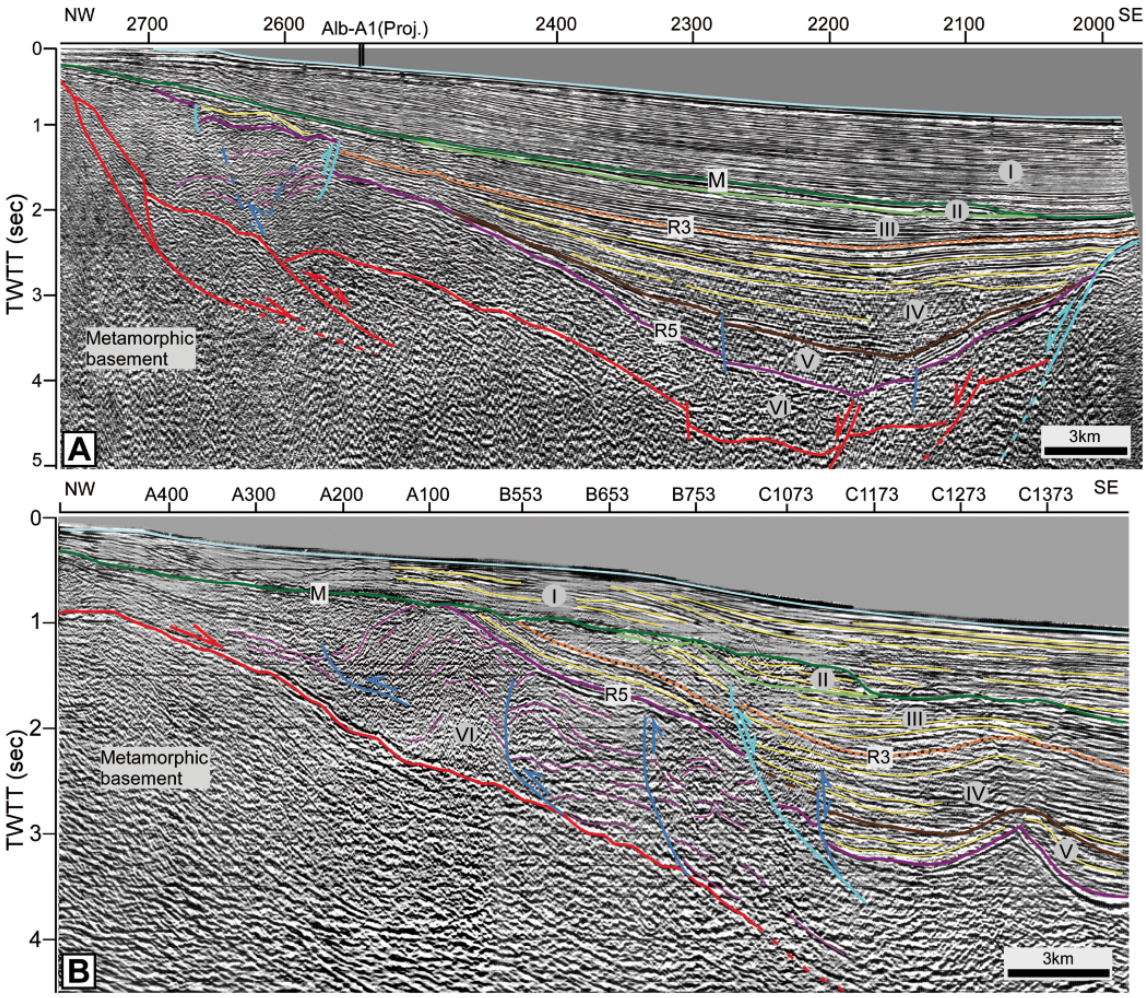

Figure 1.30. Interpreted seismic profiles of the Malaga Basin (location in Figure 1.29) (from Suades et al., 2013). Units are according to Comas et al. (1999). Reflectors are drawn in purple for unit VI and in yellow for the rest of the sedimentary sequence. A) Line EAS-098 showing the seismic architecture of the north-eastern part of the basin. B) Line ALB-015 showing the flank North at south-western sector.

Deep structures in the basement imaged from deep-seismic reflection profiles in the northern half of the Alboran Basin have been interpreted as extensional shear zones, presumably associated with major extensional detachments in the Betic Zone and most probably active already during the first extensional stage (Watts et al., 1993; Comas et al., 1999) (Fig. 1.28). The main extensional episode is the second one, which controls the sedimentary infill of the Malaga Basin occurred from Langhian to Lower Tortonian (units V

and IV in Figs. 1.30 and 1.31). During this time interval, in the eastern part of the basin, most of the extension was accommodated by both the low-angle detachment on top of the basement of the northern flank and its counter-fault that bounds the Site 976 (Suades et al., 2013) (Fig. 31). In the western part of Malaga Basin, the northwestern flank shows extensional structures (now partially inverted) that affected both the basement and the whole Miocene infill (Fig. 1.30A). The extensional system observed has been often related with the extension observed onshore in the Western Betics (García-Dueñas et al., 1992).

While the west Alboran Basin has up to 8 km of Neogene sediment fill (Torné et al. 2000), much of the central and eastern Alboran Sea is underlain by Neogene volcanics (Booth-Rea et al. 2007) (Figs. 1.27). In the westermost part the basement has been drilled only in site 976 sampling rocks attributed to the Blanca group of the Alpujarride. Another peculiarity of the West Alboran Basin tectonic inversion and compressional deformation within the sedimentary infill ceased by the end of the Messinian (Suades et al., 2013). This timing is consistent with the observations in the Late Miocene sediments obtained 20 kilometers to the north onshore, as reported in Chapter 2.

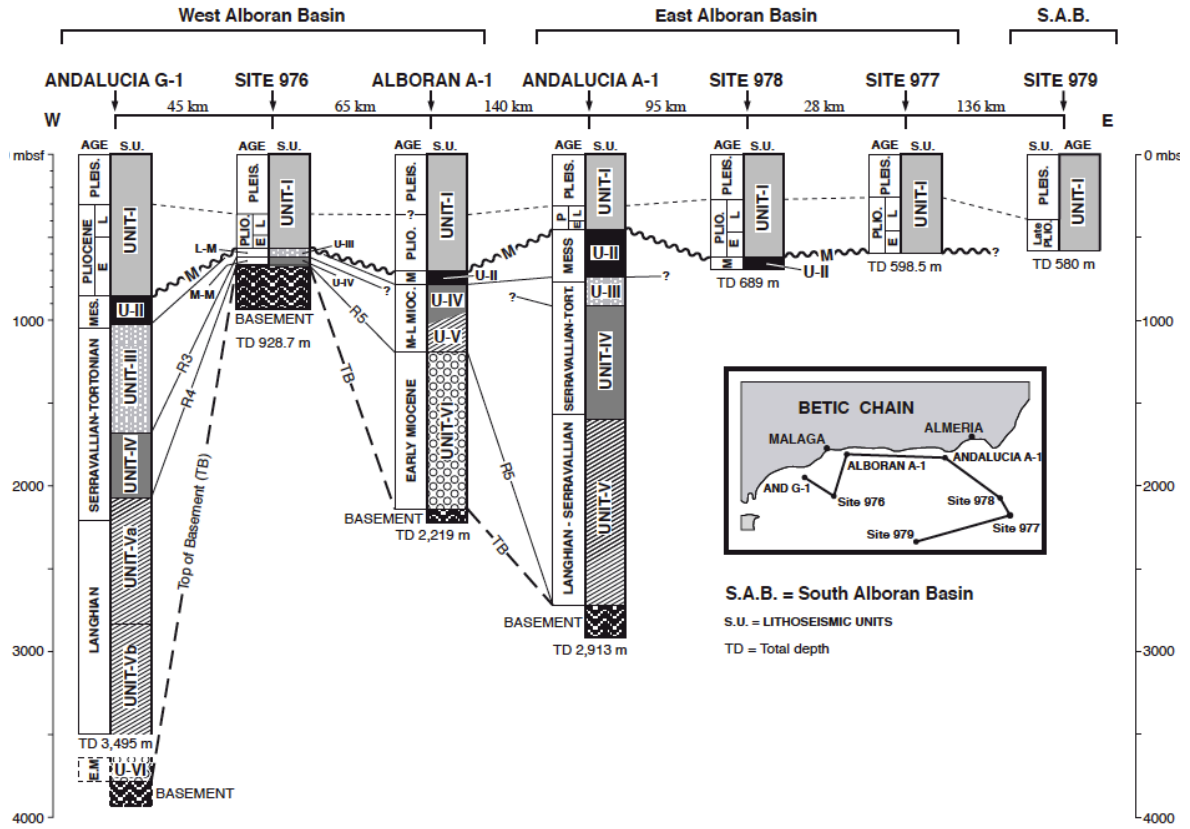

Figure 1.31. Correlation between sedimentary sequences sampled at Sites 976, 977, 978, and 979 and in commercial wells on the Iberian shelf (from Comas et al., 1999). The diagram shows ages, seismic units, major regional reflectors, and drilled metamorphic basement. The correlations are based on MCS analysis, logging, and stratigraphic data. Seismic units and R-reflectors according to Comas et al. (1992). M = Messinian unconformity. The inset map shows locations of commercial boreholes, connecting lines between holes refer to relative positions and distances in kilometers shown at the top of this figure.

Intramontane basins

The emergent areas of the Alboran Domain have experienced up to 1.200 m of regional uplift starting from the end of the Tortonian (Braga et al. 2003; Romagny et al., 2014). This fact permits to observe at the surface in the central and eastern Betics Middle and Late Miocene sediments, partly similar to the ones deposited on the Alboran Domain offshore (compare the logs in 1.31 and 1.32), that crop out scarcely in the westernmost part of the Betic Cordillera.

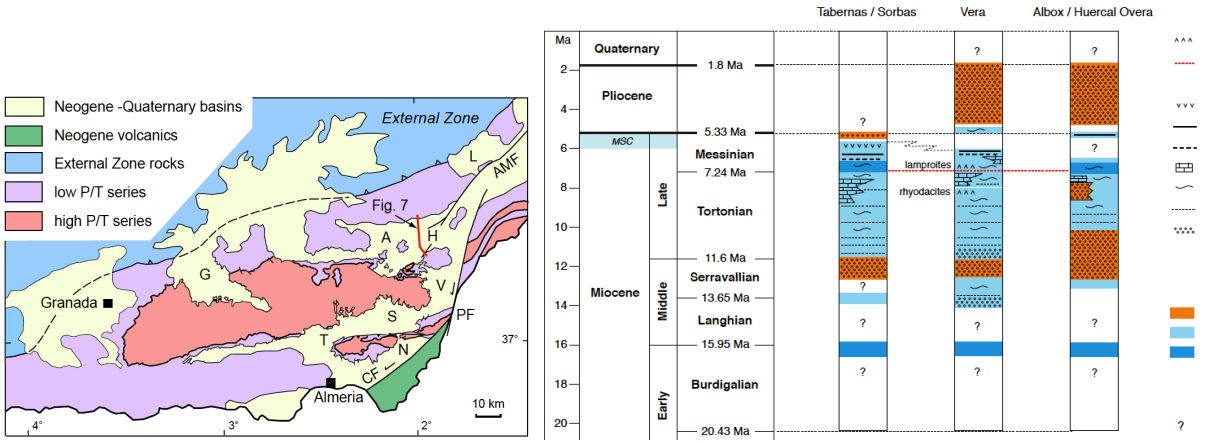

Figure 1.32. MSC = Messinian Salinity Crisis. Note that the stratigraphy is represented on a time scale not a length scale to emphasize correlations between coeval deposits as well as the hiatuses in the different basins. Symbols on the right lists from top to bottom are: volcanoclastic, ashes, evaporites, sapropel, diatomite, reef, marls, turbidites, conglomerates layers. Continental deposit are in orange, marine deposits in pale blue, deep marine deposits dark blue. Question marks represent hiatuses (from Vissers, 2012).

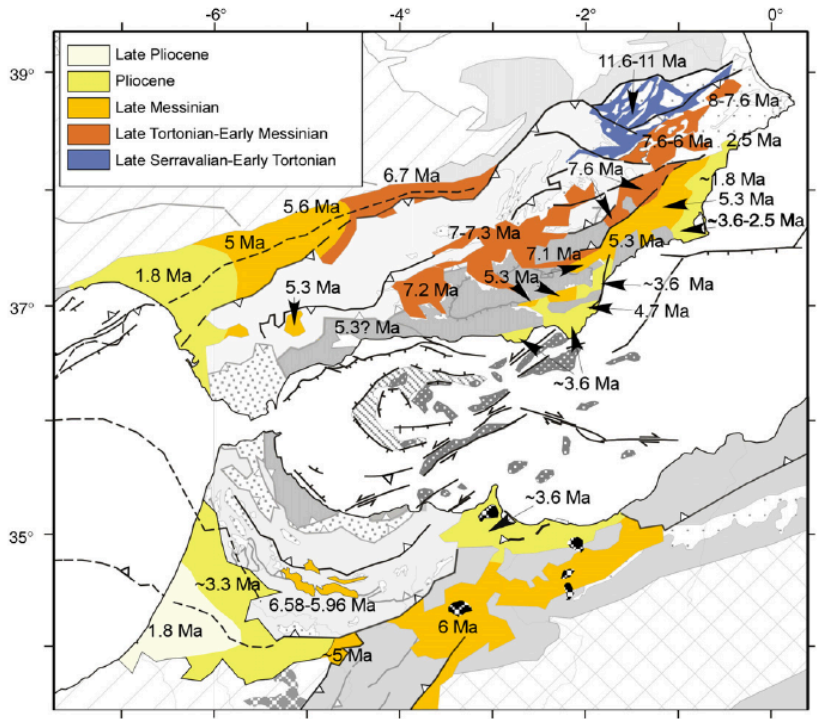

Figure 1.33. Map of the Betic–Gibraltar–Rif orogenic system showing the age of the marine to non-marine transition for the different sedimentary basins onshore (from Iribarren et al., 2009).

Numerous basins in the eastern and central Betics formed indeed in the middle to late Miocene. The basins have a coarse synrift fill of Serravallian to early Tortonian age, evolving from continental to marine, and a postrift fill of late Tortonian and younger age, which evolves from marine to non marine with different timing from W to E (Fig. 1.33) as a result of the Messinian and younger uplift of the Betics (Iribarren et al., 2009; Meijninger and Vissers, 2006).

Most of the basins formed in response to southwest-directed extension, with conjugate sets of northwest-trending normal faults (Meijninger and Vissers, 2006). Some of them are continuous on top of the Subbetics. This is the case of the Ronda Basin. The Ronda basin is as well associated with prominent northwest- and north-trending normal faults (Kirker and Platt, 1998; Ruiz-Constán et al., 2009) that control also the distribution of the tortonian-messinian sediments on the Alboran Domain (Lopez-Garrido and Sanz de Galdeano, 1999). The Ronda basin is an unequivocal sign of extension in the Western Betics and gives clear timing for the structures. In Figure 1.34a the sediments are flat-lying on top of Jurassic limestone, verticalized along a strike-slip fault (Martín-Algarra et al. 1987), and in Figure 1.34b are tilted at the NW border of the Ronda basin (Jiménez-Bonilla et al., 2011).

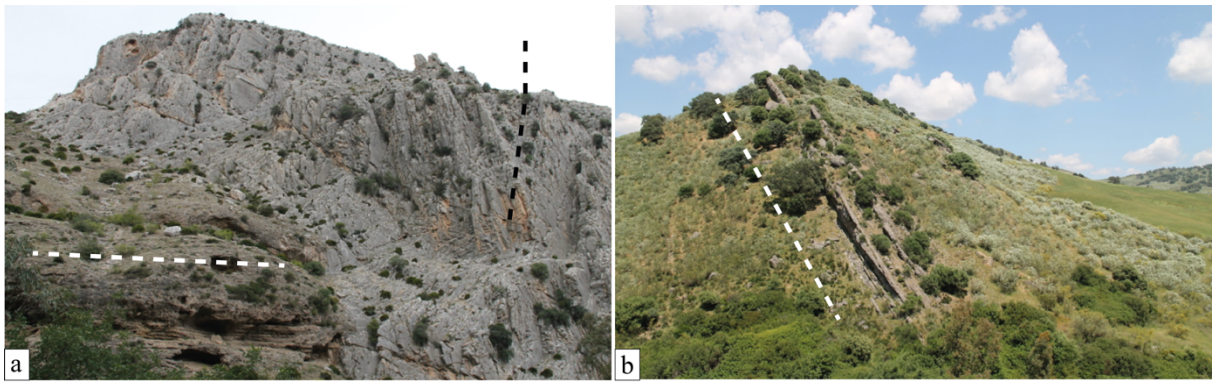

Figure 1.34. Intramontane Tortonian basin in the Western Betics along the IEZB and in the westernmost part of the Ronda Basin. (a) El Chorro area, (b) 20 km NNW of Ronda. The white dashed line highlights the general trend of the late Miocene sediments. The black line underlines the verticalized layering in the limestones (Photographs by G. Frasca).

The tertiary basin cropping out in the eastern betics are related to a prominent set of N to NE trending sinistral strike-slip faults (de Larouzière et al., 1988; Montenat and Ott d'Estevou, 1999; Rutter et al., 2012). The basins, however, are not, systematically located on the releasing bends of these faults, and the activity on the faults is essentially late Miocene to Quaternary, i.e., after most of the basins had ceased to be active depocenters. This fact suggests the areal extent of the basins and the amount of extension suggested by their internal structure appear to require significant crustal thinning during their formation (Meijninger and Vissers, 2006) and origin is probably related to extensional exhumation of the NFC and not to strike-slip faults interpreted in term of N-S Nubia-Iberia convergence (Vissers, 2012).

Several of these basins are physically continuous not only with the Subbetics as in the case of the Ronda basin, but also with the foreland basins. This is the case of the Granada basin that may have reactivated an early Miocene basin at the same location, and it is

undergoing now active normal faulting (Martínez-Martínez et al. 2006) and, hence, have a multiple origin (Platt et al., 2013).

Guadalquivir foreland basin

The large flexural foreland basins (Guadalquivir and Rharb) results from the emplacement of the external thrust wedge of the Alboran Domain onto the Iberian and African continental margins (Fig. 1.35).

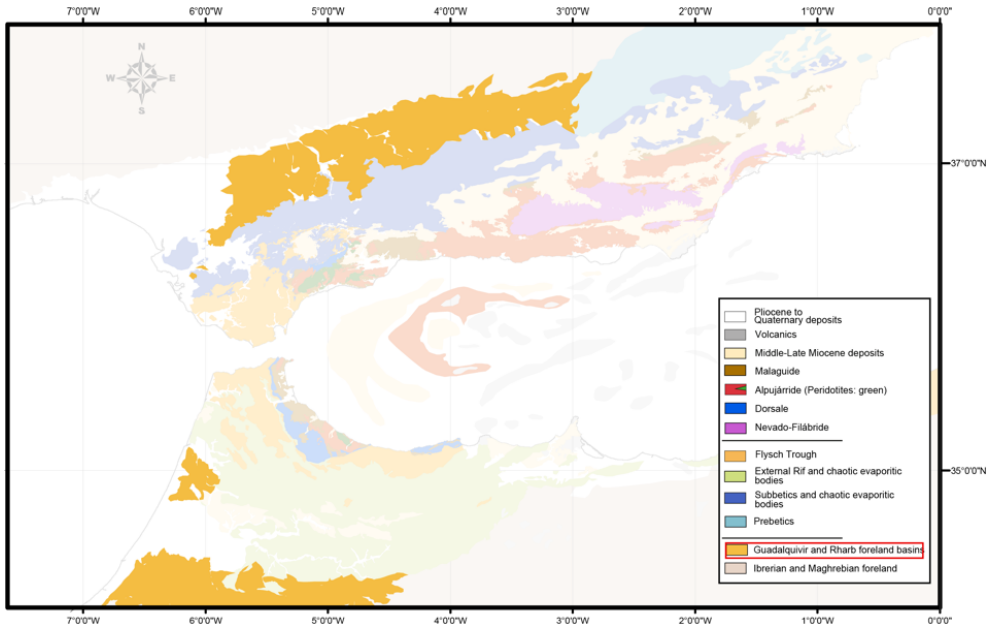

Figure 1.35. Tectonic map of the Alboran region (modified from Frasca et al., 2015). In orange the sediments of the Guadalquivir and Rharb basin

The Miocene to Quaternary sediments forming the basins delineate the northern and southern terminations of the Betic-Rif arc. The transition from the external thrust belt to the foreland sediments is an area of re-sedimented Mesozoic material embedded in evaporites and clays called "Guadalquivir allochthons" in the Betics (Platt et al., 2013; Ruiz-Constán et al. 2012a) (see Fig. 1.7b). Thrusting started during the early Miocene (Berástegui et al., 1998; Fernández et al., 1998; Flinch, 1993; García-Castellanos et al., 2002). Shortening continued, apparently continuously, until the end of the Miocene, migrating northwest toward the present thrust front in the Guadalquivir Basin (Berástegui et al. 1998; Ruiz-Constán et al., 2012b).

The first basins along the northern border of the Betic Cordillera emerge from a marine environment at late Serravallian–early Tortonian times (starting at about 11 Ma) on the Prebetic, located in the north-easternmost part. The distribution in time of the isopachs show a shifting towards the west, while in the Rharb basin a change towards the south and the south-west is observed. A great part of sediments have been deposited during the late Miocene.

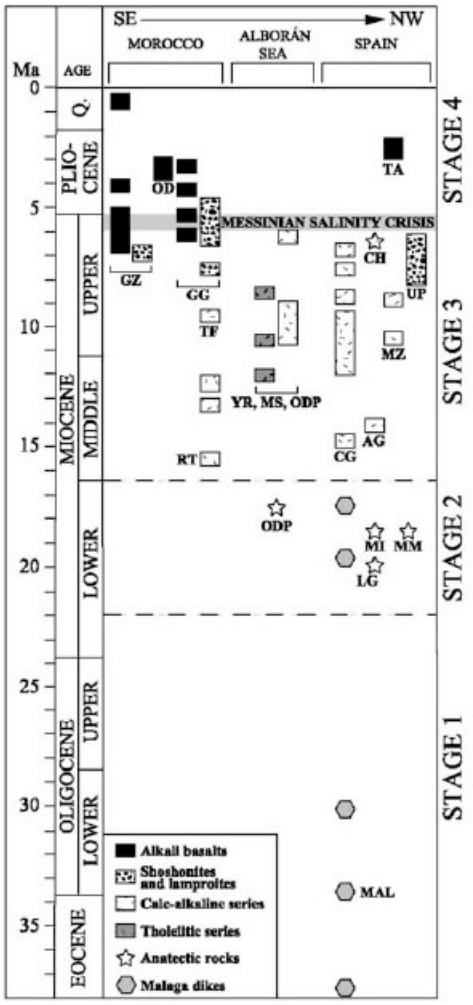

Figure 1.36. Chronologic table of the igneous activity in the Alboran region summarizing the 40Ar/39Ar age data (from Duggen et al., 2004). The magmatic evolution of the Alboran region can be divided into four stages: (1) Eocene to Lower Miocene tholeiitic to calcalkaline Malaga dikes, (2) Lower Miocene crustal anatexis related to a large-scale thermal event, (3) Middle to Upper Miocene tholeiitic and calc-alkaline magmatism, and (4) Upper Miocene to Lower Pliocene shoshonitic and lamproitic magmatism and Lower Miocene to Quaternary alkali basalt volcanism. Transition from subduction-related to intraplate-type volcanism overlaps with the Messinian Salinity Crisis. Abbreviations: GZ, Guilliz; OD, Oujda; GG, Gourougou; TF, Trois Furches; RT, Ras Tarf; ODP, Ocean Drilling Program Holes 977 and 978; YR, Yusuf Ridge; MS, Mansour Seamount; MAL, Malaga dikes; CG, Cabo de Gata; AG, Aguilas; MI, Mijas; LG, leucogranites; MM, Mar Menor; MZ, Mazarron; CH, Cerro Hoyazo; UP, ultrapotassic rocks (lamproites); TA, Tallante. Q, Quaternary.

1.1.4 Volcanism and magmatism

The volcanism in the Betic-Rif is generally considered as subduction related (Duggen et al., 2004), although the predominant intermediate to silicic character of the volcanics onshore suggests assimilation of continental crust (Turner et al. 1999) and possibly removal of the lithospheric mantle (Platt et al., 2013). Four main stages can be envisaged in the chemical evolution of the magmatism in the Betic Rif (see in the chronologic table of Duggen et al., 2004, in Figure 1.37), with the main activity between 18 and 0.45 Ma ago (Duggen et al. 2004).

The oldest volcanic rocks (~18 - 8 Ma) are *calc-alkaline* and are present mainly in the center of the Alboran Basin while in Spain they crop out only close to Cabo de Gata (Lonergan and White, 1997) (red color and red arrow in Fig. 1.38) The tufitic volcanoclastic products deposited at the end of the Burdigalian in the Internal-Median Subbetics (Soria, 1994) testify the proximity of the Iberia margin to the volcanic centers in the Alboran Domain at that time and indicate that the slab was already below the present-day Alboran sea at 18 Ma.

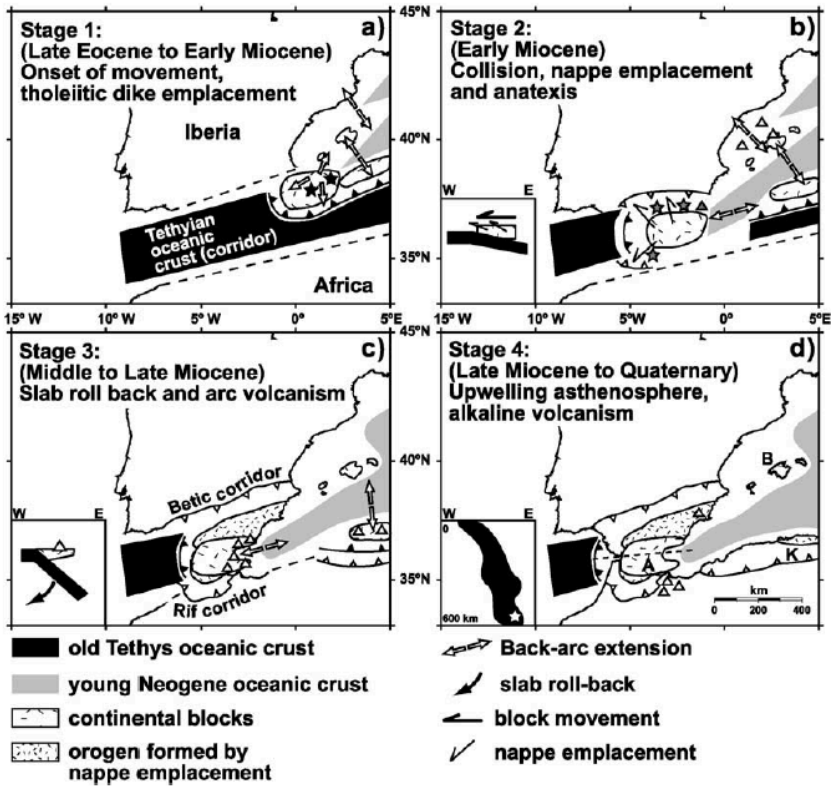

Figure 1.37. Tectonic model for the evolution of the Alboran system (from Duggen et al., 2004).

High-K volcanics are the second broad suite of volcanics that occurred in the region. These rocks have a wide variety of compositions, from shoshonitic to lamproitic, and were erupted between ~9-4Ma (Lonergan and White, 1997) (Fig. 1.37). Perez-Valera et al. (2013) use the Messinian lamproites in the eastern Betic, coeval to strike-slip movements, to suggest tearing at upper mantle level in the eastern Betics.

The most recent suite of volcanics are the *alkali-basalts* that erupted from ~5Ma to ~1Ma (Lonergan and White, 1997). Alkali-basalt are reported also towards middle atlas and the tell region by Duggen et al., 2005. This type of volcanism tends to occur in the more external parts of Rif and Betics and is often associated with extension (Lonergan and White, 1997) (Fig. 1.38).

Based on the geodynamic model of Duggen et al. (2004) (Fig. 1.37), magmatism during these stages results from (1) back-arc extension in a subduction setting, (2) emplacement of the Alboran domain onto the Iberian and African continental margins, (3) release of hydrous fluids and sediment melts from subducted Tethys oceanic lithosphere into

the mantle wedge beneath the Alboran Basin, and (4) delamination of subcontinental lithosphere associated with upwelling of asthenosphere beneath southern Iberia and mainly northwestern Africa. Shift in geochemistry from calc-alkaline to potassic before the end of the magmatism, is a peculiar feature of subduction-environment and observed also in the Aeolian-Calabrian magmatic arc (Duggen et al., 2003), although if in the meditrranean case, small anomalies with respect to the classical "Pacific-style" arc magmatism are observed.

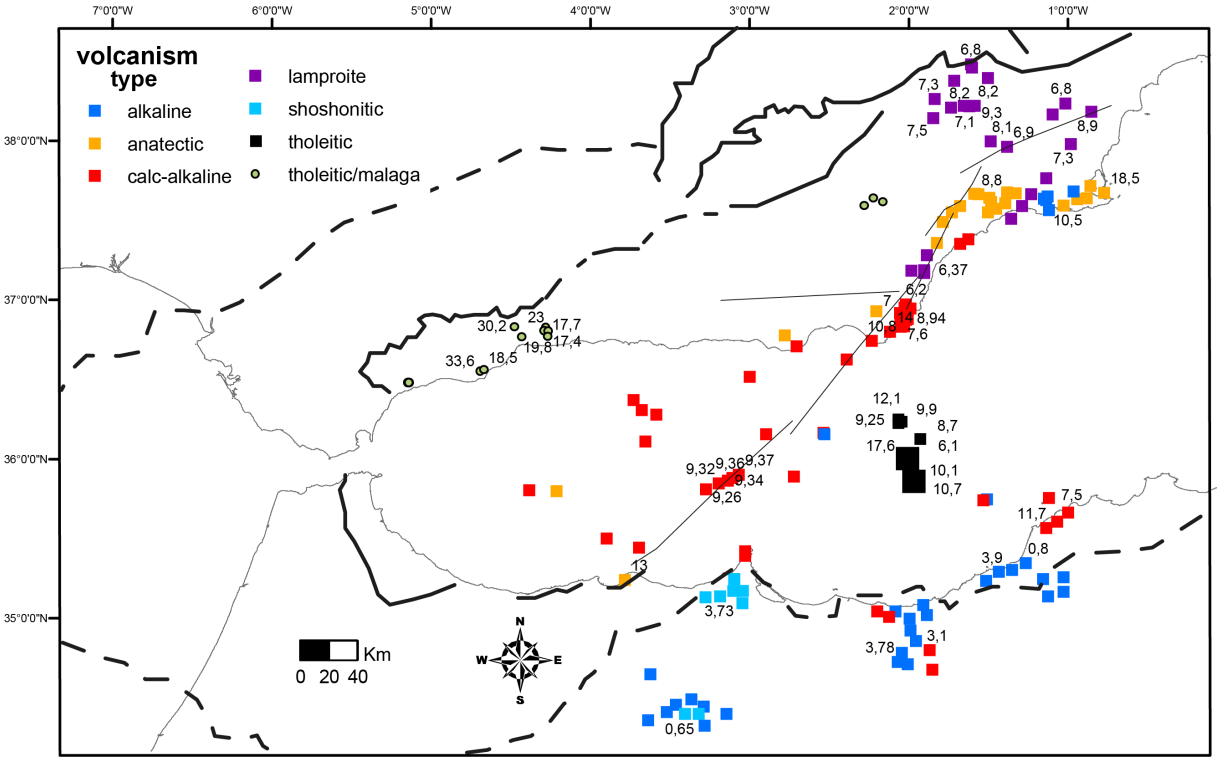

Figure 1.38. In the map is reported the distribution of the volcanism in the Alboran region. The anatectic products in the westernmost Alboran Domain are not represented in the Figure and have a different origin of the rhyolitic products in the eastern Betics (Duggen et al., 2004). Data compiled mainly from Chalouan et al., 2008; Duggen et al., 2004; Perez-Valera et al., 2013; Turner et al., 1999). The compilation is extracted from our GIS database (151 data) (see section 1.6, Methods).

To complicate this scenario, the existence of "anorogenic" or "intraplate" volcanic activity in areas very close to the subduction systems or in hinterland positions. Partial melting at 22-18 Ma, ascribed to a large-scale thermal event related to collision (Duggen et al., 2004) or to strike-slip faults (Rossetti et al., 2013, 2010). A different interpretation taking into account the structures is proposed in chapter 4. Furthermore in the western part of the chain in an anomalous position mantle-related tholeitic andesitic dike (Malaga dikes) are cropping out in the hinterland and have been dated recently at 33 Ma (Esteban et al., 2013; Torres-Roldán et al., 1986). A possible origin of this volcanism is discussed in Chapter 3.

In this framework, we will now discuss in more detailed the open questions related to the Gibraltar arc system.

1.2 Gibraltar arc

The arcuate thrust belt that bounds the Alboran Domain to the west is usually called

Gibraltar arc. Three main groups of tectonic units characterize the arc and are not observed in the rest of the Betic-Rif: in ascending order are the Subbetics, the Flysch Trough and the Dorsale (described in sub-section 1.1.1 and 1.1.2). The first two are in the External Zone, the last one in the Alboran Domain at the boundary with the External Zone (Fig. 1.4). In the next three subsections we resume the models proposed for the arc formation and the direction of displacement of the Alboran Domain proposed by each research group, underlining from where the data used come from. Then, we present the paleomagnetic data published for the whole Betic Cordillera. Finally, we discuss the Miocene extension described in the Alboran Domain and contemporaneous to the shortening in the Gibraltar arc.

The relationships between structures in the External Zone, already described in literature, and the coeval structures inside the Alboran Domain is of capital importance to the comprehension of the formation of the arc. This subsection, through a review of the literature, aims to introduce mainly Chapter 2.

1.2.1 Direction of emplacement

In this sub-section we summarize the observations from the Western Betics and the different hypotheses on the Alboran Domain displacement. Structural studies in the whole arc have shown radial pattern of the slip vectors in the External Zone that was interpreted as a result of either westward motion of the extending Alboran Domain (Balanyá et al., 2007) or radial motion of the Alboran Domain due to extensional collapse (Platt et al., 2003a). In the first case, the Alboran Domain motion would be westward with a radial distribution of kinematic vector, opening with a glacier-front style (Balanyá et al., 2007) (Fig. 1.39a).

The swing in slip-vectors in the External Zone, from E-W north of Gibraltar to NW north of Ronda is an effect of strain partioning from arc normal shortening (black arrow) to arc parallel extension (Balanyá et al., 2007, Fig. 1.39a). In constrast, Kirker and Platt (1998) suggest a N120° unidirectional motion of the Alboran Domain in the Western Betics (Fig. 1.39b). The main difference between these two scenarios is that the first one postulate the existence of a dextral transpressive E-W zone (Torcal region: Balanyá et al., 2007, Balanyá et al., 2012) while the second one a N120° dextral strike-slip fault zone for Platt et al., 2003a (see discussion in Balanyá et al. 2007, summarized in Fig. 1.40) that actually could correspond to the Zafarraje-Nogaje fault zone of Fernandez-Ibañez and Soto (2008). The dextral strike-slip faults in the area that can result from these pattern have been also described in the pastby Martín-Algarra (1987), Sanz de Galdeano (1990) and Sanz de Galdeano and López-Garrido (2012a), (2012b).

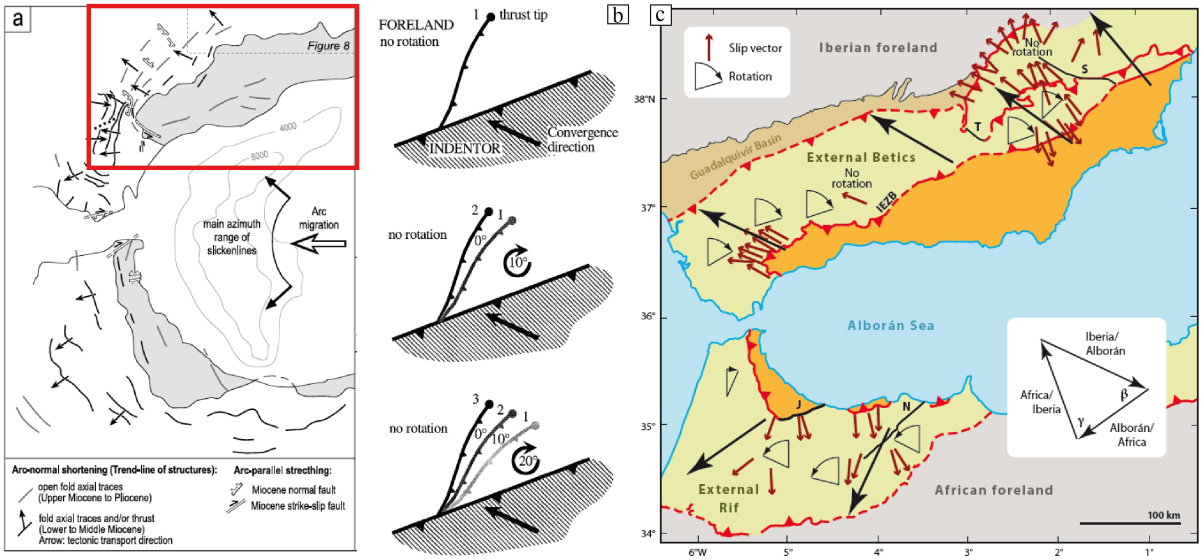

Figure 1.39. Different hypotheses for the External Zone shortening direction. (a) Diverging pattern of slip vectors in the Western Betics; (b) Unidirectional displacement and rotation of the thrust sheets (Kirker and Platt, 1998); (c) Unidirectional displacement all along the Betic Cordillera (Platt et al., 2013).

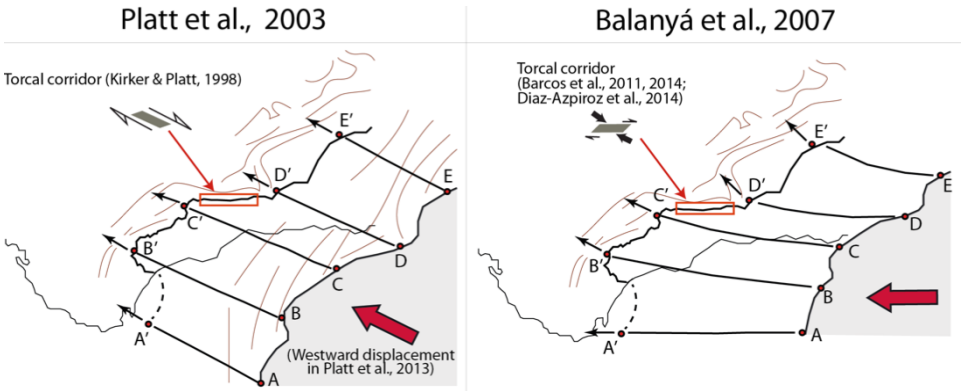

Figure 1.40. Displacement of the Alboran Domain with respect to the fold and thrust belt of the Western Subbetics and Betic Flysch Trough, as proposed by Platt et al. (2003) and Balanyá et al. (2007). Initial contour of the Alboran Domain from Kirker and Platt (1998).

1.2.2 Paleomagnetism and rotations

The vertical axis rotation revealed by paleomagnetic data is an important aspect of the kinematic evolution of the Gibraltar arc (e.g. Calvo et al., 1994; Cifelli et al., 2008; Mattei et al., 2006; Osete et al., 1988; Platzman, 1992; Platzman et al., 1993; Platzman et al., 2000; Platt et al., 1995) (Fig. 1.41). Vertical axis rotations, mostly clockwise in the Betic segment and counter clockwise in the Rif segment of the belt, have been used to confirm the geodynamic models that suppose a westward propagation of the system and in particular the roll-back model (see next section 1.3) (Fig. 1.42). These rotations provide essential information on the pattern of deformation around the arc and raise questions about the significance of the kinematic data acquired in the field. If the rocks can be rotated of large angles about vertical axes during the deformation, then the same can be true for the structures in the rocks. Kirker and Platt (1998) state concerning this point that in the Western Subbetics

arc the structures are active during the rotation and that the displacement persist with the same direction after the rotation permitting the preservation of the unidirectional slip vectors observed.

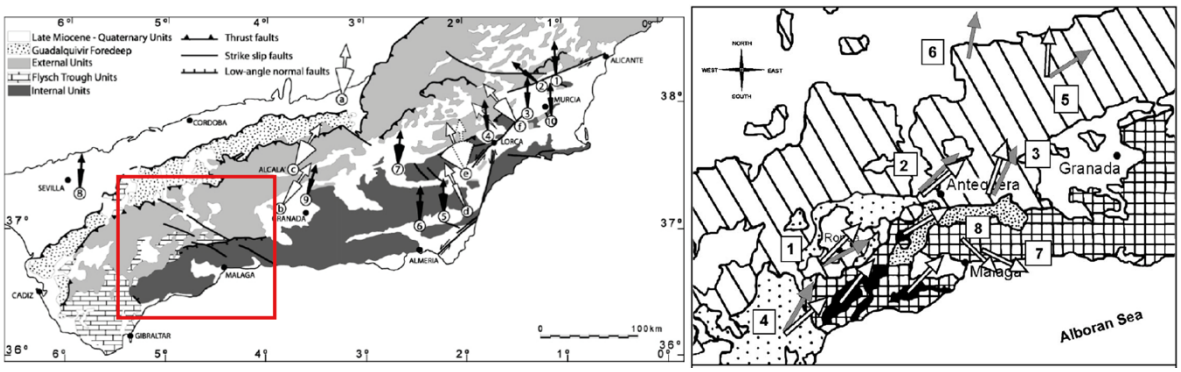

Figure 1.41. Paleomagnetic declinations (and relative confidence limits) from Neogene sediments in the Betic chain. White arrows come from Mattei et al. (2006) and indicate cumulative paleomagnetic declinations for each study basin. Black arrows come from previous studies and are indicative of mean paleomagnetic declination deduced in single magnetostratigraphic sections. See Mattei et al. (2006) for references. Red square report the area in Figure 1.44. Block rotations in the Ronda-Málaga region from Villasante-Marcos (2003). Data from other studies are also included and described in Villasante-Marcos et al. (2003). Tertiary paleomagnetic vector is indicated with a white arrow and the Jurassic paleomagnetic declination with a grey arrow.

The paleomagnetic data in the Western Betics side of the arc come largely from sites in the Jurassic and Cretaceous carbonates of the Subbetic units close to the boundary with the Alboran Domain. These units record a long and composite geologic history encompassing Jurassic and Cretaceous rifting and then subduction-related orogenic processes since the Late Cretaceous. As a consequence, a very complex rotation and magnetization histories have been documented in Villalaín et al. (1994). Osete et al. (2004) showed that this widespread secondary remagnetization event took place in Mesozoic sediments all along the belt. These factors can be a strong handicap for a proper interpretation of the paleomagnetic data.

The remagnetization imprints a deformed wedge with a variable structural trend. Consequently, the remagnetization event would have occurred after the main deformation. Crespo-Blanc and Campos (2001) considered that the main shortening deformation episode took place during the Late Burdigalian in the Western Betics. Consequently, the remagnetization that led to the same paleomagnetic declinations on different side of the western subbetics arc should have accurred after the Langhian and the rotation as well. Unfortunately, in the Western Betics, no Miocene sediments have been sampled in the past (Fig. 1.41) and the most probable hypothesis is that remagnetization occurred at different time before and during the deformation. Some of the rotations continued to early Pliocene times in the Betic basins (Mattei et al., 2006) and have been related to Nubia-Iberia compression that would still produce further bending of the arc. Then, at the end of the deformation history, there was still a slight clockwise rotation of the whole region of 10–15º. For the Rif side of the arc Cifelli et al. (2008) show an anticlockwise rotations also in Upper Miocene deposits (Fig. 1.41).

Concerning the Alboran Domain, the mantle bodies rotate of 30º to 50º clockwise about a vertical axis (Feinberg et al., 1996; Villasante-Marcos et al., 2003; Osete et al., 1988). Analyses are coming from magnetite in peridotites and serpentinites (Villasante-Marcos et al., 2003; Berndt et al., 2015) or from leucocratic granitic dikes inside the mantle (Feinberg et al., 1996). An anticlockwise rotation is reported from the Rif (Berndt et al., 2015). A clockwise rotation is reported also from the Malaga Dikes, but considerably larger, 118±14º (Calvo et al., 2001). This rotation is almost 70º higher than the Ronda Peridotite rotation that accurred in the last 20 Ma: if the age of the dikes is 33 Ma (Esteban et al., 2013), the rotation is 5.4º per million year. A strong clockwise has been registered before in the Alboran Domain than in the External zone.

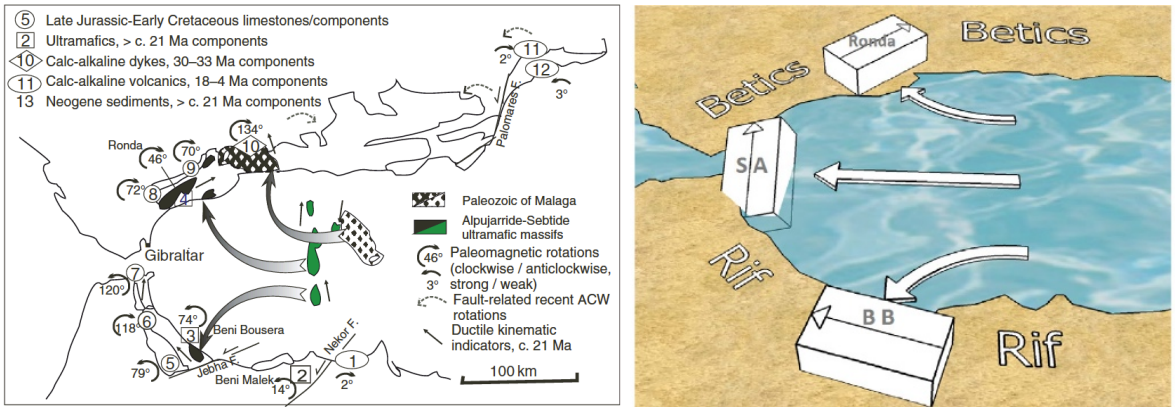

Figure 1.42. Paleomagnetic rotations (mean site values) in the Betic-Rif Belt (from Chalouan et al., 2008, and from Berndt et al., 2015). The inferred approximate N–S strike of the pre-Early Miocene orogen is shown schematically by the alignement of the three ultrabasic bodies in the mid-Alboran area in the figure on the left (Chalouan et al., 2008). This also restores the main ductile shear directions of the west Gibraltar Arc, as reported by Reuber et al. (1982), Balanyá et al. (1997), Martínez-Martínez et al. (2002), into an broadly N-S trend. On the right, no rotation have been observed in the Ceuta Peridotite close to the Gibraltar Strait (Berndt et al., 2015).

1.2.3 Extension coeval to compression

While the thrust sheets were emplaced to form the Gibraltar arc a widespread extension took place in the Alborna Domain and at the boundary between Internal and External Zone (García-Dueñas et al., 1992). Subsidence in the Alboran Basin has been justified with the action of detachment faults individuated in low angle normal faults onshore in the Western Betics. The age is mainly defined on the base of the infilling of the basin offshore to the Serravallian describe in subsection 1.1.3. (Comas et al., 1992). The repetitions of the tectonic units (García-Dueñas et al., 1992) and the lateral variation in thickness in the Alboran Domain (Sánchez-Gómez et al., 1999) have been ascribed to these low angle normal faults (Fig. 1.43). Further work by Crespo-Blanc and Campos (2001) show that also the Subbetics is affected by the Serravallian extension that is mainly top to the SSE (Fig. 1.43).

QUESTIONS

The formation of the Gibraltar arc implies strong rotation, the role of thrusts, strike-slip and extensional faults during at least the last 20 Ma, with however contrasting tectonic hypotheses. This brief review allows identifying key areas where to collect new structural data in order to constrain the **direction**, the **timing** and the **amount** of **displacement** of the **Alboran** Domain, and also the coexistence of compression and extension in the Gibraltar system. This will be the main objective of Chapter 2.

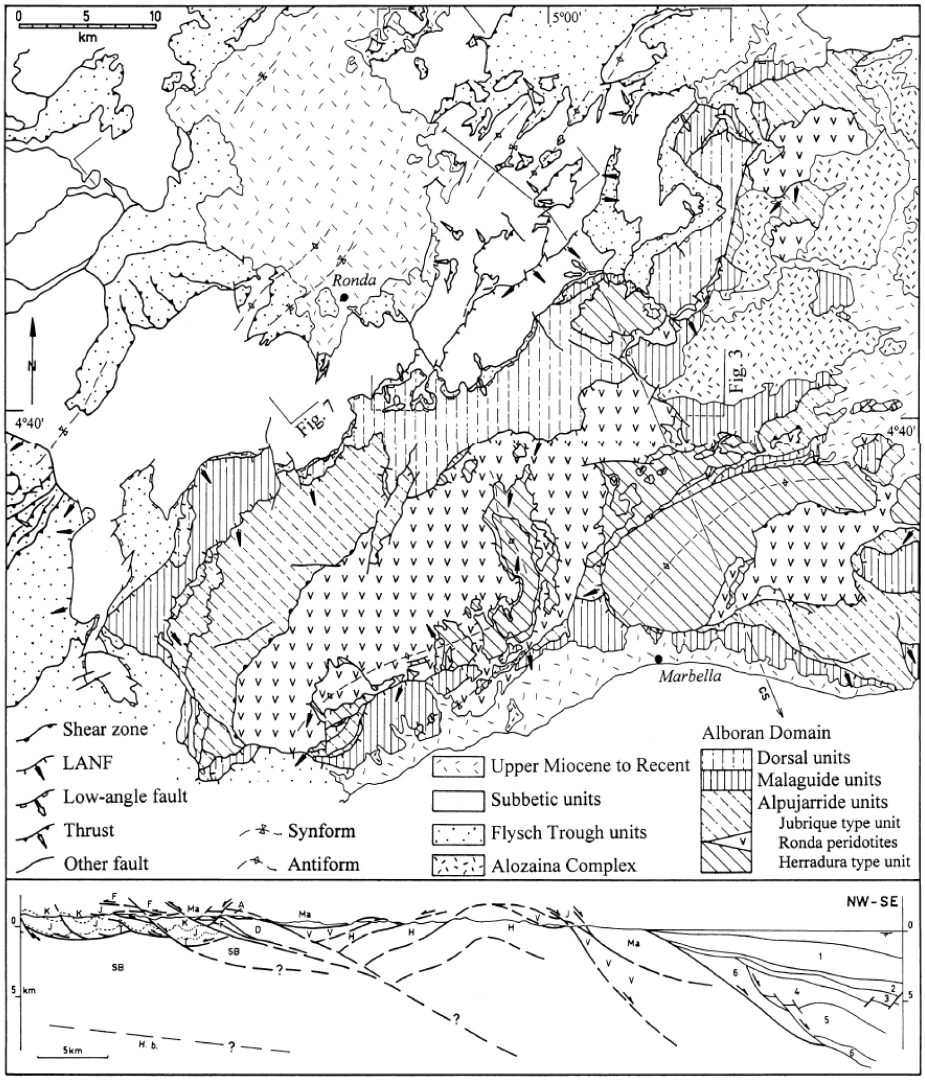

Figure 1.43. Tectonic map of the Western Betics (from Crespo-Blanc and Campos, 2001). Arrows are kinematic indicators along low-angle faults. Synform and antiform are Upper Miocene very open folds. Relationships between the Internal Subbetic units (T, Triassic, J Jurassic; K Cretaceous to Paleogene), F: Flysch Trough; D Dorsale; Ma Malaguide, H Alpujarride, V peridotite are exposed in the cross-section below.

1.3 Tectonic models for the Alboran system features

Two main types of models have been proposed in the past to explain how semi-radial thrusting around the external Gibraltar arc could have occurred coevally with the extension reported from the internal Alboran Domain: convective-removal of lithospheric mantle due to

gravitational instabilities and slab rollback. In this section, we go through a broad selection of models. This is useful, firstly, to introduce the main geophysical and tectonic characteristics of the region and secondly, to illustrate the main differences between the models in order to discuss their coherence with the contribution of the present study.

A first category of models looks for causes in the relative movement between the plates that bound the region (see sub-section 1.3.2). These models have been dismissed in favour of a second category, more popular, proposes the role of oceanic subduction or convective removal of a thickened lithosphere (Platt et al. 2013). Platt and Vissers (1989) have suggested convective removal as working hypothesis 25 years ago, but in the last two years have proposed oceanic subduction rollback as base of the tectonic evolution (Platt et al., 2013; Van Hinsbergen et al., 2014; Johanesen et al., 2014).

The rest of the section is divided in four subsections. In the first sub-section we describe the diffuse plate boundary, the tertiary relative movements between the plates and GPS data. In the second subsection we present the Alboran micro-plate extrusion model. The convective removal and delamination models are detailed in the third subsection where also recent tomography from the region is presented. The fourth subsection is entirely devoted to slab rollback in the area, and to the debate already summarized in figure I.3 in the introduction.

1.3.1 A diffuse plate boundary between Iberia and Nubia

GPS and seismic data suggest that active deformation in the Alboran region is pretty complex and cannot be explained simply by the right lateral motion along the Iberia–Nubia plate boundary, which is a diffuse plate boundary.

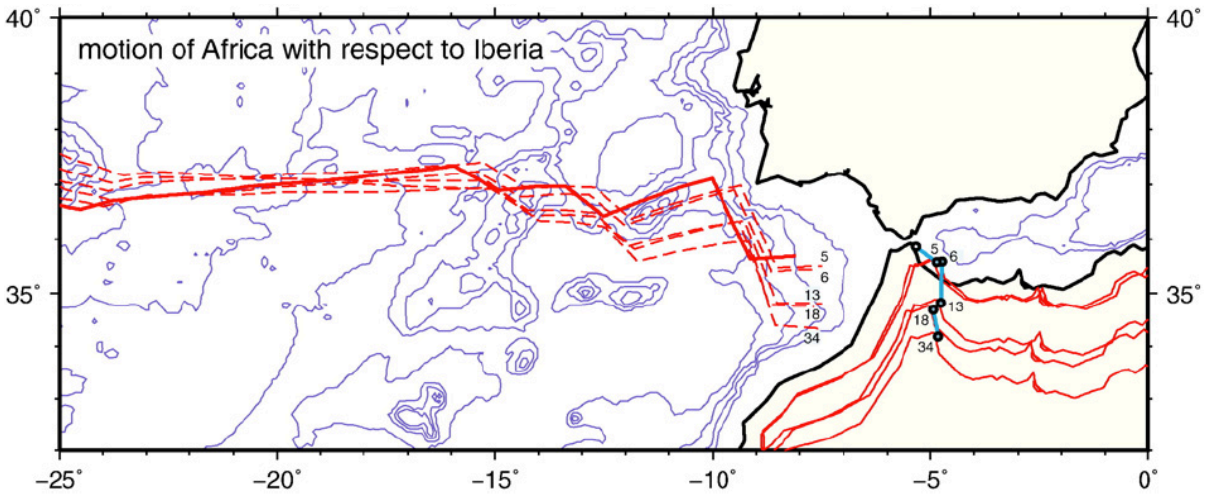

Figure 1.44. Motion of Africa with respect to Iberia (from Vissers and Meijer, 2012). Positions of Africa and the Azores Gibraltar Fracture Zone are shown with respect to Iberia for chrons 34, 18, 13, 6 and 5 at, respectively, 83 Ma, 39.3 Ma, 33.1 Ma, 19.2 Ma, 9.9 Ma.

Indeed, GPS motions relative to Africa (Fig. 1.45, left) in the Alboran system change significantly from area to area. In western Morocco, the stations show systematic motion

toward the ESE (relative to Iberia). Stations in the central part of the Rif Mountains indicate a significant southwestward motion (3.5 to 4.0±0.3 mm/yr) with respect to Africa (Fadil et al., 2006). Furthermore, north of the Alboran Sea, stations in the southwestern Betics indicate west–southwest motion (~3 mm/yr, relative to Iberia). In the vicinity of the Gibraltar arc two stations show slow motion towards the SE relative to Africa with less than 1±0.4 mm/yr (Vernant et al., 2010).

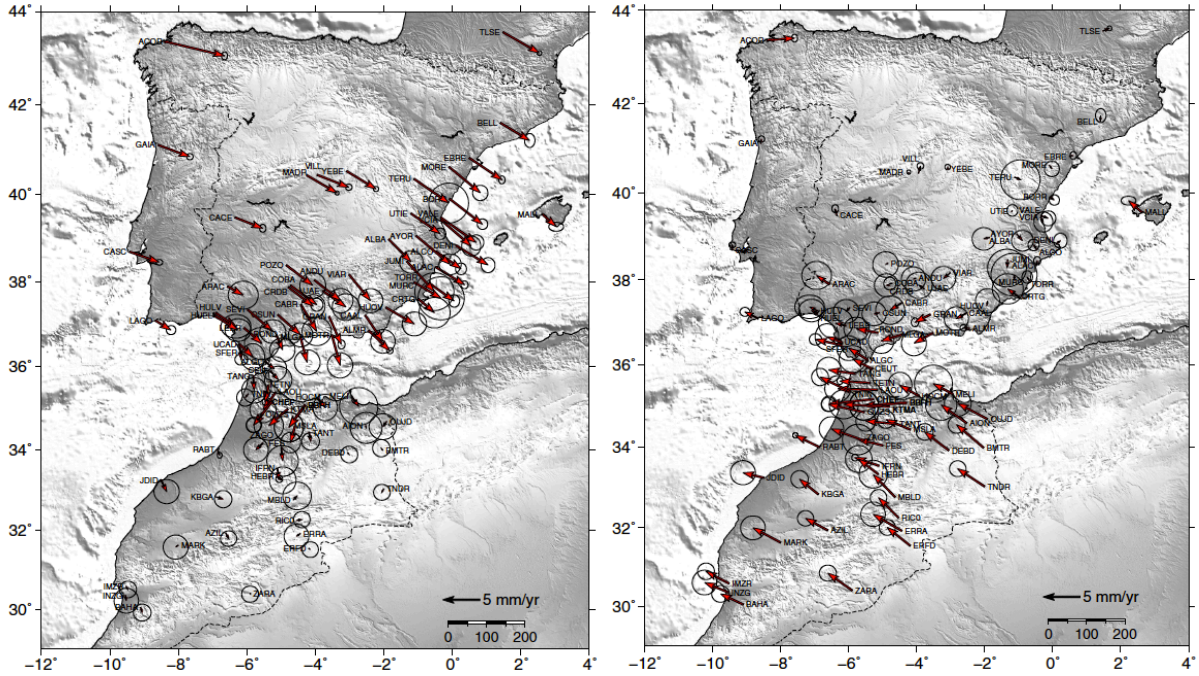

Figure 1.45 On the left, GPS site velocities with respect to *Africa* and 95% confidence ellipses. On the right, GPS site velocities relative to *Eurasia* and 95% confidence ellipses. (From Koulali et al., 2011).

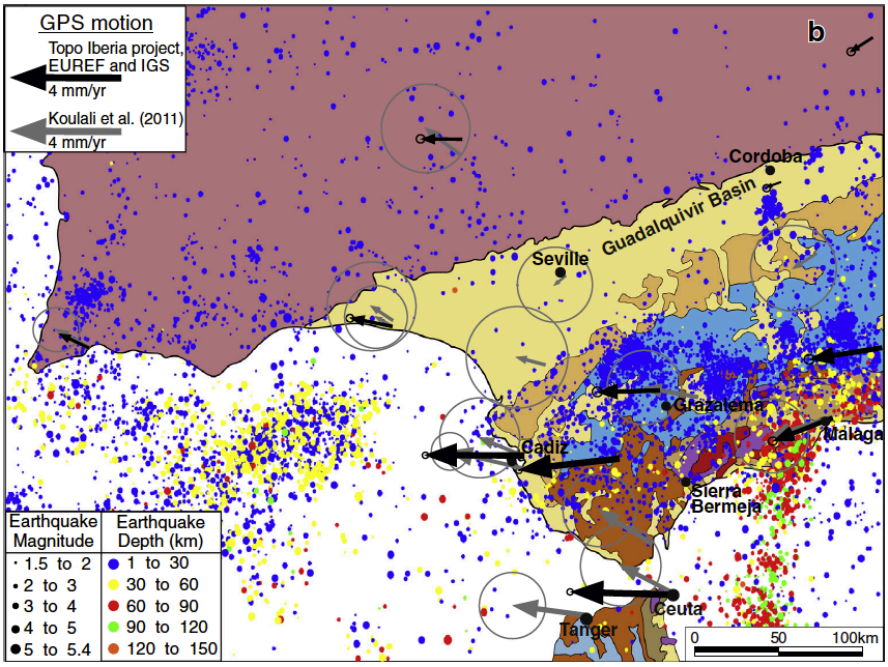

Figure 1.46. Tectonic sketch of the area studied in Gonzalez-Castillo et al. (2015) including seismicity (database of Instituto Geográfico Nacional, www.ign.es) and CGPS data. Residual velocity field is referred to Eurasia and 95% confidence ellipses.

GPS velocities relative to Eurasia (Fig. 1.45, right) exhibit a consistent westward motion of the stations located in the Western Betics with displacement increasing toward south and west, reaching maximum values in the Gibraltar Strait area (4.27 mm/yr in Ceuta, CEU1, and 4.06 mm/yr in San Fernando, SFER). This motion is distinct from the motion of the sites in central, eastern and western Iberia where the expected NW–SE Eurasia motion direction dominates. This behavior suggests that deformation mechanisms affecting the Alboran region could be associated with those seen in the Rif (Fadil et al., 2006), forming a large distributed deformation zone along the Gibraltar arc (Koulali et al., 2011).

1.3.2 Microplate westward extrusion

Crustal extrusion and lateral escape of an Alboran micro-plate have been proposed originally by Andrieux et al., 1971 (Fig. 1.47). They have proposed that a rigid, westward-moving Alboran micro-plate could have caused the radial thrusting around the Gibraltar region. Strike-slip shearing along the lateral boundaries of the supposed exotic rigid indenter has been observed all along the Betics (Sanz de Galdeano, 1996) and in the eastern sectors of the Rif (Olivier and Blanc, 1984). The micro-plate hypothesis has been abandoned as subsequent studies have shown that extension and thin crust are main features of the Alboran Domain (Comas et al., 1999) and are not explained by this model.

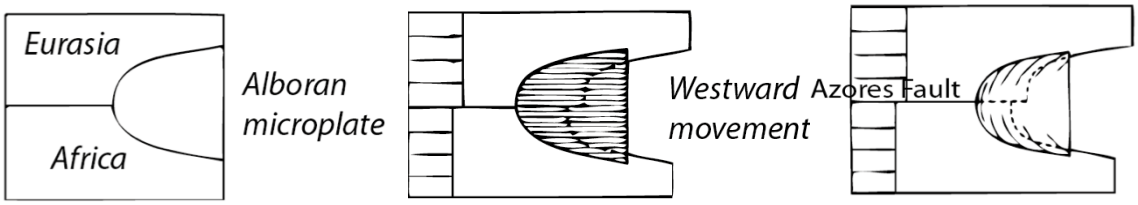

Figure 1.47. Gibraltar arc geometrical model (from Andrieux et al., 1971). On the left, situation before plate relative displacement. In the middle, thrusting of the Alboran microplate on top of Europe and Africa. On the right, folding accomodates the Alboran micro-plate emplacement.

Rebai et al. (1992) and Morel and Meghraoui (1996) repropose the idea of a lateral extrusion to explain the active crustal transpressional deformation occurring within the Gibraltar arc. The westward extrusion-escape of the internal Rif ca. orthogonal to the Nubia–Eurasia convergence direction is accommodated by the presence of active strike-slip fault systems. In particular, the extruded sector is bounded southward by the left-lateral Trans-Alboran Shear zone (TASZ, Fig. 1.3) and northward by the right-lateral Zafarraya-Niguelas fault system (NFZ, Fig. 1.3) (Fernandez-Ibañez and Soto, 2008), which should accomodate the escape/extrusion process.

Apart from this model of extrusion, most models evoke the role of mantle dynamics (slab) in the origin of the Betic-Rif Cordillera, involving classicaly 1/ sinking of lithosphere and 2/ rising of buoyant asthenosphere mantle (Figs. 1.48 and 1.51). The postulated flow of material causes a pattern of extensional and contractional tectonics in the overlying crust, with

associated structural responses and thermal imprint (studied in chapter 2 and 4 respectively). The lithospheric thickening beneath the Gibraltar Arc and the adjacent thinning in the Alboran Basin has given rise to four main families of geodynamic models. The main differences, following Platt et al. (2013), concern whether oceanic lithosphere is involved and whether the sinking lithosphere behaves as a viscous fluid or a rigid slab.

Slab rollback (Frizon de Lamotte et al., 1991; Royden, 1993; Lonergan and White, 1997) that can still be active (Gutscher et al., 2002), and slab break-off (Zeck, 1996; Wortel and Spakman, 2000) need a subducting slab. In what follow, the extreme options are clearly ditinguhished for purpose of exposition although they can act together. the delamination, for example, can occur during roll-back, but also convective removal. a geodynamic discrimination can likely be done only at the scale of the whole orogenic system. This is outside the objectives of this regional work.

1.3.3 Convective removal of lithosphere mantle roots and mantle delamination

Both convective removal (e.g. Platt and Vissers, 1989; Platt et al., 2003) and mantle delamination (e.g. Seber et al., 1996; Calvert et al., 2000) imply the disappearance of the lithosphere mantle beneath the Alboran crustal domain (Fig. 1.48).

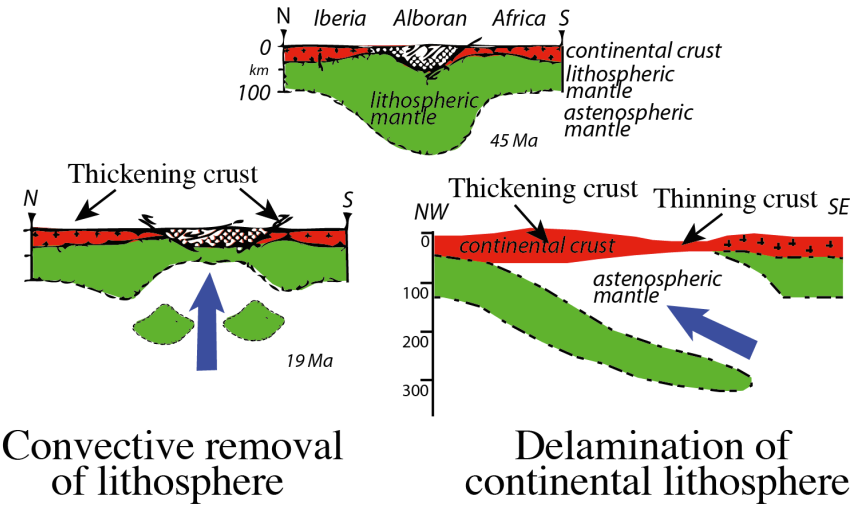

Figure 1.48. Upper mantle processes beneath the Alboran Domain might leave a trace in the mantle rocks cropping out in the western betics. At the top initial situation with thickening of the lithospheric mantle (*a*) delamination (e.g., Calvert et al. 2000), convective removal of lithosphere (Platt & Vissers 1989). Redrawn after Platt and Vissers, 1989 and Platt et al., 2013.

Convective removal

The first model, presented as a working hypothesis by Platt and Vissers (1989), proposes that removal of a thickened lithosphere root by thermal convective processes has happened in Late Oligocene-Early Miocene, in conjunction with the steady Africa–Eurasia

convergence (Platt et al., 2003). Late Cretaceous through Paleogene convergence between Africa and Eurasia has created a zone of thick crust (~Internal Zone) that was located in the area between present-day Morocco and southern Spain. Thus, the first implication is that the **amount** of total **displacement** is relatively small: estimates of Miocene crustal shortening in the external thrust belt range from 150 to 200 km for Platt et al., 2003.

The supposed collisional ridge in the area between present-day Morocco and southern Spain was underlain by a thick, cold, and gravitationally unstable lithosphere mantle that has been removed by thermal convective processes into the mantle. The large increase in potential energy led to horizontal stresses that resulted in extension and **exhumation** of lower crustal rocks (e.g. **peridotites** within the Internal Zones) through action of several cross-cutting detachments (Platt et al, 2003) and the formation of an extensional basin (the Alboran basin).

The radial horizontal stresses, combined with the continued convergence of Africa and Eurasia, were accommodated by coeval shortening within the External Betic and Rif mountain belts throughout the Miocene. The postulated **direction** of **displacement** is thus radial to the center of the collapse, i.e. the Alboran basin. Both mass-balance considerations and seismological evidence (Seber et al., 1996; Calvert et al., 2000) suggest sinking of lithospheric mantle during this process, but evidences for a corresponding **migration** of the locus of **extension** within the Alboran domain are doubtful (Docherty and Banda, 1995).

The **timing** of the thickening event is not well determined, but available radiometric and stratigraphic data suggest a late Eocene age (Vissers et al., 1995). The evidence therefore suggests a **delay** of 25 Ma between the crustal-**thickening** event and the onset of crustal **thinning**. This delay is a characteristic and predicted feature of the process of convective removal of thickened lithospheric roots beneath collisional orogens (Houseman and Molnar, 1997) and, accorfing to Platt et al. (2003) is not predicted by the other mechanisms for postorogenic extension. The thermal evolution of the Alboran crust indicates heating during rapid exhumation and contemporaneous reset ages in the belt. Platt et al. (1998) elaborate that the only plausible way to explain this thermal history is the removal of most of the lithospheric mantle beneath the collisional orogen immediately before exhumation started.

The slab has been for long time not clearly imaged. Indeed, the intermediate and deep seismicity in the area is highly localized, and do not resemble that of a Wadati-Benioff zone (Fernandez-Ibañez and Soto, 2008). Furthermore, until the works of Bezada et al. (2013) and Bonnin et al. (2014), in previous tomographic models the imaged shape of cold material was more consistent with the one predicted for an amplifying and laterally propagating Rayleigh-Taylor instability developed from the lower lithosphere (Houseman and Molnar, 1997) (Fig. 1.49).

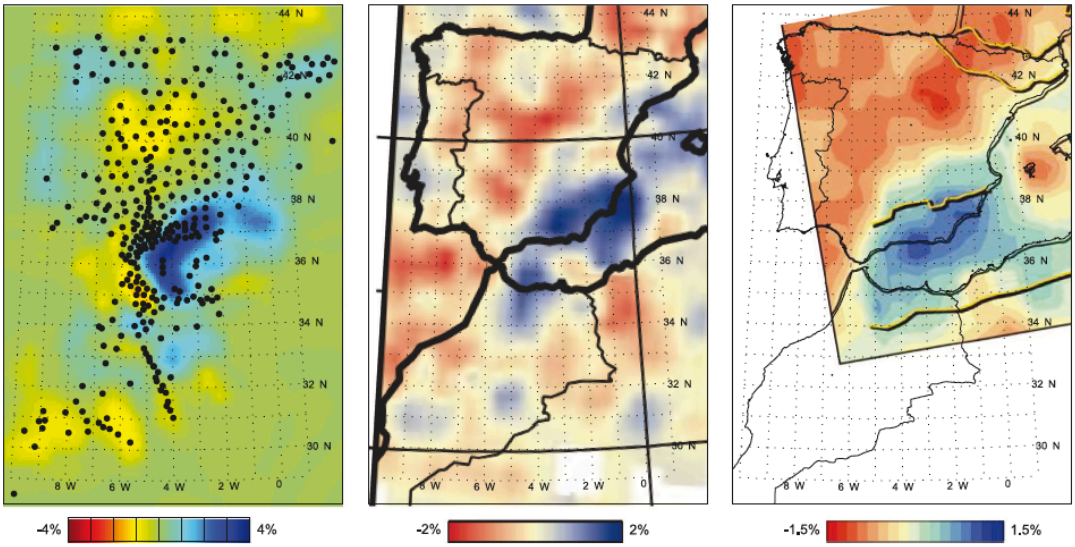

Figure 1.49. High-velocity anomaly images in an horizontal slice at a given depth (from Bezada et al., 2013). Left: Bezada et al. (2013) at 435 km; Center: Piromallo and Morelli (2003) at 450 km. Right: Spakman and Wortel (2004) at 440 km. Note the arcuate shape of the anomaly in Bezada at this depth is not imaged in the older models that in opposite support more a blob-like shape of the anomaly.

Delamination

The delamination model initially proposed by Garcia-Duenas et al. (1992) and Seber et al. (1996) shares many similarities with the convective removal hypothesis of Platt and Vissers (1989). The main difference between the two models centers on how the lithospheric root was removed from the crust. Lithospheric thickening during the Late Cretaceous through Paleogene resulted in a large gravitationally unstable lithospheric root beneath a NE striking zone of thickened crust. Possibly induced as a consequence of some convective removal, this root mechanically detached from the crust and was replaced by hot asthenosphere (Fig. 1.47). The lithosphere peeled back to the west and northwest where it may still be attached beneath portions of Spain (Calvert et al., 2000). Heating of the crust, uplift and extension in the Alboran area are the results of the loss of the lithospheric root, along with the inflow of hot asthenospheric material.

Calvert et al. (2000) interpreted the high velocity bodies imaged beneath the Alboran region to be delaminated lithosphere. Calvert et al. (2000) noted that the high velocity body could be interpreted as a subducted slab (which would support the slab rollback model), but favored the delaminated lithosphere model because of the petrological work by Platt et al. (1998), which suggested the process of slab rollback would be incapable of producing the P-T-t paths found in the metamorphic assemblages in the Alboran basement rock. Crustal delamination from the downgoing subcontinental mantle has been proposed to explain the peculiar kinematics, especially of the Rif region, in present-day GPS data (Pérouse et al., 2010). Following this debate, delamination during slab rollback is nowadays the most common interpretation.

Worth to note are the recent Ps receiver function analyses that indicate the existence of the top of the slab (Thurner et al., 2014). Beneath the Guadalquivir Basin in the west, the RFs show a fairly strong flat Moho signal at 30 km, consistent with active source results (Torné et al., 2000) (Fig. 1.50). Beneath the western Betics, the Moho signal weakens and dips eastward to ~45 km depth over a distance of ~50 km. Below the Moho in the central Betics, a second positive event extends from ~80 km depth in the west up to ~53 km depth in the east, where it intersects the shallower Moho event. Based on surface wave tomography, Thurner et al. (2014) correlate the deeper positive event with the top of the Alboran slab (Fig. 1. 50e).

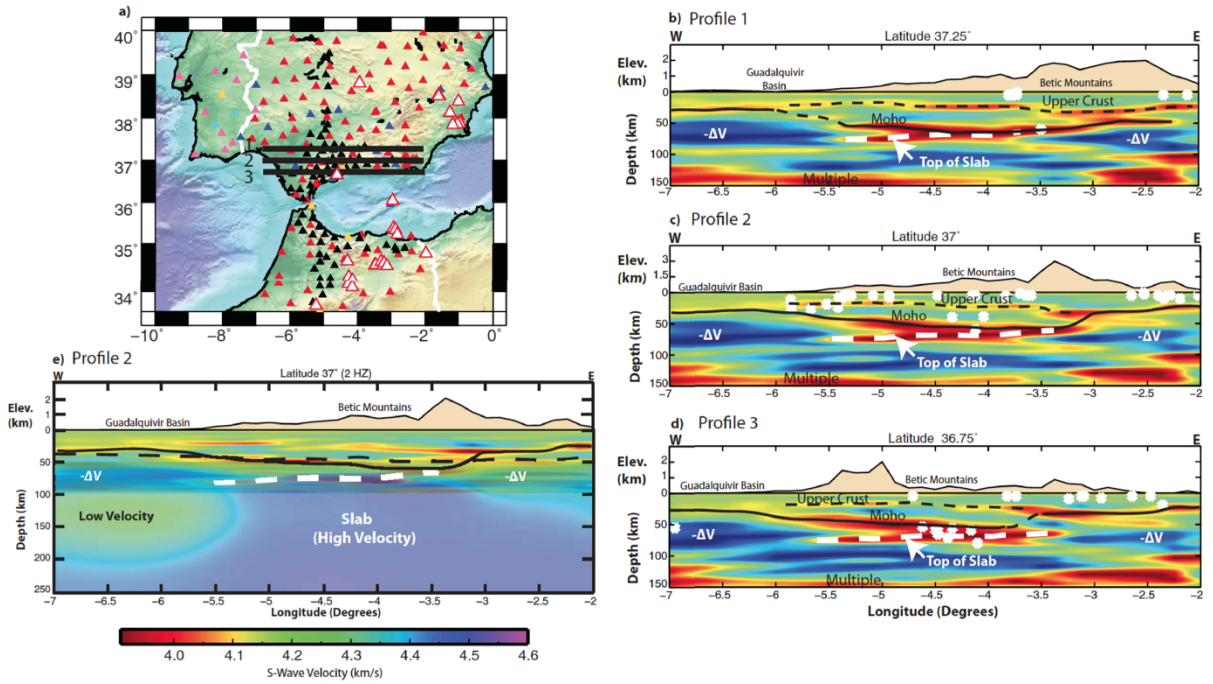

Figure 1.50. a) Map showing the location of CCP profiles at 37.25º, 37º, and 36.75º latitude, marked by the black lines. (b) 1 Hz CCP profile at latitude 37.25º. (c) 1 Hz CCP profile at latitude 37º. (d) 1 Hz CCP profile at latitude 36.75º. The black dashed line marks a strong midcrustal event. The black solid line marks the continental Moho. The deepest, positive event, interpreted as the top of the slab, is marked by the white dashed line. The white diamonds mark earthquake hypocenter locations. 2DV indicates the locations where strong negative events suggest a negative velocity gradient. (e) The 2 Hz receiver functions and the Rayleigh wave tomography results along latitude 37º. We can see that the deep positive RF event coincides with the top of the high velocity slab and the strong negative events in the west and east coincide with the tops of low velocity zones seen in the surface waves (Thurner et al., 2014)

Note that break-off of a rigid NW dipping subducted slab beneath Iberia (Blanco and Spackman, 1993 and Zeck, 1999) or of a S dipping subducted slab (Tubía et al., 1992) has been also proposed to explain the orogenic collapse. However, there are two important problems with these models: 1) the total convergence between Africa and Eurasia (<400km) is less than the length of the subducted slab interpreted to have broken off (~600km); and 2) the high P-wave velocity zones in the upper mantle do not correspond to a NW dipping slab or SE dipping slab (the zone appears to dip to the east; see tomography results in Figure).
Note that a slab can break-off also during rollback during the tearing of the subducting lithosphere.

1.3.4 Rollback of a subducting oceanic lithosphere

Royden (1993) and Lonergan and White (1997) were the first to propose slab rollback as a driving mechanism for the formation of the Betic-Rif arcuate system. In the area between Iberia and Northern Africa, a Late Cretaceous-Paleogene subduction zone had a NW-SE to N-S orientation and involved NE to E dipping subduction of the Tethyan oceanic crust. As the rate of subduction (driven by slab-pull forces) exceed the rate of convergence, the subduction zone began migrating to the west in the Late Oligocene-Early Miocene (Fig. 1.52a).

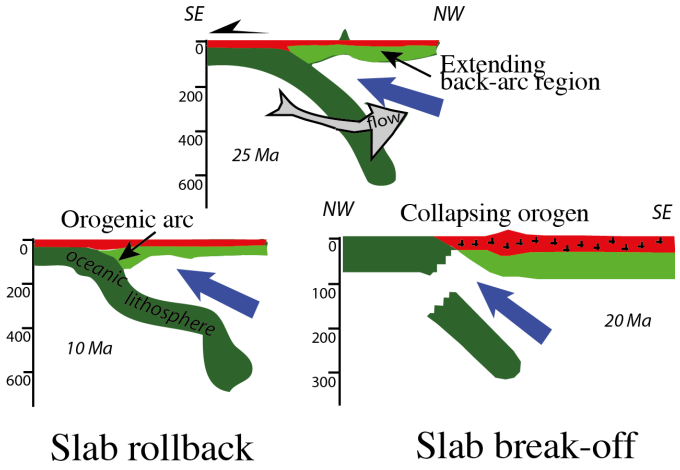

Figure 1.51. Upper mantle processes beneath the Alboran Domain might leave a trace in the mantle rocks cropping out in the western betics: slab rollback (Lonergan & White 1997, Royden 1993) and slab break-off (e.g., Blanco & Spakman 1993) can be caused by different behaviour oceanic subducting lithosphere. Redrawn inspired by Platt et al. (2013) and Faccenna et al. (2004).

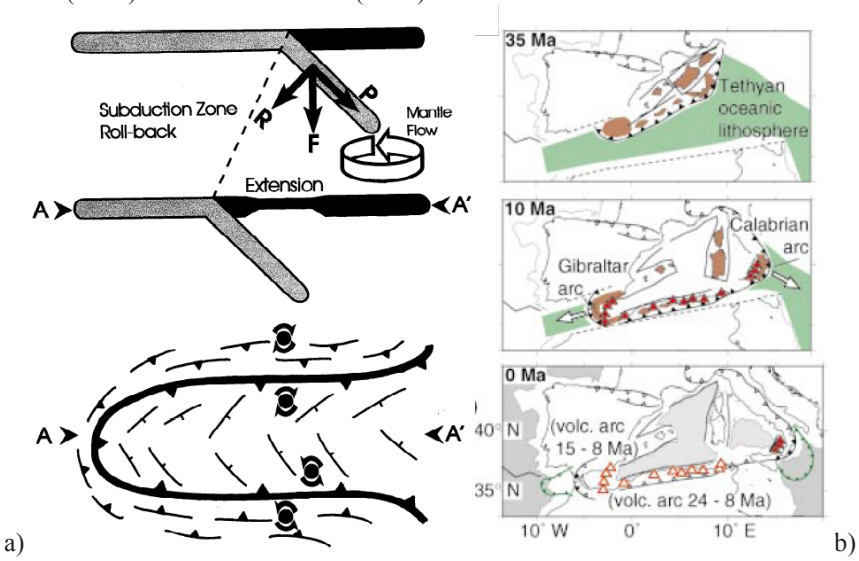

Figure 1.52. Slab rollback in the Western Mediterranean. (a) Cartoons with idealized kinematic evolution of subduction zone roll-back. At the top the E-W cross-section along the system before the rollback, in the middle the cross-section after the roll-back. Below a plan view of the orocline with extension and rotation reported (Lonergand and White, 1997). (b) Rollback evolution in the Western Mediterranean (from Gutscher et al., 2002)

As the subduction zone migrated westward, the crust of the former collision ridge (the Alboran Domain) has been broken up and dispersed while the crust immediately behind this region was extensively thinned. In the northern and southern portions of the subduction zones, the westward movement slow down as the buoyant continental crust of Iberia and Africa is encountered, while in the central portion of the subducting trench, westward migration continue. This result in northward emplacement of the Internal Zone onto southern Iberia and southward emplacement of the Internal Zone onto Northern Africa contemporaneous to extension in the overriding plate during clockwise rotation on the Iberia side and anti-clockwise rotations in the Maghrebian side (Lonergan and White, 1997; Gutscher et al., 2002; Rosenbaum and Lister, 2004). The imaged slab below the Alboran region is one of the main reason of the success of this model nowdays (Fig. 1.53).

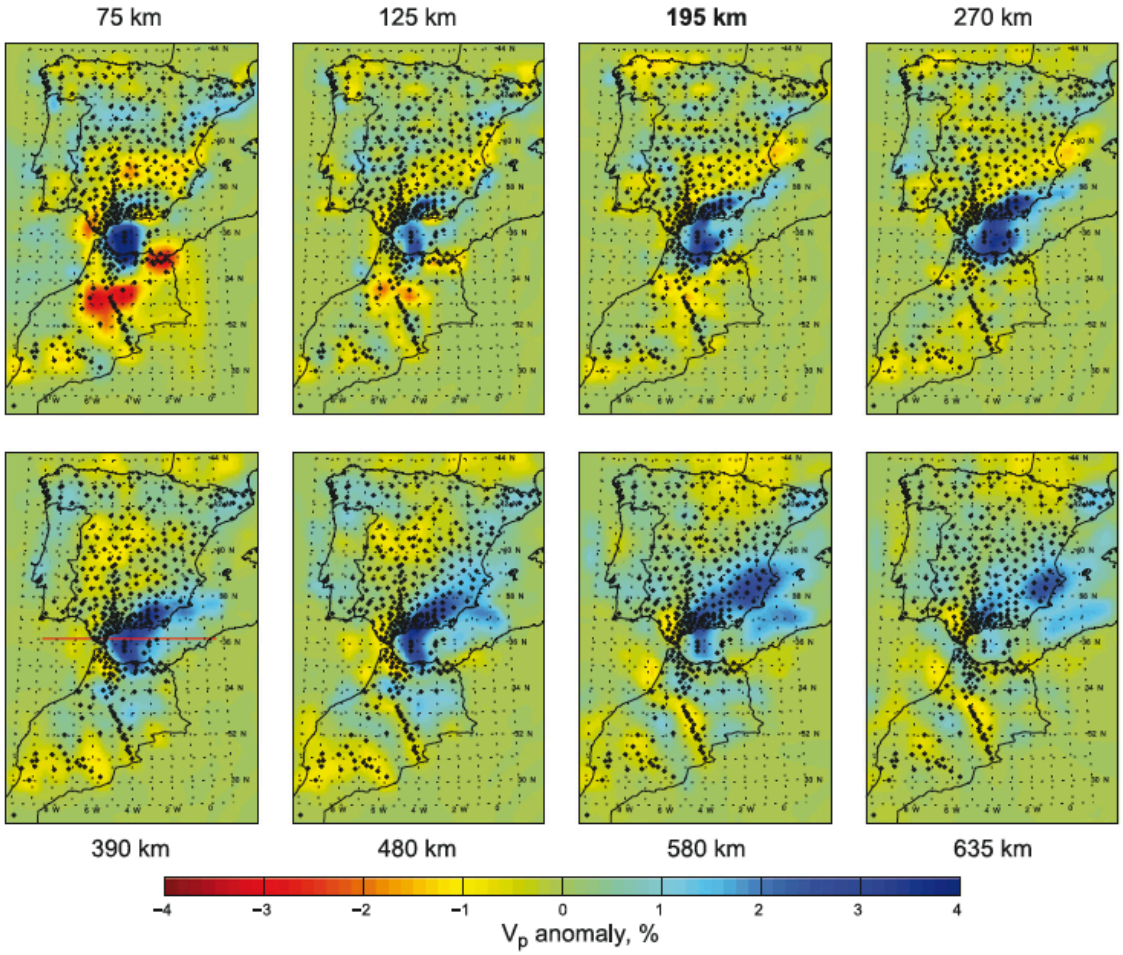

Figure 1.53. Horizontal slices through the final model at different depths as indicated on the figure (from Bezada et al., 2013)

Alternatives on timing and direction roll-back

The amount of slab rollback and the direction of trench migration is matter of controversy (Faccenna et al., 2004; Jolivet et al., 2006; Guegen et al., 1998; Spakman and

Wortel, 2000; Rosenbaum and Lister, 2004 Duggen et al., 2004; Booth-Rea et al., 2007; Gutscher et al., 2002; Spakman and Wortel, 2004; Frizon de Lamotte et al., 2009; Van Hinsbergen et al., 2014; see summary in Chertova et al., 2014). Three end-members models can be envisaged, involving a slab initially dipping more towards the north, towards the south or towards the east.

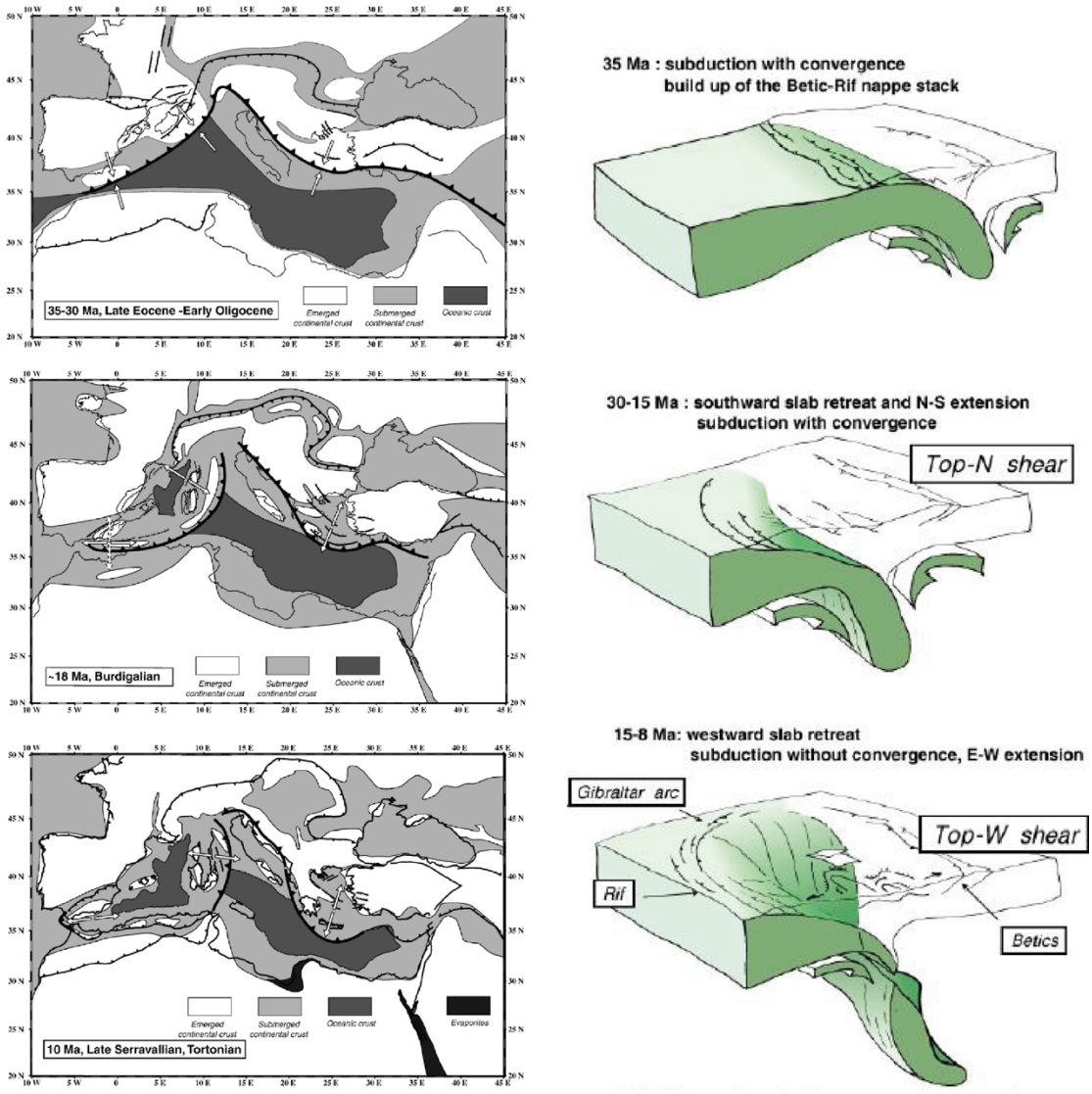

Figure 1.54. On the left, paleogeographic and paleotectonic maps of the Mediterranean region from Jolivet et al. (2006) for 30 Ma, 18Ma and 10 Ma NB: oceanic crust is shown only in the Mediterranean domain, not in the Atlantic Ocean and Black Sea.

A first family of interpretations considers an initial northwest-dipping subduction along the west-central Mediterranean (from Gibraltar or southeast of Iberia to Corsica) initiated in Oligocene and rolled back mainly to the south and then to the west (Faccenna et al., 2004; Jolivet et al., 2006; Guegen et al., 1998; Spakman and Wortel, 2000) (Fig. 1.55). Jolivet et al. (2006) propose a first stage of nappe stacking of Alpujarride and Nevado-Filabride during subduction before 30 Ma. A shearing top to the north during southward retreat and N-S extension until 18 Ma and then until the Messinian a shearing top to the west.

In the second family, a short N-S trending subduction zone located south of the Baleares islands rolled back westward during the upper Miocene (Frizon de la Motte et al., 2009; Rosenbaum et al., 2004; Van Hinsbergen et al., 2014) (Fig. 1.55). This model, envisaged by Rosenbaum et al. (2002) and Rosenbaum and Lister (2004), receive a wide consensus and is also supported by many other authors (e.g., Booth-Rea et al., 2007; Gutscher et al., 2002; Spakman and Wortel, 2004; Frizon de Lamotte et al., 2009; Van Hinsbergen et al., 2014). The westward drifting driven by a subduction rollback is large and fast. Important assumptions of the model are: i) the Alboran domain with HP–LT rocks formed far to the east of its present position travelling between 200 and 800 km; ii) the trench associated with slab-rollback turns clockwise around an anchor point located in the present eastern termination of the Betics leading to a total trench rotation of ~180° in the Betic segment; and iii) at 16 Ma (Frizon de Lamotte et al., 2009) or 21 Ma (Van Hinsbergen et al., 2014) the trench and the accretionary wedge displaced westward forming a continuous subduction front along the Betics and the Rif and a strong extension to the east.

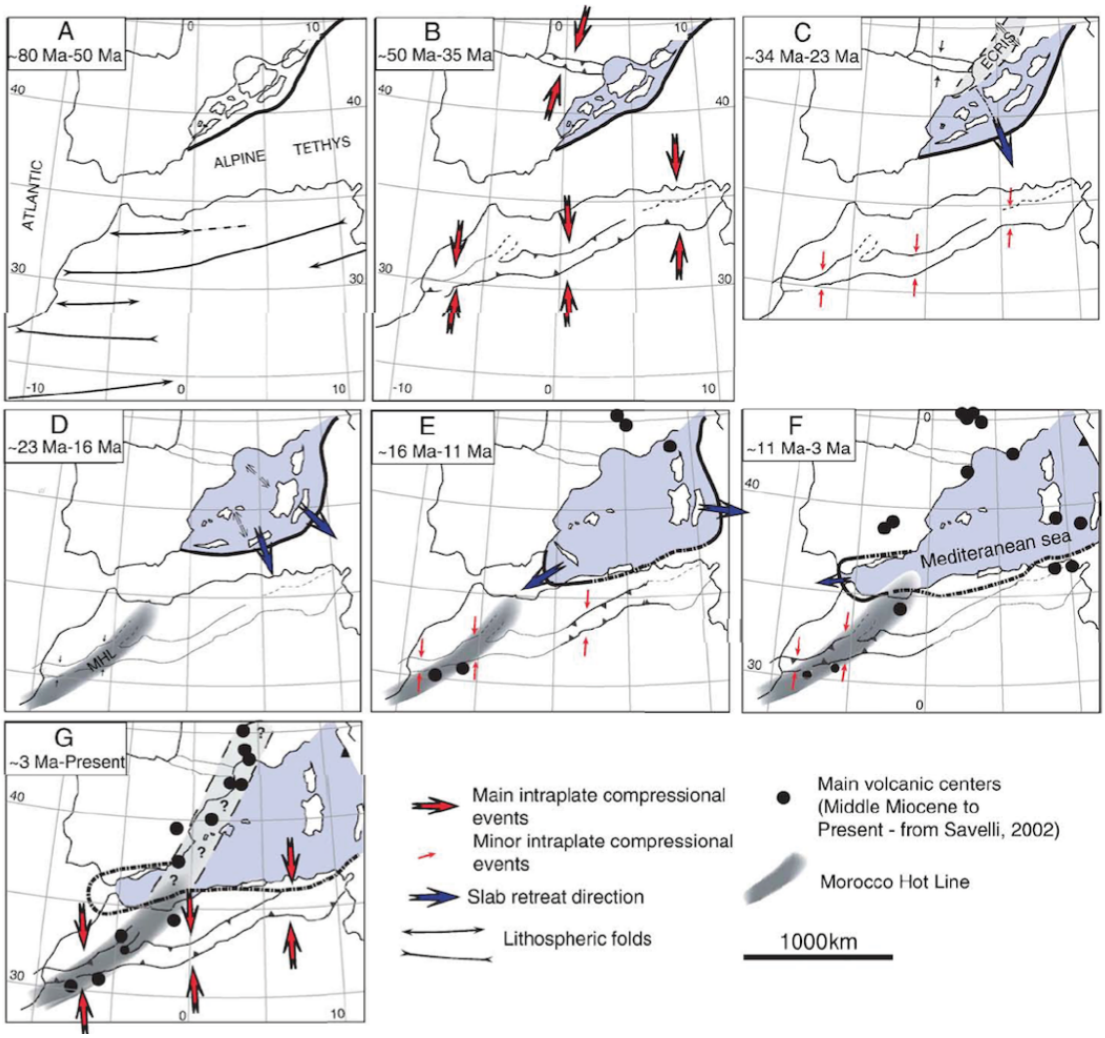

Figure 1.55. Schematic kinematic scenario for the Maghreb and western Mediterranean since the Upper Cretaceous (Frizon de Lamotte et al., 2009). A: Initiation of the subduction of the Alpine Tethys and development of lithospheric folds in the Maghreb area; B: First general inversion of the Atlas basin (first Atlas event) followed by the initiation of the slab roll-back in the Mediterranean area; C and D: Slab roll-back, development of the Tell-Rif accretionary prism, formation of the West Mediterranean basin (violet color) as an oceanic (or with thinned continental crust) basin. The southern termination of

the European Cenozoic Rift System (ECRIS) is indicated and also the possible initiation of the Morocco Hot Line (MHL). E and F: docking of the Kabylies (pertaining to the AlKaPeCa domain) on the African margin, tearing of the lithosphere along the North-African margin and development of the MHL. G: second inversion of the Atlas system (second Atlas Event). At that time, the slab is almost completely detached.

A third category considers an initial subduction zone dipping to the S-SE under the African margin (Alpine-type) that rolled back first northward and progressively to the NW (Vergés and Fernández, 2012). The reconstruction is mainly based on data coming from the Betic Cordillera. Subduction starts in the Upper Cretaceous and the involvement of the Iberia margin occur at the end of the Oligocene and the beginning of the Miocene (Fig. 1.56).

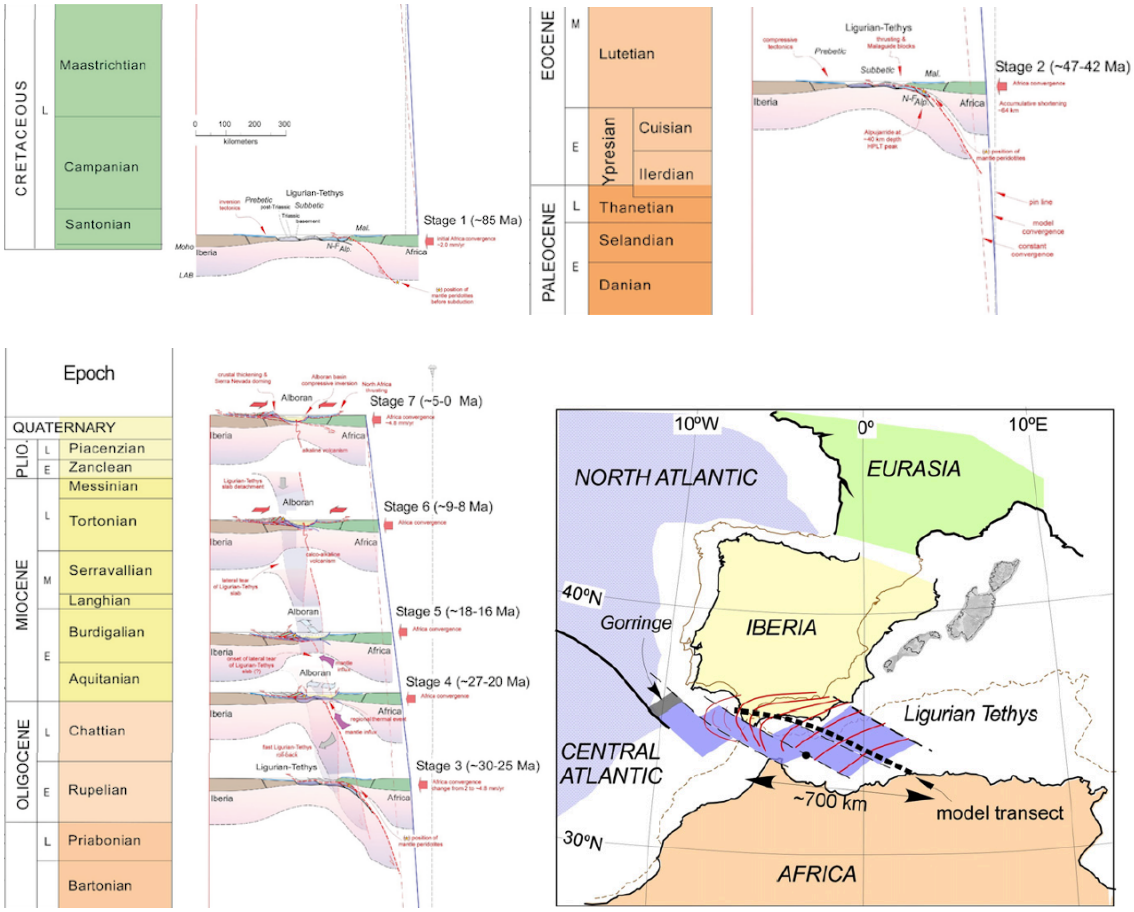

Figure 1.56. Crustal kinematic model showing the general evolution of the Betic–Rif system and its timing (see location in Fig. 7). The different steps are based on the chosen time periods, which are constrained by geological and geophysical data as discussed in the text and in Fig. 8. The dashed line on the right side of the model represents a constant rate of Africa convergence from Upper Cretaceous to present. The blue line shows the modeled convergence velocity, which increases in the last 30 m.y. Below rightMap reconstruction of the proposed Ligurian–Tethys domain between Iberia and Africa during Late Cretaceous before the onset of the African convergence. Most reconstructions of this area depict an irregular and segmented geometry for the Atlantic–Alpine–Tethys corridor. The dashed thick line shows the approximate trace of the section used to illustrate the proposed kinematicmodel depicted in Fig. 9. Thin continuous and dashed brown lines show the present positions of Iberia and Africa, respectively.

QUESTIONS

Apparently all these hypotheses and the models described hereabove are supported by data and it is difficult to choose the best hypothesis based on the published information. Fieldwork data presented in the following two chapters permit to identify the main structural features related to **displacement** of the Alboran rocks and to the structures responsible for the **mantle** exhumation. The position of the trench at 20 Ma appears to be a key to decipher between the above mentioned models.

1.4 The Ronda Peridotite: field, working hypotheses and geophysical insights

The integration of the Ronda Peridotite exhumation and crustal emplacement is key to constrain the geodynamics scenario of the Western Mediterranean. This section describes the main geological features of the Ronda Peridotite and aims at introducing mainly Chapter 3 and 4. However, the poliphasic deformation and the complex history related to the emplacement led to plenty of hypothetical tectonic model. In the following, three subsections follow a general overview. The first subsection describes the structures and the lithology at the top of the Ronda Peridotite, the second one the base of the Ronda Peridotite and the metamorphic rocks below, the third subsection the different mantle exhumation models proposed.

The Ronda Peridotite crops out close to the Gibraltar strait in Southern Spain. Together with the Beni Bousera massif in the Rif they form the largest subcontinental mantle body exposed at the surface in the world (Afiri et al., 2011; Darot, 1974; Obata, 1980; Johanesen et al., 2015; Kornprobst, 1974; Reuber et al., 1982; Frets et al., 2014). The position of the mantle rocks, exactly where the arcuate trend bends, coincides with the gravity anomaly reported for example by Bonini et al. (1973) and Torné et al. (2000). The Ceuta serpentinitic sliver is the link between the Spanish and the Moroccan peridotite bodies and suggests an original continuity between the peridotitic outcrops on the two sides of the arc (Sánchez-Gómez et al., 2002) (Fig. 1.57).

Some authors have put the serpentinite at Cabo de Gata and Beni Malek in relation with Ronda (Michard et al., 2014; Sánchez-Gómez et al., 2004) but these serpentinites emerge in a different structural position in the belt, in the Infrarif, and are not related with the Alboran outcrops. The Ronda-Beni Bousera mantle are indeed pinched in between Alboran crustal rocks that are ascribed to the Alpujarride tectonic group and contain, as a main peculiarity, diamonds or graphite pseudomorphes after diamonds (Pearson et al., 1989; Davies et al., 1993). We can divide the Ronda Peridotite into three massives: Sierra Bermeja, Sierra Alpujata and Carratraca, which are clearly connected by small serpentinitic outcrops

(Navarro-Vilá and Tubía, 1983; Sánchez-Goméz et al., 1999) (Fig. 1.57).

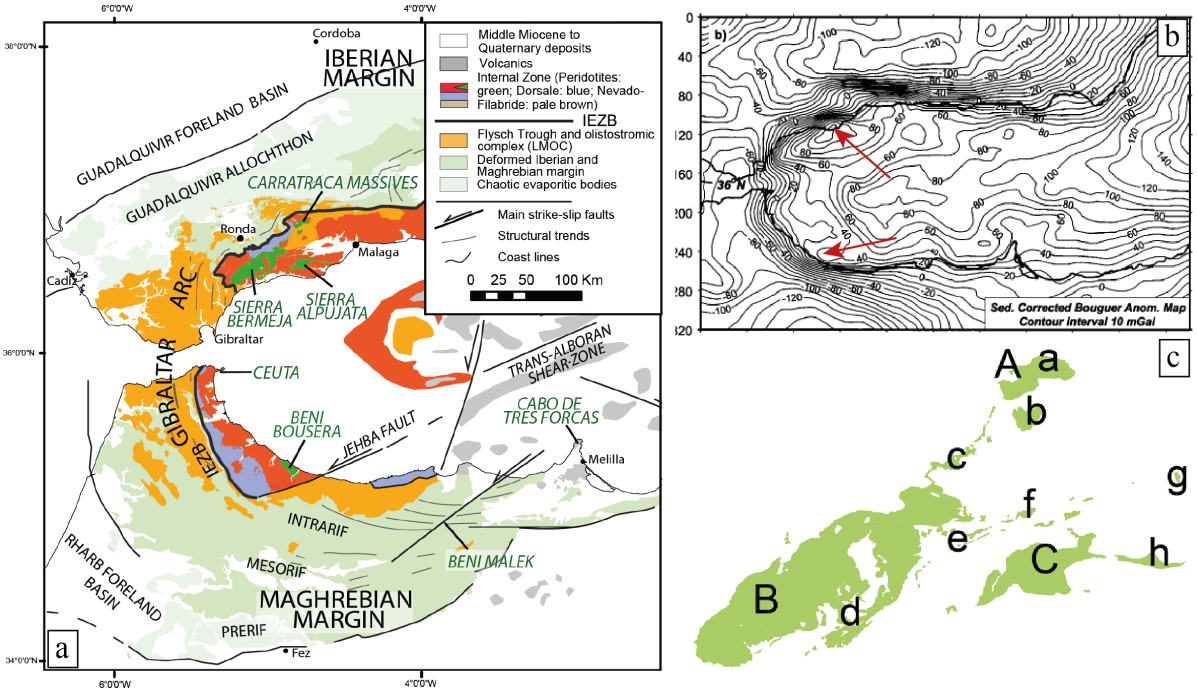

Figure 1.57. (a) Position of the main peridotite and serpentinite bodies in the westernmost Betic-Rif region (modified after Frasca et al., 2015). (b) Arrows show the gravity anomaly highs close to the Ronda and Beni Bousera Peridotite outcrops. (c) Location of the Ronda Peridotite outcrops. A: Carratraca; B: Sierra Bermeja; C Sierra Alpujata (reported also on the figure on the left). a: Sierra de Agua; b: Sierra de la Robla; c: Tolox-Yunquera serpentinitic outcrops; d: Montemayor slivers; e: Istán serpentinites; f: Sierra Pelada; g: Cartama serpentinites; h: Sierra de Mijas.

These three massives composing the Ronda peridotite have as a main characteristic the roughly concentric pattern of all three peridotite facies (i.e., garnet-, spinel- and plagioclase-peridotite facies; Obata, 1980) in a coherent outcrop of 300 km^2. Several structural-petrological studies of this massif (Lenoir et al., 2001; Précigout et al., 2013; Soustelle et al., 2009; van der Wal and Vissers, 1993, 1996) show that the three facies domains are related to and coincide with the progressive development of three different structural domains (Fig. 1.58). These structural domains are (1) foliated garnet-bearing peridotites at the top of the massif, (2) coarse-grained granular spinel peridotites in the central part, and (3) porphyroclastic plagioclase tectonites at the base. The km-scale grt-sp mylonite defines the top of the mantle sliver (Precigout and Van der Wal) and was formed in conditions of subcontinental mantle with decreasing P conditions, starting at 85 km, by grain size reduction and dynamic recrystallization (Balanyá et al. 1997; Argles et al., 1999 ; Tubía et al., 2004; Précigout et al., 2007; Précigout et al., 2013). The plagioclase tectonites define the base (Van der Wal and Vissers, 1996) and developed in shallower conditions because the deformation evolved to low-T and low-P mylonites (Hidas et al., 2013; Hidas et al., 2015) (Fig. 1.58). In the next two subsections we describe first the top and associated crustal rocks and then the base with the underlying rocks.

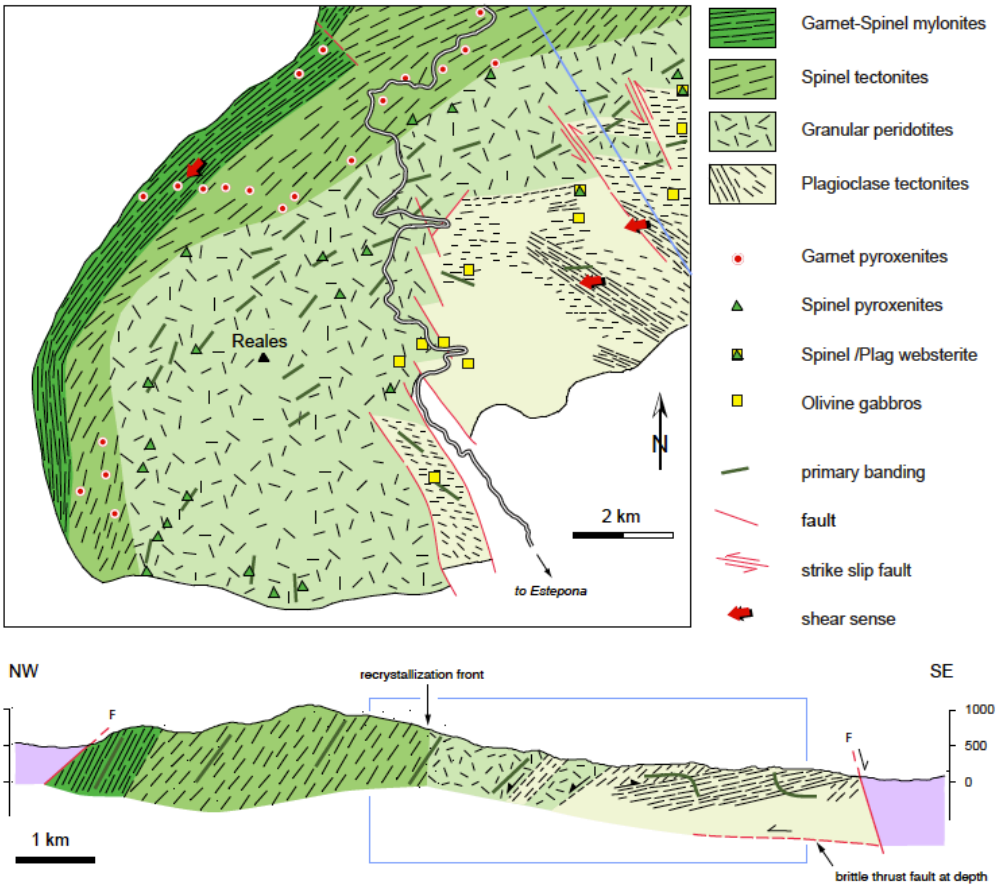

Figure 1.58. Structural map and cross section of the Ronda peridotite of the western Sierra Bermeja (see Fig. 1.57) (Vissers, 2012). Note that cross-section is partly outside the map area, and is presented at a larger scale than the map, to allow more detail (location of cross-section shown partly in Fig. 1.64). Domain in the blue rectangle represents part of the section seen along the (blue) section line in the northeast corner of the map.

1.4.1 Exhumation and HT metamorphism

Crust-mantle extensional shear zone

At the top of the Sierra Bermeja a progressive transition from near coaxial thinning to strain localization in the Ronda garnet-spinel mylonite is the result of grain size reduction and subsequent activation of low-temperature grain size -sensitive processes (Précigout et al., 2007). During lithosphere thinning coaxial deformation dominates at incipient extension (Précigout et al., 2013), while the shear deformation component becomes more dominant as continental necking takes place. Note that for Johanesen et al. (2015) simple shear deformation has been always dominant. S-C structures form at the beginning of the deformation and then discrete shear bands at ~40° form as a consequence of the steepening of the main shear plane with the increase of the continental thinning (Précigout et al., 2013) (Fig. 1.59).

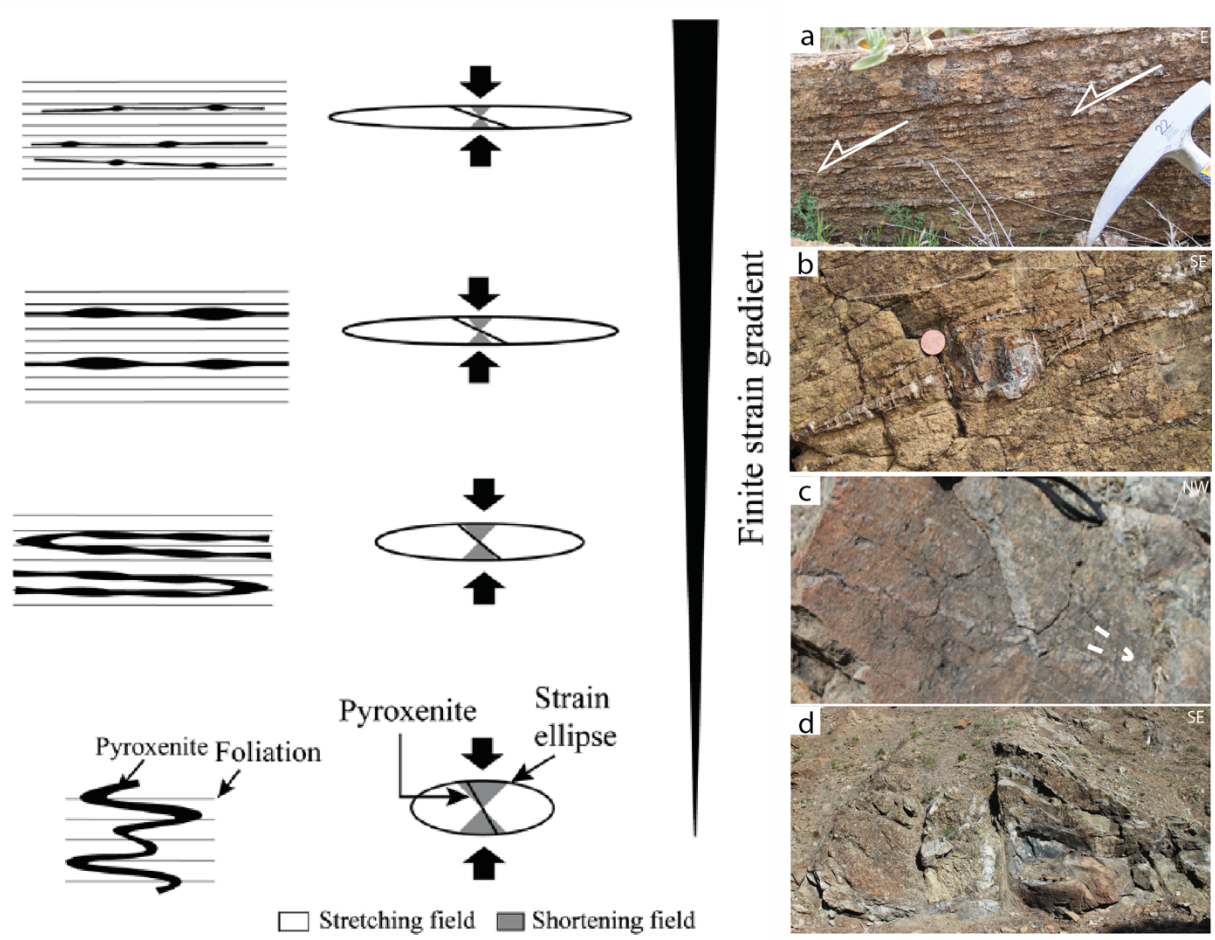

Figure 1.59. Deformation pattern of meter-scale pyroxenites from the granular peridotite to the Grt/Spl mylonite. This evolution describes a change in deformation pattern of passive lines (pyroxenites) from shortening (folding) to stretching (boudinage) fields with increasing ductile strain of the peridotites (from Précigout et al., 2013). The outcrop pictures are from the Carratraca massif (Photographs by G. Frasca). (a) Shear bands at ~40°; (b) boudinated garnet-pyroxenite layer in the spinel-tectonites; (c) stretched and folded pyroxenite layer; (d) folded pyroxenite layer.

The P-T path reconstructed by Garrido et al. (2011) is based on petrographic evidence for the existence of prekinematic, coarse-grained garnet lherzolite assemblages (2.4-2.7 GPa and 1020-1100ºC) in the garnet-spinel mylonite domain, demonstrating that the Ronda peridotite equilibrated at ~85 km depth before shearing. The synkinematic garnet and spinel assemblages overprint the garnet lherzolite assemblages at 800-900ºC and 1.95-2.00 GPa (Fig. 1.60a). The decompressional cooling path and high pressure recorded by garnet-spinel mylonites rule out their formation by near-isobaric cooling above a subduction-collision wedge or during or after the emplacement of the peridotite massif into the crust and favour the interpretation of the formation at early stages of lithosphere extension.

Moreover, gabbroic rocks similar to those occurring in the mantle section of ophiolites or continent–ocean transitions crop out in the plagioclase tectonite (Fig. 1.60c) domains of the Ojén and the Ronda orogenic peridotite massifs as discordant dikes and anastomozing patches, respectively (Hidas et al., 2015) (Fig. 1.60a). Geochemical evidence shows that Ronda gabbroic patches and Ojén discordant dikes crystallized from similar parentalmelts with an island arc tholeiitic affinity. Ojén gabbros represent magmatic segregates in dikes, while

Ronda gabbroic patches record crystallization of trapped melts in dunite channel at decreasing melt mass upon cooling. Intrusion of Ojén gabbro dikes is coherent with the stress field that formed the high temperature, ductile plagioclase tectonite foliation and then attests for a mantle igneous event prior to the intracrustal emplacement of the massif. Geothermobarometric data and liquidus mineralogy indicate that gabbro crystallization occurred at shallow depths (0.2–0.5 GPa) in a 7–16 km thick lithospheric section (Hidas et al., 2015).

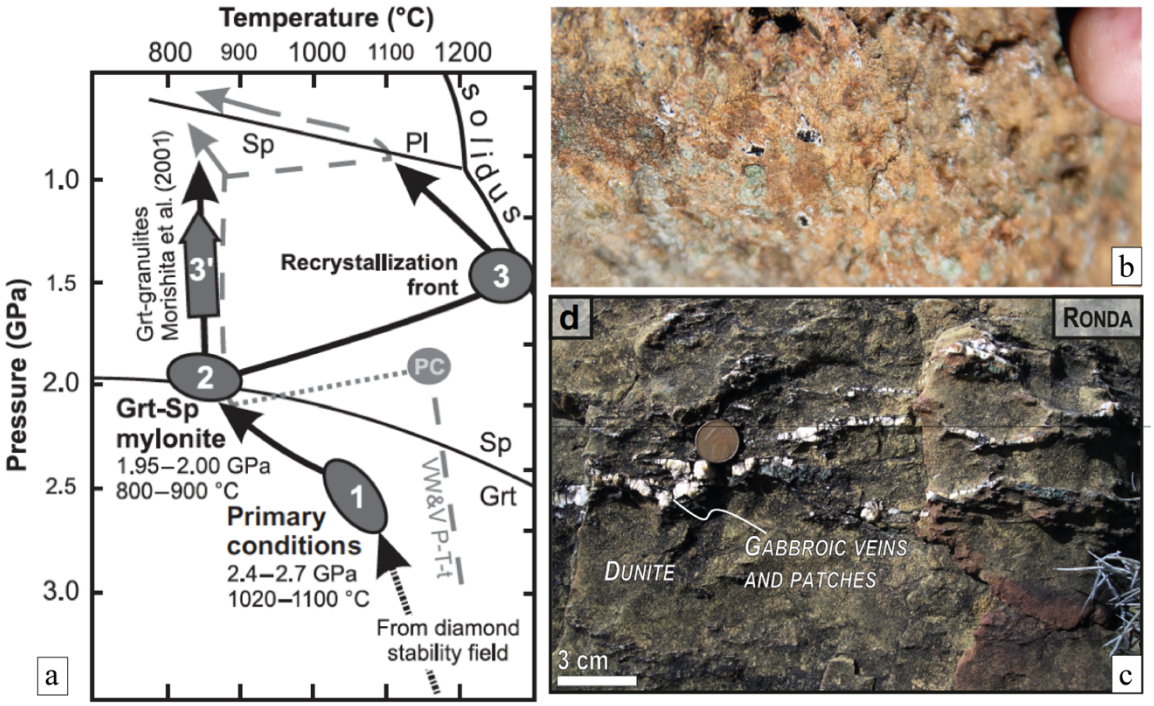

Figure 1.60. Characteristics of the Ronda Peridotite. (a) New pressure-temperature-time (P-T-t) path for the Ronda peridotite (black path; dark gray ellipses depict different equilibration stages) and previously proposed P-T-t path (Van der Wal and Vissers, 1993; gray path labeled VW&V P-T-t). PC—primary conditions of Van der Wal and Vissers (1993); Grt—garnet; Sp—spinel; Pl—plagioclase. (b) Plagioclase–peridotite in the Tolox region (Photograph by G. Frasca). (c) Gabbro veins intruding the spinel tectonite (from Hidas et al., 2105).

The crustal envelope: attenuated section of continental lithosphere

The Jubrique Group is at the top of the Ronda Peridotites and consists of the Jubrique Unit and the overlying Benarraba imbrications (Balanyá et al., 1997). Specifically, the Jubrique Unit (Balanyá et al, 1997) contains a 5-km-thick metamorphic succession of, from bottom to top, garnet gneiss, migmatite gneiss, staurolite-bearing schists, chloritoid-bearing schists, fine-grained schists, quartzites, and carbonate rocks, with little or no evidence of recrystallization (Loomis, 1972; Sanz de Galdeano et al., 1999) (Fig. 1.61).

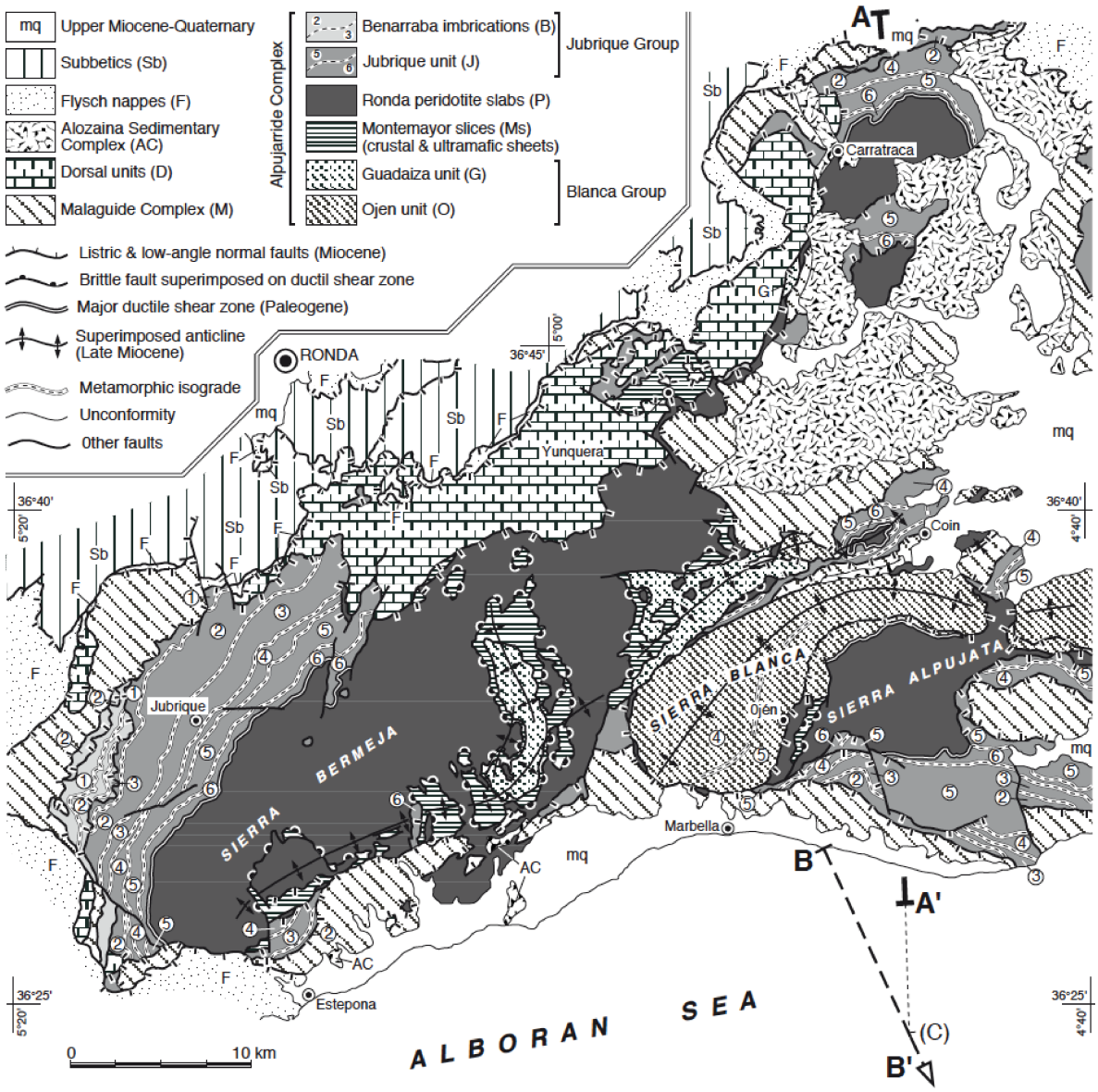

Figure 1.61. Tectonic map of the Western Betics Alboran Domain by Sánchez-Gómez et al., (1999)

The Jubrique unit has upward-decreasing metamorphic grade, with metamorphic isograds parallel to the main foliation and to the lithological contacts (Negro et al., 2006) (Fig. 1.62). At the base, mylonitic gneisses provide peak conditions of ≈850 °C and 12–14 kbar, corresponding to cores of large garnets with inclusions of kyanite and rutile Barich et al., 2014). Probably these conditions are related the hercynian HP commonly reported in the area (Zeck and Whitehouse, 2002; Ruiz Cruz and Sanz de Galdeano, 2014). Thermodynamic modeling and conventional thermobarometry of mylonitic gneisses provide then post-peak conditions of ≈800–850 °C and 5–6 kbar, represented by rim regions of large garnets with inclusions of sillimanite and ilmenite, cordierite-quartz-biotite coronas replacing garnet rims, and the matrix with oriented sillimanite (Barich et al., 2014).

This general parallelism is produced during an extensional event (Argles et al., 1999; Balanyá et al., 1997; Torres-Roldán, 1979); at the same time, the Jubrique Unit thinned probably one-third untill to one-twentieth of its original thickness (Argles et al., 1999;

Balanyá et al., 1997). Thus, the surprisingly complete lithological sequence of the Jubrique Unit roughly corresponds to a segment of condensed continental crust (Balanyá et al., 1997). The top of the crustal section (Benarrabá imbrications for Balanyá et al., 1997) consists of lithologic sequences similar to the upper third of the Jubrique Unit, normally comprising chloritoid-bearing schists up to the formation of carbonates and, more locally, staurolite-bearing schists in a lowermost position.

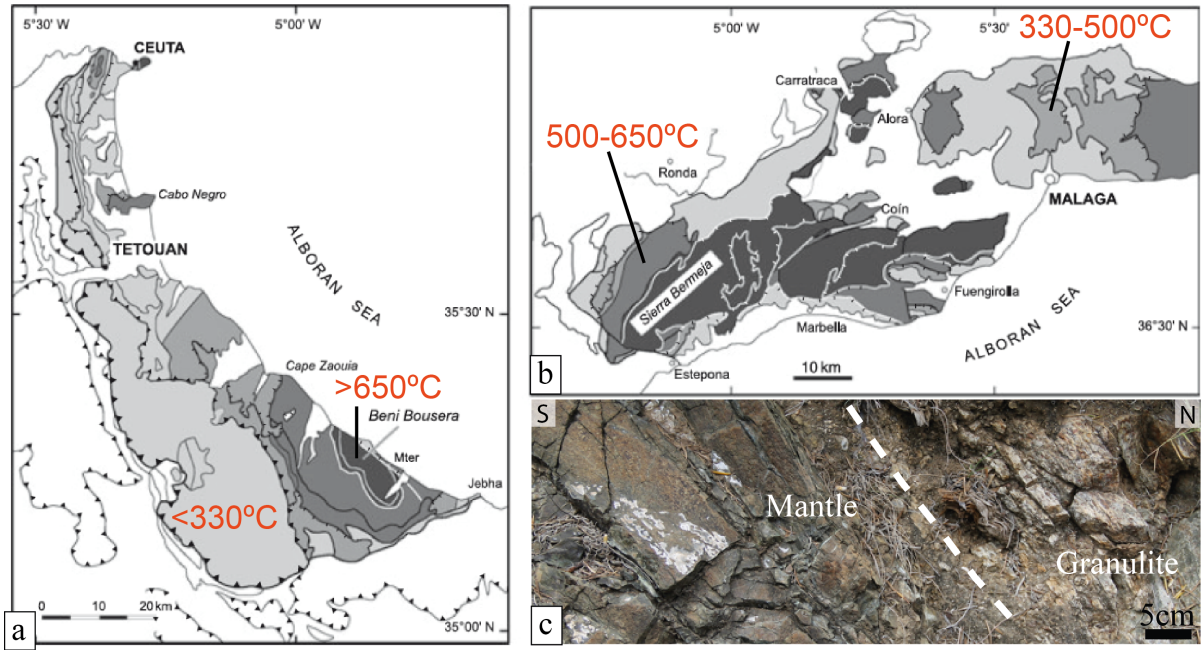

Figure 1.62. Map of the isotherm in the Rif and in the Western Betics (b). The T associated to the colours is indicated on the figure. (c) A unique continuous exposure of the crust-mantle interface, reported and sampled by Argles et al. (1999), in the north-eastern Sierra de Agua (Carratraca, Photograph by G. Frasca).

The exhumation and the cooling of the mantle along the extensional shear zone located at its top is dated in garnet pyroxenites (Sm-Nd age of 21.5 ± 1.8 Ma on garnet and clinopyroxene, Zindler et al., 1983) (mean Lu-Hf ages of 25 ± 1 Ma or 24 ± 3 Ma on garnet (Blichert-Toft et al., 1999; Pearson and Nowell, 2004). Moreover, the stretched leucosomes within the foliation (U-Th-Pb age of 21.37 ± 0.87 Ma on monazite, Gueydan et al., 2015, and U-Pb age of 22.0 ± 0.3 Ma on zircon, Platt et al., 2003b) give similar result.

1.4.2 Emplacement and HT metamorphism

The Ronda Peridotite Thrust

Melting and melt-rock interaction processes at the base of the Ronda Peridotite have occurred during the peridotite emplacement into the crust along high-temperature plagioclase-facies shear zones developed in the deeper parts of the spinel-facies granular peridotites. Most plagioclase tectonites show a top-to-N directed shear, but a later set of narrower plagioclase tectonite shear zones show south and west directed displacements (Van der Wal and Vissers, 1996). The syntectonic plagioclase assemblages indicate that the shear zones developed

during exhumation of the peridotite toward crustal levels (Hidas et al., 2013). Cooling ages of hornblende bearing leucocratic dikes (~22 Ma; Esteban et al., 2011; Priem et al., 1979), transecting the plagioclase tectonites suggest that this plagioclase tectonites form before the exhumation of the peridotite (Vissers, 2012).

The thrust emplacement of the Ronda Peridotite occurs along the metamorphic sole cropping out in the Sierra Bermeja and Sierra Alpujata massives. Both of them consist of migmatites and quartzo-feldspathic mylonites mainly (Fig. 1.63), but differ in significant aspects like thickness, pressure conditions and kinematics (Tubía et al., 2013). The migmatites of the Guadaiza sole record temperatures of 725º C and pressures of 0.6 GPa (Esteban et al., 2008). Recent estimations with phase equilibria modeling of the stromatic migmatites at the base of the Ojén sole shows P-T conditions of equilibration of 0.45-0.5 GPa, 660-700 °C (Bartoli et al. 2013) (for location see Fig. 1.63B). T higher than 510ºC and a P about 0.3 GPa have been recently proposed by Mazzoli et al. (2013) for the metamorphic sole developed in the Dorsale rocks. The preservation of restitic andalusite crystals replaced by cordierite points to pre-migmatization conditions in the andalusite stability fields, at maximum temperatures of 525º-550º C and pressures of 0.35-0.45 GPa. The proposed P-T path for the Guadaiza dynamothermal aureole (Esteban et al., 2008) involves thus most probably a slight increase in pressure during the migmatization (Précigout et al. 2013).

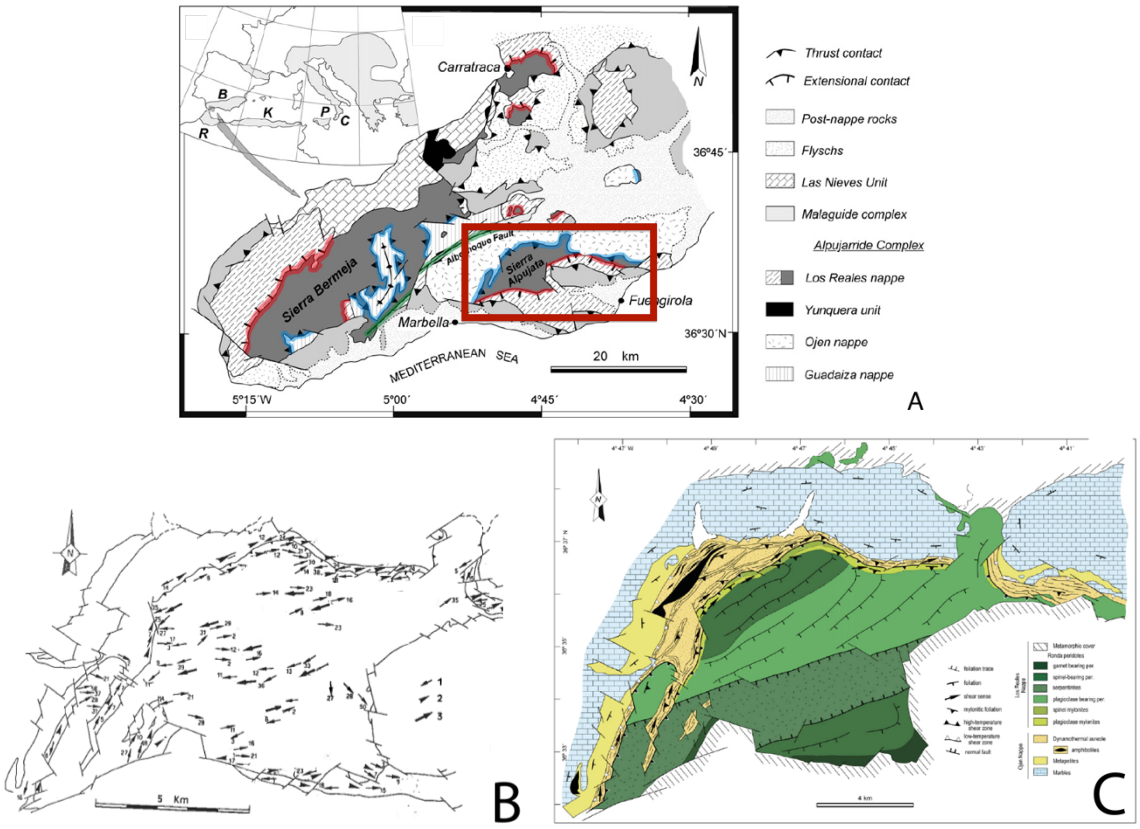

Figure 1.63. Ronda metamorphic sole and detail of the Sierra Alpujata massif (A: Simplified geological map of the western part of the Betic Cordilleras (modified from Navarro-Vilá and Tubía, 1983), showing major levels of deformation localization along the lower (blue colour) and upper (red colour) boundary shear zones of the Ronda

peridotites (from Tubía et al., 2013). B: Lineation map. In arrow labeled with 1 the numbers close to the lineations indicate the dip. In 2 and 3 the arrows indicate the sense of shear (2: low-T high-P lineation related to thrusting; 3: high-T low-P due to rising astenosphere) (from Tubía and Cuevas, 1986). C: Structural map showing the metamorphic sole of the Ojen nappe, associated to the hot emplacement of the Sierra Alpujata peridotites. Note that the basal shear zone defined by the mylonitic bands intersects the metamorphic zoning of the peridotite massif (from Tubía et al., 2013).

Alpujarride below the Ronda Peridotite

The metamorphic sole cuts across the structures (folds and axial-planar cleavage), of the underlying metamorphic schists (Esteban et al., 2008) and also at high angle with the large-scale layering in the peridotite (Figs. 1.63C).

The Blanca Group (Balanyá et al., 1997) is cropping out below the metamorphic sole and consists of, in ascending order, the Ojén, Guadaiza and Yunquera Units, all containing high-grade metamorphic rocks, also Mesozoic (Navarro-Vilá and Tubía, 1983; Esteban et al., 2005).

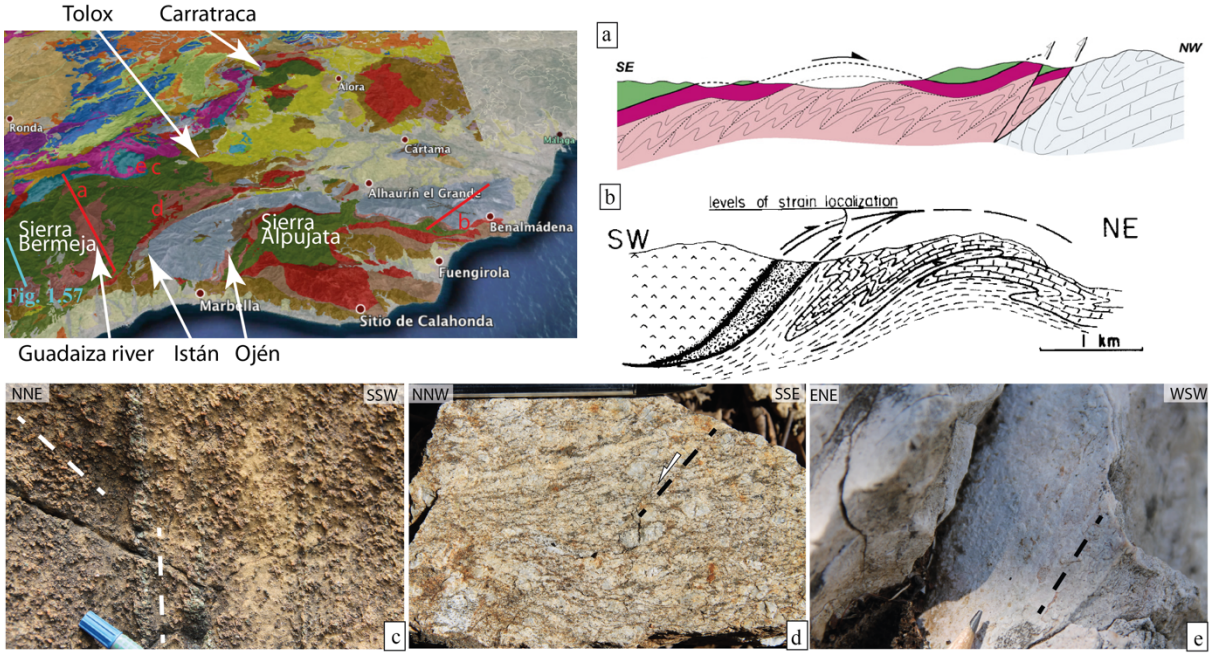

Figure 1.64. 3D view of the geological map on Google Earth topography (see section 1.6, Methods) with position of the localities cited in the text. (a) SE-NW cross-section (Esteban et al., 2008) and (b) SW-NE cross-section (Tubía et al., 1997). Photographs (by G. Frasca) for deformation close the metamorphic sole. (c) Foliation intersecting at high-angle a piroxenite layer. (d) Migmatites in the metamorphic sole of the Ronda Peridotite Thrust. (e) Marble in the Dorsale with a lineation defined by elongated calcite and tremolite. Locations of the photographs and of the cross-sections are reported on the 3D view.

The Ojén Unit, which underlies the Alpujata peridotite massif, is a large-scale recumbent syncline whose reverse limb crops out at the Sierra Blanca in the core of a late superimposed Miocene anticline (Fig. 1.64B). The recumbent synclinal core contains thick marbles (Triassic protoliths) and the limbs contain high-grade schists, amphibolites, and gneissic rocks (Sanz de Galdeano and Andreo, 1995). Minor folds and a penetrative axial-plane foliation overprint the main foliation (Orozco and Alonso-Chaves, 2012). The highest pressure in the Ojén metamorphic sole is recorded by eclogitoids preserved as boudins in amphibolites. Minimum estimated conditions at the metamorphic peak yield 790º±15 C and

1.74 ±0.1 GPa (Tubía and Gil Ibarguchi, 1991). The decompression path starts with an increase in temperature. However, the Lower Miocene age of the peak pressure is questionable and the age obtained is most probably related to the HT event (Sánchez-Rodriguez and Gebauer, 2000).

The Guadaiza Unit contains a monotonous sequence of quartzites, high- and medium-grade schists, gneiss, and minor amounts of metamafics. Marble bodies are included within a thick fault zone overlying the unit (Sánchez-Gómez et al., 1999).

The Yunquera Unit is composed of migmatitic gneisses and Mesozoic metasediments (marbles and schists) (Esteban et al., 2005; Martín-Algarra, 1987). The age of the HP metamorphism in the metasediments of this unit is unknown.

1.4.3 Models for the Ronda Peridotite exhumation

The tectonic processes postulated to justify the exposure at the surface of the Ronda peridotites changed through time. The idea of a **mantle "diapirism"** was the first one to arise to explain the outcrops of the Ronda peridotites and developed by Van Bemmelen (1969) and Loomis (1972). These authors associate the emplacement of the Ronda and Beni Bousera peridotite massifs with the gravitational emplacement of the Betic nappes. This hot "astenospheric diapir" is considered as well responsible for the metamorphism in the Alpujarride/Sebtide (Loomis, 1972).

The concept of diapirism has been then progressively abandoned, with few rare exceptions (e.g. Tubía et al., 2004), and substituted by core-complex structures (Doblas and Oyarzun, 1989) (Fig. 1.65a) or by rift structures (Tubía and Cuevas, 1986) (Fig. 1.66). Starting then with Lundeen (1978) the rift hypothesis has been criticized and the thrust emplacement has been emphasized (Tubía and Cuevas, 1986; Vauchez and Nicolas, 1991). A strike-slip kinematics has been often related to the rifting-exhumation hypothesis, leading to the hypothesis of a transpressional extrusion of a mantle wedge (Darot, 1974; Tubía and Cuevas, 1986; Vauchez and Nicolas, 1991; Tubía et al., 1997; Mazzoli and Martín-Algarra, 2011) (Fig. 1.65b).

The timing of this extrusion and exhumation is also debated. Late- to post-Variscan extension has been proposed on the base of the Variscan ages of the zircons in the high-temperature rocks at the boundary with the Ronda Peridotites (Ruiz Cruz and Sanz de Galdeano, 2014). Moreover, spinel from peridotites is reported as clastic in Mesozoic rocks (Kornprobst, 1976). As a second hypothesis, the transcurrent movement between the Iberia and Africa plates can permit rifting and exhumation during Upper Cretaceous (Reuber et al., 1982). In this case a subduction follows the break-up of Pangaea and the opening of the Tethyan Ocean (Chalouan et Michard, 2004; Vissers et al., 1995; Van Hinsbergen et al., 2014 Van der Wal and Vissers, 1993; Vissers *et al.*, 1995) (Fig. 1.65c). Modern geochronology suggests abandoning all these hypotheses in favour of a Lower Miocene crustal emplacement.

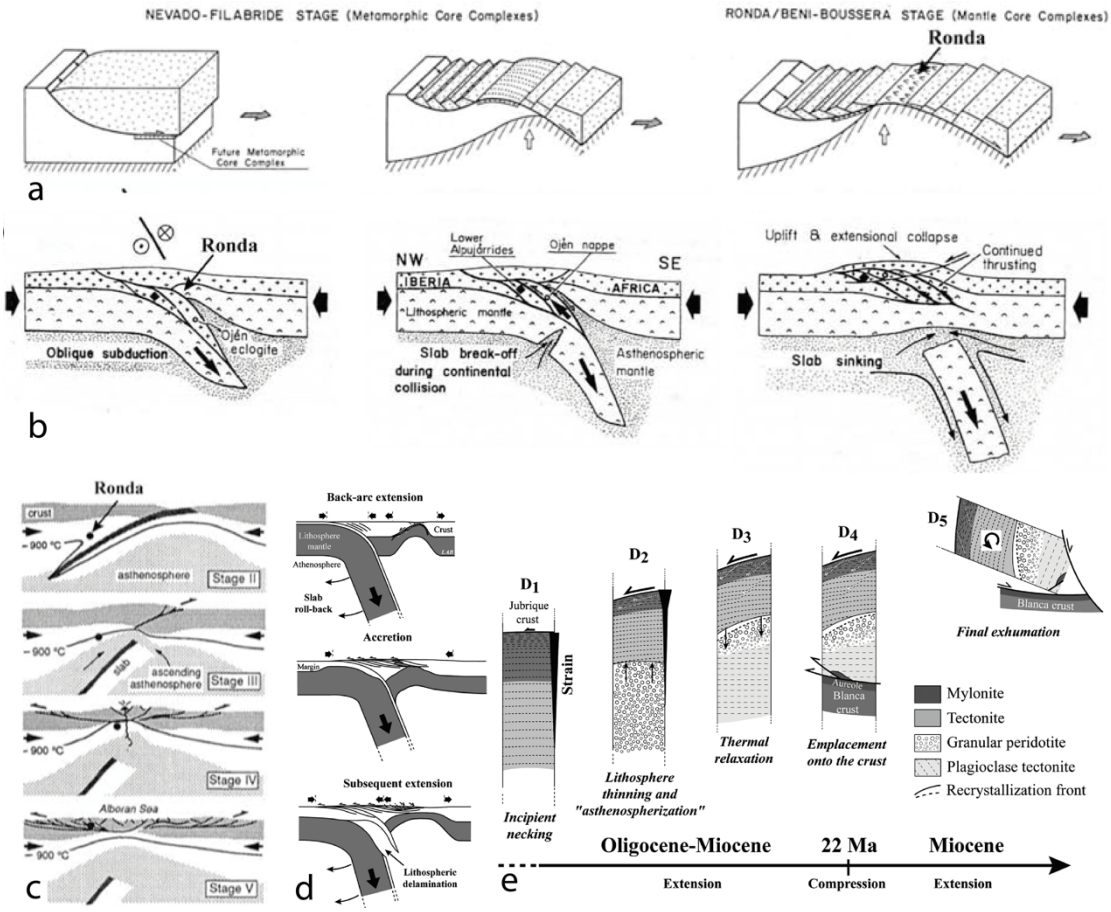

Figure 1.65. Tectonic models for the Ronda Peridotite exhumation. (a) Core-complex exhumation (Doblas and Oyarzun, 1989). (b) Oblique extrusion along a subduction zone (Tubía et al., 1992). (c) Gravitational collapse (Van der Wal and Vissers, 1993) and (d) back-arc rift inversion (Précigout et al., 2013). (e) Stages of the evolution from extension to emplacement (Précigout et al., 2013).

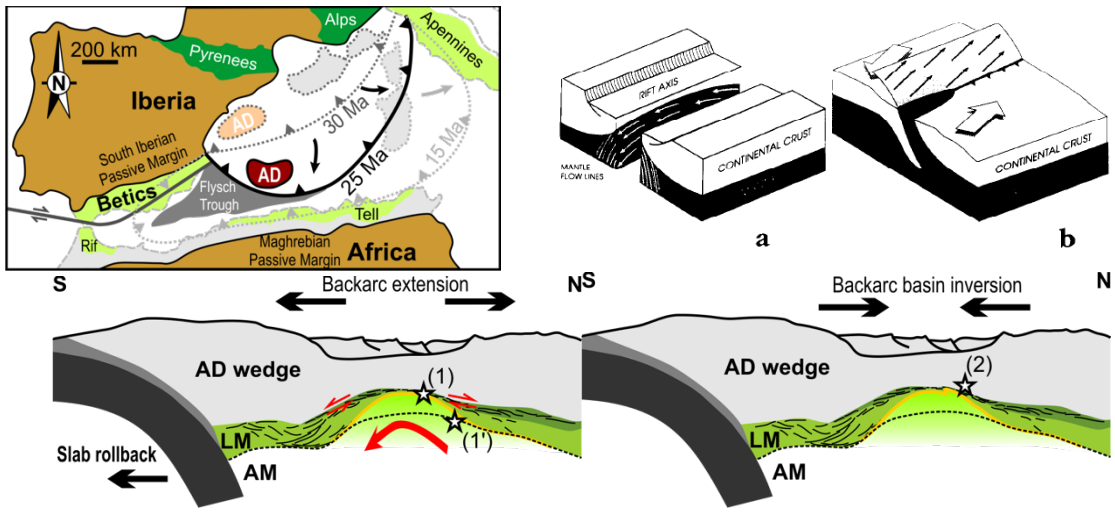

Figure 1.66. Top left, geodynamic reconstruction showing the tectonic scenario proposed for the westernmost Mediterranean for the Late Oligocene–Early Miocene. AD, Alborán Domain including Ronda Peridotite (From Hidas et al., 2013). Top right, reconstruction of the rift-inversion after Tubía and Cuevas (1986) with a strike-slip kinematics (from Vauchez and Nicolas, 1991). The inversion occurs in the Alboran Domain, although if the exact location is not specified. Below, on the left, north–south cross-section for the Late Oligocene back-arc extension. In the figure, (1) denotes the formation of grt–spl mylonites owing to back-arc extension and (1') refers to partial melting at the base of the lithosphere induced by asthenospheric upwelling. Below, on the right

north–south cross-section for the Late Oligocene–Early Miocene back-arc basin inversion that led to kilometre-scale folding, referred as (2) in the figure (from Hidas et al., 2013). No strike-slip displacement are supposed in this case.

Two main scenarios have been proposed for the Lower Miocene tectonic evolution of the Ronda Peridotite. The first scenario involves the action of crosscutting detachment faults during the extensional collapse of the Betic-Rif chain (Van der Wal and Vissers, 1993; Platt et al., 2003d) (Fig. 1.65c). In this proposal the Ronda Thrust is an extensional shear zone and the garnet-spinel mylonite at the top of the Ronda Peridotite, described above in the section, is related to the subduction (Van der Wal and Vissers, 1996). The second scenario involves Oligocene back-arc lithospheric extension and subsequent tectonic inversion as reported in several recent papers (e.g. Garrido et al., 2011). In this case the garnet-spinel mylonite at the top is the structure accomodating the back-arc extension (Fig. 1.66). However, uncertainites remain in the timing, the location and the kinematics of the inversion (e.g. Hidas et al., 2013; Vauchez and Nicolas, 1991) (Fig. 1.66).

QUESTIONS

Recent works indicated that the extensional structures were responsible of mantle exhumation during the rifting to a maximum depth of 15 to 20 km (Garrido et al., 2011; Précigout et al., 2013). However, a very shallow depth is associated to gabbro intrusions into the mantle (Hidas et al., 2015). The **amount** of **thinning** is the aim of the investigation in chapter 3. The **timing** of the exhumation is studied further in Chapter 4 where we verify also the sequence of **extension** and **compression** events described above in the first two subsection. The paleomagnetic rotation described can, at least partly, be justified by the strike-slip faults that accompany the Ronda Peridotite Thrust described in Chapter 2. Another open question is where the exhumation of the Ronda Peridotite has happened. The answer has great importance for the geodynamical reconstruction of the western Mediterranean. Field data from study in chapter 2 suggest that the amount of displacement of the Ronda Peridotite after the exhumation is limited.

1.5 SUMMARY OF MAIN QUESTIONS AND CONTRIBUTIONS

1.5.1 Question 1: Alboran displacement relative to Iberia

The direction of the Alboran displacement has been debated in the past. The question is which structures in the Western Betics accommodate the motion. Three kinds of faults commonly reported in the literature (N140, N50 and E-W trending) can have a role in the displacement. Furthermore, the timing of the motion along this faults need investigation: the relationships between structures and deposition of the terrigenous basin has thus to be clarified. Moreover,

the amount of displacement has to be estimated. For this reason, we focus not just in the External Zone at the boundary with the Alboran Domain but also inside the Alboran Domain where it is possible to individuate reference surface displaced by the deformation zones.

METHODS

The approach started with a **compilation** of maps from literature and the creation of 3D model using google earth topography. **Re-mapping** of key areas has permitted to understand the relative relationships of the structure. The relation between thrusting and extension and strike-slip is resolved with structural **geometrical analyses** of the fault system and fault zones, during the collection of data on fault mirrors along the large-scale deformation zones. Furthermore, the acquisition of outcrop-scale folds data and the analyses of large-scale folding via the foliation trajectories have helped the comprehension of the tectonics of the area. Next, strain **kinematics** is extracted using FaultKin software with the support of FSA software. The estimation of the timing of the structures and of the amount of displacement is permitted by an additional field study devoted to the **sedimentary deposits** and literature collection of the ages. Finally, samples for **U-Th/He** dating are collected, in collaboration with Patrick Monié, with the goal to define the very late stage of uplift of rocks.

OUTCOMES: Chapter 2

The Alboran Domain is moving westward relative to Iberia during Lower Miocene. The consequences of this motion are the coeval action of the three kinds of faults in the Alboran Domain and at the boundary with External Zone and the syn-tectonic deposition of a mainly Burdigalian terrigenous basin. The major E-W dextral strike-slip corridors, one of them newly identified, are interpreted as lithosphere structures reflecting tearing of the subduction slab at uppermost mantle level. The observed strain pattern is compatible with the nowadays GPS velocity-field data.

1.5.2 Question 2: Amount of continental lithosphere thinning

Extreme extension with gabbro intrusions has been recently reported (Hidas et al., 2015), but this is not in agreement with the thickness of the crust estimated from the previous study. As well, the age of the extensional structures reported from the crustal rocks is reported as, at least partly, younger than the thrust (Crespo-Blanc and Campos, 2001).

METHODS

After having constrained the thrust-related deformation and structures (Chapter 2), we have identified a key area to study rift-related structure: the **Carratraca** area is reported with extremely thinned crust and different sense of shear in the crust.

A large amount of measurement of main foliation, stretching lineation and analyses of **shear criteria** in the crustal envelope coupled with re-mapping permit the creation of a map with the crustal sense of shear at different levels. As also done for the previous study a

database of structural data published in the area and a relational GIS database with the new data in which each structures is reported georeferenced and with description of the feature has been done. The study of the **basin** close to key area associated to structures permits to define a relative timing for the thinning. The geometrical and kinematic analyses of the faults affecting the crustal envelop permits to address the sampling of a fault breccia for **Ar-Ar dating**, done in collaboration with Patrick Monié, along one of this fault.

OUTCOMES: Chapter 3

A unique preservation of the ductile deformation during rifting is observed in the crust at the top of Carratraca mantle massif. Extension is mainly accommodated by ductile deformation that allows the extreme thinning of the ductile crust and the juxtaposition of the upper crustal rocks to the mantle. The sense of shear is changing inside the crust during the rifting with important implications for the mechanics of the rifting. The rift is most probably Oligo-Miocene in age since brittle fault gouge related to rifting, posterior to the ductile deformation, have the same Lower Miocene Ar-Ar age of all the micas defining the fabrics in the Western Betics. Moreover, the base of the basin transgressive on the Alboran Domain is reported as Oligo-Miocene in age.

1.5.3 Question 3: From extension to thrusting

The literature shows two structures associated at the top and at the base of the mantle. Most authors indicate that the thrust at the base of the Ronda Peridotite is younger than the extensional structure at the top of the Ronda Peridotite. However, geochronological constraints are rare since HT metamorphism is evoked to have reset most of the previous ages (Monié et al., 1994).

METHODS

Fieldwork permits to establish the relative chronology between the structures. To obtain an absolute chronological value we perform a targeted collection of samples on the bases of the suitable database for the Betic-Rif chain. These samples, collected in areas where no previous ages were obtained before, are used for geochemical, petrographical and geochronological analyses. The geochronological analyses permit to obtain the absolute age of the magmatism. The U-Pb ages on zircons are obtained from the collaboration with Marc Poujol.

OUTCOMES: Chapter 4

We identify two stages of crustal melting: the first associated with the final period of the mantle exhumation, the second with the thrusting. The collected dikes are precisely dated at 22,5 and 20 Ma. These ages are consistent with the rift preceeding the thrust and indicate that the switch was extremely fast. The influence on the evolution of the low-T thermochronological data is also investigated.

1.6 Methods

Information Technologies (IT) have the capability to improve the usefulness of scientific information and their applications in earth sciences allow to make geological data more sharable among different users. This section illustrates the knowledge path followed for the analysis of the complex structural and geological setting described in the chapter. The approach is based on several working steps with a pre-fieldwork planning based on bibliographic work, a fieldwork stage and a sampling stage, with natural interplays between the different steps. In the next three subsections we go through the methods used during these steps.

1.6.1 Bibliographic work

The conceptual plan deriving from bibliographical investigations drives the acquisition of field data and gives rules for the GIS representation of the geological features (pre-fieldwork stage). The approach starts thus with a compilation of the published maps of the area. We georeferenced 115 maps of the western Betics and of the whole Betics. For the Rif the maps derive mainly from Chalouan et al. (2008) and Michard et al. (2014), for the Central Betics we used mainly the works of Platt and coworkers, and of Booth-Rea et al. (2005) and Azañon and Crespo-Blanc (2000) (Fig. 1.67). In the Western Betics all the papers cited in the references of this chapter have been used, when the articles contain a geological map. All the maps from the IGME (Instituto geologico-minero de España) have been used as well.

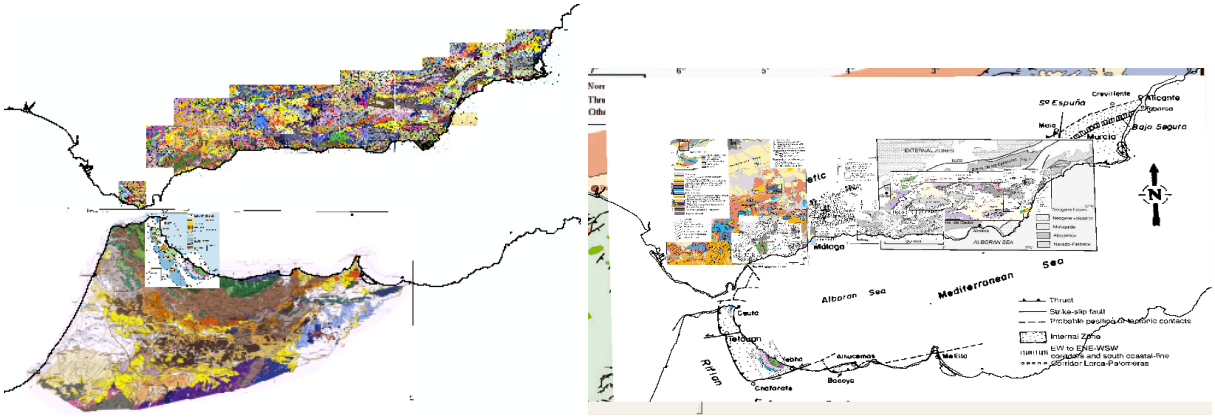

Figure 1.67. Compilation of the georeferenced maps used for the preliminary analyses before the fieldwork.

The new GIS database built initially with the synthesis of these data has more than 5500 polygons with different shapes. Five characteristics are attributed to each polygon: domain, major tectonic group, tectonic unit, type of rocks and age. The database is very useful to compile informative maps because different combinations of the attributes lead to different maps. Examples of possible combinations are reported throughout this chapter.The complexity of the polygons geometry is illustrated in Fig. 1.68, while Figure 1.68b contains a map in which different combinations of the attribute mainly based on the ages or the lithologies can be possible as reported in Figure 1.68b. Then, a second map in which the

different levels inside the crust and the different formations in the Subbetics are with different colours. The main challenge, beside dealing with the large size of the data, is the need to enforce consistencies between different sources.

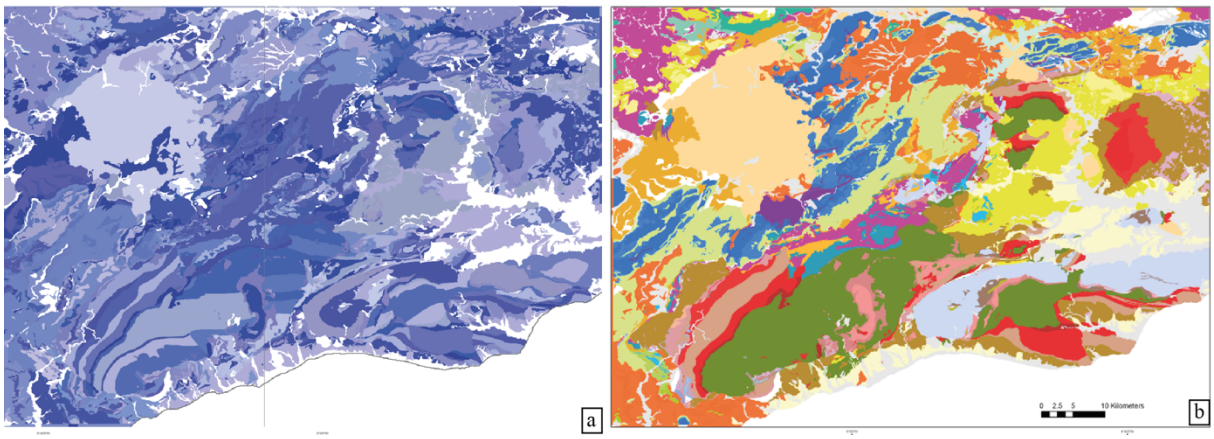

Figure 1.68. Synthesis of the previous geological maps integrated with new observations. The scale is the same in both figures. (a) All the polygons are reported with different tonalities of blue. (b) The subdivision is mainly based on the attribute age, in combination with the lithology. Violet indicates Triassic rocks, Jurassic in blue and Cretaceous in green. Different tonalities of yellow and orange indicate the Miocene sediments. Different colours in the crust represent different structural levels described in section 1.4.

The flexibility of the method allows for finer or more coarse map which can used to visualize features at different scales. The resulting maps can be enriched by the addiction of symbols bearing further information such as lineations with senses of shear (Fig. 1.69) and geochronological data (Fig. 1.70). The analysis of the previous papers permit to locate the sense of shear attributed to different structures by different authors. Also in this case a large table of georeferred attributes (715) permits the appearance or disappearance of different sense of shear if brittle or associated to particular metamorphic conditions.

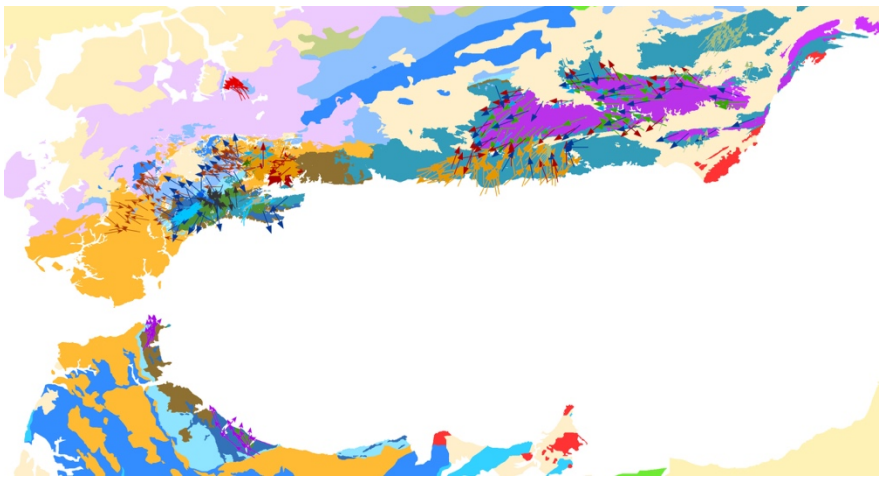

Figure 1.69. Lineations (senses of shear) and the slip-vectors from brittle strucutres reported in the literature (from Augier et al., 2005c; Chalouan et al., 2008; Crespo-Blanc and Campos, 2001; Azañon and Crespo-Blanc, 2000; Balanyá et al., 1997; Kirker and Platt, 1998; Pedrera et al., 2012; Rossetti et al., 2005; Simancas and Campos, 1993; Johnson et al., 1997; García-Dueñas et al., 1992; Martínez-Martínez et al., 2002; Booth-Rea et

al., 2003; Argles et al., 1999; Tubía et al., 2013; Mazzoli and Martín-Algarra, 2011; Luján et al., 2006). Same scale as Fig. 1.70.

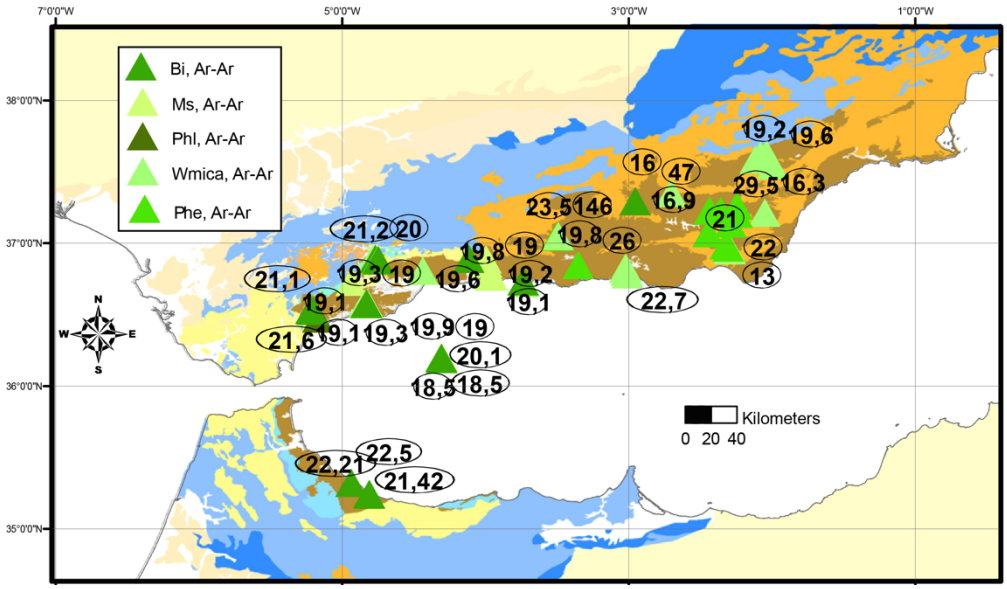

Figure 1.70 Ar-Ar data on micas from the Betic-Rif region. (Rossetti et al., 2010; Platt et al., 2003a, Platt et al., 2005; Monié et al., 1991, 1994). Age older than 23 Ma are collected in structural higher units of the Alboran Domain.

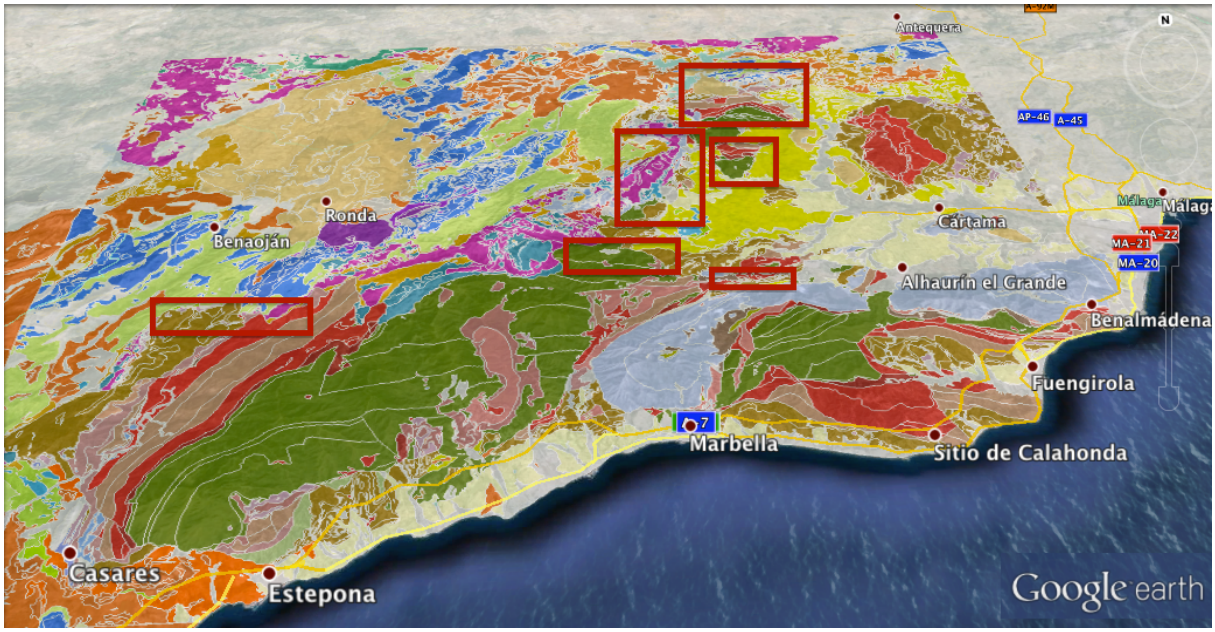

Figure 1.71. Representation of the GIS polygons in the 3D model on Google Earth. The white lines bound the all the polygons and the red square define the area re-mapped in the present study.

The map has been used also to locate the samples used for dating by the previous authors. Furthermore, from the analysis of the published literature it is also possible to extract the whole dataset of the geochronological data, which is also accomodated in a table of attributes (361 samples). The table contains for each sample the following information: the method used, the source paper, the name of the sample, the tectonic unit, the age, the standard

deviation, the number and the length of the tracks for the fission tracks ages (when reported) and the altitude of the sample (derived from the DEM when not reported in the paper). The compilation of a detailed attribute table permits to compare old and new data and to evaluate its quality. An example of visualization is on figure 1.70.

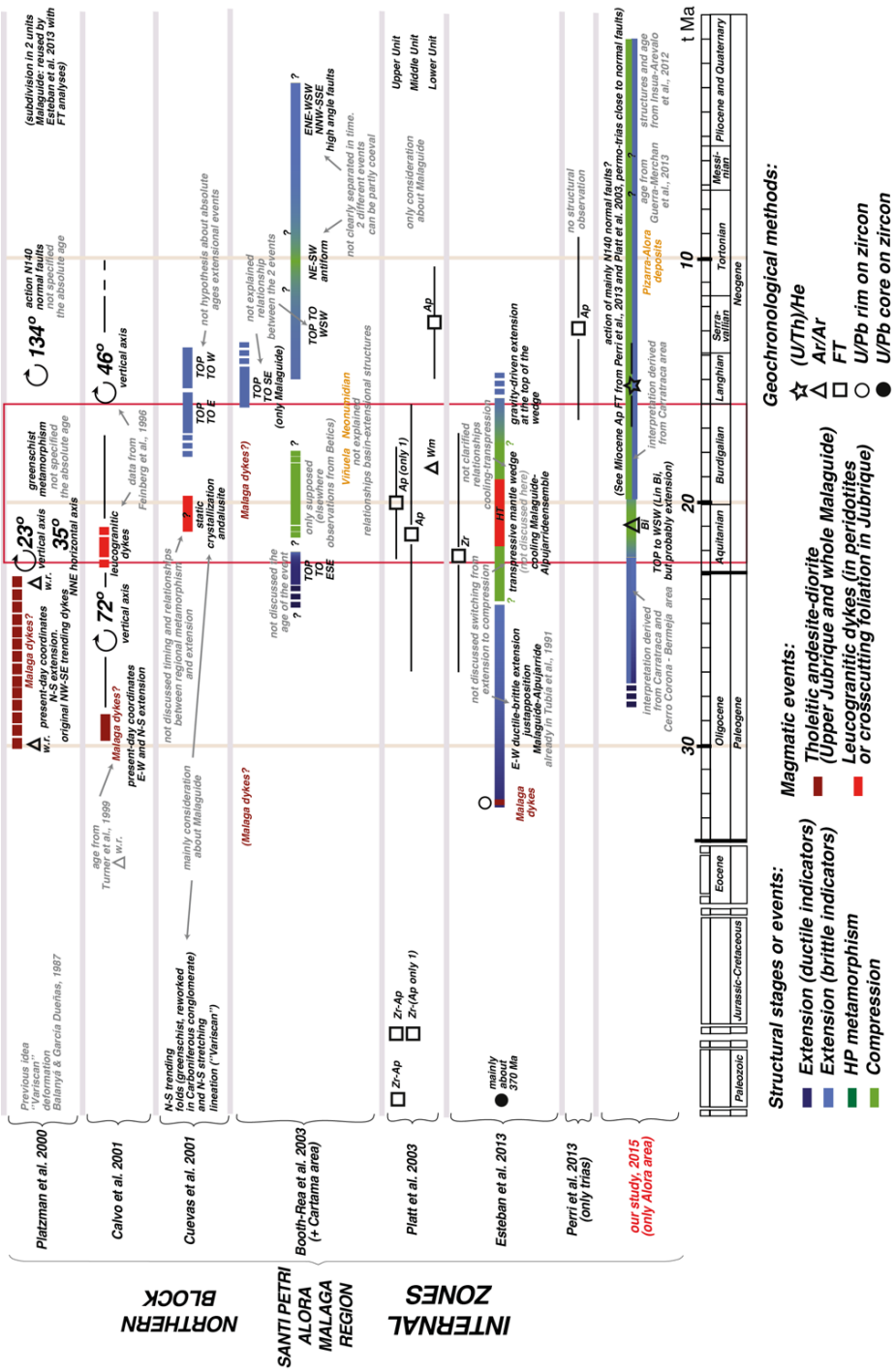

Figure 1.72. A schematic representation of the different of the structural and geological evolution of the units cropping out in the hills north of Malaga with comments. Each paper proposes new data and often integrates observation from other areas. The abbreviation "w.r." stands for "whole rock" (dating).

Attaching altitude information to the polygons and the samples allows to construct a full and complete 3D model (Fig. 1.71). This 3D model is specially useful to reveal

inconsistencies and gaps in the data. Indeed, subsequent fieldwork had the goal of resolving them.

To understand the debate and the disagreement on the evolution of the area between the different working groups and to individuate the best area for the purpose of the present study, the literature study was accompanied by schematic representations of the different opinion of the research group for different areas. Figure 1.72 contains this scheme for the Alora region: the complexity of the questions and strong differences between the interpretations clearly are apparent from the analysis of this small region, one of the least studied portion of the Western Betics.

1.6.2 Fieldwork

The fieldwork campaign lasted for 15 weeks during which structural data were collected. The work is organized in three classical stages. First, the description of the rocks, the measurement and description of planar structural elements (foliation, axial planes and faults) and linear structures (fold axes and lineations) (8734 measurements). Second, the analysis of the structural elements (stereographic projections, histograms) and their interpretation in relation with the "regional" observations. Third, interpolation and generalization at the macroscale with realization of foliation trajectories and the creation of the geological map (lithological boundaries, faults) and representative geological cross-sections (Balestro et al., 2010). A relational GIS database with the new data in which each structure is reported and georeferenced with a description of the main features. The possibility to define relationships between the structural entities in the attribute table built for the structural elements permits to couple for example foliation, lineation and C' shear planes in the database: this allows for faster and more effective statistical analyses. Furthermore, the coordinates associated to each measurement permit to locate exactly each station of measurement and each outcrop (Fig. 1.73). Moreover, each data has a "quality" attribute that defines the «weight» of the data in the postfieldwork stage.

The concepts of style groups, orientation groups and overprinting relationships between fabrics are the bases of the structural fieldwork (e.g. McClay, 1987). Unfortunatly geochronology on minerals defining the fabrics (in this case micas and intra-foliation monazites) often gave the same age and thus did not permit any insight into the age of the fabrics. Since it is not possible to obtain direct chronological information from the fabrics, we had to date the dikes associated with the structures can permit to attribute age to structures. This explain the interest of sampling the leucocratic dikes in the western Betics.

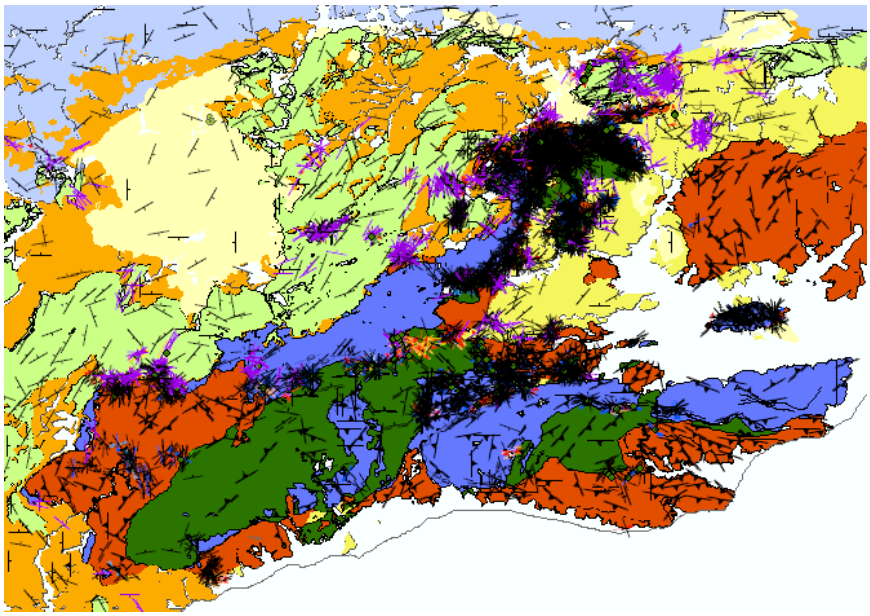

Figure 1.73. Location of the structural elements collected during the present study on a simplified geological map. The black measurement are foliation, the coloured ones are fault planes. In green are reported the Ronda Peridotites. In blue Blanca and Dorsale Units. In red the crustal envelope of the Ronda Peridotite. The Miocene sediments are orange or yellow. The coherent Subbetics sediments are light green and the chaotic deposits are violet.

1.6.3 Geochronology

The fieldwork and literature study has permitted to identify the sampling location that are expected to give the best indications about the age of structures. Besides, IT-based approach makes retraceability of the decisional processes possible. In the rest of the subsection we briefly describe the three dating methods that we have used.

Zircon U–Pb dating

Uranium–lead (U–Pb) dating is one of the most refined of the radiometric dating schemes and perfectly applies to our purpose, i.e. dating leucogranite intrusions. Uranium-lead dating has been performed on zircons ($ZrSiO_4$), though it could be used on other minerals such as monazite or titanite, not dated or not observed in the collected samples. The zircon incorporates U and Th atoms into its crystalline structure, but strongly rejects lead. Therefore we can assume that the entire lead content of the zircon is radiogenic. The U-Pb dating method relies on two separate decay chain, the uranium series from ^{238}U to ^{206}Pb, with a half-life of 4.47 billion years and the actinium series from ^{235}U to ^{207}Pb, with a half-life of 704 million years. These decay routes occur via a series of alpha and beta decays. the whole decay process can be described by a single decay equation, relating the ratio of parent atoms remaining (e.g. 238U) and final daughter atoms (e.g. 206Pb*) to time:

$$^{206}Pb^*/^{238}U = e^{\lambda_{238} t} - 1$$

where e is the exponential function, t is time, and l is the decay constant specific to this decay scheme, i.e. $\lambda_{238} = 1.55125e^{-10}$. $^{206}Pb^*$ refers to the radiogenic 206Pb accumulated in the crystal as a result of the decay of 238U.

To concentrate minerals suitable for U-Pb dating, classic mineral separation procedures have been applied using the facilities available at Géosciences Rennes. The samples were crushed to obtain a powder fraction with a diameter of 250 µm. Heavy minerals were successively concentrated by Wilfley table and heavy liquids. Magnetic minerals were then removed with an isodynamic Frantz separator. Part of the work has been done by Sophie Maziers during her M1 stage. Zircon grains were carefully handpicked under a binocular microscope and embedded in epoxy mounts. The grains were then hand-grounded and polished on a lap wheel with a 6 µm and 1 µm diamond suspension, successively. Zircon grains were imaged by reflected light (RL) and cathodoluminescence (CL) using a Reliotron CL system equipped with a digital color camera available in Géosciences Rennes. U-Pb geochronology of zircon was conducted by in-situ laser ablation inductively coupled plasma mass spectrometry (LA-ICPMS) using a ESI NWR193UC excimer laser coupled to a quadripole Agilent 7700x ICP-MS equipped with a dual pumping system to enhance sensitivity. Ablation spots of diameters of 25 to 30 µ with repetition rates of 3 Hz were used throughout. The data were corrected for U-Pb and Th-Pb fractionation and for mass bias by standard bracketing with repeated measurements of the GJ-1 zircon (Jackson et al., 2004). Data reduction is carried out using the GLITTER® software package developed by Macquarie Research Ltd. (Jackson et al., 2004). Concordia ages and diagrams were generated by Marc Poujol in Rennes using Isoplot/Ex (Ludwig, 2001).

Biotite and muscovite ^{40}Ar-^{39}Ar step-heating

Argon-argon dating works because Potassium-40 decays to Argon-40 with a known decay constant. ^{40}Ar/^{39}Ar closure temperatures are a function of crystal diffusional length-scale, composition and structure, and cooling rate. The samples are heated incrementally: this process, known as "step heating", provides additional information on the age of the sample. Reheating events and diffusion of argon from the boundaries of the grain can result in lower ^{40}Ar/^{39}Ar ages near the boundaries of the grain. A more representative age of initial cooling is given by the "plateau age", where the edge effects give way to a constant ^{40}Ar/^{39}Ar date. Many studies have been carried out to investigate diffusion by domains and diffusion rates of Ar in different minerals. In addition to theoretical calculations, estimates of closure temperature ranges have also been inferred from the pattern of age discordance in minerals from a single locality using different dating methods. The closure T estimates are reported in Figure 1.74. Two samples have been collected during this study and the analysis has been performed by Patrick Monié and description in Chapter 3 and mainly in the third annex.

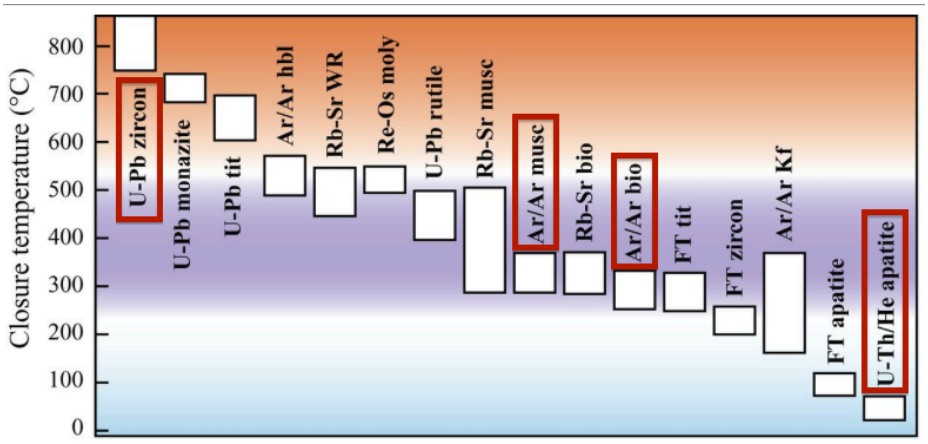

Figure 1.74. Table of the closure T for different dating methods. Red rectangles highlight the methods used during the present study.

Apatite (U-Th)/He (AHe)

The apatite (U-Th)/He thermochronometer (Zeitler et al., 1987) is based on the accumulation of radiogenic ^{4}He from the decay of ^{235}U, ^{238}U and ^{232}Th series nuclides. Laboratory diffusion experiments of apatites indicate that the helium is partially retained at temperatures between 40°C and 80°C, values which are apparently insensitive to chemical composition of the apatitesand only slightly sensitive to grain size (Wolf et al., 1996). The depth range that corresponds to this temperature range, marked in red in Figure 1.74, is termed partial retention zone (PRZ). At temperatures below 40°C most helium is retained in the apatite crystal, and above 80°C most helium is lost. Using this method is possible to obtain important information concerning the shallower movements of the rocks. This method will be then mostly useful in Chapter 2 where we will deal mainly with brittle structures that are supposed to be active in recent times. The apatites were obtained by a procedure similar to the one for the zircons in Géosciences Montpellier, but without the using the Wilfrey table. Most laboratory work has been done by Cyprien Astoury. The hand-picking of the apatites that satisfied good standards of quality, the calculation of the correction factor, and He analyses have been done by myself, while the U and Th isotopes by Michael Bonnin.

Chapter 2

Structural record of Lower Miocene westward motion of the Alboran Domain in the Western Betics, Spain

The article composing this chapter has been accepted to Tectonophysics

Gianluca Frasca[1,2*], Frédéric Gueydan[2], Jean-Pierre Brun[1]

[1] Géosciences Rennes, Université Rennes 1, UMR 6118 CNRS, Campus de Beaulieu, 35042 Rennes Cedex, France

[2] Géosciences Montpellier, Université Montpellier 2, UMR 5243 CNRS/INSU, Place E. Bataillon, CC60, 34093 Montpellier Cedex, France

*Corresponding author e-mail and telephone number: gianluca.frasca@univ-rennes1.fr; +33649326203

Abstract

In the framework of the Africa-Europe convergence, the Mediterranean system presents a complex interaction between subduction rollback and upper-plate deformation during the Tertiary. The western end of the system shows a narrow arcuate geometry across the Gibraltar arc, the Betic-Rif belt, in which the relationship between slab dynamics and surface tectonics is not well understood. The present study focuses on the Western Betics, which is characterized by two major thrusts: 1/ the Internal/External Zone Boundary limits the metamorphic domain (Alboran Domain) from the fold-and-thrust belts in the External Zone; 2/ the Ronda Peridotites Thrust allows the juxtaposition of a strongly attenuated lithosphere section with large bodies of sub-continental mantle rocks on top of upper crustal rocks. New structural data show that two major E-W strike-slip corridors played a major role in the deformation pattern of the Alboran Domain, in which E-W dextral strike-slip faults, N60° thrusts and N140° normal faults developed simultaneously during dextral strike-slip simple shear. Olistostromic sediments of Lower Miocene age were deposited and deformed in this tectonic context and hence provide an age estimate for the inferred continuous westward translation of the Alboran Domain that is accommodated by an E-W lateral (strike-slip) ramp and a N60° frontal thrust. The crustal emplacement of large bodies of sub-continental mantle may occur at the onset of this westward thrusting in the Western Alboran domain. At lithosphere-scale, we interpret the observed deformation pattern as the subduction upper-plate expression of a lateral slab tear and its westward propagation since Lower Miocene.

KEYWORDS: Western Betics; strike-slip corridors; thrust and lateral ramps; slab tearing.

2.1 Introduction

In the Mediterranean, the correlation between P-wave tomographic models that reveal the present-day 3D complexity of slab geometry and surface geology has permitted to reconstruct the subduction upper-plate deformation during slab rollback. The trench curvature that progressively increased during trench retreat (Faccenna et al., 2004; Rosenbaum et al., 2004) is laterally accommodated by slab tearing along northern Africa (Wortel and Spakman, 2000), in Central Mediterranean, and along western Anatolia, in the Aegean (Brun and Sokoutis, 2010; Jolivet et al., 2013), explaining the progressive formation of the Calabrian and Hellenic arcs, respectively.

The western termination of the Mediterranean realm in the Alboran-Gibraltar arc domain is far less understood. The diffuse plate boundary between Africa and Eurasia is an arcuate system defined by two Alpine belts, the Betics in Spain and the Rif in Morocco (Chalouan et al., 2008; Crespo-Blanc and Frizon de Lamotte, 2006; Platt et al., 2013) that developed during the convergence between Africa and Eurasia plates (Dewey et al., 1989; Mazzoli and Helman, 1994; Rosenbaum et al., 2002; Schettino and Turco, 2011; Vissers and Meijer, 2012). The formation of the Gibraltar arc is viewed as extensional collapse of a previous existing belt (e.g. Platt et al., 1989), driven by i) continental lithospheric delamination, with different direction (Docherty and Banda, 1995; García-Dueñas et al., 1992; Seber et al., 1996), and/or ii) slab rollback (Faccenna et al., 2004; Frizon de la Motte et al., 2009; Lonergan and White, 1997; Rosenbaum et al., 2004; Royden, 1993), with also

possible lateral accommodation by continental lithosphere delamination in Morocco (Fadil et al., 2006; Pérouse et al., 2010).

The earlier tomographic images (Blanco and Spakman, 1993) have lead to various contrasted interpretations (e.g. comment to Gutscher et al., 2002, by Platt et al., 2003c). The most recent tomographic models (Bezada et al., 2013; Bonnin et al., 2014; Palomeras et al., 2014; Thurner et al., 2014) display a very localized, subvertical, well-resolved high Vp anomaly below the Gibraltar arc, which further suggests subduction rollback as the geodynamical process responsible for the arcuate belt along the plate boundary. However, interpretations that significantly differ in terms of timing, direction of displacement and amount of slab rollback have been proposed (Faccenna et al., 2004; Gueguen et al., 1998; Gutscher et al., 2012; Spakman and Wortel, 2004; Vergés and Fernández, 2012).

The present study aims at providing geological and structural constraints on the timing and direction of displacement of the Alboran Domain in the Western Betics. In this paper, we first describe the geological setting of the Betic-Rif belt and more specifically the northern branch of the Gibraltar arc, the Western Betics, which is characterized by the presence of the Ronda Peridotites, the largest sub-continental mantle body in the world. New structural and kinematic data are presented that document the coeval development of E-W dextral strike-slip corridors and N60° trending thrust faults. We propose that the northern part of the Gibraltar arc has been formed, mainly during the Lower Miocene, by the westward motion of the Alboran Domain, accommodated by simultaneous E-W trending lateral ramps and N60° frontal thrust. The E-W strike-slip deformation zones, acting as lateral ramps of the moving and extending hinterland, more likely correspond to an upper-plate expression of slab tearing at depth.

2.2 Geological setting

2.2.1 Overview of the Betic-Rif arc

Figure 2.1 presents a simplified tectonic map of the Betic-Rif system. A major tectonic contact, hereafter called the Internal-External Zone Boundary (IEZB; Platt et al., 2013) divides the tectonic system in two zones: 1/ the Internal Zone, also called the Alboran Domain (red, dark green, blue and grey in Fig.2.1), characterized by metamorphic rocks with variable metamorphic grades and ages; and 2/ the External Zone, composed of two main tectonic domain: the Subbetics (in Spain) / Intra- and Meso- Rif (in Morocco) that consist in a non-metamorphosed Mesozoic and Tertiary sedimentary cover on top of the Iberian/Maghrebian basement (pale green in Fig.2.1) and the Flysch Trough Complex (Cretaceous to Miocene sediments, orange together with Miocene deposits of the Western Betics in Fig.2.1).

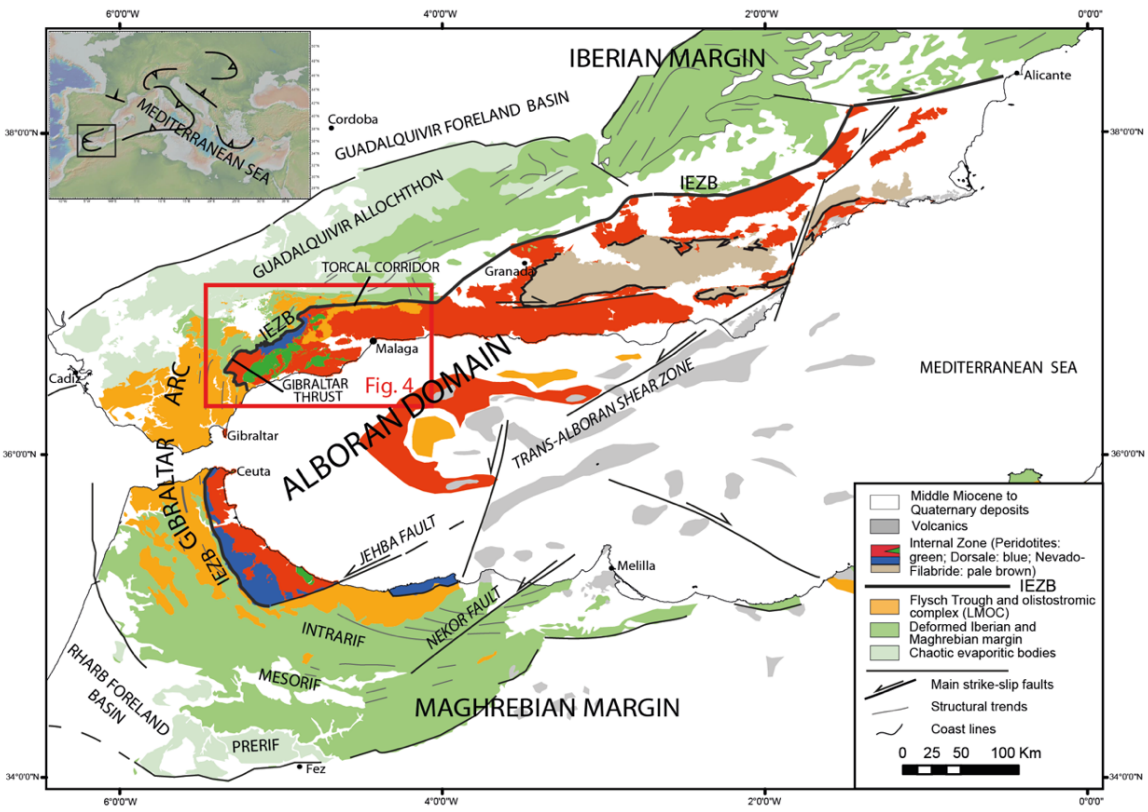

Figure 2.1. Simplified tectonic map of the Betic-Rif belt (Redrawn for the Betics after IGME: **http://info.igme.es/cartografia/magna50.asp?c=s** and Crespo-Blanc and Frizon de Lamotte (2006), for the Rif after Chalouan et al. (2008) and for the Alboran Domain after Martínez-García et al. (2013)). Left-up corner inset: Location in the Mediterranean (from GeoMapApp, http://www.geomapapp.org). Red rectangle: Location of the study area.

The Internal Zone**,** or **Alboran Domain**, is structurally made of a nappe pile of three tectonic units, which are, from bottom to top: the Nevado-Filabride, the Alpujarride and the Malaguide (see Didon et al., 1973; Egeler and Simon, 1969; Torres-Roldán, 1979).

The *Nevado-Filabride* is cropping out only in the central and eastern part of the Betics and is mainly composed of Paleozoic orthogneisses and graphitic schists with a thin Permo-Triassic cover (light brown in Fig.2.1, Bakker et al., 1989; García-Dueñas et al., 1988; Martínez-Martínez et al., 2010; Platt et al., 1984). Late Jurassic metamorphosed mafic (Hebeda et al., 1980; Puga et al., 2011) and ultramafic (Padrón-Navarta et al., 2008; Puga et al., 1999) rocks occur locally and are interpreted as Tethysian oceanic remnants affected by a Tertiary (Monié et al., 1991; Platt et al., 2006) high-pressure metamorphic event. Note that the Nevado-Filabride has no equivalent in the Rif.

The *Alpujarride*, Sebtide in the Rif, mainly consists of Paleozoic/Early Mesozoic crustal rocks (several tectonic units with different tectonic evolution, e.g. Booth-Rea et al., 2005) that contain large bodies of sub-continental peridotites (Ronda and Beni Bousera Peridotites, Obata, 1980). The Alpine metamorphic grade generally increases westward (Tubía et al., 1992), from high-pressure/low-temperature south of Granada (Goffé et al., 1989) to medium-pressure/high-temperature in the Western Betics (Platt and Whitehouse, 1999). The Alpujarride is characterized by a strong Oligo-Miocene extensional deformation (Argles et al 1999; Balanyá et al., 1997; Précigout et al., 2013) and by a widespread Lower

Miocene high-temperature metamorphic event (Monié et al., 1994). The age of an earlier high-pressure metamorphic event is debated: Paleozoic for Zeck and Whitehouse, 2002; Eocene for Platt et al., 2005; Oligocene for Monié et al., 1991; Lower Miocene for Tubía et al., 2013. The Mesozoic cover in the Alpujarride Unit is exclusively Triassic (e.g. Martin-Rojas et al., 2009, 2014).

The *Malaguide* (Ghomaride in the Rif; Durand-Delga, 1963, 1980) is composed of Paleozoic rocks with Hercynian low-grade metamorphism (Chalouan and Michard, 1990). Close to the Alpujarride, the Alpine metamorphic grade increases (Negro et al., 2006) with occurrence of andalusite (Cuevas et al., 2001; Platzman et al., 2004), partly suggesting a common evolution for Malaguide and Alpujarride during the regional Alpine metamorphism (Torres-Roldán, 1979). The non-metamorphic cover is Mesozoic to Paleogene (Chalouan et al., 2008; Martín-Algarra et al., 2009; Perri et al., 2013).

In the westernmost part of the Betic-Rif system, the Internal-External Zone Boundary (IEZB) is marked by the *Dorsale* units (Bourgois, 1978; Martín-Algarra et al., 2004a), which are composed of deformed and locally metamorphosed at high-grade Triassic-Jurassic sediments. The relationship between the Dorsale and the other units of the Alboran Domain is still debated: belonging to the Alpujarride, according to Chalouan et al. (2008) and Wildi et al. (1977), or belonging to the Malaguide, according to Balanyá and García-Dueñas (1987) and Sanz de Galdeano et al. (2001b), Didon et al. (1973).

The **External Zone** is characterized by a fold and thrust belt of Miocene age (Burdigalian-Langhian, Crespo-Blanc and Frizon de Lamotte, 2006) that affects two domains, called Subbetics and "Flysch Trough Complex". The *Subbetics* are the Mesozoic to Tertiary sedimentary cover partly detached from the Iberian margin basement, equivalent to Infra and Meso-Rif for the Maghrebian margin (see discussion in Crespo-Blanc and Frizon de Lamotte, 2006). The Subbetics are divided into several tectonic units (External Subbetics, Median Subbetics and Internal Subbetics), mainly based on their paleogeographic position during the Jurassic and the observed differences in sedimentary facies of the Cretaceous deposits (García-Hernández et al., 1980; Martín-Algarra et al., 2004c; Vera et al. 2004).

Along the Gibraltar arc, deep marine clastic sediments, called hereafter the "*Flysch Trough*" (Martín-Algarra et al., 2004b; Luján et al., 2006; Stromberg et al., 1998; orange in Fig.2.1) lies structurally on top of the Subbetics. The Flysch Trough that was deposited during the Lower Cretaceous (Thurow and Kuhnt, 1986) in a structural depression floored by oceanic or thinned continental crust, probably related to a transform setting (Biju-Duval et al., 1977; Dercourt et al., 1986), is mainly composed by Miocene (Guerrera et al., 2012) terrigenous sediments. The "Flysch Trough" is organized in a coherent accretionary prism north of Gibraltar (Luján et al., 2006) and is divided in two main groups: 1/ slivers of Cretaceous sediments at the base, considered as separated tectonic units (Martín-Algarra, 1987) and 2/ large amounts of Paleogene to Miocene flysch-type deposits, considered as pre-compression and Aquitanian to Lower Burdigalian in age (Martín-Algarra et al., 2004b). The sediments are usually separated in several units on the base of the relative abundance of quartz or lithic fraction (Aljibe quartzose, Algeciras only lithic and Bolonia a mix of both component, Martín-Algarra et al., 2004b, see Fig.2.2 for a summary of different lithological units).

Sedimentation ends in the Lower Miocene, marking the onset of the main shortening event in the Flysch Trough (Luján et al., 2006).

Lower Miocene-Quaternary foreland sediments delineate the northern and southern terminations of the Betic-Rif arcuate belt: the Guadalquivir Basin in the Betics and Rharb Basin in the Rif (Berástegui et al., 1998; Fernández et al., 1998; Flinch, 1993, white in Fig.2. 1). The transition between the Subbetics and the foreland sediments is an area of re-sedimented Mesozoic material embedded in evaporites and clays called "Guadalquivir allochthons" in the Betics (pale olive-green in Fig.2.1; Platt et al., 2013; Ruiz-Constán et al. 2012a). It is characterized by a scarcity of outcrops that prevents good structural analysis (Sanz de Galdeano et al., 2008).

2.2.2 Geodynamical scenarios of the Alboran region

Although the overall geometry of the Betic-Rif belt is relatively well defined (see Chalouan et al., 2008; Crespo-Blanc and Frizon de Lamotte, 2006; Platt et al., 2013 for review), its tectonic origin has been matter of debate in the past. Several geodynamical scenarios have been proposed to explain the arcuate geometry of the Alboran system and are reviewed here in their order of appearance.

Andrieux et al. (1971) postulated that an exotic microplate has indented the Iberian and Maghrebian margin. Strike-slip shearing along the lateral boundaries of the supposed exotic rigid indenter has been observed all along the Betics (De Smet, 1984; Sanz de Galdeano, 1990) and in the eastern and southern sectors of the Rif (Leblanc, 1990; Olivier, 1981). In particular, the major sinistral trans-Alboran shear zone (De Larouzière et al., 1988) is underlined by volcanism (grey in Fig. 2.1) and extends unambiguously for at least 400 km from the Eastern Betics (Bousquet, 1979; Pacquet, 1969; Rutter et al., 2012) to Morocco (Olivier and Leblanc, 1984) through the Alboran Sea (Booth-Rea et al. 2007). However, extension described in the Alboran Domain (Argles et al., 1999; Balanyá et al., 1997; García-Dueñas et al., 1992; Précigout et al., 2013) is not explained by this interpretation that must be therefore ruled out.

Platt and Vissers (1989) then formulated a first hypothesis that takes into account the existence of low-angle normal faults in the Alboran system, postulating a gravitational collapse of a previous mountain belt behind the formation of the Betic-Rif arc. This collapse should have induced a radial displacement around the Alboran Domain with contemporaneous compression in the foreland and extension in the hinterland. García-Dueñas et al. (1992) invoked a delamination of continental lithosphere to explain a similar deformation pattern in the Betic-Rif belt.

Nowadays, the most commonly accepted geodynamic scenario refers to the rollback of a subducting slab (Royden, 1993) to explain the arcuate evolution of the Betic-Rif External Zone and the extensional structures in the Alboran Domain (Lonergan and White, 1997; Royde, 1993). Furthermore, the spatial distribution of the different types of volcanism

(Duggen et al., 2004), the shifting along the Betics of the marine-continental transition in onshore sedimentary basins (Iribarren et al., 2009), and the tectonic evolution of the Ronda Peridotites (Afiri et al 2011; Garrido et al., 2011; Johanesen et al. 2014; Précigout et al., 2013) also suggest a subduction rollback origin for the mountain belt and its metamorphic units. However, the amount of slab rollback and the direction of trench migration is matter of controversy (see review in Chertova et al., 2014). A first category of interpretations considers an initial northwest-dipping subduction along the west-central Mediterranean (from Gibraltar or southeast of Iberia to Corsica) initiated in Oligocene and rolled back first to the south and then to the west (Faccenna et al., 2004; Gueguen et al., 1998; Jolivet et al., 2006). In a second category, a short N-S trending subduction zone located south of the Baleares islands rolled back westward during the upper Miocene (Frizon de la Motte et al., 2009; Rosenbaum et al., 2004; Spakman and Wortel, 2004; Van Hinsbergen et al., 2014). Subduction of the Moroccan continental margin may trigger crustal delamination from the downgoing sub-continental mantle and could explain the peculiar kinematics of the Rif with respect to Iberia in present-day GPS data (Fadil et al., 2006; Pérouse et al., 2010). A third category considers an initial subduction zone dipping to the S-SE under the African margin (Alpine type) that rolled back first northward and progressively to the NW (Vergés and Fernández, 2012).

The direction and timing of the Alboran Domain displacement, that is the subduction upper-plate, is therefore a key issue to discriminate between different models. A tectonic study such as the one presented here cannot alone definitely rule out some of the proposed models. However, our study provides new geological and structural constraints, collected in key areas of the Western Betics that allow constraining the Lower Miocene displacement history of the Western Alboran Domain.

2.2.3 Lower Miocene extension and compression in the Western Betics

The timing and direction of displacement in the Alboran Domain has been partly constrained by the deformation in its western part, mainly in the External Zone (Balaya et al. 2007;Kirker and Platt, 1998) and Dorsale units, in the Western Betics (Mazzoli and Martín-Algarra, 2011) and in the Rif (Vitale et al. 2014a, 2014b). Figure 2.2 summarizes the Miocene tectonics of the Western Betics that is marked by the succession of compressive and extensional events (see Balanyá et al., 1997 and comment by Platt, 1997; Crespo-Blanc and Campos, 2001).

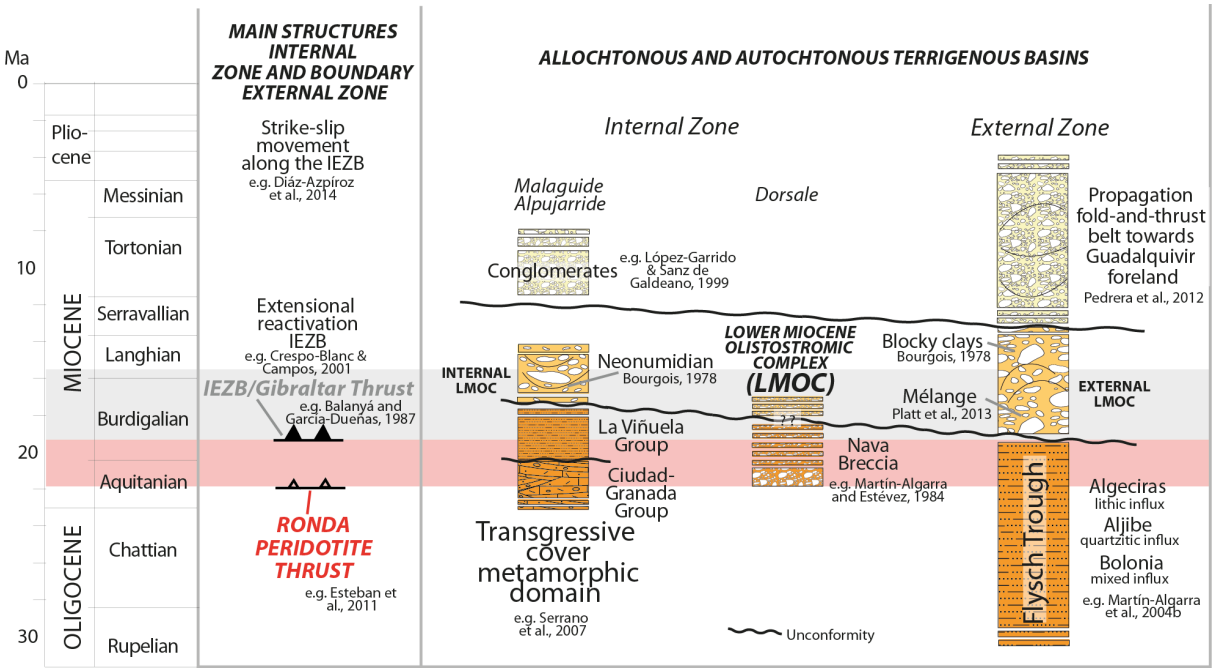

Figure 2.2. The main Miocene tectonic events of the Western Betics (after Crespo-Blanc and Campos, 2001; Díaz-Azpiroz et al., 2014; Esteban et al., 2011 and Kirker and Platt, 1998) and the Lower Miocene deposits (after López-Garrido and Sanz de Galdeano, 1999; Serrano et al., 2007; Martín-Algarra et al., 2004a, 2004b, 2004c).

The Flysch Trough Complex is affected by an upper Burdigalian/Langhian shortening event giving an external fold and thrust belt (Luján et al., 2006) with coeval deposition of external lower Miocene olistostromic complex (e.g. Martín-Algarra et al., 2004b, Platt et al., 2013, Fig. 2.2 and see discussion in section 3.3). Consistently, Balanyá and García-Dueñas (1987) have proposed that the IEZB in the Western Betics (called by them "Gibraltar crustal thrust") formed during that main shortening event. In this paper, we will use the term Gibraltar thrust for the thrust-related portion of the IEZB that trends roughly N60° in the western Betics. The E-W portion of the IEZB will be denoted Torcal fault zone (Fig. 2.1).

Structural studies in the Western Betics have shown radial slip vectors in the External Zone that were interpreted as a result of either westward motion of the extending Alboran Domain (Balanyá et al., 2007) or radial motion of the Alboran Domain due to extensional collapse (Platt et al., 2003a). For Balanyá et al. (2007), the Alboran Domain motion would have been westward with a radial distribution of slip-vectors in the External Zone, from E-W north of Gibraltar to NW north of Ronda, as an effect of strain partioning from arc normal shortening to arc parallel extension (Balanyá et al., 2007; Fig. 2.3). In contrast, Kirker and Platt (1998) suggest a N120° unidirectional motion of the Alboran Domain in the Western Betics (Fig. 2.3b). The main difference between these two scenarios is the existence of a dextral transpressive E-W zone for Balanyá et al., 2007 (Torcal region; Balanyá et al., 2012) and N120° dextral strike-slip fault zone for Platt et al. (2003a) (see discussion in Balanyá et al. 2007; summarized in Fig. 2.3).

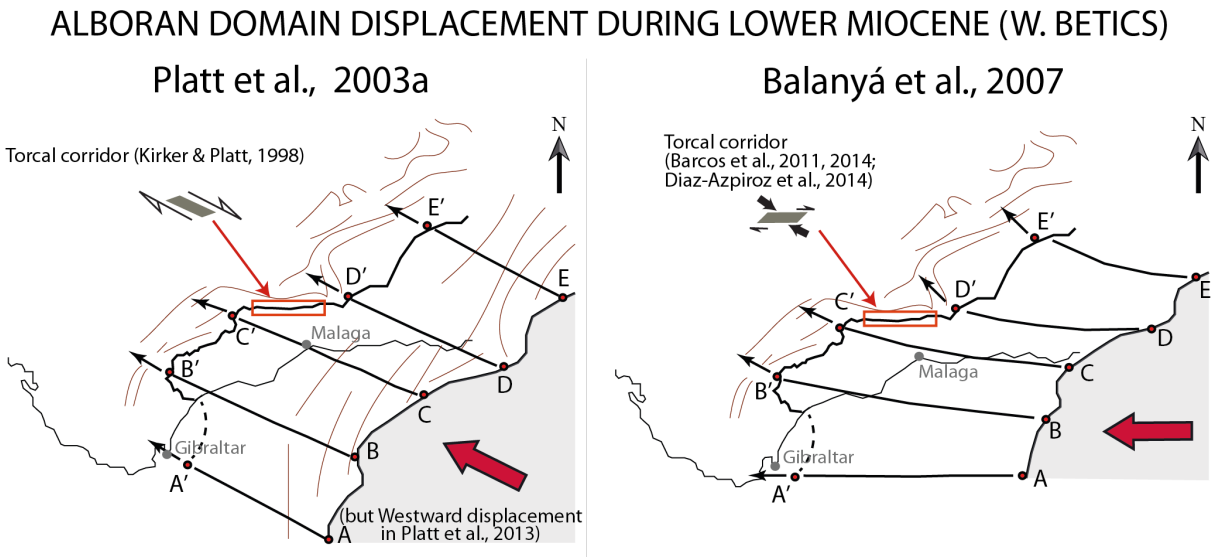

Figure 2.3. Displacement of the Alboran Domain with respect to the fold and thrust belt of the Western Subbetics and Betic Flysch Trough, as proposed by Platt et al. (2003a) and Balanyá et al. (2007). Initial contour of the Alboran Domain from Kirker and Platt (1998).

Such a motion of the Alboran Domain implies shortening at the front (mainly in the External Zone) and extension in the moving domain (Alboran Domain, Platt et al., 2013). In western Alboran, a major stage of extension occurred during Serravallian and is marked offshore by the large amount of subsidence in the Alboran basin (Comas et al., 1992) and onshore by extensional reactivation along the IEZB. Widespread low-angle normal faulting, mostly in the western part of the Alboran Domain, is considered to result from this major extensional event (García-Dueñas et al., 1992).

2.2.4 Extensional exhumation and thrusting of the Ronda Peridotites

The largest onshore exposure worldwide of sub-continental mantle (Ronda and Beni Bousera), which is characterized by three typical metamorphic facies (Grt/Sp-peridotites, Granular Sp-peridotites, Pl-bearing peridotites; Obata, 1980), is a key geological feature of the Alboran Domain along the Gibraltar arc (Darot, 1974; Kornprobst, 1974; Obata, 1980).

These bodies of mantle rocks are characterized by: 1/ an extreme continental lithosphere thinning registered in both peridotites and surrounding crustal rocks and 2/ thrusting of the exhumed mantle into the Alboran Domain, allowing the final exhumation of peridotites at crustal depths (see review in Précigout et al., 2013). Sub-continental mantle exhumation was accommodated by extensional ductile shear in the upper part of the Ronda peridotitic bodies (in white in Fig. 2.4, Garrido et al., 2011; Précigout et al., 2013) and in the Alpujarride (Argles et al., 1999; Balanyá et al., 1997) and the Malaguide (Booth-Rea et al., 2003; Cuevas et al., 2001) in the Malaga area.

The regional foliation in the Alpujarrides crustal rocks is marked by medium-

pressure/high-temperature assemblages that recorded a decrease in pressure (Argles et al., 1999; Balanyá et al., 1997). Simultaneously, mantle rocks have registered a continuous decompression from garnet stability field to spinel-peridotite facies (Garrido et al., 2011), associated with ductile strain localization in the very top of the mantle section (Précigout et al., 2013). The occurrence of syn-tectonic partial melting (Marchesi et al., 2012) confirms the syn-exhumation mylonitization hypothesis. A similar tectonic evolution occurs in the Beni Bousera peridotites (Afiri et al., 2011; Frets et al., 2014). The complex polycyclic history that characterizes the mantle section, as suggested by occurrence of pseudomorphs after diamond (Davies et al., 1993) and by Hercynian, Jurassic and Alpine ages (Montel et al., 2000; Sánchez-Navas et al., 2014; Sánchez-Rodriguez and Gebauer, 2000), allows a certain degree of freedom for interpreting the age of continental lithosphere thinning.

The basal surface of the peridotites slices is a "hot" thrust (Esteban et al., 2008, Tubía et al., 1997), which will be called hereafter the Ronda Peridotites Thrust, observable in the Western Betics and very locally in the Rif (e.g. Ceuta). Partial melting in crustal rocks below the "hot thrust" yields a cluster of ages between 22 Ma and 20 Ma (Esteban et al., 2011), supporting a lower Miocene age for the "hot" thrusting.

Previous tectonic scenarios either do not consider the presence of mantle rocks (Andrieux et al., 1971) or proposed very different mechanisms and ages for mantle rock exhumation: i) mantle core complex (Doblas and Oyarzun, 1989), ii) extrusion of a mantle wedge during transpression along a subducting slab (Mazzoli and Martín-Algarra, 2011; Tubía et al., 1994), iii) successive detachment faults during extensional collapse of the Betic-Rif chain (Platt et al., 2003d; Van der Wal and Vissers, 1993) and iv) the inversion of a thinned back-arc lithosphere during slab rollback (Garrido et al., 2011 ; Précigout et al., 2013). Ages of exhumation are also strongly variable: i) Paleozoic (Kornprobst, 1976; Ruiz Cruz and Sanz de Galdeano, 2014), ii) Mesozoic (Tubía et al., 2009; Van Hinsbergen et al., 2014) and iii) Oligo-Miocene (Hidas et al., 2013; Précigout et al., 2013).

2.2.5 Objectives of the study

The above review of previous studies regarding the Alboran region, and more specifically the Western Betics, shows that a major contractional event started during Lower Miocene in both the western External Zone (IEZB and fold-and-thrust belt in the Flysch Trough: Burdigalian/Langhian) and in the western Alboran Domain (Ronda Peridotites Thrust: Aquitanian). This lower Miocene shortening event occurs during the motion of the Alboran Domain, whose direction remains to be constrained (E-W or N120°, as shown in Fig. 2.3). Our study is therefore focused on the relative development of the IEZB and the Ronda Peridotites Thrust during lower Miocene in relation with the motion of the Alboran Domain. It aims: at 1/ mapping at regional-scale the strike-slip deformation zones involved in the internal deformation pattern, 2/ constraining the timing of deformation, and 3/ providing rough estimates of regional-scale shortening.

Consequently, the pre-Miocene history, related to the subduction and exhumation of the Alpujarride and to the unroofing of the Ronda Peridotites, and the mid-Miocene to present-day history, related to Serravallian extension in the Alboran Basin with supposed extensional reactivations onshore and recent contractional events (Fig. 2.2), are beyond the scope of the present paper. Nevertheless, we later discuss in the paper the implications of our tectonic model to the Lower Miocene to present day evolution of the Western Betics.

2.3 Lower Miocene tectonics of the Western Alboran Domain

2.3.1 Data acquisition

The tectonic map shown in figure 2.4 presents the major tectonic features of the Western Alboran Domain and of the boundary with the External Zone. This map combines our own work (four months of fieldwork; around 8000 measurements) and previously published structural and geological data (IGME maps of Cano Medina, 1990; Cano Medina and Ruiz Reig (1990); Chamón Cobos et al., 1972; Cruz San Julían, 1990; Del Olmo Sanz et al., 1984, 1990; García de Domingo et al. 1994; Moreno Serrano et al., 1991; Piles Mateo et al., 1972a, 1972b; Pineda, 1983; and maps from Esteban et al., 2008; Sánchez-Gómez et al., 1999, 2002; Sanz de Galdeano and Andreo, 1995; Tubía et al., 1997). We identify four main areas (analyzed in sections 4 and 5) where contractional, extensional and strike-slip structures involving post-lower Burdigalian formations are unconformably covered by Late Tortonian - Early Messinian Conglomerate (López-Garrido and Sanz de Galdeano, 1999; Martín et al., 2001; Figs. 2.4 and 2.5). Therefore, the deformation patterns that we infer started during lower Miocene. Other recent studies also suggest that strike-slip deformation zones were active in Pliocene times (Díaz-Azpiroz et al., 2014) implying that the inferred deformation kinematics has been active from Mid-Miocene to present day. The fact that these structures do not show any systematic cross-cutting relationships suggests their coeval development. Fault slip-data were collected mainly in the External Zone at the boundary with the Alboran Domain where the IEZB has an arcuate trend and around major E-W fault trending zones within the Alboran Domain.

Foliation trajectories and bedding envelopes outline the existence of large-scale faults and the deformation pattern of the Alboran Domain (Figs. 2.6 and 2.8). Local observations (fault geometries and kinematic indicators) and constraints deduced from geological and structural maps (lithostratigraphy and foliation trajectories) are used to identify and describe map-scale structures (as summarized in Fig. 2.4). Local observations and structural data analysis are reported in sections 4 and 5. The overall kinematics of the Western Betics during lower Miocene deformation are described and interpreted in section 6.

2.3.2 Tectonic units

Figure 2.4 shows the two main tectonic contacts that characterize the Western Betics. 1/ The IEZB (Platt et al., 2013) separates the External Zone from the overlying Alboran Domain and is delineated by Lower to Middle Miocene sediments that contain blocks of the overlying Alboran rocks ("Blocky-clays" deposits, Bourgois, 1978: External LMOC, little white dots on orange in Fig. 2.4).

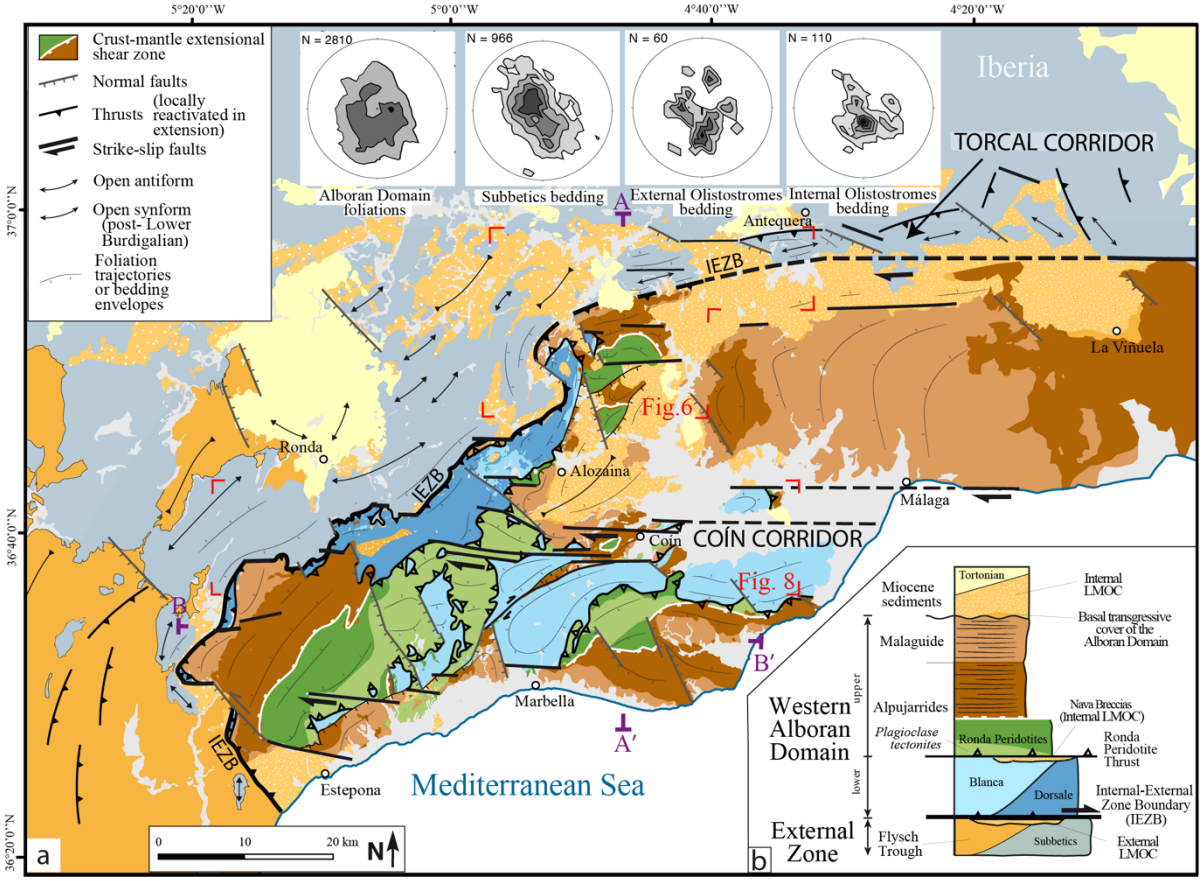

Figure 2.4. (a) Simplified structural map of the Western Betics (redrawn after IGME (**http://info.igme.es/cartografia/magna50.asp?c**=s) and our own mapping) with location of the cross-sections AA' and BB' of Fig. 2.5. (b) General vertical section, showing the two main tectonic contact (IEZB and Ronda Peridotites Thrust) and the main tectonic units, from bottom to top: Subbetics and Flysch through unit, Blanca and Dorsale, Ronda Peridotites, Alpujarride, Malaguide, Internal and External LMOC and Tortonian sediments. Red marks: location of Figs. 2.6 and 2.8. Stereoplots of the foliation in the Alboran domain (2810 measurements) and of the bedding in the Subbetics, External and Internal Olistostromes (1136 measurements) are shown in the top of the figure.

The age of these sediments are however not well established, between Burdigalian and Mid Miocene and formed by gravitational dismembering of the Alboran front (Suades and Crespo-Blanc, 2013). 2/ The Ronda Peridotites Thrust divides the Western Alboran Domain into two units. The Lower Western Alboran Unit is made of unmetamorphosed sediments (Dorsale) and metamorphic rocks ("Blanca"). The Upper Western Alboran Unit is a slice of thinned continental lithosphere (peridotites and crustal rocks). In the Western Betics, the IEZB is

marked from West to East by the Gibraltar Thrust in the Gibraltar area (Balanyá and García-Dueñas, 1987) and the E-W Torcal fault zone (Martín-Algarra, 1987). As mentioned above, the Torcal fault zone has been described as either a N120° dextral strike-slip zone (Platt et al., 2003a) or a N90° strike-slip deformation zone (Balanyá et al., 2012). EW and NS cross-sections (Fig. 2.4) show the tectonic superposition of the Western Betics units and the major fault zone.

The Upper Western Alboran Unit corresponds to a strongly attenuated continental lithosphere section, whose thickness is as low as 5 km (cross-section in Figure 2.5 and García-Dueñas et al., 1992) showing from bottom to top: 1/ the Ronda Peridotites (sub-continental mantle, dark green; Fig. 2.4), 2/ the Alpujarrides crustal rocks (dark brown; Fig.2. 4), locally denoted Jubrique Unit (Balanyá et al., 1997) or Los Reales Nappe (including the Ronda Peridotites; Navarro-Vilá and Tubía, 1983) that corresponds to a deep- to mid-crust rock-pile as shown by the decrease in metamorphic grade from granulite to low grade schists, in which lithostratigraphic repetitions may occur (Balanyá et al., 1997) and 3/ the Malaguide (light brown; Fig.2.4) that is made of upper crustal rocks, weakly or non metamorphosed (Martín-Algarra, 2004a).

The base of the Upper Western Alboran Unit is underlined by plagioclase-bearing peridotites (light green; Figs. 2.4 and 2.5) whose foliation developed in low-pressure conditions (Hidas et al., 2013), very well developed in the vicinity of the Ronda Peridotites Thrust and cross-cutting the previous garnet-spinel foliation (Précigout et al., 2013). This leads Hidas et al. (2013) to suggest that the plagioclase tectonites marked the thrusting related-deformation within the peridotites. Moreover, previous studies (Esteban et al., 2008; Mazzoli et al., 2013) have shown that the thrusting of the Ronda Peridotites and its crustal envelope on top of the Lower Western Alboran Unit occurred at low pressure and high temperature. The Ronda Peridotites Thrust is responsible for a dynamo-thermal contact metamorphism in the Lower Western Alboran Unit (i.e. “hot” thrusting) and to the intrusion of leucogranite dikes that cross-cut the Ronda Peridotites and its crustal envelope (Cuevas et al., 2006; Tubía et al., 1997). All the above considerations from the literature support our tectonic division of the Western Alboran Domain in two major units (Upper and Lower Western Alboran) separated by a major thrust. The clustering of leucogranite dike ages between 22 and 20 Ma (Esteban et al., 2011) shows that the Ronda Peridotites Thrust has a Lower Miocene age. Note that the subdivision in two units of the Alboran Domain is not relevant for Central and Eastern Betics where HP/LT units (e.g. Nevado-Filabride) with no equivalent in the Western Betics crop out below the Alpujarride (Platt et al., 2006) and where the Alpujarride does not contain mantle slivers.

The Lower Western Alboran Unit is composed mainly by “Blanca” rocks that consist mainly of a gneissic basement locally migmatitic (Acosta-Vigil et al., 2014; Sánchez-Rodriguez, 1998) covered by Triassic marbles (Sanz de Galdeano and Andreo, 1995). Locally, tectonic slivers made of Triassic (dolomitic-) and Jurassic (cherty-) limestones (O’Dogherty et al., 2001), called Dorsale Units (Martín-Algarra et al., 2004a), underline the footwall of the Ronda Peridotites Thrust and the hanging-wall of the Gibraltar Thrust. At regional scale, these Dorsale Units underline the Gibraltar Thrust in both Betics and Rif (Expósito et al., 2012; Martín-Algarra, 1987; Olivier, 1984). Conglomerates, considered post-Lower

Aquitanian (Felder, 1980), locally marked the Ronda Peridotites Thrust found on top of the Dorsale Units (Nava Breccia; dotted orange in Fig. 2.4) (Bourgois, 1978; Martín-Algarra and Estévez, 1984). Note that high-temperature metamorphism has been recently described in Dorsale Units located immediately below the peridotites (forsterite in dolomitic marble, Mazzoli et al., 2013). From the above metamorphic arguments, we propose that the "Blanca" rocks and the Dorsale Units correspond to the same tectonic unit (i.e. the Lower Western Alboran Unit), with variable degrees of high-temperature metamorphism and deformation resulting from the "hot" peridotites thrusting.

2.3.3 Lower-Mid Miocene Olistostromic Complex (LMOC)

Chaotic deposits, interpreted as of Lower to Mid Miocene age (Fig. 2.2) (Martín-Algarra et al., 2004c), characterize the Western Betics: the "Blocky-clays" formation in the External Zone and the Neonumidian formation on the Alboran Domain rocks (Bourgois, 1978). For sake of simplicity, these two Lower to Mid Miocene Olistostromic Complexes (LMOC) are called hereafter, according to their present-day location, External LMOC deposit on the External Zone and the Internal LMOC on the Alboran Domain (Fig. 2.2 and dotted orange in Fig. 2.4). Since Miocene sedimentation in these two basins is very similar, the transition in the northern sector of the Western Betics between Internal LMOC and External LMOC is not easy to identify (Crespo-Blanc and Campos, 2001), suggesting that these two basins were most likely connected at that time (Bourgois, 1978; Martín-Algarra, 1987).

This olistotromic deposit composes the major part of the Alboran Domain cover and has been previously called Alozaina complex (e.g. Balanyá et al., 2007). However, the base of the transgressive cover of the Alboran Domain (Fig. 2.2) that crops out mainly near Alozaina and La Viñuela, (orange without dots; Fig. 2.4) is usually divided in two formations (see Fig. 2.2): Ciudad-Granada at the base and La Viñuela at the top (Serrano et al., 2007). The stratigraphic succession is characterized by a deepening trend upward with a change in sedimentation-type at around 20 Ma, corresponding to the temporal boundary between the two formations (Serrano et al., 2007). The sediments were deposited exclusively on the Malaguide in the Ciudad Granada formation. In the La Viñuela formation the deposition started at 20 Ma involving metamorphic rocks of the Alboran Domain and locally peridotites (Aguado et al., 1990). The major part of the Alboran terrigenous sediments is composed of Lower to Mid-Miocene olistostrome-type deposits (LMOC), with blocks of Alboran Domain (Malaguide and Dorsale; Martín-Algarra, 1987) and of Flysch Trough Complex (Suades and Crespo-Blanc, 2013).

2.3.4 Map-scale faults

The Western Alboran Domain shows at map scale three main types of structures: strike-slip faults (Sanz de Galdeano, 1990; Sanz de Galdeano et al., 2001a), thrust faults and related folds (Balanyá and García-Dueñas, 1987; Kirker and Platt, 1998) and normal faults (Crespo-Blanc and Campos, 2001; García-Dueñas et al., 1992; Platt et al., 2003b).

Several strike-slip faults have been identified in the Western Alboran Domain with various orientations and either sinistral or dextral offsets (Balanyá et al., 2007; Sanz de Galdeano and López-Garrido, 2012a, 2012b; Sanz de Galdeano et al., 1998; Sosson et al., 1998). A N140°-trending sinistral fault is located to the NW of Estepona (Fig. 2.4) (Balanyá et al., 2007; Kirker and Platt, 1998; Sanz de Galdeano et al., 1999). E-W trending dextral faults are located in the Subbetics (Bourgois, 1978; Martín-Algarra, 1987) and at some places in the Alboran Domain (Sanz de Galdeano et al., 1996, 2001a; Tubía et al., 1997). These strike-slip faults were considered to be second order structures related to compression (Platt et al., 1995). Recently, a structural study (Díaz-Azpiroz et al., 2014) suggested that the deformation pattern associated to the Torcal fault zone was dominated by E-W dextral shearing between Upper Miocene and Present. The present-day seismicity is moreover consistent with such deformation kinematics (Balanyá et al., 2012; Ruiz-Constán et al., 2012b). In the following, we argue that such a deformation pattern was mostly acquired during Lower Miocene but has most probably been active since then, corresponding to a single, although complex, deformation event. Our structural mapping documents the geometry and kinematics of two main strike-slip corridors that are major regional-scale tectonic features in the study area. The term "strike-slip corridor" is here used to pick out elongated and broad deformation zones characterized by dominant along-strike displacements. The Torcal corridor corresponds to the northern boundary of the Alboran Domain that is in contact with the External Zone. The Coín corridor separates a northern domain dominated by Dorsale Units and Internal LMOC sediments from a southern domain dominated by Ronda Peridotites and the "Blanca" rocks, as displayed at map scale (Fig. 2.4) and highlighted in the N-S cross-section (Fig. 2.5). Structural evidence for dextral strike-slip shear in these corridors was previously described by Barcos et al. (2011, 2014), Sanz de Galdeano and López-Garrido (2012a, 2012b) and Díaz-Azpiroz et al. (2014) for the Torcal de Antequera corridor and by Tubía et al. (1997), Sanz de Galdeano et al. (2001a) for the Coín corridor.

The orientation of thrusts (mainly N45°-50°, with the exception of the Flysch Trough) and related folds in the External Zone is based on previously published geological maps and our own mapping (in the vicinity of the IEZB) (Fig. 2.4). Jurassic formations outcrop in the core of open antiforms that likely reflect the presence of blind thrusts in the External Zone (as drawn in cross-section; Fig. 2.5). In the Alboran Domain, the Ronda Peridotites Thrust is strongly deformed in the hanging-wall of the IEZB (Fig. 2.4 and cross-sections in Fig. 2.5), as shown by the tectonic windows in which the Lower Western Alboran Unit crops out (south-west of Coín).

Normal faulting is widespread in the Western Betics. A strong extensional reactivation, mostly during Serravallian (see section 2), has been proposed for the IEZB, leading some

authors to draw the IEZB as an extensional contact (Balanyá et al., 1997; Crespo-Blanc and Campos, 2001; García-Dueñas et al., 1992). Although the Ronda Peridotites Thrust is indeed slightly reactivated in extension at some places (e.g. in the vicinity of Alozaina; Fig. 2.4), this major extensional reactivation of previous thrusts is nevertheless questioned by several studies (Kirker and Platt, 1998; Mazzoli and Martín-Algarra, 2011; Esteban et al., 2013). Our objective is here to constrain the structure related to thrusting and not to discuss later reactivations. From our structural work, the most common map-scale normal faults trend N140° (Balanyá et al., 2007) and crosscut all the lithological contacts in the Alboran Domain and in the Subbetics (Fig. 2.4). These normal faults controlled the deposition of Upper Miocene (Late Tortonian to Early Messinian; Martín et al., 2001) sediments, in elongated basins trending N140° to the North-West of Ronda (Jiménez-Bonilla et al., 2011; Ruiz-Constán et al. 2009) (Fig. 2.2) and in the Alboran Domain, near Álora (López-Garrido and Sanz de Galdeano, 1999; Martín et al., 2001) (Fig. 2.4).

2.3.5 Cross-sections

Our regional-scale cross-sections (Fig. 2.5), based on our own structural data and previously published cross-sections that considered available geophysical data (Balanyá et al., 1997; García-Dueñas et al., 1992; Mazzoli and Martín-Algarra, 2011), show the relationships in time and space between the two main thrusts (Ronda Peridotites Thrust on top and Gibraltar Thrust/IEZB below) and the strike-slip corridors.

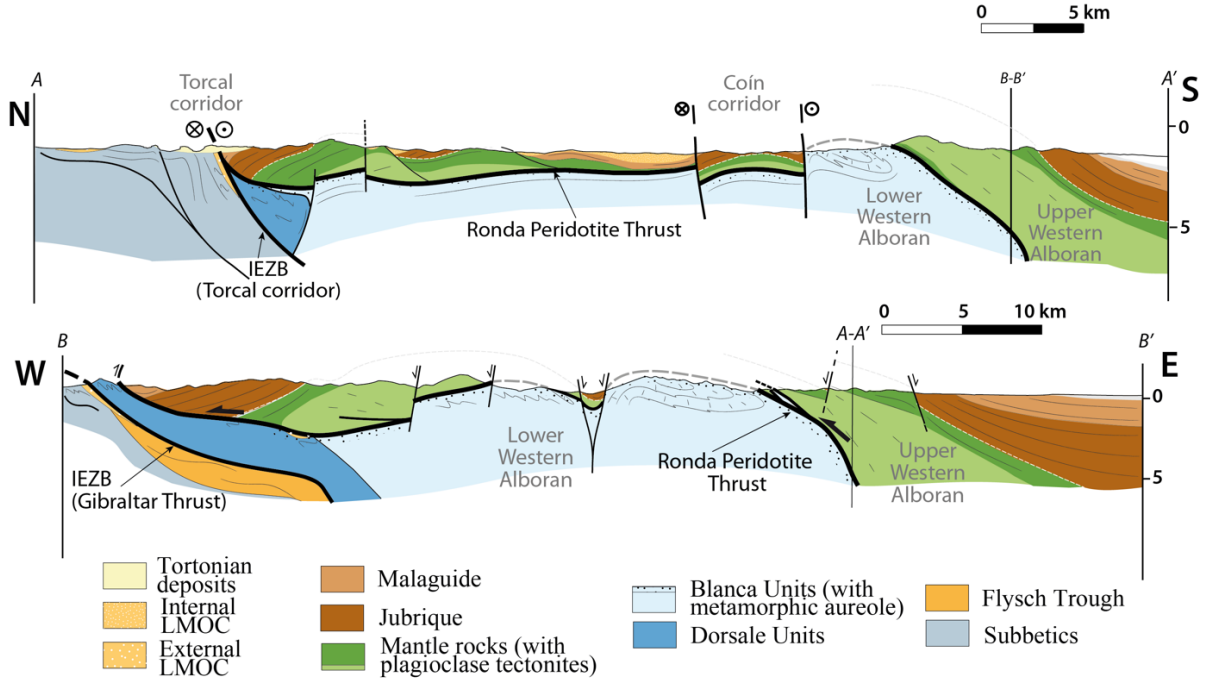

Figure 2.5. Synthetic cross-sections (see location in Fig. 2.4). Interpretation below 5 km is omitted due to the lack of geophysical data.

Cross-section AA' that is N-S oriented shows the relationship between the thrusts and

the strike-slip corridors of Torcal to the North and Coín to the South, which are deformation zones, few kilometer wide, marked by abrupt changes in lithology.

Between the two corridors, the Ronda Peridotites Thrust is involved in broad synclines and anticlines close to the major strike-slip faults but maintains an almost flat-lying attitude. The Internal LMOC sediments, only observed in the northern block (between the Torcal and Coín Corridors) are deposited and deformed in such a syncline.

Cross-section BB', that is E-W oriented, highlights the relationship between the Gibraltar Thrust (the N60º-trending segment of the IEZB) and the Ronda Peridotites Thrust that is folded in the hanging-wall of the Gibraltar Thrust. Moreover, the Upper Western Alboran Unit is dipping westward on top of the Ronda Peridotites Thrust in the westernmost part of the cross-section. This geometry suggests a thrust-propagating system with a hanging-wall ramp lying on top of a footwall flat. Conversely, to the East, the relationship between Upper and Lower Western Alboran Units corresponds to hanging-wall flat lying on top of a footwall ramp. The Gibraltar Thrust with a similar geometry acted in the same thrust-propagating system, resulting in a typical pile of in-sequence thrust-sheets. The deformation is accommodated along a few-hundred meters thick metamorphic sole but imply local inversion of the litho-stratigraphy in the footwall and in the hanging-wall (Fig. 2.5).

2.4 The Torcal strike-slip corridor

The IEZB is characterized by a regional-scale arcuate shape in the northern part of the map where it evolves from N60° (Gibraltar thrust) to E-W (Torcal fault zone) (Fig. 4). A more detailed structural map of the IEZB in the northern Western Betics summarizes our structural mapping (see foliation trajectories in Fig. 2.6a and stereoplot Fig. 2.6b).

The map displays (Fig. 2.6a): 1) the Subbetics Units: Triassic clays and evaporites (violet), Jurassic massive limestones (blue) and layered Cretaceous marly-limestones (green); 2) the Upper Western Alboran Unit: Malaguide rocks (brown), Jubrique rocks (red) and peridotites, often serpentinized (green); 3) the Lower Western Alboran Unit (Dorsale and "Blanca" rocks in blue) and 4) sedimentary basins: Internal LMOC (pale yellow with little white dots), External LMOC (pale yellow with big white dots) and Tortonian-Messinian conglomerates (beige). The IEZB is strongly arcuate and fault data were therefore collected in several areas that could be representative for both almost N-S and E-W trends observed. In this area, map-scale relationships between normal, thrust and dextral strike-slip faults suggest their at least partly simultaneous development. Field measurements were made, as far as possible, on fault-mirrors cross-cutting the main pre-existing lithological discontinuities, and only in sectors where at map scale the three different types of faults (normal, thrust and dextral strike-slip) could be observed with a geometrically compatible pattern. Faults with non-ambiguous slip indicators were mainly identified at the boundaries between layered Cretaceous carbonates (green) and massive Jurassic carbonates (pale blue) in the Subbetics and along the lithological contacts between Jubrique gneisses and Malaguide slates and between marbles and schists in the Alboran Domain.

Fault kinematic analysis was made using the methodology of Marrett and Allmendinger (1990). Using the FSA software of Célérier (2013), we extracted from each fault population the strike-slip, normal and thrust faults with dispersion of slip-vector orientation of maximum 40º with reference to a hypothetical pure fault with the same attitude. We calculated the average incremental principal strain axes and, in order to better visualize the results and data dispersion, the contour of the principal strain axes has been also obtained with the FaultKin software of Marrett and Allmendinger (1990). Detailed strain analyses of the corridor are provided in the supplementary material (also for the Coín Corridor) and the related overall strain pattern is given in Figure 2.6c.

Structural data (foliation strike and dip, fault-slip, fold axes) are derived from our structural mapping (conducted at a 1:50000 scale) and from available data for the area East of Álora (Booth-Rea et al., 2003) and North of the Huertas y Montes village (Crespo-Blanc and Campos, 2001). Foliation trajectories and bedding envelopes were constructed using around 900 measurements of the main foliation in crustal and mantle rocks and bedding in Mesozoic and Miocene sediments.

2.4.1 Structures of the El Chorro sector

The E-W corridor, along 30 km, is marked in the Subbetics by ENE trending en-échelon anticlines affecting competent Jurassic limestones (Fig. 2.4). The Torcal and El Chorro anticlines are separated by an 8 km long depression, filled by thin and partly deformed olistostromic sediments (Fig. 2.6a). The IEZB limits the anticlines to the South and corresponds to the master fault of the Torcal corridor deformation zone, as evidenced by the steepening of bedding and foliation at its vicinity (right side of Fig. 2.7a). Sub-horizontal Tortonian sediments lie unconformably on top of upward bent older layers of the El Chorro area (left side of Figs. 2.6a and 2.7a) providing an important time constraint for the deformation along the Torcal corridor.

Three sets of faults, E-W dextral strike-slip, N60° thrust and N140° normal, are responsible for the morphology of the *en échelon* anticlines and are widespread in the corridor. E-W dextral strike-slip fault zones bound the Torcal de Antequera massif to the North and South. The El Chorro sector is composed by an overall ENE trending anticline, well developed in its eastern part, delimitated by N140° normal faults to the East and by a N60° transpressional fault zone to the South, in lateral continuity with the southern dextral strike-slip fault of the Torcal area (Fig. 2.6a). The cylindrical best fit of bedding and foliation surfaces measured in the El Chorro sector in stereographic projection (Fig. 2.6b; box in Fig. 2.6a) gives an ENE trending axis, marked in the field by a big-scale box fold in the eastern part of El Chorro sector. A NE-trending thrust and an E-W strike-slip fault are located in the core of the anticline (inside the box of Fig. 2.6a).

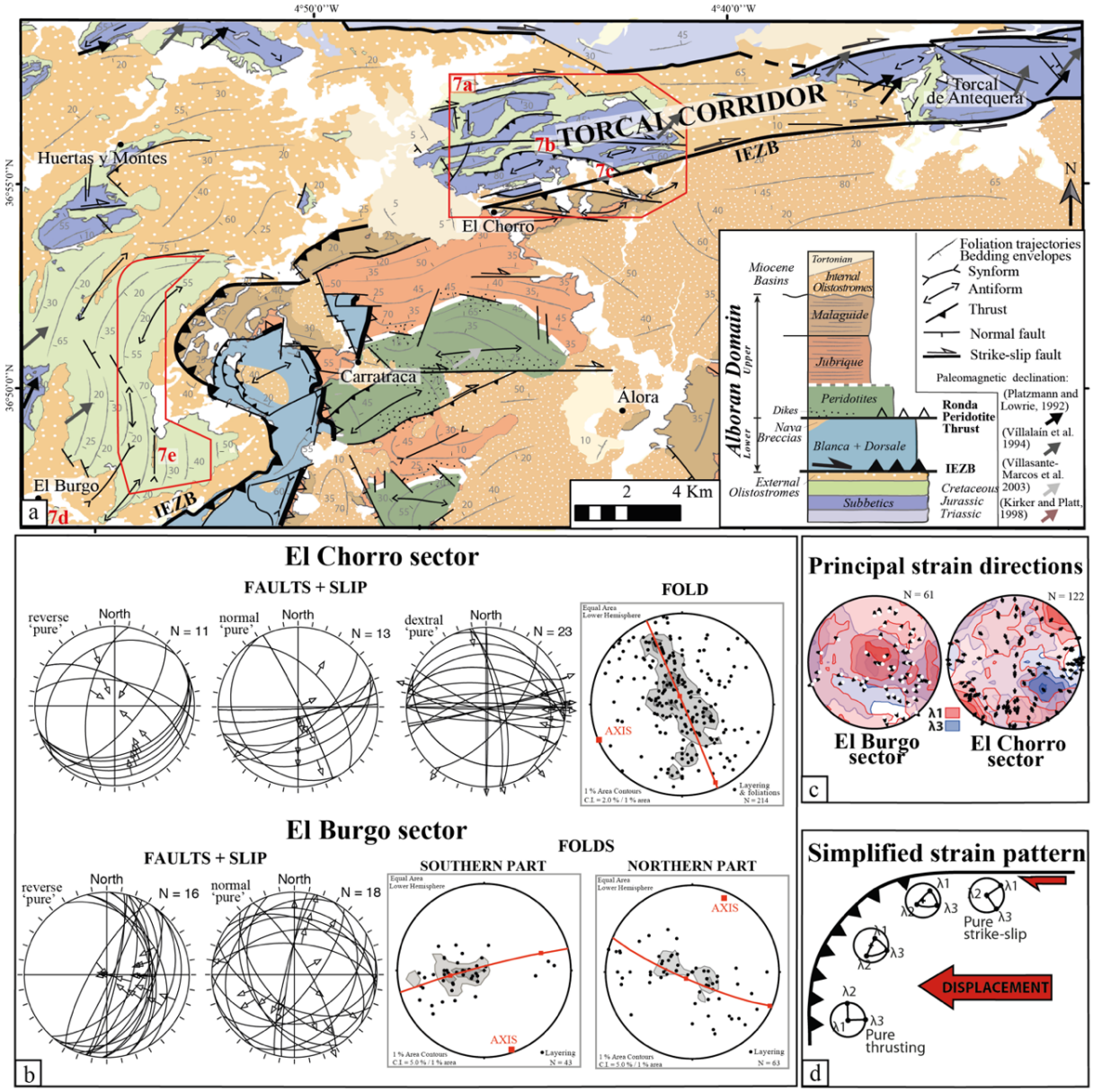

Figure 2.6. (a) Structural map of the Torcal corridor between El Burgo and the Torcal de Antequera (lithotypes after our own mapping and previous works (Argles et al., 1999; Barcos et al., 2011; Cano Medina, 1990; Chamón Cobos et al., 1972; Cruz San Julián, 1990; Del Olmo Sanz et al., 1990). A synthetic vertical section shows the main tectonic units and contacts. Red numbers indicate the location of Fig. 2.7 photographs. Paleomagnetic declination for the Subbetics and for the Alboran Domain are drawn after Platzman and Lowrie (1992), Villalaín et al. (1994) and Villasante-Marcos et al. (2003). (b) Stereoplots of data collected in the areas marked in red on the map of Fig. 6a (lower hemisphere; Schmidt net; using OSXStereonet: version 9.2.0. **http://www.ux.uis.no/~nestor/work/programs.html** and Fsa: Fault slip analysis software. Version 35.1. http://www.pages-perso-bernard-celerier.univmontp2.fr/software/dcmt/fsa/fsa.html). Faults with an oblique slip-vector (higher than 20° from the ideal pure-slip vector for each fault) are not reported; (c) Principal strain directions obtained with FaultKin (http://www.geo.cornell.edu/geology/faculty/RWA/programs/faultkin.html). For sake of clarity, only striaes and slip directions are indicated with the contours of λ1 (red) and λ3 (blue) distribution obtained for each fault mirror measured. For a detailed strain analysis of the corridor see *supplementary material*. (d) Simplified evolution of the principal strain directions from frontal to lateral ramps of Fig. 2.6a. Red arrow: displacement of the Alboran Domain. Figure S1 in supplementary material presents a complete description of the principal strain directions.

Outcrop-scale reverse faults in the El Chorro sector show a dispersion with a distribution in 3 families: N50°, N70° and N110°. Despite this variation, probably due to

lithological heterogeneities, the related slip-vectors display a remarkably constant trend N160°. This indicates that all these reverse faults are kinematically compatible with a N160° direction of shortening, which is almost perpendicular to the IEZB in this region.

Strike-slip faults oriented E-W or WSW-ENE are sub-vertical. Small R-type shear planes (Fig. 2.7b) and calcite fibers in veins usually mark the slip direction on fault surfaces. In the El Chorro area, their average trend is N80° with a scattering of almost 50° and a high dispersion in the plunge angle (stereoplot; Fig. 2.6b). The slip-vectors always plunge at low-angle dominantly eastward, suggesting a vertical movement of the Subbetics relative to the Alboran Domain. E-W right-slip vertical faults do not cut the open fold responsible for the arcuate outcrop pattern of the Flysch sediments west of Ardales, which marks the western end of the corridor, in the Huertas y Montes region.

Normal faults are often marked by pull-apart type veins, showing usually calcite step structures, or by wear grooves in the contact strain zones between massive Jurassic limestones and layered Cretaceous marly-limestones (Fig. 2.7c). Trend dispersion of these faults dipping at high or low angles is large but with maxima around N140° and E-W (Fig. 2.6b).

The absence of a systematic cross-cutting relationship between E-W dextral strike-slip, N70° thrust faults and N140° normal faults suggests a coeval development of these three sets of faults. This indicates principal directions of shortening and stretching trending N160° and N70°, respectively. *En-échelon* folding in the Subbetics, underlined and bounded by E-W dextral strike-slip faults, suggests that the whole set of faults resulted from E-W strike-slip simple shear, with locally a possible but small component of pure shear due to rheological contrasts between different lithological formations.

2.4.2 Structures of El Burgo sector

NE of El Burgo, the IEZB has an average N20° trend at map scale. However, the combination of N50° thrust segments, N140° normal and rare strike-slip fault segments locally accommodate the IEZB arcuate geometry. In the study sector, bedding envelopes and fold axial traces follow the Gibraltar Thrust/IEZB contour at map scale (Fig. 2.6a).

The trend variation of the folds from the northern part, close to Ardales, to the southern part, close to El Burgo, is also illustrated in Figure 2.6b. The pole of the cylindrical best fit of bedding pole stereoplot swings by almost 45°, keeping a sub-horizontal plunge. Therefore, no significant vertical movement can be postulated from the bedding strike and dip data. Folds in the layered Cretaceous marly-limestones can vary from tight to open, mainly as a function of their distance from the Gibraltar Thrust. They correspond to fault-propagation folds (Fig. 2.7d) whose dominant asymmetry indicates a top-to-the- W-NW sense of shear, consistent with the ramp-flat structures observed in the field (Fig. 2.7e). As in the El Chorro sector, normal faults have a variable trend with a mean at N140° (Fig. 2.6b). The associated slip vectors show roughly a N50° direction of stretching.

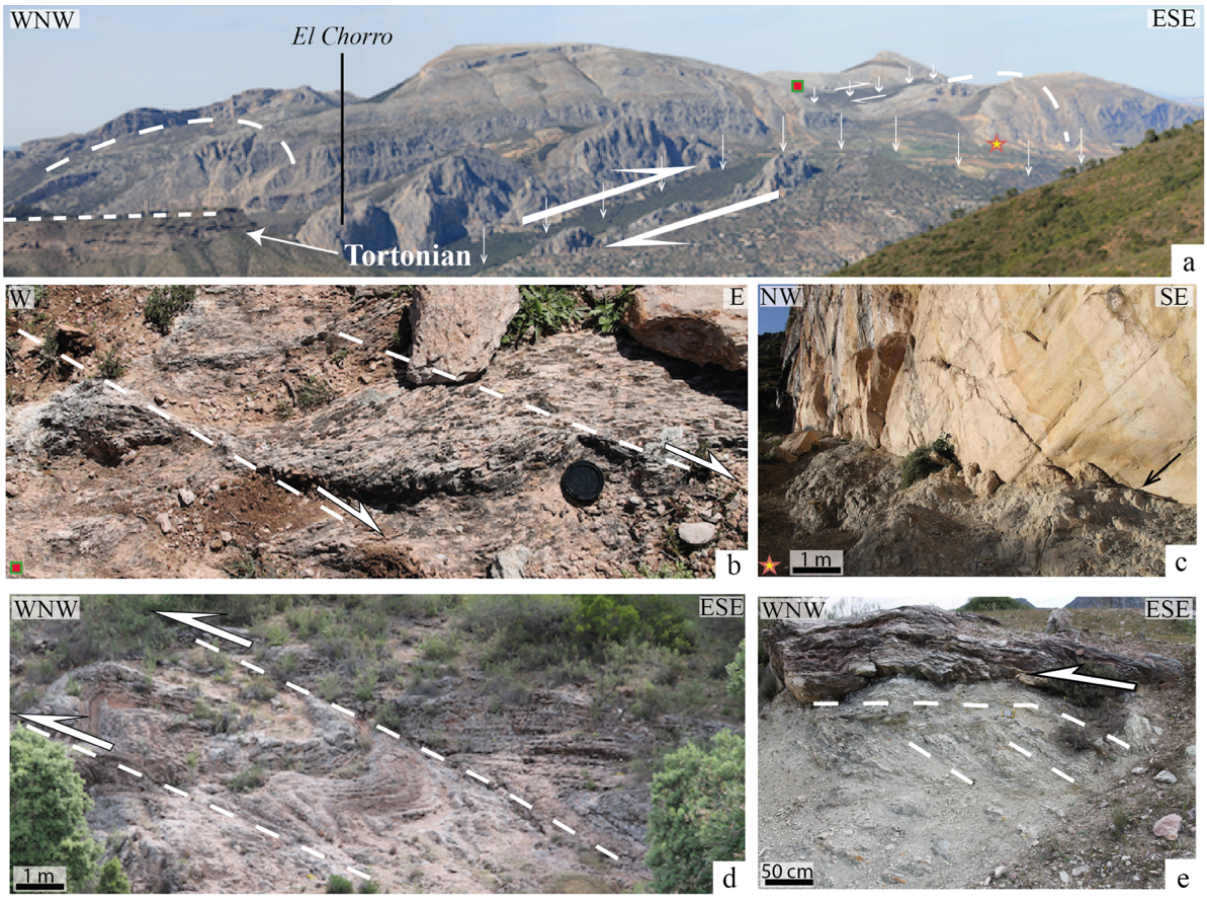

Figure 2.7. Some typical structures of the El Chorro sector (see location in Fig. 2.6a): (a) Panoramic view of the Torcal strike-slip deformation zone and of the anticline NE of El Chorro village. Note the flat-lying Tortonian on the left-side. Square and star indicate the location of Figs. 2.7b and c, respectively. (b) Riedel-type shear planes indicating a dextral slip in an E-W vertical fault zone inside Upper Cretaceous marly-limestones. (c) Normal fault with a strong oblique dextral-slip component at the contact between Jurassic limestones and Cretaceous marly-limestones. (d) Fault-propagation-folds and (e) a flat-and-ramp structure, show a top-to-the-WNW sense of shear in the Upper Cretaceous marly-limestone close to El Burgo.

2.4.3 Strain and kinematics

In El Chorro sector, N70° trending thrust, E-W dextral strike-slip and N140° trending normal faults are found to be synchronous. The whole set of data acquired in this region indeed shows a 3D strain tensor with principal strain axes λ_1 trending N45º, λ_2 steeply dipping to the NW, and λ_3 trending N135°, indicating a transpressional regime. Moreover, the strain derived from the entire set of measurements in the El Burgo sector shows a plunge increase of λ_1 and shifting of λ_3 slightly towards a N100° trend, suggesting a thrust component increase (see schema Fig. 2.6d). This deformation pattern implies a large-scale vertical zone of dextral strike-slip simple shear with principal directions of shortening and stretching trending N135° and N45°, respectively. At regional-scale, this implies a N90° direction of displacement of the Alboran Domain with respect to Iberia. This westward motion is accommodated by a lateral strike-slip ramp to the north (Torcal corridor) and a frontal thrust ramp to the west (Gibraltar Thrust). This is responsible for the general change in dip direction of the IEZB from N60° to E-W. An increase of the amount of dextral shear

along the corridor likely explains the evolution of fold axis trend from N40° to N70° from north of El Burgo to El Chorro. Furthermore, clockwise block rotations measured by paleomagnetism (Platzman and Lowrie, 1992; Villalaín et al., 1994) (see paleomagnetic declinations in Fig. 2.6a and 2.8a) are in agreement with such a deformation pattern with simple shear and rotations involving also the frontal thrust ramp of the system (Gibraltar Thrust of the El Burgo sector).

Internal deformation within the Alboran Domain is also consistent with this E-W dextral simple shear. East and south-east of Carratraca, the interconnection between a WSW-ENE thrust fault, that reactivated a previous extensional structure (Argles et al., 1999; Esteban et al., 2004), E-W dextral strike-slip fault and a N140° trending normal fault-zone supports this overall strain pattern. Moreover, the leucogranite dikes, associated with the Ronda Peridotites Thrust, are more abundant in the vicinity of the E-W serpentinite fault gouges, suggesting also an interplay between E-W strike-slip faulting and "hot" thrusting.

The overall geometry of the Internal LMOC is controlled at map scale (Figs. 2.4 and 2.6a) by a N60° trending syncline whose orientation is compatible with the inferred principal strain directions. Because the type of sedimentation is mainly olistostromic in this basin (Suades and Crespo-Blanc, 2013), we suggest that the LMOC was deposited during the deformation along the strike-slip corridors. The Internal LMOC can therefore be interpreted as a piggy-back basin deposited and deformed during the westward motion of the Alboran Domain and, in the other hand, the contemporaneous and connected External LMOC as chaotic mélange deposited at the front of the advancing nappe and involved in the deformation (wildflysch). Late Tortonian-Early Messinian sediments, controlled by N140º normal faults NW of Malaga (Fig. 2.4) generally seal the previous structures. The deformation pattern described therefore occurs in Lower to Mid Miocene in time (Fig. 2.6). Note that the Late Tortonian – Early Messinian sediments are locally deformed (north of the Torcal strike-slip corridor), suggesting a continuous deformation from Lower Miocene to Upper Miocene (Díaz-Azpiroz et al., 2014; Insua-Arévalo et al., 2012).

2.5 The Coín dextral strike-slip corridor

The Coín strike-slip corridor is characterized by the map-scale predominance of E-W trending dextral strike-slip faults. With a general E-W trend along 50 km, the corridor involves the whole Alboran Domain (Fig. 2.8a; same colour captions than in Fig. 2.6a). The IEZB and the Subbetics sediments mark the western tip of the dextral fault zone and the E-W trending coastline starting in Malaga (Fig. 2.4) is its eastern end.

The Coín high strain deformation zone is around 4 km wide and divides the Alboran Domain in two E-W elongated lower strain blocks, as exemplified in the N-S cross-section (Fig. 2.5). The northern block displays the largest domain of Lower to Mid Miocene olistostromic sediments (LMOC) whose deposition is syn-kinematic with the strike-slip corridors. The southern block displays the deeper parts of the Alboran Domain with a large exposure of the Ronda Peridotites, the Ronda Peridotites Thrust and the "Blanca" rocks of the

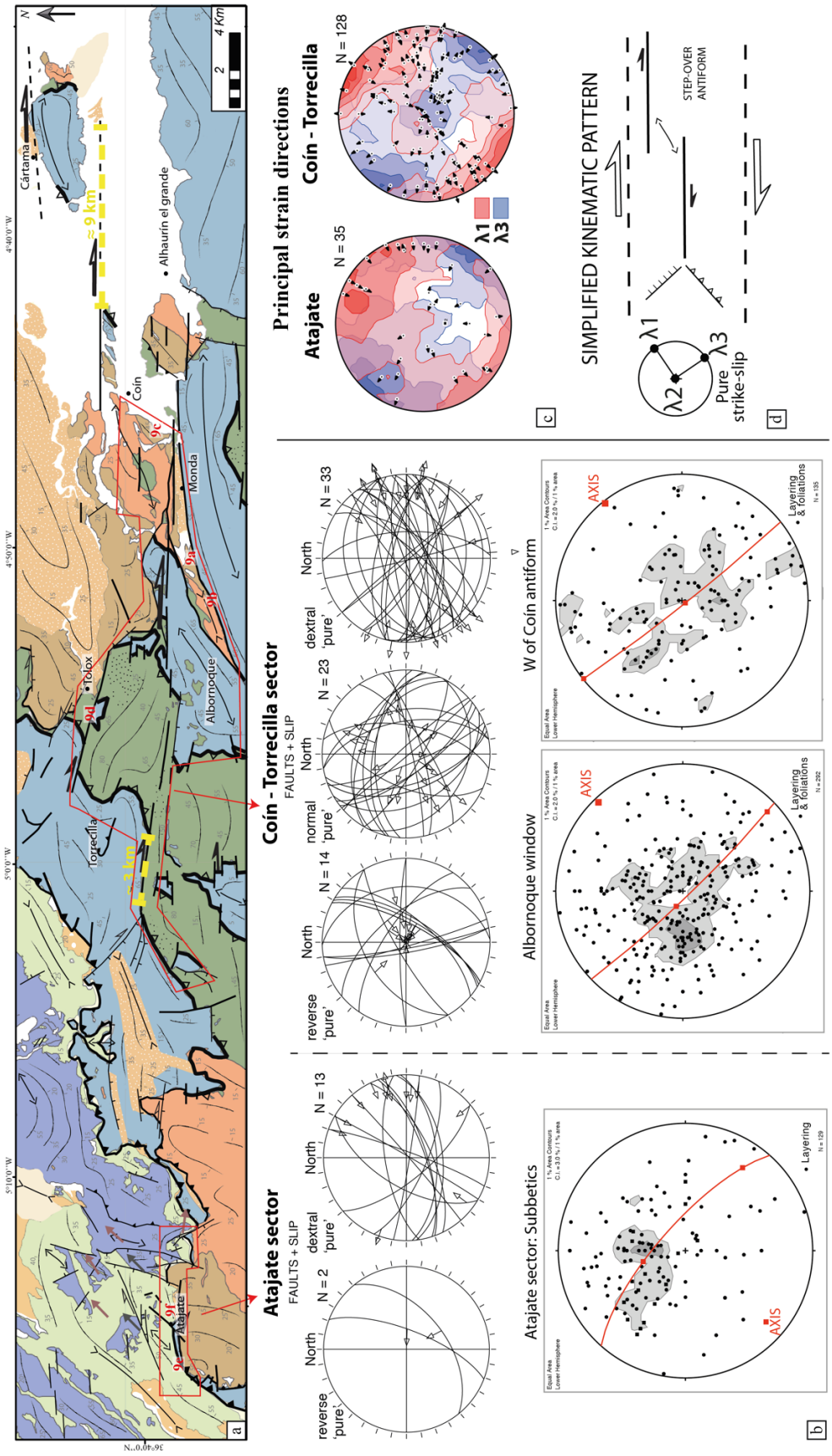

Figure 2.8. (a) Structural map of the Torcal corridor between El Burgo and the Torcal de Antequera (lithotypes after our own mapping and previous works (Argles et al., 1999; Barcos et al., 2011; Cano Medina, 1990; Chamón Cobos et al., 1972; Cruz San Julián, 1990; Del Olmo Sanz et al., 1990). A synthetic vertical section

shows the main tectonic units and contacts. Red numbers indicate the location of Fig. 2.7 photographs. Paleomagnetic declination for the Subbetics and for the Alboran Domain are drawn after Platzman and Lowrie (1992), Villalaín et al. (1994) and Villasante-Marcos et al. (2003). (b) Stereoplots of data collected in the areas marked in red on the map of Fig. 2.6a (lower hemisphere; Schmidt net; using OSXStereonet: version 9.2.0. http://www.ux.uis.no/~nestor/work/programs.html and Fsa: Fault slip analysis software. Version 35.1. http://www.pages-perso-bernardcelerier.univmontp2.fr/software/dcmt/fsa/fsa.html). Faults with an oblique slip-vector (higher than 20° from the ideal pure-slip vector for each fault) are not reported; (c) Principal strain directions obtained with FaultKin (http://www.geo.cornell.edu/geology/faculty/RWA/programs/faultkin.html). For sake of clarity, only striaes and slip directions are indicated with the contours of λ1 (red) and λ3 (blue) distribution obtained for each fault mirror measured. For a detailed strain analysis of the corridor see supplementary material. (d) Simplified evolution of the principal strain directions from frontal to lateral ramps of Fig. 2.6a. Red arrow: displacement of the Alboran Domain. Figure S1 in supplementary material presents a complete description of the principal strain directions.

Lower Western Alboran Unit. Fault data were collected with the same criteria than those of section 4, in areas along the E-W trending corridor where at map scale the relationships between normal, thrust and dextral strike-slip faults could suggest a coeval action.

2.5.1 Internal deformation of the Alboran Domain

The Alboran Domain is characterized by three main sets of faults trending N50°, N90° and N140° and a minor fourth set trending N-S (Fig. 2.8a). The major set is the E-W-trending dextral strike-slip faults. The map-scale E-W trending faults are more common in the eastern part of the map (Fig. 2.8a) and are progressively replaced towards the west by splay faults with different orientations and kinematics (Fig. 2.8d), suggesting a progressive decrease of displacement towards the west.

The eastern part of the Corridor shows that the Ronda Peridotites Thrust is cut by E-W dextral strike-slip faults with a minimum apparent offset of 9 km (East of Cartama; Fig. 2.8a). In the Coín–Torrecilla sector, the E-W strike-slip faults occur usually with a few meters wide brecciated zones, surrounded by highly fractured rocks. Flower structures (Fig. 2.9a) and tightly asymmetrical folds in the Malaguide slates (Fig. 2.9b) mark the dextral shearing in the fault damage zones. Fault mirrors within fault core zones display often grooves, striaes and slickenlines with plough marks (Fig. 2.9c). At outcrop scale, the trend of pure dextral strike-slip faults is scattered around an average E-W trend indicating that they probably represent minor shear planes (e.g. P- and R-shear planes of the Riedel shear model) oblique to the major shear surface (Fig. 2.8b). Rotation of foliation trajectories (South of Alhaurín, Fig. 2.8a) also supports the existence of major map-scale dextral strike-slip fault zones (e.g. in the panoramic view of Fig. 2.9d). Similarly, in the Albornoque window close to Coín, a SW-NE trending antiform developed in the zone of dextral strike-slip faults step-over (Fig. 2.8a) and explains the dispersion in trend and dip angle of bedding and foliation measurements (Fig. 2.8b). The depocenter geometry of the Internal LMOC was controlled by a N70° syncline to the East of Tolox, providing a Lower Miocene age for the NW-SE shortening. Conversely, flat-lying Late Tortonian – Early Messinian conglomerates are found in the vicinity of the Cartama anticline and hence post-date the inferred deformation pattern.

N140°-trending normal faults (Fig. 2.8b) with a short horizontal length were identified at outcrop-scale by offsets, deflections and sigmoidal shapes of foliations trajectories in the fault damage zones. In this sector (south-west of Torrecilla), the Ronda Peridotites Thrust is cut by an E-W strike-slip fault (3 km of horizontal offset, Fig. 2.8a), explaining the change in trend of the thrust faults from N60° to N-S north of the strike-slip fault (Fig. 2.8b). Note that the E-W strike-slip corridor ends onto the Ronda Peridotites Thrust into a N140°-trending normal fault to the North and N70° thrust fault to the south. This strongly suggests that the strike-slip and normal faults and the Ronda Peridotites thrust developed more likely simultaneously.

2.5.2 The IEZB near Atajate

To the East and West of Atajate (Fig. 2.8a), the trend of the IEZB progressively evolves towards the south from NE-SW, to E-W and then to NNE-SSW again. Strain along the IEZB is thus partitioned in strike-slip (Fig. 2.9e), NE-SW-trending IEZB, and thrust, E-W-trending IEZB, segments. The E-W strike-slip fault zone does not cross-cut the External LMOC to the West of Atajate, but implies a clockwise rotation of the fold axes (Fig. 2.9f) in the Subbetics.

2.5.3 Strain and kinematics

Along the Coín Corridor, like along the Torcal corridor, the different fault sets do not show any systematic cross-cutting relationship, suggesting a coeval development of thrust, strike-slip and normal faults. The dominance of E-W dextral strike-slip faults indicates a dextral simple shearing along the corridor, with a NW-SE direction of shortening and NE-SW direction of stretching. Moreover, the whole set of acquired fault data shows a pure strike-slip 3D strain tensor in the Coín sectors (128 data). The E-W strike-slip system merges into the IEZB, steepened and with a strike-slip kinematics only close to Atajate where the trend is generally E-W. The kinematic analysis (Fig. 2.8c) shows a distribution of the principal strain directions similar to the Alboran Domain pattern. The same type of relationship between the Ronda Peridotites Thrust and the strike-slip corridor strongly suggests that the same kinematics (i.e. NW-SE shortening and NE-SW stretching) controlled the motion of the Ronda Peridotites Thrust.

The trend of folds in the Subbetics evolves from NNE to ENE, suggesting a westward motion of the southern block with respect to the northern block. The Coín corridor is thus a deformation zone located inside the westward moving Alboran Domain, with a southward increase of displacement. The strike-slip fault offset decreases from East to West: around 9 km near Cartama, 3 km in Torrecilla (offset of the Ronda Peridotites Thrust) and merging then into IEZB (Fig. 2.8a).

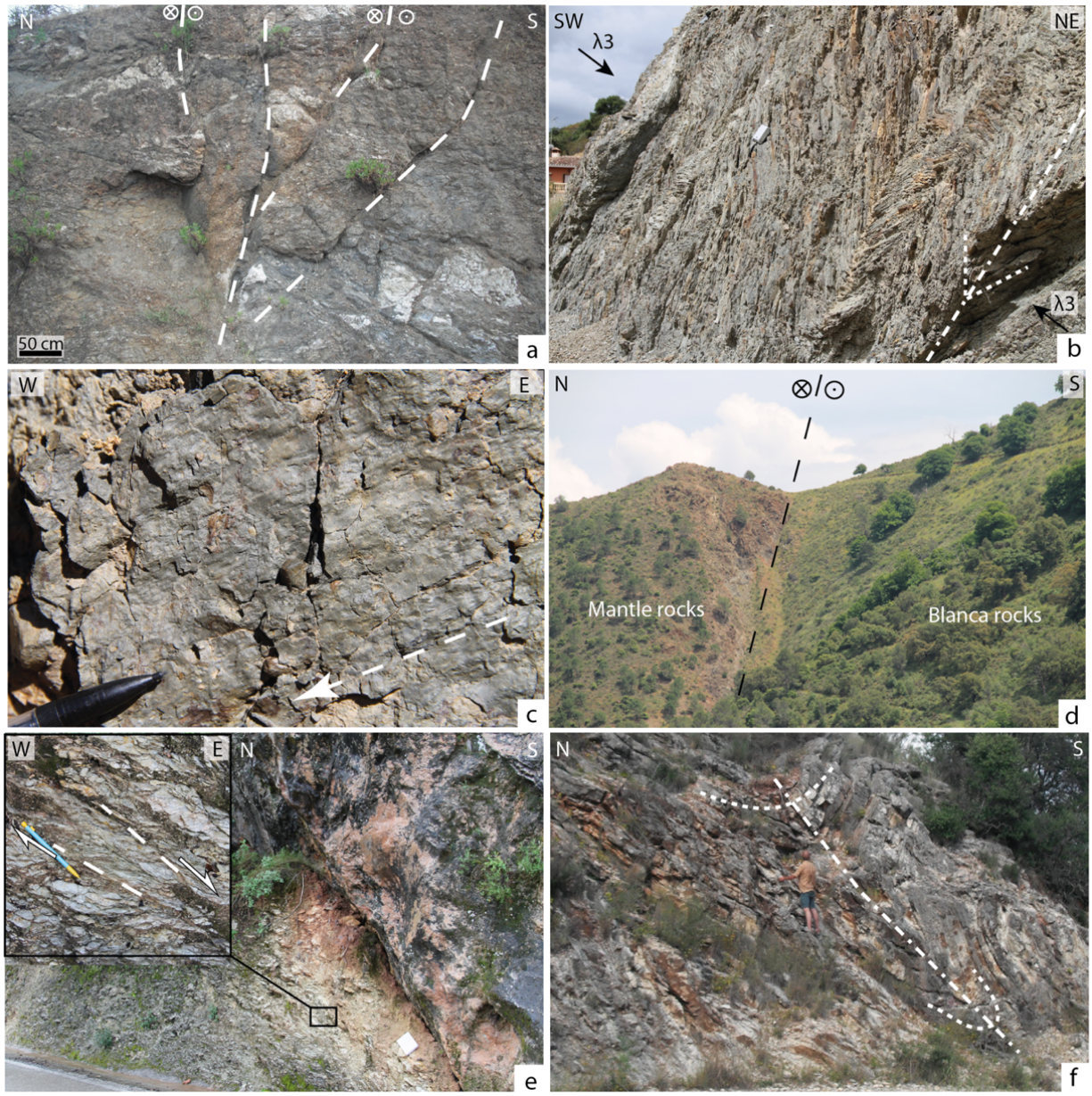

Figure 2.9. Some typical structures of the El Chorro sector (see location in Fig. 2.6a): (a) Panoramic view of the Torcal strike-slip deformation zone and of the anticline NE of El Chorro village. Note the flat-lying Tortonian on the left-side. Square and star indicate the location of Figs. 2.7b and c, respectively. (b) Riedel-type shear planes indicating a dextral slip in an E-W vertical fault zone inside Upper Cretaceous marly-limestones. (c) Normal fault with a strong oblique dextral-slip component at the contact between Jurassic limestones and Cretaceous marly-limestones. (d) Fault-propagation-folds and (e) a flat-and-ramp structure, show a top-to-the-WNW sense of shear in the Upper Cretaceous marly-limestone close to El Burgo.

2.6 Lower Miocene coeval thrusting and strike-slip faulting

2.6.1 Westward motion of the tectonic units along the IEZB

The more likely tectonic scenario that explains the Lower Miocene deformation pattern observed in the Western Betics is a continuous westward translation of the tectonic units composing the Alboran Domain, with reference to Iberia.

The motion of the Alboran Domain is accommodated by two main movement zones: a N60°-trending frontal thrust ramp (i.e. the Gibraltar Thrust) and an E-W lateral (strike-slip) ramp (i.e. the Torcal corridor). The combination of these two ramps (Boyer and Elliott, 1982) explains the arcuate geometry of the IEZB observed at their intersection, with trends roughly around N60° to the West and E-W to the North. The N-S strain gradient across the Alboran Domain leads to strain localization along the Coín Corridor. Brittle deformation affected the whole Western Betics with coeval N140° normal, N60° thrust and E-W strike-slip faults that are all compatible with an E-W-trending strike-slip simple shear whose principal directions of shortening and stretching trend N135° and N45°, respectively.

This interpretation is consistent with the conclusion drawn by Balanyá et al. (2007) concerning the N90°-trending Torcal strike-slip corridor. In addition, we suggest a transpressional regime along this corridor, as recently proposed by Díaz-Azpiroz et al., (2014). In a westward motion, transpressional deformation may be related to boundary effects along the lateral ramp between the moving Alboran Domain and the External Zone. As a consequence, any N120° strike-slip corridor in the Torcal area (Platt et al., 2003a) must be ruled out.

The novelty of our work is to show that an E-W strike-slip corridor developed inside the Alboran Domain, with a simple shear deformation pattern, strongly supports a westward displacement of the whole Alboran Domain (Fig. 2.10). This dextral simple shear at regional-scale also explains clockwise rotation of tectonic units (Platzman and Lowrie, 1992; Platt et al., 1995). Radial slip vectors in the External Zone (Balanyá et al., 2007; Platt et al., 2013, Figs. 2.3 and 2.10) are not incompatible with such a westward motion (the dispersion in slip-vectors due to thrust-sheets rotation is demonstrated geometrically in the appendix of Kirker and Platt, 1998).

Neither the bulk amount of shortening accommodated by the IEZB nor the amount of westward displacement along the corridors can be precisely estimated since i) no available reflection seismic line images the whole study area, ii) the tectonic units have not a constant thickness, and iii) deformation is accommodated in several splays at the tip of the strike-slip corridors with no reliable displacement markers on their two sides. However, an important outcome of our study is that the amount of strike-slip displacement decreases westward. In the Torcal corridor, the evolution of fold axis trend from N70° to N40° along the lateral strike-slip ramp of the IEZB suggests a westward decrease of dextral displacement. Likewise, the measured horizontal offset in the Coín Corridor decreases westward from 9 km to 3 km.

2.6.2 Relationship between Ronda Peridotites Thrust and IEZB, and ages of deformation

On the basis of the new collected structural data (maps Figs. 2.6 and 2.8 and cross-sections Fig. 2.5), we propose that the piling up of thrust units in the Western Betics occurred in two time steps. First, the Ronda Peridotites Thrust brought a portion of thinned continental lithosphere (Upper Western Alboran Unit, Précigout et al., 2013) on top of the Lower Alboran. This "hot thrusting" (i.e. bringing the hot base of a lithosphere section on top of upper crustal rocks) leads to i) high-temperature metamorphism of the footwall units, up to partial melting, and intrusion of acid dikes (Cuevas et al., 2006; Tubía et al., 1997) in the Upper Western Alboran Unit and ii) peridotite deformation in the plagioclase facies (Hidas et al., 2013; Précigout et al., 2013) and iii/ mafic dikes intrusion in the Ronda Peridotites with a geochemical signature indicating incipient subduction of Blanca-type rocks under the peridotites (Marchesi et al., 2012). During a second stage, more likely during the Lower to Mid Miocene (compare to Fig. 2.2), the IEZB lead to the emplacement of the previous nappe stack of the Alboran Domain onto the External Zone. However, the connection between the Ronda Peridotites Thrust and the IEZB (Gibraltar thrust) close to Atajate (Fig 2.4) may suggest a partly coeval activity of these two thrusts.

Our structural work supports that the second thrust-stage corresponds to a westward motion of the Alboran Domain accommodated by lateral (strike-slip) and frontal (thrust) ramps. Similarly, the arcuate geometry and the trend of the Ronda Peridotites Thrust close to the Coín Corridor also suggest a westward motion during the first stage of deformation. This interpretation is furthermore consistent with the deformation observed in the Dorsale Units (Mazzoli et al., 2013). Note that deformation patterns in the Lower Western Alboran Unit and at the base of the Ronda Peridotites indicate senses of shear top to NNW, NW or SW (Esteban et al., 2008; Mazzoli et al., 2013; Hidas et al., 2013), consistent with our analysis, but also top to ENE (Tubía et al., 1997). These local complexities can partly be related to a change in emplacement direction of the Upper Western Alboran Unit between 22 and 20 Ma.

On the above bases, we propose that the westward displacement of the Alboran Domain most probably started with the thrust emplacement of the Ronda Peridotites on top of the Lower Western Alboran Unit, at 22-20 Ma. Upper Miocene to Pliocene deformation, with similar kinematics, is moreover supported by field data (Díaz-Azpiroz et al., 2014), suggesting a continuous deformation along the E-W strike-slip corridors, from Lower Miocene to present day. Present-day seismicity (Ruiz-Constán et al., 2012b) and GPS displacement pattern (Koulali et al., 2011) are consistent with such a westward motion, accommodated by coeval strike-slip, thrust and normal faulting. The present-day GPS displacement of 2-3 mm/year (Koulali et al., 2011) would yield to an average displacement of 40-60 km during the past 20 Ma. Although the present-day displacement is not necessarily relevant for the past, it is worth noting that the length of the Internal LMOC that underlines the displacement along the Torcal corridor between La Viñuela and Alozaina is close to 60 km (Fig. 2.4).

2.6.3 Restored Miocene evolution of Western Alboran Domain

We propose a reconstruction of the Alboran Domain during Miocene times involving a component of E-W dextral simple shear at regional scale (Fig. 2.10). The progressive westward migration of the active front, from the Ronda Peridotites Thrust (lowermost Miocene), to the IEZB (lower Miocene) and to the External Zone thrusts (mid- to upper Miocene) is partly accommodated by strain localization along E-W strike-slip corridors.

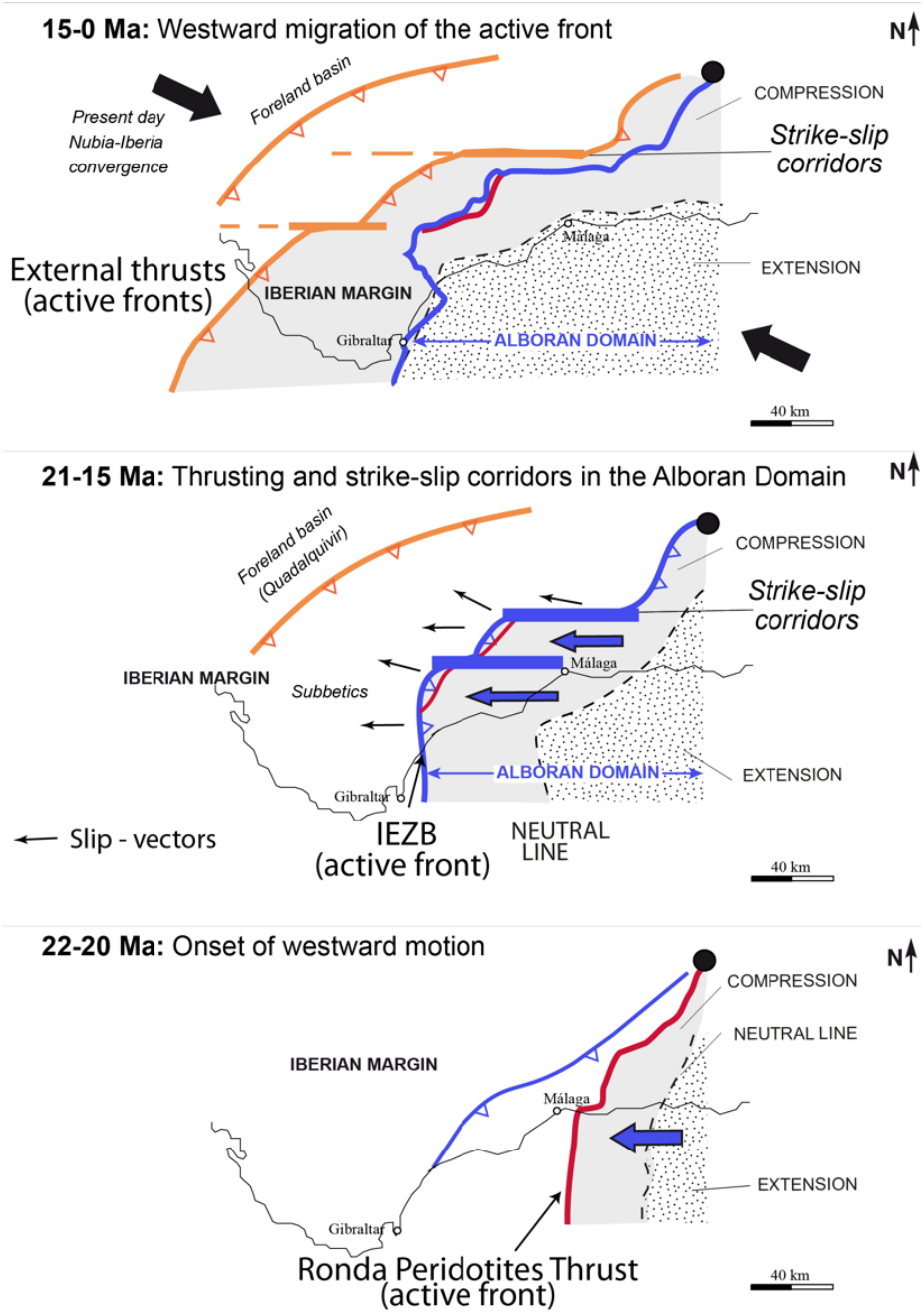

Figure 2.10. Three-stage sketch of the westward displacement of the Alboran Domain from Lower Miocene to present day the progressive development of thrusts and strike-slip corridors. A thick line marks the Active front and domains sustaining compression or extension are respectively in white or dotted-white. The three successive stages are from bottom to top 1/ Onset of westward motion (22-20 Ma) marked by the Ronda peridotites thrust (thick red line), 2/ westward motion of the Alboran domain (22-15 Ma) mainly accommodated by the IEZB

(thick blue line) and strike slip corridors (blue E-W bands), 3/ westward migration of the active front in the External Zone (15-0 Ma, thick orange line), leading to an extensional reactivation (dotted domain) of the Alboran domain. Black arrows: Present-day Nubia-Iberia direction of convergence in the northern part of the Gibraltar arc (from Vernant et al., 2010).

The E-W orientation of the strike-slip corridors implies a westward movement of the whole thrusting domain. The former region of shortening is thus reactivated in extension, as suggested for the Alboran Domain during Serravallian time (García-Dueñas et al., 1992). The coeval development of E-W strike-slip faults, N60º thrusts and N140º normal faults is moreover compatible with a NE-SW convergence between Africa and Europe during Miocene times (Mazzoli and Helman, 1994; Fig. 2.10). A change in direction of plate convergence from N-S to NE-SW (Vissers and Meijers 2012) could likely explain the onset of the westward motion of the Alboran Domain, accommodated by dextral strike-slip corridors at the boundary with the Iberia margin.

At lithosphere scale, the lateral ramp (Torcal Corridor) corresponds to the northern limit of deep mantle seismicity clusters observed in the Betics and in the Alboran Sea (Buforn et al., 2004; Calvert et al., 2000). Recent tomographic images confirm that the E-W trending northern limit of the Alboran Domain is the edge of a subduction system (Bonnin et al., 2014; Thurner et al., 2014). The lateral slab tearing that is imaged by tomographic models accommodated slab rollback at upper mantle depths. It might be thereby accompanied at crustal levels by the localization of westward displacement within the strike-slip corridors of Torcal and Coín (Fig. 2.10). The trenchward decrease of the amount of strike-slip displacement in the corridors strongly sustains this interpretation. Our structural and kinematic analysis can thus provide a geological description of the deformation pattern associated to slab tearing, over a 80 km distance. Slab tearing may have initiated during Lower Miocene and progressively lead to a complete lateral slab detachment, from East to West during Upper Miocene, triggering partly the Messinian salinity crisis (Duggen et al., 2003; García-Castellanos et al., 2011).

2.7 Conclusion

The major results of our study can be summarized as follows:

1/ Lower Miocene tectonics of the Western Betics resulted from a westward motion of the Alboran Domain, with respect to Iberia, accommodated by a lateral E-W dextral strike-slip ramp (Torcal corridor) and a frontal N60º thrust ramp (Gibraltar Thrust). The connection between these two major tectonic boundaries explains the arcuate geometry of the Internal-External Zone Boundary (IEZB).

2/ Strain localization during dextral simple shear of the Alboran Domain gave birth to the E-W Coín strike-slip corridor.

3/ The westward motion of the Alboran Domain led to a classical piling up of thrust units through the following thrust sequence: 1) the Ronda Peridotites Thrust, 2) the IEZB system and 3) external thrusts within the Subbetics. The crustal emplacement of large bodies of sub-continental mantle may therefore have occurred at the onset of this westward thrusting

4/ The onset of the westward motion of the Alboran Domain is constrained by the synkinematic deposition of the Lower to Mid Miocene (Burdigalian-Langhian) Olistostromic Complex (LMOC), in both the Internal and External Zones, and by the age of leucogranite dikes related to the Ronda Peridotites Thrust at around 22-20 Ma.

5/ A continuous westward motion of the Alboran Domain and hence of the active front is then recorded from 22-20 Ma to present day, more likely related to a continuous slab tearing at the northern edge of the Alboran domain. The E-W strike-slip corridors described in this study may be the crustal signature of slab tearing that accommodates the westward trench retreat at upper mantle depths.

ANNEX I: Fault-slip data

Figures 2.S1 and 2.S2, show the provenance of the fault-slip data shown in Figures 2.6 and 2.8. The data were collected along map-scale fault zones, segments of tectonic fault systems (respectively the northern IEZB, in the El Burgo - Torcal arc and the Coín corridor). In Figure 2.S1 and 2.S2, fault zones are reported with black lines and study areas with red boxes. Fault measurements made within the fault zones or their immediate vicinity, in case of too strong rock alteration in the fault zone, are reported in stereoplots (lower hemisphere projection; Schmidt net). Low-angle dipping normal faults systems were not taken into account in this study, since we focus on the Lower Miocene tectonics of the Western Betics.

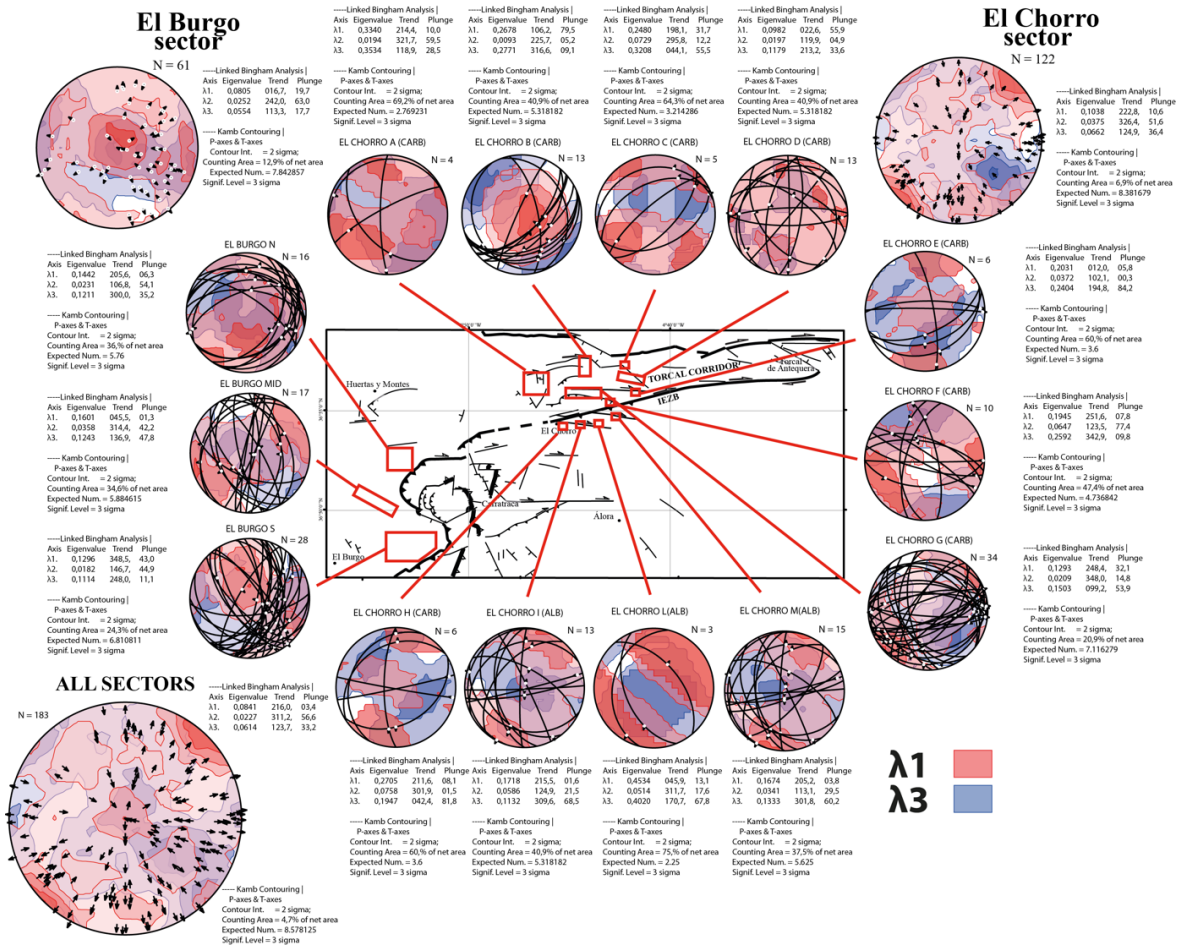

Figure 2. S1. Location of the study-areas along the Torcal corridor and the Gibraltar Thrust.

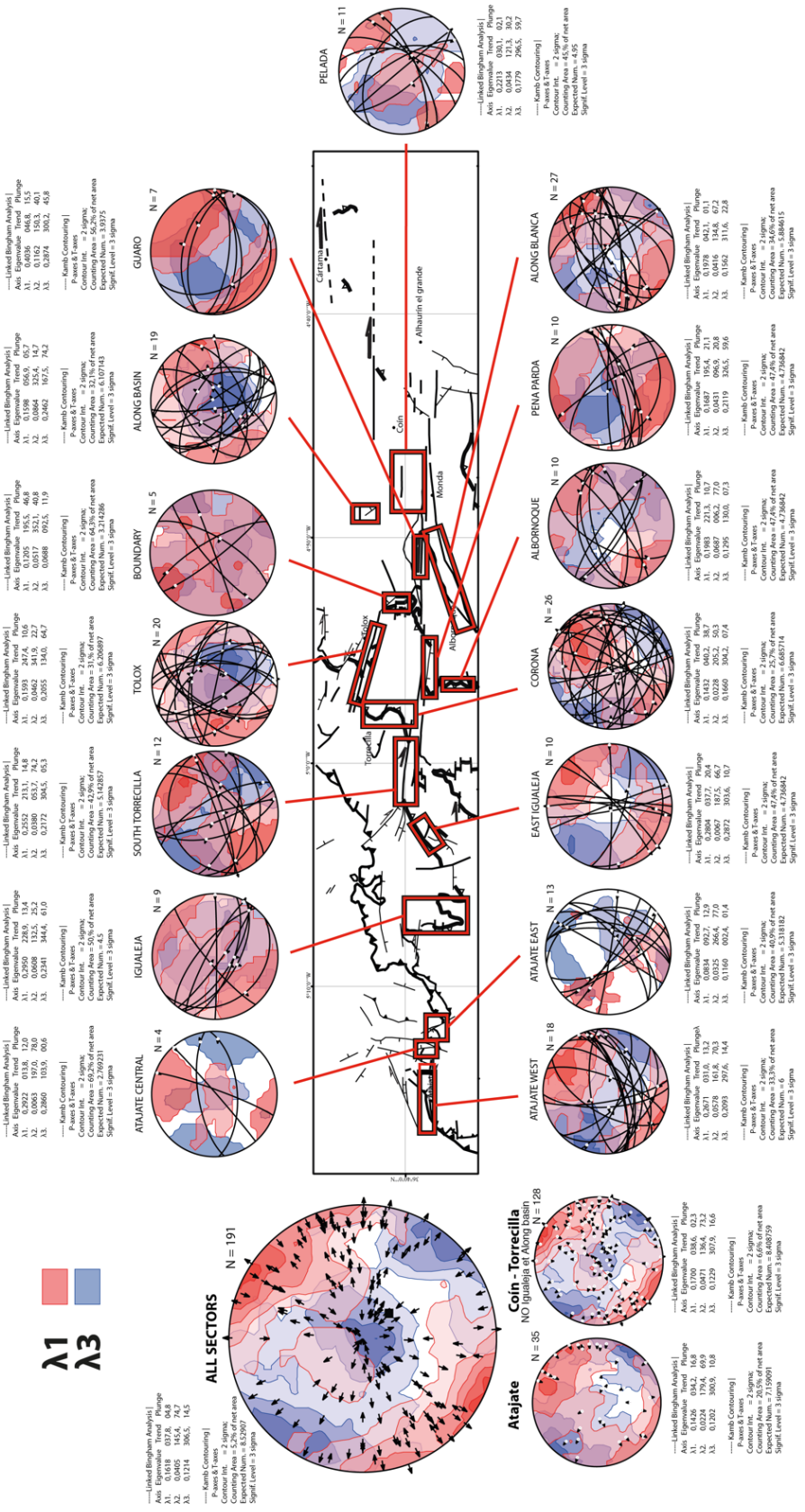

Figure 2.S2. Location of the study-areas along the Coín corridor and the Gibraltar Thrust.

Uncertainties of kinematic analysis can derive from: 1/ effects of post-faulting block rotation, 2/ sampling representativity of the entire fault population, 3/ relative weight of the data

collected, 4/ strain heterogeneity, due to lithological/rheological variations. The kinematic analysis of faults reported in figures S1 and S2, (using the methodology of Marrett and Allmendinger 1990), provides an estimate of the data uncertainties and scattering. Contours of the principal strain axes (blue: principal direction of shortening λ_3; red: principal direction of stretching λ_1) were calculated using all faults collected in each sector and were reported using the FaultKin software of Marrett and Allmendinger (1990) (http://www.geo.cornell.edu/geology/faculty/RWA/programs/faultkin.html). The overall strain patterns calculated for the whole data sets are shown in Figures 2.6 and 2.8.

ANNEX II: (U-Th)/He thermochronology

The content of this annex is not part of the published manuscript and will be published elsewhere.

The Alboran Domain underwent very fast exhumation during the Oligocene - Lower Miocene interval (synthesis in Platt et al., 2013 and chapter 4). However, no data are available for the more recent exhumation period, despite the fact that Tortonian to Messinian sediments are uplifted, as commonly described in the Alboran Domain since the theses of Peyre (1974) and Bourgois (1978). We present in this annex the preliminary results of a low-temperature thermochronologic study (apatite (U-Th)/He; AHe) of rocks collected in the Alboran Domain, aiming to date the Neogene exhumation history of the westernmost Alboran Domain, and relate it to the fault system described in this chapter.

Sampling strategy

We collected eight samples, four north of the Coín corridor and four south of the Coín Corridor, at different structural levels and on each side of the major N140-trending normal faults. We have collected the samples at similar altitudes because our sampling was constrained to avoid the abundant carbonatic lithologies that do not allow the use of the AHe method. From four of the eight samples we could not obtain a good amount of high quality apatites, necessary for the study. On the whole, 16 apatite single crystals were dated, 4 from each sample (12 from the Upper Western Alboran unit and 4 from the Lower Alboran unit).

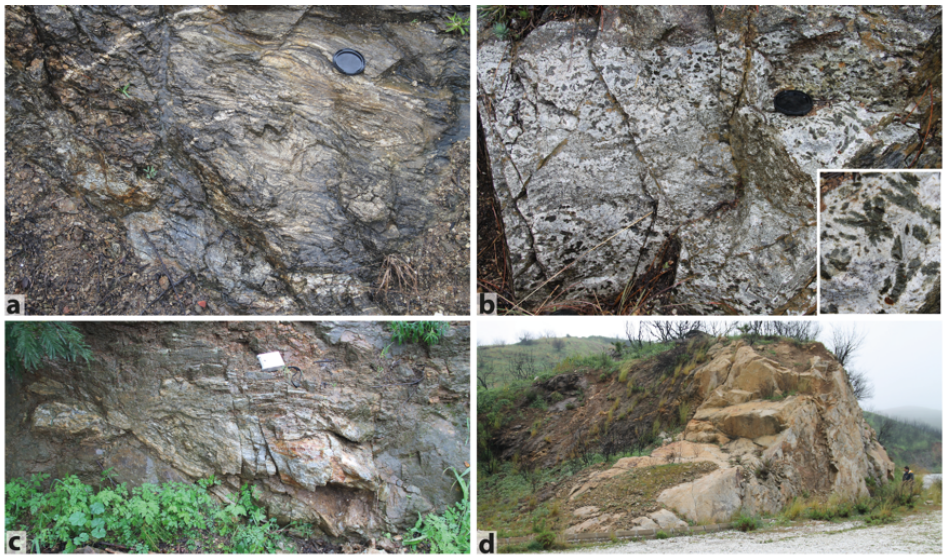

Figure 2.S3. Four example of rocks collected during fieldwork. (a) Gneissic migmatite in the Ojén Unit, sample GFD1. (b) Granite intrusion with pinite pseudomorphs after cordierite (inset), sample GFD6. (c) Metapegmatite in the uppermost Alpujarride, sample GFD3. (d) Diorite intruding the uppermost Alpujarride, sample GFD4.

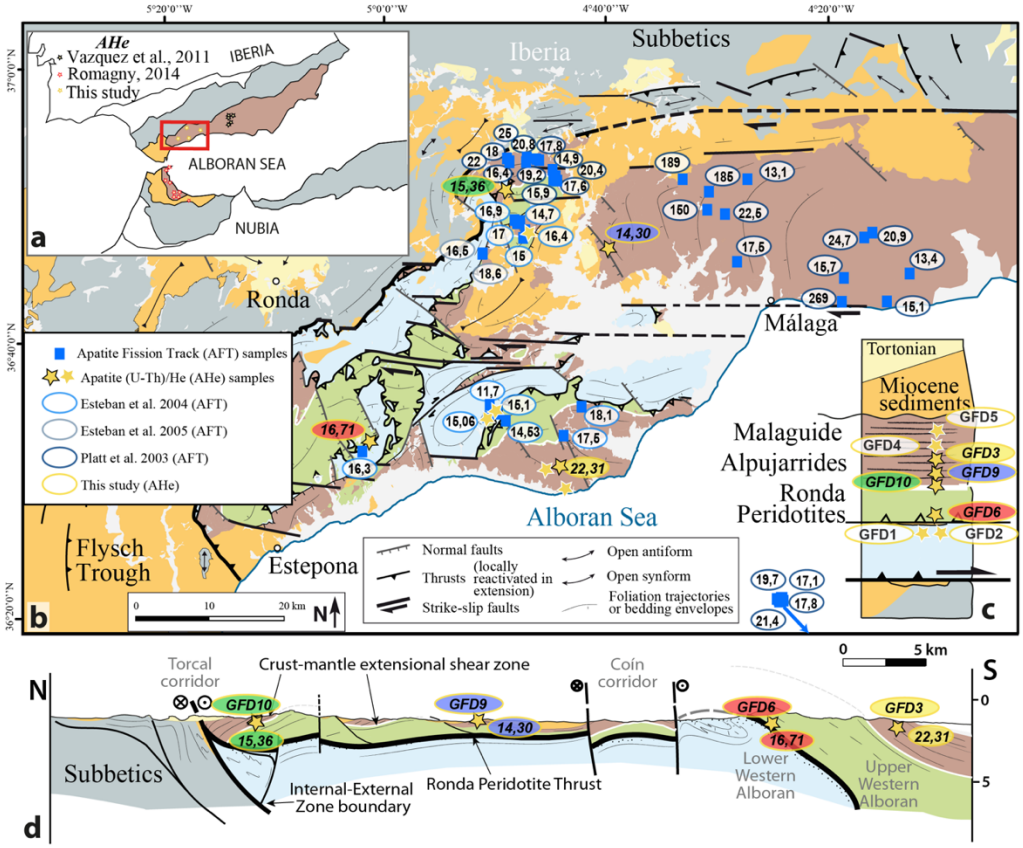

Figure 2.S4. Location of the collected samples in the tectonic map of the Western Betics and location projected on the N-S cross-section. Apatite Fission Track ages reported from the area are located on the map.

Results and ages

The U-Th/He results presented here are the first ones for the Alpujarride units of the Betic Cordillera. The ages obtained after the chemical analyses have been calculated using the Qt_Ft software for realistic crystal shapes (Gautheron et al., 2009), scaled on the base of the reference Durango samples. The four AHe ages are comprised between 22.3 ± 0.21 and 15.32 ± 0.31 Ma and no Tortonian or Messinian ages were identified. AHe ages are close in time to the apatite fission tracks ages reported for the area (see Esteban et al., 2004, 2013), indicating a very rapid cooling.

The age proposed in the table DR1 are calculated excluding the apatite with eU value higher than 120. In three samples, AHe ages have been found to vary significantly between each apatite. The observed important variability appears to be mainly the result of samples heterogeneity. This heterogeneity may due to anisotropic helium diffusion at the rock-scale that can be peculiarly effective within metamorphic rocks (e.g. Farley et al., 1996).

Table 2.DR1. Apatite (U-Th)/He data from the Western Betics. [eU] = [U238] + 0.235[Th232] in ppm. Ft were calculated using Qt-FT software for realistic crystal shapes (Gautheron et al., 2009).

	elevation (m)	U238 (ppm)	Th232 (ppm)	U/Th	He4	eU	length (µm)	radius (µm)	Calculated ages	Ft	Corrected ages (Ma)	Corrected age after Durango	Weighted mean ages (Ma)	Weighted mean age after selection (Ma)
GFD3a	288	131,76	3,89	0,03	128,44	132,67	248,15	192,59	19,83752	0,842	23,56	23,71 ± 0,21		
GFD3b	288	61,80	1,71	0,03	60,24	62,20	233,33	150,00	20,4152	0,845	24,16	**22,34 ± 0,26**		
GFD3c	288	44,72	2,47	0,06	43,59	45,30	335,00	188,89	21,91726	0,842	26,03	**23,24 ± 0,21**		
GFD3d	288	15,10	0,79	0,05	14,72	15,28	269,00	160,00	19,34942	0,838	23,09	**21,35 ± 0,37**	22,66 ± 0,81	**22,31 ± 2,31**
GFD6a	456	21,89	1,41	0,07	21,34	22,22	184,44	152,22	13,46595	0,839	16,05	**16,15 ± 0,18**		
GFD6b	456	78,23	4,31	0,06	76,27	79,25	304,72	183,33	15,93975	0,795	20,05	18,54 ± 0,19		
GFD6c	456	24,33	3,12	0,13	23,71	25,06	201,39	138,89	15,29003	0,791	19,33	**17,25 ± 0,15**		
GFD6d	456	24,28	2,93	0,12	23,67	24,96	254,00	215,00	20,57396	0,836	24,61	22,76 ± 0,23	18,68 ± 2,04	**16,71 ± 0,55**
GFD9a	468	29,92	2,64	0,09	29,17	30,54	250,00	138,89	18,1076	0,812	22,3	22,44 ± 0,34		
GFD9b	468	20,28	1,59	0,08	19,77	20,66	295,00	168,00	12,64868	0,836	15,13	**13,99 ± 0,2**		
GFD9c	468	8,66	0,80	0,09	8,44	8,84	258,33	127,78	12,3039	0,882	13,95	**12,46 ± 0,07**		
GFD9d	468	23,59	2,46	0,11	23,00	24,17	286,67	193,06	14,51664	0,816	17,79	**16,45 ± 0,13**	16,34 ± 3,11	**14,30 ± 1,43**
GFD10a	232	33,81	7,74	0,23	32,96	35,63	233,06	161,11	11,74433	0,793	14,81	**14,90 ± 0,14**		
GFD10b	232	53,23	19,03	0,37	51,89	57,71	359,17	219,17	16,66258	0,851	19,58	**18,11 ± 0,14**		
GFD10c	232	31,38	10,42	0,34	30,59	33,83	266,67	177,78	11,38305	0,777	14,65	**13,08 ± 0,17**		
GFD10d	232	68,66	12,15	0,18	66,93	71,52	280,56	200,56	16,89864	0,814	20,76	19,20 ± 0,26	16,32 ± 2,33	**15,36 ± 1,82**

The youngest AHe ages we obtained correspond to apatite with lowest uranium contents (Fig. 2.S5 and Table DR1). Shuster et al. (2006) showed that uranium effective concentration

([eU]) in apatites influence the (U-Th)/He system closure temperature, and that the temperature of the upper boundary of the PRZ can reach ~30ºC for uranium-poor apatites ([eU] < 5 ppm). This could explain the correlation between AHe ages and [eU] in our samples (Fig. 2.S5). However, we could not find any significant correlation between the AHe ages and the crystals size as proposed by Farley et al. (1996) (Fig. 2.S5). Some AHe ages have been found to be older than AFT ages obtained from rocks in the same area (GFD3, 22.31 Ma). This could be related to He implantation from U- and/or Th-rich neighboring phases within the rocks. This implantation is especially likely in the metapegmatite of sample GFD3, a lithology often rich in U-bearing minerals.

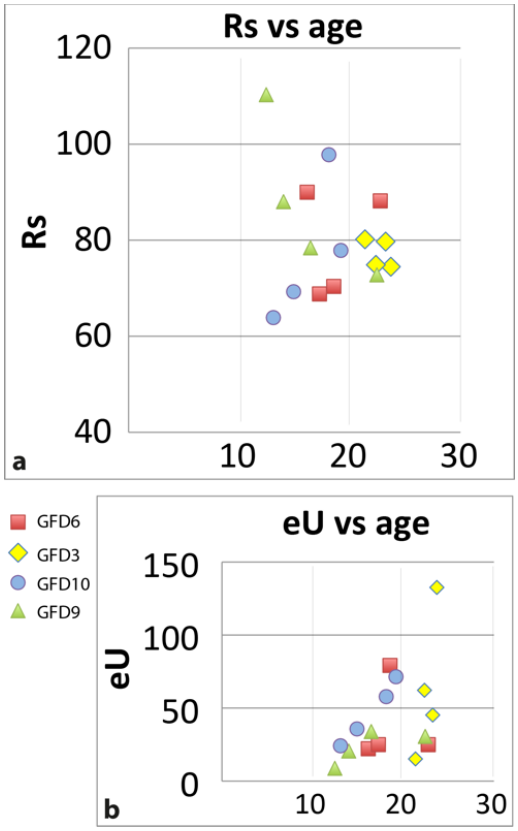

Figure 2.S5. Diagrams showing the mean radius and the eU against the ages in the analysed apatites.

This data lead us to conclude that exhumation probably occurred very rapidly between 22 and 17 Ma until rocks reached the top of the PAZ (80° to 60°C), as modelled for similar rocks from the other branch of the arc (Romagny et al., 2014). This very fast exhumation have brought the present-day outcropping rocks at depths less than 2-3 km already before the late Miocene. Furthermore, it must be noticed that mean AHe ages from the Western Betics rocks are much older than the ones from the Nevado-Filabride in the Central Betics, which are comprised between 6.2 and 12.9 Ma (Vazquez et al., 2011). The different AHe ages suggest a diachronous exhumation between the lowermost structural levels in the Western Betics (Alpujárride Blanca Group) and in the Central Betics (Nevado-Filábride). Note that no data are available in the Alpujárride from Central and Eastern Betics and a comparison is thus not possible.

ACKNOWLEDGEMENTS

This work was funded by the European Union FP7 Marie Curie ITN “TOPOMOD”, contract 264517. Alexandre Pichat and Hugo Humbert are acknowledged for the help during fieldwork. Thanks to Anne Delplanque for help in drawing Figure 2.4 and 2.5 and to Bernard Célérier for useful discussions. Very constructive comments made by an anonymous reviewer and Guillermo Booth Rea, as well as the professional handling of the Editor, helped to improve the manuscript.

CHAPTER 3

Hyper-stretching in a continental rift up to mantle exhumation (Western Betics, Spain)

The article composing this chapter has been submitted to Marine and Petroleum geology

Gianluca Frasca[1,2], Frédéric Gueydan[2], Jean-Pierre Brun[1], Patrick Monié[2]

[1]Géosciences Rennes, Université Rennes 1, UMR 6118 CNRS, Campus de Beaulieu, 35042 Rennes Cedex, France

[2]Géosciences Montpellier, Université Montpellier 2, UMR 5243 CNRS/INSU, Place E. Bataillon, CC60, 34093 Montpellier Cedex, France

Abstract

The identification of the main structures that result from continental rifting at magma-poor margins is essential to constrain the necking processes of the continental lithosphere. Brittle faults, often termed mantle detachments, are considered to play a major role in the formation of magma-poor rifted margins. However, ductile shear zones in the deep crust and mantle are rarely identified whereas they likely play an important mechanical role that remains to be constrained. The Western Betics (Southern Spain) shows an exceptional exposure of a strongly thinned continental lithosphere, formed in a supra-subduction setting during Oligocene-Lower Miocene, giving access to the entire crust and the upper part of the mantle. Variations in crustal thickness is used to quantify crustal stretching that may reach values larger than 2000% where the ductile crust almost disappear, defining a stage of hyper-stretching. Opposite senses of shear top-to-W and top-to-E in the crust-mantle extensional shear zone and close to the brittle-ductile transition in the crust, respectively. Where the ductile crust almost disappears, concordant top-to-E-NE senses of shear are observed in both upper crust and serpentinized mantle. Late high-angle normal faults, dated by ^{40}Ar-^{39}Ar step heating method at ca. 21 Ma, cross-cut the previously hyper-stretched domain involving both crust and mantle in tilted blocks. The western Betics exemplifies, probably better than any previous field example, the changes in deformation processes that accommodate the progressive necking of a continental lithosphere and that can be summarized in three successive steps: i/ a mid-crustal shear zone and a crust-mantle shear zone, acting synchronously but with opposite senses of shear accommodate ductile crust thinning and ascent of the sub-continental mantle, ii/ hyperstretching localizes in the neck, leading to an almost disappearance of the ductile crust and bringing the upper crust into contact with the subcontinental mantle, each of them with their already acquirred opposite senses of shear, and iii/ high-angle normal faulting, cutting through the Moho, and related block tilting ends the full exhumation of mantle in the zone of localized stretching.

3.1 Introduction

During the last decade, the exhumation of subcontinental lithospheric mantle in rifted margins became a commonly recognized tectonic feature. In the Iberia margin, the case-study for magma-poor continental margin (Beslier et al. 1990; Boillot et al., 1980; Boillot et al. 1987; Brun and Beslier, 1996; Whitmarsh and Miles, 1995), the crustal thickness decreases abruptly in a short horizontal distance (75 km, Péron-Pinvidic and Manatschal, 2009; Whitmarsh et al., 2001) leading to wide mantle exposures directly to the sea-floor. The sudden extreme thinning of the continental crust has been well imaged (Péron-Pinvidic et al., 2007; Ranero and Perez-Gussinyé, 2010) and ascribed in the past to polyphasic and complex activity of ductile and brittle structures (Manatschal et al., 2001, Péron-Pinvidic and Manatschal, 2007). However, at first glance, "necking" and "hyperextesion" are the two stages typically recognized in passive continental margin evolution (Doré and Lundin, 2015).

The final stage of lithosphere thinning, so-called "hyperextension", is characterized by

coupled continental brittle crust and mantle: faults penetrate into the mantle and "extensional allochtons" of upper crust lie in direct contact with the mantle (Beslier et al., 1993; Manatschal et al., 2001). This final stage of rifting is now well documented worldwide, e.g. in the South Atlantic (Contrucci et al., 2004; Moulin et al., 2005), in the Red Sea (Cochran and Karner, 2007) and in Norway (Osmundsen and Ebbing, 2008) and also from what is observed in obducted margins in the Swiss Alps (Manatschal, 2004; Mohn et al., 2012, and references therein). Normal faults and detachment faults shape the final stages of the rift, partly obliterating the earlier structures that are responsible for a large part of lithosphere thinning.

The bulk process responsible for lithospheric thinning up to continental breakup results from a "necking" instability characterized by a strong decoupling between brittle crust and mantle. However, the late stages of stretching (i.e. "hyperextension") may obliterate the earlier stages of the "necking" process. Furthermore, it is difficult to obtain a detailed resolution of this stage from seismic data (see Reston, 2007 for a detailed discussion) and entire sections of rifted lithosphere are rarely exposed in the field. However, the large bodies of subcontinental mantle exposed in the Alboran region, show that major extensional shear zones at the crust-mantle interface are coeval with the sub-continental mantle exhumation (Afiri et al., 2011, Frets et al., 2014, Précigout et al., 2013). In the other hand, analogue and numerical models reveal that large ductile shear accommodates crust-mantle decoupling and hence controls the subcontinental mantle exhumation process during lithosphere necking (Brun and Beslier, 1996; Gueydan et al., 2008). However, many aspects of the relationships between upper crustal faulting and crust-mantle ductile deformation during necking remain poorly understood. As an example, fault displacements observed in seismic lines always remain rather small compared to the overall crustal thinning. To reconcile such discrepancies various solutions have already been considered: i) large-scale crustal detachments (Lister et al., 1986, Manatschal et al., 2001; Mohn et al., 2012), ii) upper crustal brittle faulting accommodated by lower crustal flow (Brun and Beslier, 1996; Gueydan and Précigout, 2014; Ranero and Perez-Gussinyé, 2010) or iii) depth-dependent mechanisms of thinning at different levels in the crust (Davis and Kusznir, 2004; Reston, 2007).

In the present paper, we describe new structural and geochronological data from an outstanding field example of continental rifting up to mantle exhumation in a supra-subduction setting in the Western Betics (Southern Spain). The stretched continental crust section associated to the Ronda Peridotites in the western Alboran Domain is a prime location to observe and measure the effects of stretching at all levels of the continental lithosphere (Argles et al., 1999; Balanyá et al., 1997; Précigout et al., 2013; Tubía and Cuevas et al., 1986). In this study, we document the changes in deformation processes that accompany the progressive necking of the continental lithosphere.

3.2 Geological setting

The *Betic-Rif* belt is divided into an internal metamorphic zone (Alboran Domain) and an external, un-metamorphosed, zone (Inset of Fig. 3.1). The Internal-External Zone Boundary (IEZB) separates the Alboran Domain from an external thrust-and-fold belt (e.g. Chalouan et al., 2008; Crespo-Blanc and Frizon de Lamotte, 2006). Tertiary foreland basins

wrap to the North, West and South the belt (Fernández et al., 1998; Flinch,1993) (shaded in inset of Fig. 3.1). The external zone is composed by sediments mainly derived from the subducting Iberian and Maghrebian margins (pale grey in inset of Fig. 3.1) and the Alboran Domain is nowadays a portion of the upper plate of the western Mediterranean subducting system (dark grey in inset of Fig. 3.1), (e.g. Garrido et al., 2011; Platt et al., 2013). A large part of the Alboran Domain stands below the sea level, corresponding to the Alboran Sea basin (Comas et al., 1999; Watts et al., 1993) whose development is mostly coeval with Miocene shortening in the arcuate External Zone (Balanyá et al., 1997; García-Dueñas et al., 1992; Platt et al., 2013), as also observed in the other circum-Mediterranean belts.

The metamorphic tectonic units of the Alboran Domain contain in the westernmost sector the world largest sub-continental mantle outcrops, so-called Ronda Peridotites. The *exhumation* mechanism and timing of the *Ronda Peridotites* have been and are still *matter of controversy***.** Among the proposed mechanisms of mantle rock exhumation are: i) mantle core complex (Doblas and Oyarzun, 1989), ii) crosscutting detachment faults during the extensional collapse of the Betic-Rif chain (Platt et al., 2003a; Van der Wal and Vissers, 1993), iii) transpressional extrusion of a mantle wedge (Mazzoli and Martín-Algarra, 2011; Tubía et al., 1997; Tubía et al., 2013), and iv) inversion of a thinned back-arc lithosphere during slab rollback (Garrido et al., 2011; Hidas et al., 2013; Précigout et al., 2013). Ages proposed for the exhumation also strongly vary: i) Paleozoic (Kornprobst, 1976; Ruiz Cruz and Sanz de Galdeano, 2014), ii) Mesozoic (Van Hinsbergen et al., 2014; Vissers et al., 1995) and iii) Oligo-Miocene (Hidas et al., 2013; Précigout et al., 2013).

3.2.1 The Ronda – Beni Bousera subcontinental mantle

The *Ronda Peridotites* in southern Spain consist in three main massives, called Bermeja, Alpujata, Carratraca massives (Fig. 3.1). Several smallest mantle outcrops connect the three larger massives suggesting the original continuity of a single mantle sliver (Navarro-Vilá and Tubía, 1983; see Didon et al., 1973 for an alternative view). Furthermore, the Ronda Peridotites in the Western Betics were probably originally continuous with the Beni Bousera massif (Sánchez-Gómez et al., 2002) on the Rifean side of the Gibraltar arc (inset in Fig. 3.1) and then dismembered during the Miocene formation of the Gibraltar arc (Balanyá et al., 1997; Berndt et al., 2015; Chalouan et al., 2008; Frasca et al., 2015). The peridotites display a kilometer-scale petrological zoning with Grt/Sp-peridotites at the top, granular and porphyroclastic Sp-peridotites in the middle and Plag-bearing peridotites at the base (Obata, 1980). The Ronda Peridotites sliver is separated from the Alboran continental crustal rocks by *two major tectonic contacts*: i) the Ronda Peridotites "hot" Thrust at the base and ii) the Crust-Mantle extensional shear zone (respectively black and white colors in map and cross-section of Fig. 3.1) at the top (Mazzoli et al., 2013; Johanesen and Platt, 2015; Précigout et al., 2013; Tubía et al., 1997).

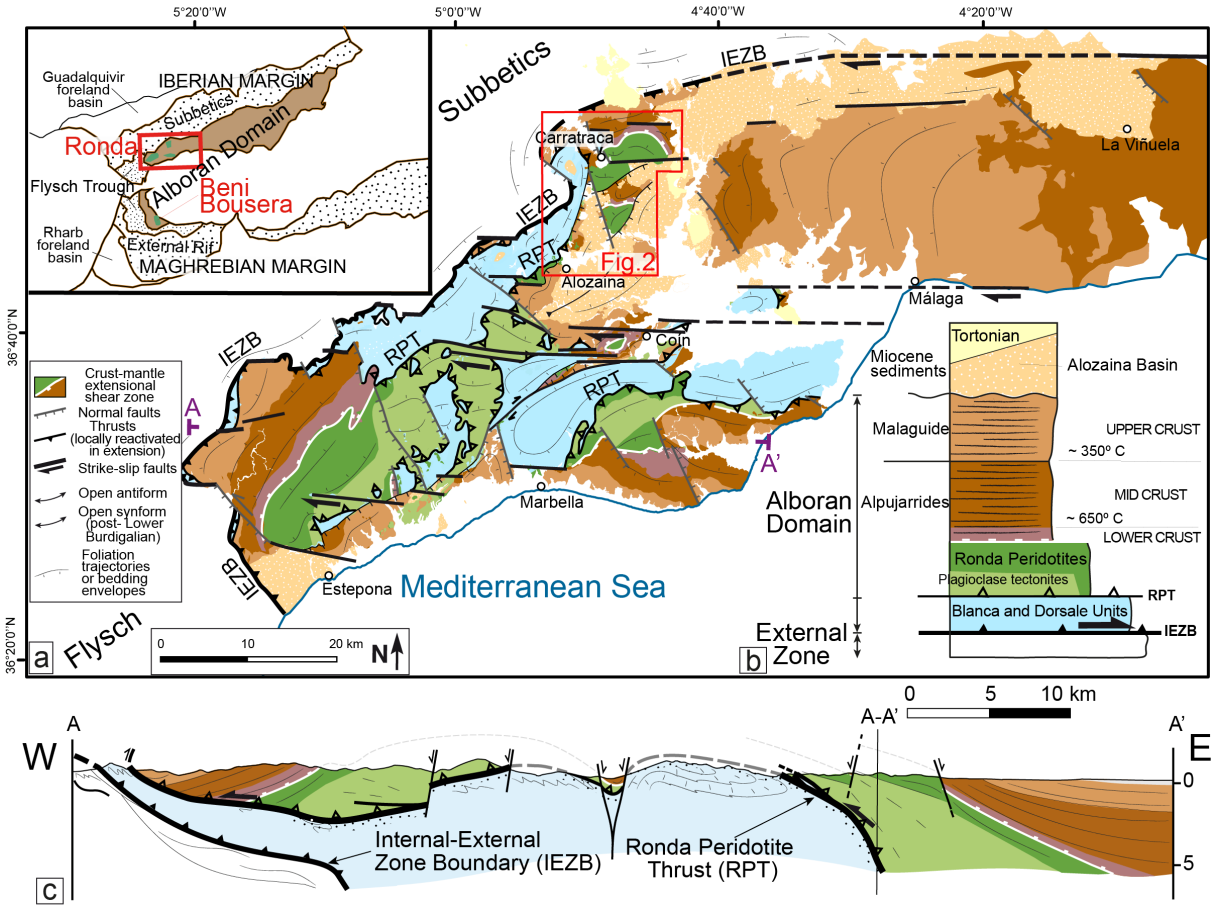

Fig. 3.1. A/ Tectonic map of the Western Betics with foliation trajectories adapted from Frasca et al. (2015). The Western Alboran Domain: mantle rocks Ronda peridotites with plagioclase tectonites), lower, middle and upper crustal rocks (pale green), Crustal rocks below the Ronda peridotites (e.g. Blanca and Dorsale, Frasca et al., 2015) (Pale blue), Lower Miocene Alozaina basin (Beige) and Tortonian basins (Light yellow). Major tectonic contacts: Ronda Peridotites thrust (RPT), Internal External Boundary Zone (IEZB), Crust-Mantle extensional Shear Zone (White line). Top left inset: overview of the Betic-Rif belt with the position of the Ronda – Beni Bousera mantle bodies in the Western Alboran Domain. Bottom rigtht inset: synthetic vertical section of the lithological and tectonic units of the Western Betics. B/ E-W cross-section (location AA' in A/).

The *Ronda Peridotites Thrust* is a "hot" thrust (Esteban et al., 2008; Tubía et al., 1997) characterized by a metamorphic sole with: 1/ partial melting in the footwall metamorphic rocks with ages ranging between 22 Ma and 19 Ma (Esteban et al., 2011), and 2/ high-temperature minerals in the basal Mesozoic sediments deformed during Lower Miocene (HT: Mazzoli et al., 2013; deformed Lower Miocene Nava Breccia: Mazzoli and Martín-Algarra, 2011). The Plagioclase tectonites (Fig. 3.1) usually mark in the mantle rocks the deformation along the Ronda Peridotites Thrust (Hidas et al., 2013; Précigout et al., 2014).

Conversely, the *Crust-Mantle Shear Zone* shows structural and petrological evidences of an extensional nature (Argles et al., 1999; Balanyá et al., 1997; Précigout et al., 2013; Sánchez-Gómez et al., 1999; Tubía and Cuevas, 1986). Garnet-spinel mylonites mark the Crust-Mantle Shear Zone with a top-to-SW shearing in the Bermeja massif (Précigout et al., 2013), top-to-E shearing in the Alpujata massif (Tubía and Cuevas, 1986), a variable sense of shear in the Carratraca area (Tubía et al., 2004), and top-to-NW sense of shear in the Beni

Bousera massif (Afiri et al., 2011; Frets et al., 2014). Simultaneously, mantle rocks have recorded a continuous decompression, from the garnet stability field to spinel-peridotite facies (Garrido et al., 2011; Afiri et al., 2011), related to ductile strain localization at the very top of the mantle units (Précigout et al., 2007, 2013). Syn-kinematic partial melting confirms the syn-exhumation mylonitization (Marchesi et al., 2012). Nevertheless, all mantle massives are dominated by spinel lherzolites in which mafic layers are common (Garrido and Bodinier, 1999). The granular plagioclase-peridotites at the base are separated from the overlying spinel tectonites by a "recrystallization front" that marks the asthenosphere boundary (Lenoir et al., 2001; Soustelle et al., 2009; Van der Wal and Vissers, 1996) that is not exposed in the Carratraca massif (Tubía et al., 2004).

3.2.2 Stretching in the Western Alboran crust

The Western Alboran crustal envelope is mainly made of Paleozoic rocks divided in two tectonic units, Alpujarride and Malaguide, that formed an alpine nappe-stack most probably during an Eocene subduction (Platt et al., 2013; Vergés and Fernández, 2012). This Alpine nappe stack thus composes the Alboran crust, on top of the Ronda peridotites lithosphere mantle, during the Oligo-Miocene evolution (Torres-Roldán, 1979; Tubía et al., 1992). The pre-Oligocene juxtaposition of these two tectonic units is testified by the intrusion of Oligocene tholeitic dykes in both units (Esteban et al., 2013). As shown in the following, the Oligo-Miocene evolution of the Alboran crust is mainly associated with crustal thinning.

The *regional foliation* that is defined by medium-pressure/high-temperature mineral assemblages showing a decrease in pressure (Argles and Platt, 1999; Argles et al., 1999; Balanyá et al., 1997) became parallel to the Crust-Mantle shear zone in the Alpujarrides crustal rocks during the crustal thinning (Fig. 3.1, Précigout et al., 2013; Gueydan et al., 2015; Balanyá et al., 1997; Sanchez-Gomez et al., 1999). The Alpujarride crustal rocks are sometimes divided for sake of simplicity in granulites, migmatites, gneisses and schists (Chalouan et al., 2008). Hereafter, following partly the field observations of Argles et al. (1999) and Balanyá et al. (1997), we divide the crust into three lithological groups, namely lower, middle and upper crust (generalized vertical section in Fig. 3.1). The *lower crust* is composed by pelitic granulites, characterized by cm size garnet porphyroclasts interlayered with minor marbles and rare mafic granulites, and by migmatites without garnet and often showing disrupted and folded leucosomes. The *middle crust* is made up from base to top of sillimanite gneisses, with some strongly stretched migmatitic leucosomes, of fibrolite gneisses, without leucosome but still with thin needles of sillimanite, and of andalusite gneisses, where andalusite is the only alumino-silicate observed. Quartzites, phyllites and schists with rare andalusite appear at the top of the middle crust at the transition with the upper crust. Most of the lower and middle crust rocks have amphibolite facies parageneses and partial melting is concentrated in the lower crust. The *upper crust* is composed of the Malaguide rocks made of Paleozoic non-metamorphosed slates, carbonates, clastic rocks and of scattered Permian terrigenous sediments and Mesozoic carbonates.

The lithological boundaries between lower, middle and upper crustal units roughly reflect the original 650º C and 350º C paleo-isotherms during the high-temperature Barrovian-type metamorphic event, as derived by Raman spectrometry on carbonaceous material (Negro et al., 2006; generalized vertical section in Fig. 3.1). The temperature climax is corroborated also by the evidence of partial melting at the very base of the crust (Platt and Whitehouse, 1999) and from the total resetting of low-T chronometers in almost the whole crustal section, except very shallow levels (Esteban et al., 2004; Monié et al., 1994; Platt et al., 2003a).

3.2.3 Continental rifting in a supra-subduction setting

The parallelism of foliations in crust and mantle and their development during decompression indicate that the western Alboran domain resulted from the extensional exhumation of a continental lithosphere section. However, as suggested by Hercynian, Jurassic and Alpine ages (Montel et al., 2000; Sánchez-Navas et al., 2014; Sánchez-Rodriguez and Gebauer, 2000) the mantle part of the section likely underwent a rather complex evolution. The present paper does not aim at discussing this long and complex geological evolution but only at constraining the deformation pattern resulting from rifting and related exhumation of the lithospheric mantle. In spite of local complexities, the Lower-Miocene Ronda Peridotite Thrust postdates the mantle-crust extensional shear zone, as indicated by the constant crosscutting relationships reported in the previously published maps (e.g. Esteban et al., 2008; Mazzoli and Martín-Algarra, 2011; Précigout et al. 2013; Tubía et al., 1997). Continental lithosphere thinning therefore occurs before the Lower Miocene. Since it affects an Eocene nappe-stack (Malaguide/Alpujarride), an Oligocene-early Miocene age for the thinning seems to be supported by different types of data.

The exhumation and the cooling of the mantle along the extensional shear zone located at its top is dated in garnet pyroxenites (Sm-Nd age of 21.5 ± 1.8 Ma on garnet and clinopyroxene, Zindler et al., 1983) (mean Lu-Hf ages of 25 ± 1 Ma or 24 ± 3 Ma on garnet (Blichert-Toft et al., 1999; Pearson and Nowell, 2004) and in stretched leucosomes within the foliation (U-Th-Pb age of 21.37 ± 0.87 Ma on monazite, Gueydan et al., 2015, and U-Pb age of 22.0 ± 0.3 Ma on zircon, Platt et al., 2003b) . Note that mantle was exhumed from diamond conditions (more than 150 km, Davies et al., 1993; Pearson et al., 1989) to garnet stability field (70-90 km) in a previous deformation event, most probably during Jurassic Tethyan rifting (Afiri et al., 2011; Garrido et al., 2011; Van der Wal and Vissers, 1993).

As summarized above, the foliation related to the *Crust-Mantle Shear Zone*, which affected simultaneously the crust and the upper part of the mantle, developed during decompression under high-temperature conditions. Similar senses of shear are recorded in the lower part of the crustal envelope (Balanyá et al., 1997; Argles et al., 1999) and in garnet-spinel mylonitic zone at the top of the peridotites (Afiri et al., 2011; Balanyá et al., 1997; Précigout et al., 2013; Gueydan et al., 2015). Syn-shearing temperature was high enough to induce partial melting in the crustal rocks (Argles et al., 1999; Platt and Whitehouse, 1999). Additional evidence for hot conditions of continental lithosphere stretching is the mantle-

related magmatic activity. The intrusion within the crust of tholeitic andesites and diorite dyke swarms is likely related with mantle rising (Garrido et al., 2011), considering the geochemistry of the dykes (major element composition, Duggen et al., 2004) and their spatial distribution (mainly in the Western Betics, Esteban et al., 2013). The dykes are abundant in the Malaguide and Triassic cover as well (Fernández-Férnandez et al., 2007) and in the upper and middle crust during E-W stretching (see discussion in Esteban et al., 2013). The age 33.6 ± 0.6 Ma (laser 40Ar/39Ar on a plagioclase from a basalt, determined by Duggen et al., 2004) is confirmed by U/Pb SHRIMP ages (Esteban et al., 2013). Younger lower Miocene ages (K-Ar whole rock of Torres-Roldán et al., 1986; $^{40}Ar/^{39}Ar$ step-heating age of Turner et al., 1999) can be related to the thermal cooling of the dikes controlled by the end of regional metamorphism.

The westward rollback of the Alboran subducting slab is now largely accepted to have shaped the arcuate Betic-Rif belt (Balanyá et al., 2007; Garrido et al., 2011; Johanesen et al., 2014; Platt et al., 2013; Précigout et al., 2013). Several large-scale lines of evidences as the evolution in the volcanism types (Duggen et al., 2004), the westward shift in the deposition of the foreland basin (Iribarren et al., 2009) and recent tomography images (Bonnin et al., 2014; Palomeras et al., 2014), support this hypothesis. Various scenarios have been proposed with great differences in timing, direction and amount of displacement (Faccenna et al., 2004; Gueguen et al., 1998; Gutscher et al., 2002; Lonergan and White, 1997; Rosenbaum and Lister, 2004; Vergés and Fernández, 2012; Wortel and Spakman, 2000). Whatsoever, an overall westward trench displacement is more likely responsible for rifting in the Alboran upper plate and related exhumation of the subcontinental mantle (Garrido et al., 2011; Hidas et al., 2013; Précigout et al., 2013), in agreement with the supra-subduction geochemical signature of magmatic intrusions in the Ronda Peridotites (Marchesi et al., 2012).

Rifting of the continental lithosphere and subsequent mantle exhumation thus occurred in a supra-subduction setting during Oligo-Lower Miocene Alboran slab rollback. The final emplacement of the *Ronda peridotites* corresponds to a rift inversion within the upper plate that occurred in lower Miocene accommodated by the *Ronda Peridotites Thrust* (Hidas et al. 2013; Précigout et al., 2013).

3.2.4 Positioning of our study

Following the estimates of Précigout et al. (2013) and Hidas et al. (2013), the amount of crustal thinning in the Western Alboran Domain remained moderate bringing the mantle rocks at mid-crustal levels (10-15 km). Conversely, Argles et al. (1999) and Platt et al. (2003a) suggest that crustal detachments brought mantle rocks to very shallow levels in the Carratraca area, leaving an only few km thick strongly attenuated crustal envelope. Furthermore, intrusion of gabbros in the Ronda Peridotite at the late stage of mantle thinning confirms the hypothesis of an extreme extension interesting the whole continental lithosphere (Hidas et al., 2015).

Our study focuses on rift-related structures to constrain the geometry, kinematics and amount of crustal thinning across the exhumed section of thinned continental lithosphere. We focused our study on the Carratraca region for the following reasons: 1/ this area exposes a complete lithospheric section, already rather well studied (Argles et al., 1999; Soto and Gervilla, 1991; Tubía et al., 2004), 2/ the excision of the deepest parts of the crust is well depicted in available geological maps (Cano Medina and Ruiz Reig, 1990; Chamón Cobos et al., 1972; Del Olmo Sanz, 1990), 3/ the absence of plagioclase tectonites related to hot thrusting of the peridotites on top of the crust suggest a minor reworking during rift inversion and 4/ this area has been well preserved from possible Miocene extension related to the Alboran Sea basin formation (Comas et al., 1992).

3.3 Geometry, deformation and ages of lithosphere thinning

3.3.1 Structural map of the Carratraca massives

The map of Figure 3.2a focuses on mantle rocks (green; dark green highlights the grt-sp mylonites), crustal envelope (purple, brown and beige) and overlying Alozaina basin, a terrigenous deposit of Lower Miocene age (see below for a detailed description, Sanz de Galdeano et al., 1993; Suades et al., 2013). The geological units located below the Ronda Peridotites Thrust (Fig.3.1) are not considered here as we focus on the geometry of the thinned continental lithosphere. Foliation trajectories are based on 1406 data, available as stereoplots in supplementary material (Fig. 3.S1). The N-S trending cross-section (Fig. 3.2b) is perpendicular to the main foliation trend and cuts, along 22 km, the Carratraca mantle massives, the crustal envelope and small Alozaina basin remnants on the top of it, from the El Chenil to the El Chorro region. The crust-mantle boundary dips to the North, while the Ronda Peridotite thrust is generally flat-lying. Two main high-angle normal faults, Cerro Tajo and La Robla, dip to the South and cross-cut the Ronda peridotites and its crustal envelope.

Foliations in the crustal envelope dip to the North at variable angles (Figs. 3.2a). The main foliation trend is generally parallel to the condensed isograds from granulite to greenschist facies rocks, easing the identification of lower, middle and upper crust. Approaching the upper crust the foliation strength decreases and lithological boundaries display evidence of layer-parallel brittle shear. Low-angle fault zones defined by breccias and gouges with often subhorizontal striations are characterized by jumps in P-T conditions, in particular through the Los Grenadillos fault that acts as important mid-crustal shear zone (Argles et al., 1999).

Foliation trajectories highlight the large-scale 3D geometry of the studied domain with broad anticlines cored by the peridotites massives and synclines defined by upper crustal levels and the Alozaina basin. The Cerro Tajo and La Robla faults are large-scale normal faults (Figs. 3.2a and 3.2b) that bound the peridotitic massives to the south and south-east, defining the three studied tilted blocks: Agua, Robla and Alozaina.

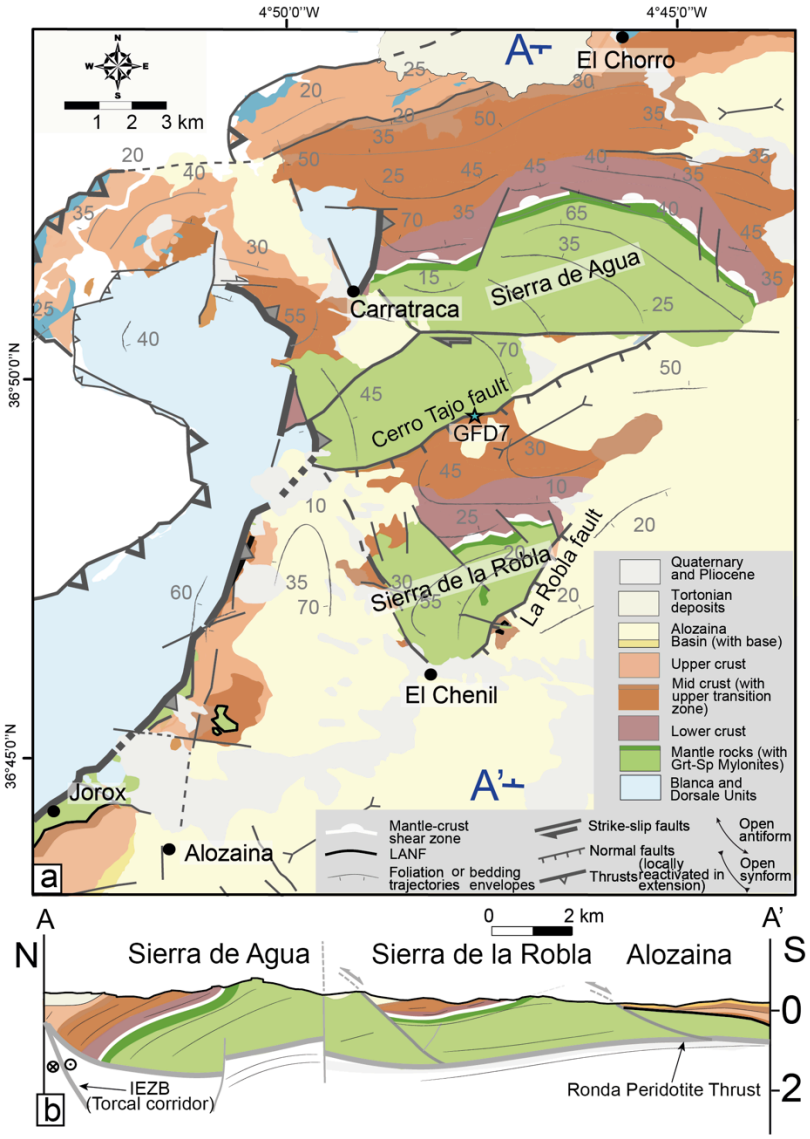

Fig. 2. (**a**) Simplified structural map of the Carratraca peridotitic massives, redrawn after personal observations and published works (Argles et al., 1999; Cano Medina and Ruiz Reig, 1990; Chamón Cobos et al., 1972; Cruz San Julián, 1990; Del Olmo Sanz et al., 1990; Frasca et al., 2015; Soto and Gervilla, 1991; Tubía et al., 2004). Foliation trajectories drawn from measurements provided in Supplementary material (Fig S1). Star: position of the sample collected for the Ar-Ar dating (GFD7). LANF: low angle normal fault. Colors like in figure 3.1. B/ N-S cross-section (location AA' in a/).

3.3.2 Ar-Ar on high angle normal faults

The Cerro Tajo and the La Robla faults are characterized at map-scale (Figs. 3.2a and b) by direct juxtaposition between mantle rocks, Alozaina basin and upper crustal rocks, indicating a km-scale normal sense offset (up to 5 km, cross-section Fig. 3.2b). Nevertheless, both faults show a polyphased kinematic history (Argles et al., 1999; Esteban et al., 2004; Soto and Gervilla, 1991). New structural data were collected from the La Robla and Cerro Tajo faults, using shear criteria (e.g. striae, Riedel-type shear faults and deflection of

foliations) observable on dm-scale fault mirrors with metric displacements in the damage zones of both faults (Figs. 3.3d and 3.3e). Similar kinematics along both faults were found with a principal direction of extension top-to-S and top-to-E, and a principal direction of shortening top-to-N-NW.

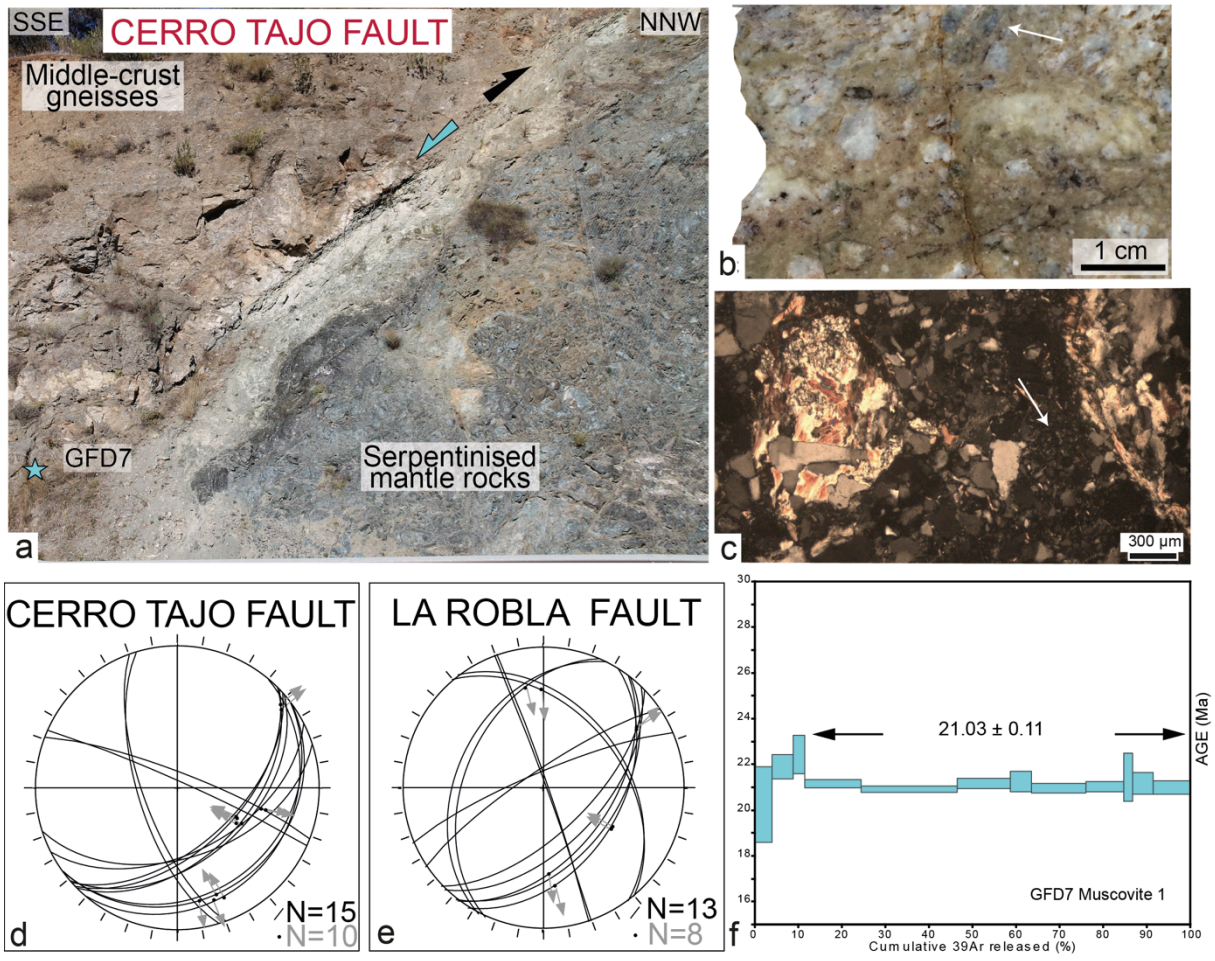

Fig. 3.3. Kinematics and age of high-angle normal faults . a/ Outcrop photographs of the Cerro Tajo fault (GFD7 in Figure 3.3). Hangingwall: the middle crust (gneisses), footwall: serpentinized mantle rocks. Star: location of sample GFD7 used for Ar-Ar dating. b/ Hand-specimen of the sampled fault breccia (GFD7). White arrow: a clast of the gneiss protolith with only biotite. c/ Thin-section from b showing the formation of muscovite pseudomorph after garnet. White arrow: very fine grains in the matrix. Stereoplots of fault surfaces (lower hemisphere projection on a Schmidt net (FSA software by Célérier, 2013: version 35.2). for Cerro Tajo fault (d) and La Robla fault (e). Great circles: fault planes. Grey arrows: striaes and motion on fault surfaces. f/ ^{40}Ar-^{39}Ar age spectrum for the mm-sized muscovite extracted from the tectonic breccia of the Cerro Tajo fault (For description of the method and analytical data see Supplementary material)

The La Robla fault has been considered as a recent normal fault (Insua-Arevalo et al., 2012). Instead, the Cerro Tajo fault has been described with movements top-to-N (Argles et al., 1999; Esteban et al., 2004) or top-to-S and dextral (Crespo-Blanc and Campos, 2001; Soto and Gervilla, 1991), during Burdigalian to Serravallian. Considering the large normal offset of these faults and their obvious control on the architecture of the area, , we collected a sample along the Cerro Tajo fault (Fig. 3.3a) of a hydrothermal tectonic breccia (Fig. 3.3b) in order to date displacement along these high-angle faults. Millimetric white micas are

pervasive in the very fine-grained matrix of the tectonic breccia (white arrow, Fig. 3.3c). They are not observed in the protolith of the breccias and define pseudomorphs after garnet (on the left in Fig. 3.3c) clearly indicating a neo-formation of the mica during shearing in presence of fluids. $^{40}Ar/^{39}Ar$ step heating method on the white micas extracted from the matrix of the tectonic breccia were conducted and the age obtained was 21 ± 0.3 Ma. Data are portrayed in an age spectrum in figure 3.3f. Details on the method, a table summarizing the data obtained and a complete set of isotopic results are given in the supplementary material. A first extensional stage top-to-S in present-day coordinates (reported also in Soto and Gervilla, 1991), most probably at ca. 21 Ma, is then followed by a reactivation in thrusting with a strong component of dextral shear (Late Burdigalian) (Esteban et al., 2004).

3.3.3 The Alozaina basin

The deposition of the *Alozaina Basin* (name as such here for sake of simplicity) (Figs. 3.1 and 3.2), is a terrigenous Aquitanian to Langhian basin that includes three main groups (Serrano et al.; Suades and Crespo-Blanc, 2013 and references therein). At the base, the Ciudad-Granada group has an Aquitanian age (22-20 Ma, dark yellow, Fig. 3.2). In the middle, La Viñuela group is Burdigalian (20-18 Ma), and at the top the Neonumidian or Numidoide olistostrome-type deposits are Burdigalian - Langhian, (around 18-15 Ma) (Bourgois, 1978; Martín-Algarra, 1987). A first typical feature of the basin is the upward deepening trend with a change in sedimentation-type around 20 Ma, when clasts of metamorphic rocks of the Alboran Domain and locally peridotites starts to be deposited in the basin (Aguado et al., 1990). A second important character of the basin is the important amount of olistostromic deposits that have been associated to thrusting in previous studies (e.g. Frasca et al., 2015; Suades and Crespo-Blanc, 2013).

Both high-angle faults (Cerro Tajo and La Robla, Fig. 3.2) are more likely contemporaneous to the deposition of the sediments in the Alozaina basin because first they display dip-parallel offsets up to 5 Km and second the distribution of the sediments is strongly linked to the location of faults. The base of the transgressive cover of the Alboran Domain (reported as dark yellow in the Alozaina Basin, Fig. 3.2a) crops out completely near Alozaina (Bourgois, 1972a, 1972b) while several smaller outcrops are scattered along the unconformity with the Alboran metamorphic rocks (Alcalá et al., 2013; Peyre, 1974; Sanz de Galdeano et al., 1993; Serrano et al., 2007). The base of the transgressive cover is lower Aquitanian, an age similar to the inferred activity of the La Robla fault through ^{40}Ar-^{39}Ar methods (Fig. 3.3). The Alozaina Basin and the high-angle faults (La Robla and Cerro Tajo) provide important relative age constraints for the tectonic evolution of the area.

3.4 Strain and kinematics in crust and mantle

The main foliation trend is generally parallel to the condensed metamorphic isograds in both crust and mantle. Two types of shear indicators are observed: ductile in mantle and lower/middle crust and brittle/ductile in middle/upper crust. Ductile shear, associated to

regional MP/HT metamorphism and foliation development during continental rifting and related crustal thinning, presents a coherent direction E-W to NE-SW. In figure 3.4, arrows represent the mean senses of shear in the lower crust and mantle (violet), and in the middle crust (dark blue). Two opposite senses of ductile shear, top-to-E and top-to-W, are observed that will be discussed in detail below. Brittle/ductile shear (light blue arrows in Fig. 3.4) that are observed in the upper crust and top middle crust can be related either to rifting/thinning or to local later reactivation. The criteria adopted for data selection are also discussed below. Figure 3.5 provide outcrop photographs of shear criteria throughout the entire thinned section of the continental lithosphere.

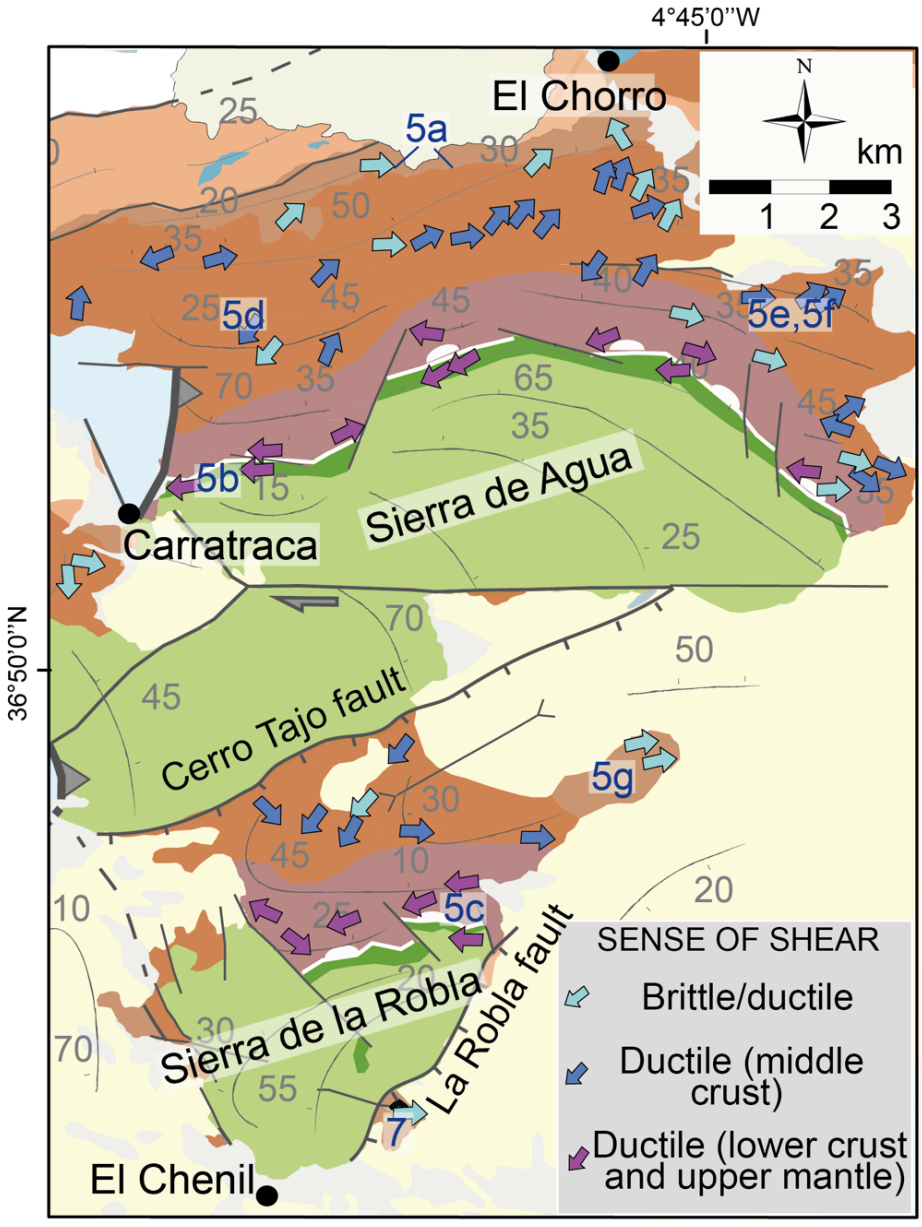

Fig. 3.4. Mean senses of shear in the Carratraca area. Ductile shear in the mantle and lower crust (Violet arrows) and in the middle crust (Blue arrows). Brittle/ductile shear, mainly observed in the upper crust (Pale blue) (For the whole set of lineation and shear criteria see Supplementary material).

3.4.1 Kinematics of ductile deformation

a) In the Crust-Mantle shear zone. In the garnet-mylonitic peridotites of the Agua and Robla blocks, the sense of shear observed is mainly dominantly top-to- W (Fig. 3.4), derived from observation of C'-type shear bands often associated with strongly stretched pyroxenite layers (Fig. 3.5b). Orthopyroxene crystals mainly define stretching lineations. Pyroxenites layers are parallel to the crust-mantle boundary (Fig. 3.4) and are deflected close to the Cerro Tajo fault and close to El Chenil defining a slight arcuate trend visible also in the dispersion of foliation poles in the stereoplots (Fig. 3.S1). In the lower crust, the main foliation is defined by biotite and sillimanite and characterized by occurrence of leucosomes lenses, locally strongly stretched and sheared. Shear bands with melt injections are abundant and show sigmoidal melt pressure shadows around garnet porphyroclasts and deflection of leucosomes against C'-type shear bands indicate a sense of shear dominantly top-to-W (Fig. 3.5c).

Stretching lineations, defined usually in kinzigites and migmatites by quartz rods and elongated K-feldspar, are subhorizontal, trending mainly E-W, almost parallel to the lineations in the garnet-mylonitic peridotites. In summary, in the Agua and Robla blocks, the crust-mantle boundary displays a top-to-W sense of shear at the base of the crust and in the top of the mantle (Fig. 3.4). Few top-to-E senses of shear are observed but only in scattered and discontinuous brittle/ductile low-angle shear zones (Fig 3.4).

b) In the middle crust, two senses of ductile shear are observed: top-to-W in the lower part of the middle crust and top-to-NE in the upper part of the middle crust. ENE to NE-trending stretching lineations are defined by sillimanite needles in the upper part of the middle crust, and by still few E-W trending quartz-sillimanite rods in the lower part. Sheath folds are common (Figure 3.5f) that could partly explain the scattering in the lineation trend observed. Sheath folds also indicate high to extremely high values of the principal direction of stretching ($\lambda_1 > 7.0$; i.e. stretching >600%) in the middle crust rocks. Deflection of foliations along C'-type planes, asymmetric boudinage of competent layers and sigma or delta tails around porphyroclasts indicate a top-to-NE sense of shear (Fig. 3.5e) and, less frequently, in the lower part of the middle crust, a top-to-W or SW sense of shear (Fig. 3.5d). No superposition pattern has been identified in the field between top-to-W and top-to-NE shear indicators, leading Argles et al. (1999) to propose a co-axial type of deformation pattern.

These two opposite senses of shear, their respective location in the lower and upper parts of the middle crust and the absence of cross-cutting relationships suggest their coeval development. Moreover, the top-to-W sense of shear in the lower part of the middle crust is in continuity with top to west shearing reported in the lower crust and mantle. In the other hand, the top-to-NE sense of shear in the upper part of the middle crust is also in continuity with the sense of shear at the transition between brittle and ductile crust (Fig. 3.4).

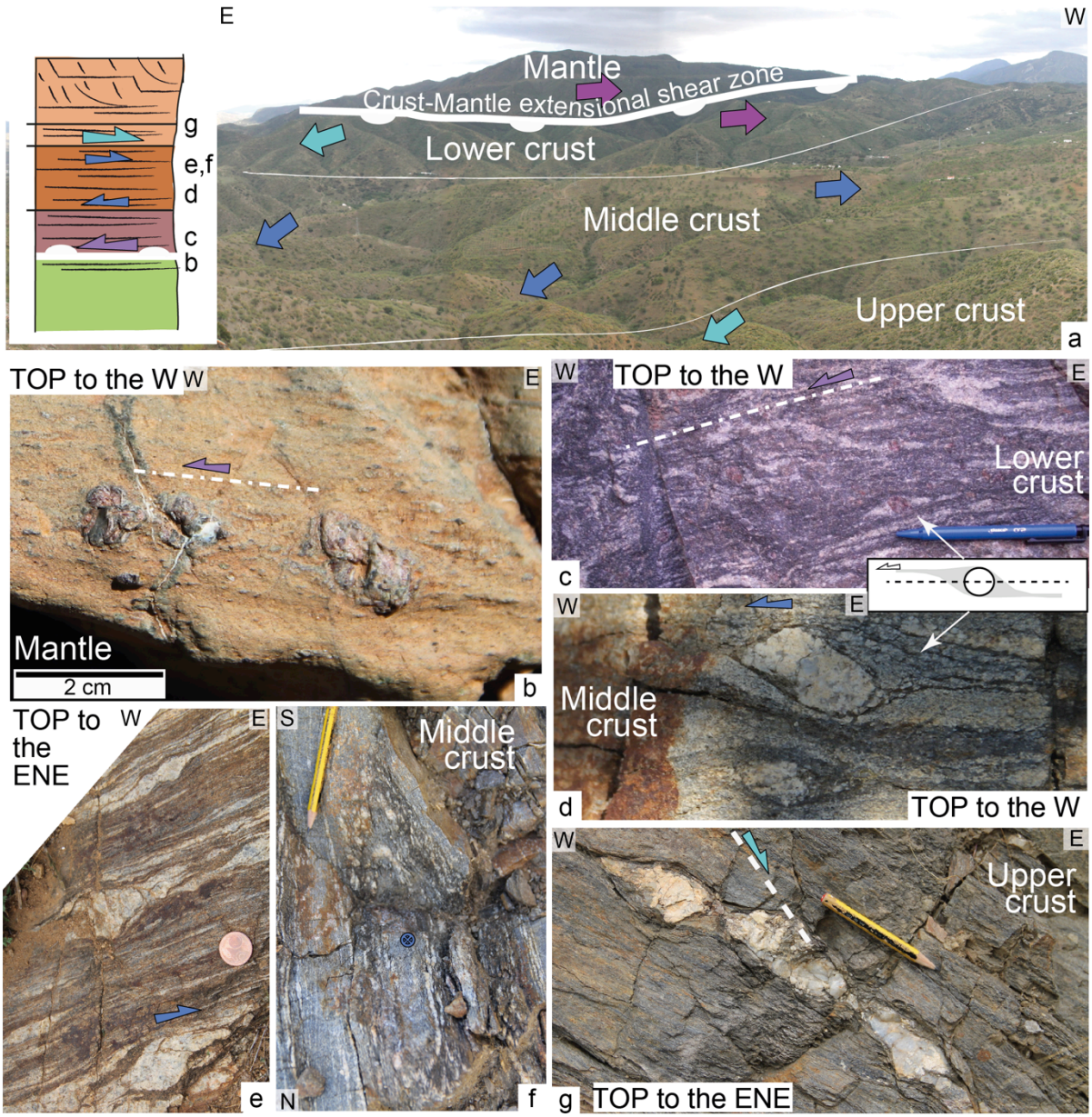

Fig. 3.5. Types of senses of shear reported in Fig. 3.4. a/ Landscape view (from point 5a on Fig. 3.4) of the thinned lithosphere in the Sierra de Agua. Left inset: Summary of senses of shear at the different lithosphere levels (not to scale; green: mantle; violet: lower crust; dark brown: middle crust; light brown: upper crust) with location of photographs (see geographic location in Fig. 3.4).. b/ Top-to-W shear in the mantle: deflection of a pyroxenite layer in the Grt-Sp mylonitic foliation. c/ Top-to-W shear in the Lower crust: melt pressure shadows around a garnet porphyroclasts and C'-type shear-bands, locally enriched in melt, in the granulites. d/ Top-to-W shear in the middle crust: sigmoidal stretched leucosome. e/ Top-to-E shear in the middle crust: sigmoidal stretched leucosome. f/ Sheath fold in the middle crust associated to top-to-E in the sillimanite gneisses indicating a high value of stretching. g/ Middle/upper crust top-to-E shear: C'-type brittle-ductile shear planes in the andalusite schists.

3.4.2 Kinematics of brittle/ductile deformation in the whole crust

In the transition between middle and upper crust, shear criteria combine mixed ductile and/or brittle features. Asymmetric boudinage and C'-type shear-planes in andalusite-bearing

quartz veins always show a top-to-E or NE sense of brittle/ductile shearing (Fig. 3.5g). The same features are observed in both Agua and La Robla blocks and this geographic distribution indicate that the observed senses of shear are related to a single deformation event and not to late local reactivations. Moreover, top-to-NE sense of shear in this ductile-brittle shear indicators are related to veins containing metamorphic minerals (Fig. 3.5g), indicating that the development of the C'-type shear bands and the regional MP/HT foliation are coeval with the overall crustal thinning.

In the upper crust, the metamorphic grade becoming very low, the absence of metamorphic mineral renders almost impossible the separation of shear sense indicators related to crustal thinning and to late reactivation, respectively. Widespread low-angle normal faults are interpreted as associated either to crustal thinning during lower Miocene (Argles et al., 1999) or to middle Miocene extensional reactivation of the Alboran domain during the formation of the Alboran basin (García-Dueñas et al., 1992).

Top-to-E-NE brittle-ductile shear indicators are also observed throughout the entire crustal section (light blue arrows, Fig. 3.4) suggesting that a late top-to-E brittle sense of shear affected the entire thinned continental crust.

3.4.3 A gradient of ductile crust thinning: hyper-stretching?

Associated with the above ductile to brittle deformation, important variation in crustal thickness can be inferred from map scale and cross-section (Fig. 2) and are summarized in Figure 6. Cerro Tajo and La Robla high angle normal fault separate the thinned continental lithosphere in three tectonic blocks (Agua, Robla and Alozaina) with strong variations in crustal thicknesses. Map-scale cross-cutting relationships indicate that variations in crustal thickness and especially in the ductile crust thickness were acquired before the high-angle normal faulting and reflect thus variation of crustal thicknesses acquired during the Oligocene-Lower Miocene rifting. This also excludes that variations in crustal thickness could be attributed to later tectonic events and in particular to thrusting.

The variations in crustal thickness can be partly related to erosion, but not for lower and middle crust that are always bounded by mantle and upper crust. A strong thickness decrease is observed in the lower crust between La Agua and La Robla blocks (average thickness values of 560 m and 370 m, respectively), while in the Alozaina block the lower crust is absent and the middle crust is preserved only in scattered lenses few tens of meters thick. As a consequence, the middle crust is locally found in direct contact with the serpentinized mantle (see below). The middle crust shows a comparable thickness variation, from 1510 m to 950 m between the Agua and La Robla blocks. The total thickness variation of the ductile crust, from 1970 m to 70 m between Agua and Alozaina blocks, corresponds to a layer-perpendicular finite strain λ_v=0.04 (i.e. 96% shortening). In plane strain this implies a layer-parallel finite strain λ_h=25.0 (i.e. 2400% stretching), defining what can be called "hyper-stretching". Such amounts of thinning-stretching are entirely related to ductile strain and cannot be simply related to high-angle normal faults. The strong gradient of layer-

perpendicular shortening observed cannot result only from simple shear and is more a combination of layer parallel shear and layer perpendicular shortening (i.e. combination of pure shear and simple shear).

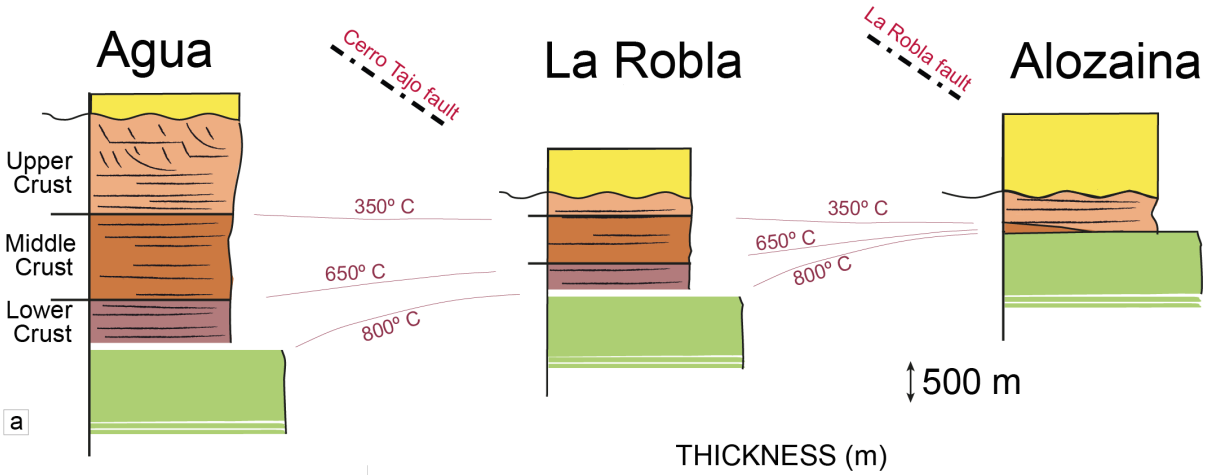

b

THICKNESS (m)

	Agua	Robla	Alozaina
Upper Crust totally or partly eroded	> 1270	0	> 480
Middle Crust	1510	950	50
Lower Crust	560	370	20
Ductile crust	1970	1070	70

Fig. 3.6. Variations in crustal thicknesses. a/ Crustal thickness estimates in the Agua, La Robla and Alozaina blocks (green: mantle; violet: lower crust; dark brown: middle crust; light brown: upper crust) (See location in Fig. 3.2). b/ Estimates of the average thicknesses of the upper, middle and lower crust in the three blocks, from mean dip of foliation and local cross-sections.

3.4.4 Kinematics of brittle/ductile deformation in the hyper-stretched continental lithosphere

In the area NE of El Chenil of the Alozaina block, the crustal section reaches its minimum thickness, and a low-angle normal fault (LANF) with top to the NE sense of shear (Fig. 3.4) juxtaposes the upper crustal rocks (Malaguide schists at the top) and serpentinized mantle rocks (Fig. 3.7a and Fig. 3.S2 for local map and measurements). Lower and middle crustal rocks are strongly stretched and only appear as meter-scale lenses (Fig. 3.6). Mylonitic peridotites as well are not preserved and upper crustal rocks are in direct contact with the spinel-tectonites through the LANF.

The fault zone thickness changes along strike from around 10 to 30 m, but maintains a

characteristic zoning (Figs. 3.7a and 3.7b). The LANF footwall is marked by a serpentinite zone, 5 to 30 meters thick, with a variable degree of brecciation and several outcrops of ophicalcites (Fig. 3.7c), suggesting the presence of hydrothermal fluids during the LANF activity. The hanging-wall (i.e. the deformed overlying crustal rocks, Fig. 3.7d) is more pervasively deformed and is characterized by gouge in the core, with clasts of quartz-veins and gneisses and locally blocks of ophicalcite. In the upper crust close to the fault zone, C'-type shear bands indicate a top-to-E-NE sense of shear (Fig. 3.7e and Fig. 3.S2 for steroplots), as in the middle and upper crust described above.

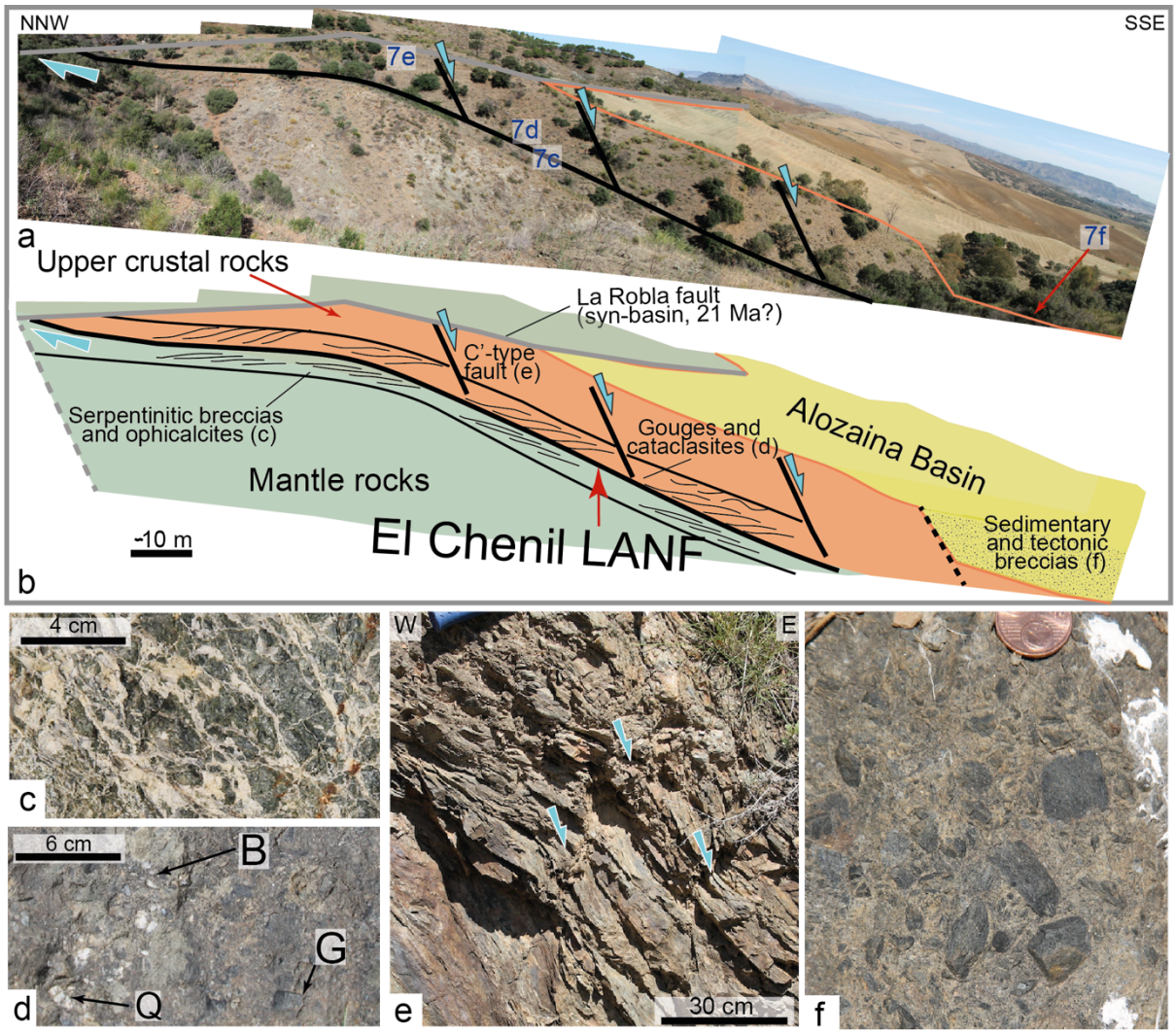

Fig. 3.7. Low-angle normal fault (LANF) in the hyper-stretched portion of the rift (El Chenil area; see location in Fig. 3.4). a/ Landscape view of the El Chenil LANF. b/ Geological interpretation of the El Chenil fault zone. Photographs of ophicalcite (c), Fault gouge in the core zone with clasts of a quartz-vein (Q), breccia (B) and gneiss (G) (d), C'-type shear bands in the upper crustal rocks indicating a top-to-E sense of shear (e). f/ Tectono-sedimentary breccia at the base of the Alozaina basin with clasts of mainly upper crustal rocks.

The LANF is cut by the high angle La Robla normal fault of Aquitanian age (Figs. 3.4, 3.7a and 3.7b), supporting a rift-related origin. Deposition of breccias and sandstones are locally controlled by C'-type shear bands in the LANF hanging-wall (Figs. 3.7a and 3.7b).

These sedimentary rocks compose the base of the Alozaina Basin (Ciudad Granada formation, Aquitanian in age) and are characterized by discontinuous angular clasts 1to10 cm large, most probably related to debris-flow with a short transport distance (Fig 3.7f).

In summary, in the Alozaina block, stretching reaches its maximum value leading to the complete omission of the ductile crust and bringing the upper crustal rocks in direct contact with the serpentinized mantle, through a LANF with top-to-E-NE sense of shear, similar to the one observed in the upper crust and opposite to one observed in the lower crust/upper mantle.

3.5 Discussion

3.5.1 Change in the sense of shear with depth

The ductile deformation that is responsible for the development of foliation and stretching lineations at regional scale is associated to a MP/HT metamorphism characterized by andalusite and sillimanite in the middle crust that lead to partial melting in the lowermost crust during lower Aquitanian. This extensional deformation triggers extreme ductile crust thinning and what we have called hyper-stretching in an EW direction and is characterized by a change in the sense of shear with depth: i) top-to-W in the mantle, lower crust and lower part of the middle crust and ii) a top-to-NE in the upper part of the middle crust and in the upper crust.

Top-to-E-NE brittle-ductile shear affected the entire thinned crustal section. The superposition of brittle-ductile deformation on ductile fabrics indicates that the originally ductile crust cooled during thinning and became part of the brittle crust during the extensional process. Consistently, in the hyper-stretched portion of the continental lithosphere, where the ductile crust thickness reaches its lowest value (less than few meters), a concordant top to NE shearing is observed in both strongly thinned crust and serpentinized mantle.

The above conclusions can be summarized graphically with their rheological implications. At the onset of extension (Fig. 3.8a), the vertical profile of displacement is bell-shaped defining: i) a top-to-E sense of shear in the upper crust and top middle crust and ii) a top-to-W sense of shear in the lower crust and the sub-continental mantle. In rheological terms, this change in shear sense with depth should be controlled by two strength peaks i) the brittle-ductile transition in the crust and ii) a high strength layer made of the sub-Moho mantle, that are separated by a weak decoupling layer (i.e. the ductile crust). Upper crust and mantle are thus mechanically decoupled, allowing the horizontal flow of the ductile crust. Two main shear zone, the midcrustal shear zone and the crust-mantle shear zone controls the horizontal displacement with opposite sense of shear. After a significant amount of extension and thinning (Fig. 3.8b) the two shear zones becomes very close, and the upper crust and mantle

becomes mechanically coupled, as exemplified by the same top to NE shearing in both crust and mantle in the hyper-stretched portion of the lithosphere.

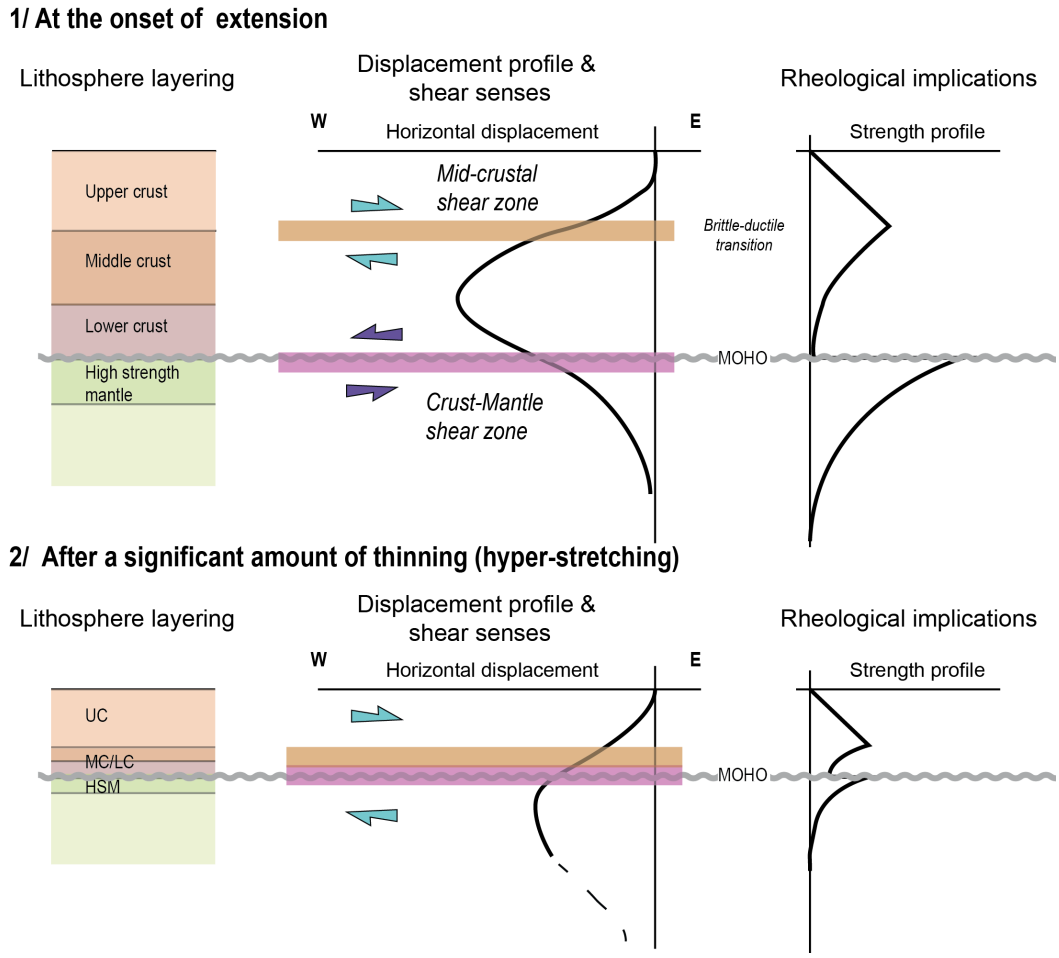

Fig. 3.8. Summary of shear sense variations with depth and their implications in terms of horizontal flow and rheology (strength profile), at the onset of extension and after a strong crustal thinning in the hyper-stretched portion of the lithosphere.

3.5.2 Some remarks concerning the Cerro Tajo and La Robla high-angle normal faults

The Cerro Tajo and La Robla faults (Fig. 3.2) are primarily normal faults which display large dip-parallel offsets up to 5 Km. During thrusting, in late Burdigalian, they have undergone some contractional reactivation with a component of dextral shear (Frasca et al., 2015; Soto and Gervilla, 1991) but not significantly affecting their large normal offset. The two faults cut trough the whole crust and the mantle controlling the block tilting of the Sierra de Agua and Sierra de la Robla. Whereas their prolongation in the Alozaina basin cannot be precisely mapped, few outcrops inside the basin indicate that the sediments are tilted in their hanging-wall (Fig. 3.S2). The Ciudad-Granada group (Serrano et al., 2007) is the first sedimentary formation deposited in the basin is Aquitanian (22-20 Ma) and is locally

controlled by top-to- E-NE C'-type shear bands in the upper crust. It is noticeable that the $^{40}Ar/^{39}Ar$ age that we obtained for the La Robla fault gouge is also Aquitanian - 21 ± 0.3 Ma - i.e. synchronous with the early sediment deposition in the Alozaina basin. On these bases, we proposed that the base of the Alozaina basin can thus be interpreted as syn-rift deposit, controlled by C'-type of structures in the upper crust.

The two faults trend at small angle to the direction of the stretching lineations in the Agua and La Robla blocks. Consequently, these normal faults cannot have developed in the kinematic continuity of the ductile deformation recorded in the tilted blocks. In fact, available paleomagnetic data show that the studied area has undergone dextral rotations up to 60° (Feinberg et al., 1996; Villasante-Marcos et al., 2003) in relation with the formation of the Gibraltar arc during slab rollback. Consequently, the rift that conducted to hyper-stretching and mantle exhumation has undergone large rotations during the late stages of its development and during inversion/thrusting (Frasca et al., 2015; Platt et al., 1995). Whereas it is beyond the scope of the present paper to elaborate on these large-scale tectonic aspects, it is especially interesting to note that these faults, whose development is rather late in the rift history, cut through a brittle mantle layer of more than 5 Km thick. This demonstrates that the extreme thinning of the continental crust in the area has permitted a quick cooling of the mantle.

3.5.3 Process of lithosphere necking in the western Betics

The geological observations and measurements carried out in the Carratraca massif of the Ronda peridotites and its crustal envelope bring new light on the process of lithosphere necking. Whereas the evolution of necking is progressive, it is, for convenience, summarized in three snapshots in figure 3.9.

The early stages of necking (Fig. 3.9a), dated between 33 and 25 Ma by Malaga dykes (Esteban et al., 2013; Turner et al., 1999), are characterized by the existence of a high strength subcontinental mantle with common sense of shear top-to-W, opposite to the sense of shear top-to-E-NE observed in the upper part of the middle crust (Fig. 3.8a). This inversion of the sense of shear with depth strongly constrains the mechanical behavior of the rifted lithosphere. It shows that the ductile middle crust plays the role of a decoupling layer (*décollement*) between the brittle upper crust and the high strength subcontinental mantle. In rheological terms, it indicates that the high strength mantle has a higher strength than the overlying (middle crust) and underlying (deeper lithospheric mantle) layers.

In addition, the inversion of shear sense within the middle crust implies that the strength peak of the high strength mantle must be higher than the strength peak of the upper brittle crust. In other terms, during the early stages of necking the lithosphere strength peak is located in the high strength mantle that exerts a dominant control on the deformation of the whole lithosphere (Fig 3.8a). Numerical models show that lithosphere necking triggers intense strain localization in the sub-continental mantle (Gueydan and Précigout, 2014) and

by crust-mantle decoupling (deep crust *décollement*) (Brun and Beslier, 1996; Gueydan et al. 2008; Nagel and Buck, 2004). Analogue models moreover exemplified that the necking process corresponds, at lithosphere scale, to a pure shear-type deformation accommodated by conjugate shear zones with opposite senses of shear, respectively at the base of the brittle crust and in the subcontinental mantle (Brun and Beslier, 1996). The strong mylonitization and thinning of the high-strength mantle (Précigout et al., 2007) allows the deeper and weaker mantle to come into contact with the crust and hence implies a strong heating of the lower crustal levels. This is in agreement with partial melting observed in the lower part of the middle crust and in the granulites of the lower crust (Platt and Whitehouse, 1999; Whitehouse and Platt, 2003). Such high geotherm (Negro et al., 2006) can be moreover related to supra-subduction settings.

The advanced stages of necking (Figs. 3.9b), dated between 25 and 22 Ma by crystallization and cooling ages within the HT foliation (Esteban et al. 2013, and compilation in geological settings), are characterized by a strong thinning of the ductile crust observed from the Agua to Alozaina blocks. The extremely large corresponding gradient of stretching (2400%) can be qualified of "hyper-stretching". The drastic decrease of the crustal thickness may trigger cooling of the attenuated crust and the initial strength profile with two peaks (Fig. 3.8a) becomes almost single peak in the localized zone of stretching (Fig. 3.8b). The crust and mantle becomes mechanically coupled and the two major shear zones (i.e. mid-crustal and crust-mantle shear zones) merge into a single, with top to NE shearing between upper crust and serpentinized mantle. Four-layers analogue models of lithosphere extension have consistently shown that the extreme boudinage of the high strength mantle brings into contact the upper part of the crust and the ductile mantle with their already acquirred opposite senses of shear (Brun and Beslier, 1996).

The late stages of necking (Fig 3.9c), dated between 22 and 20 Ma (our ^{40}Ar-^{39}Ar age on the Cerro Tajo fault and Alozaina basin), is characterized by the development of steeply dipping normal faults and related block tilting within this domain of localized stretching. This indicates that cooling follows rapidly, in the thinned crust and the underlying mantle, inducing a downward migration of the brittle-ductile transition. In the western Betics, this event of late brittle deformation characterized by the formation of large tilted blocks (Agua, La Robla, Alozaina), superposed to previous ductile fabrics, has been interrupted by thrusting and rift inversion at around 20 Ma (Frasca et al., 2015). Syn-rift deposits during this late stage, mark the onset of subsidence and the cooling of the stretched portion of the lithosphere. One can expect that, if extension would not have been interrupted by rift inversion, the normal faulting and block tilting could have continued in a core complex exhumation mode of the underlying ductile mantle.

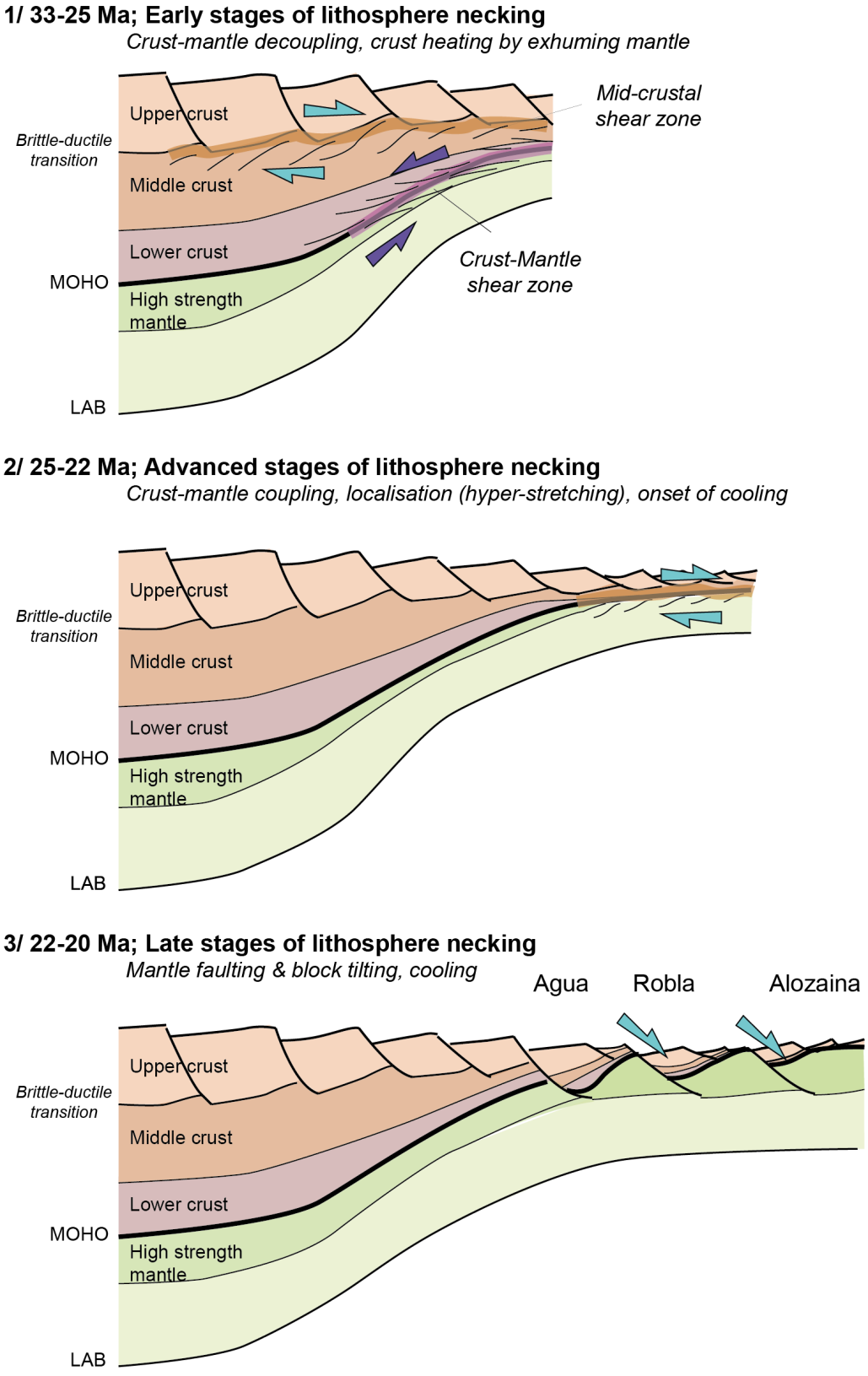

Fig. 3.9. Conceptual view of the lithosphere necking process in three main stages (See explanation in the text).

3.5.3 Comparison with previous work

In summary, what the western Betics exemplifies, probably better than any previous field example of mantle exhumation, is the changes in deformation processes that accompany the progressive necking of the continental lithosphere. The conceptual model (fig. 3.9) that summarizes our field observations and measurements is portrayed in three steps that directly result from the three major thermo-mechanical changes that occur during necking of a continental lithosphere: i) the change of shear sense with depth is controlled by the initial two-peak lithosphere strength profile, ii) the localization of stretching in the central zone of the lithosphere neck results from the intense strain localization of the subcontinental mantle and iii) the late steep normal faulting, cross-cutting the crust and mantle, results from fast cooling in the zone of hyper-stretching.

This tectonic sequence, well illustrated in the western Betics, suggests that, contrary to the habit taken in the recent years of opposing "hyperextension" to "necking" in the study of passive margins (Doré and Lundin, 2015; Manatschal, 2004) is somewhat misleading in terms of the physical processes involved. First, "necking" is the whole process (the mechanical instability) of continental lithosphere extension up to continental breakup (Brun and Beslier, 1996). Second, there is consequently no physical reason to oppose "necking" (process) to the so-called "hyperextension" (process product). Third, mantle detachment faults that are often invoked to characterize hyperextension are only a late stage of high-angle normal faulting with important block tilting. Numerical models have shown that such mantle detachment faults may develop during lithosphere extension (Lavier and Manatschal, 2006). However, in such models, a strong decrease of the friction coefficient is necessary to allow large offsets on a single fault (e.g. detachment fault, Lavier et al., 1999). On the contrary, our study shows that ductile strain localization in both the middle crust and the sub-continental mantle controls the major part of the necking process and hence sub-continental mantle exhumation at passive margins. The later stages of lithosphere necking are marked by high-angle normal faults and block tilting, involving both mantle and crust, that may continue in a core complex exhumation mode of the underlying ductile mantle for larger amounts of extension.

3.6 Conclusion

Our study, gathering field geology and geochronology, leads the following conclusions:

1/ The western Betics presents an exceptional exposure of a section of a hyper-stretched continental lithosphere with the world largest sub-continental mantle massif (Ronda Peridotites), exhumed during the Oligocene-Lower Miocene in a back-arc tectonic setting

2/ Observed variations in crustal thickness indicate amounts of stretching that may locally reach values as high as 2400 %, defining a stage of hyper-stretching.

3/ Ductile deformation associated to crustal thinning is marked by opposite senses of shear in the lower crust/sub-continental mantle and in the upper/middle crust, highlighting a mechanical decoupling between the upper crust and the localizing sub-continental mantle.

4/ In the hyper-stretched segment (i.e. lithosphere neck), the ductile crust almost disappeared and the upper crust became mechanically coupled to the underlying serpentinized mantle.

5/ On the above bases, three main successive steps characterize lithosphere necking process:

i/ First, a mid-crustal shear zone and a crust-mantle shear zone, acting synchronously but with opposite senses of shear, accommodate ductile crust thinning and ascent of the sub-continental mantle

ii/ Second, hyperstretching localizes in the neck, leading to an almost disappearance of the ductile crust and bringing the upper crust into contact with the subcontinental mantle, each of them with their already acquirred opposite senses of shear

iii/ Third, high-angle normal faulting, cutting through the Moho, and related block tilting ends the full exhumation of mantle in the domain of localized stretching.

ANNEX I

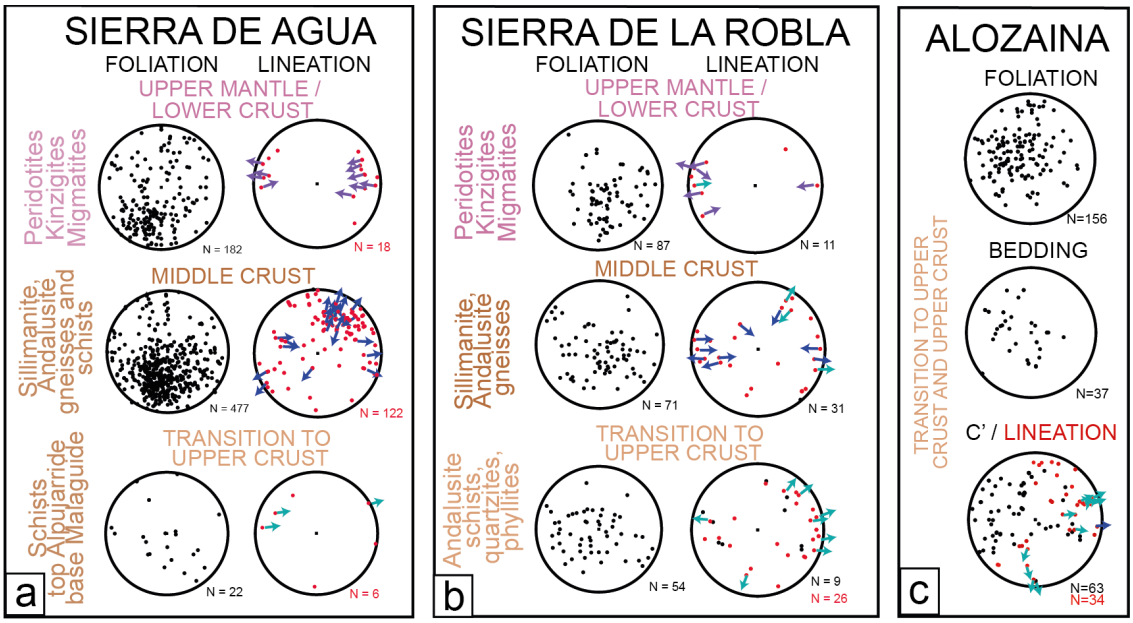

Figure 3.S1. Stereoplots of data collected in the three blocks defined in the text of the manuscript (lower hemisphere; Schmidt net; using OSXStereonet: version 9.2.0. http://www.ux.uis.no/~nestor/work/programs.html).

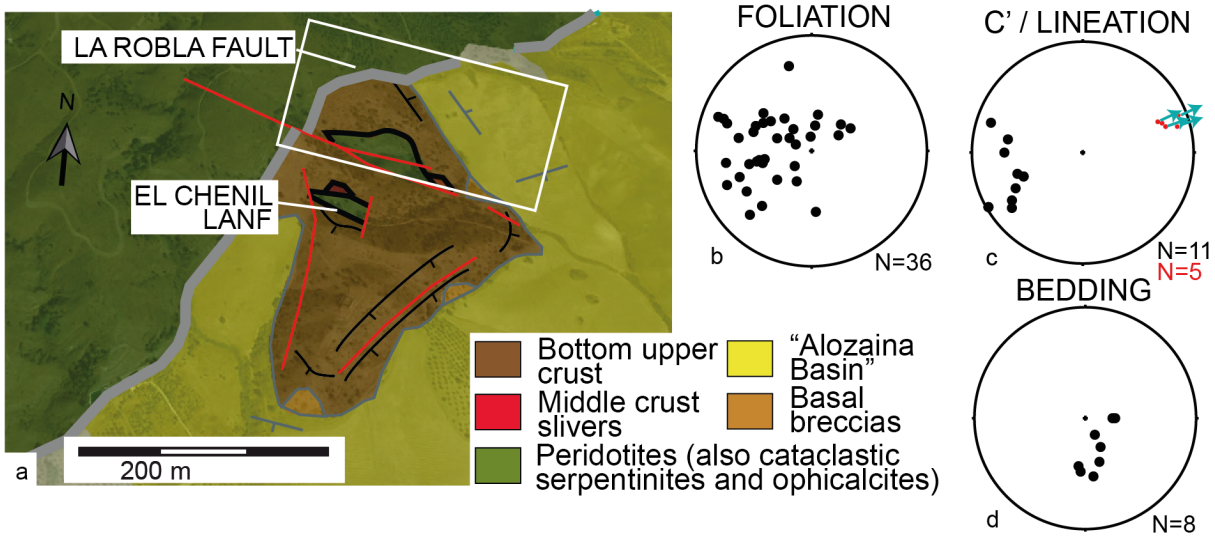

Figure 3.S2. 3D visualisation of El Chenil using GoogleEarth. (b,c,d) Stereoplots of the structural elements collected in the area reported in (a). The white rectangel

ANNEX II

$^{40}Ar/^{39}Ar$ step heating method

A fresh sample were selected in the field for single grain step-heating laser probe $^{40}Ar/^{39}Ar$ dating. The sample was crushed, sieved and single grains of micas were handpicked under binocular microscope and cleaned in ultrasonic bath using acetone and distilled water. Biotites and muscovites were packaged in aluminium foils and irradiated for 40 hours in the core of the Triga Mark II nuclear reactor of Pavia (Italia) with several aliquots of the Fish Canyon sanidine standard (28.03 ± 0.08 Ma; Jourdan and Renne, 2007) as flux monitor. Argon isotopic interferences on K and Ca were determined by irradiation of KF and CaF_2 pure salts from which the following correction factors were obtained: $(^{40}Ar/^{39}Ar)_K = 0.00969 \pm 0.00038$, $(^{38}Ar/^{39}Ar)_K = 0.01297 \pm 0.00045$, $(^{39}Ar/^{37}Ar)_{Ca} = 0.0007474 \pm 0.000021$ and $(^{36}Ar/^{37}Ar)_{Ca} = 0.000288 \pm 0.000016$. Argon analyses were performed at Géosciences Montpellier (France) with an analytical system that consists of: (a) an IR-CO2 laser of 100 kHz used at 5-15% during 60 sec, (b) a lenses system for beam focusing, (c) a steel chamber, maintained at 10^{-8} - 10^{-9} bar, with a drilled copper plate and the four samples on, (d) an inlet line for purification of gases including two Zr-Al getters, (e) a multi-collector mass spectrometer (Argus VI from Thermo-Fisher). A custom-made software controls the laser intensity, the timing of extraction/purification and the data acquisition. To measure the argon background within the system, one blank analysis was performed every three sample analyses. The ArArCalc software© v2.5.2 was used for data reduction and plotting. The one-sigma errors reported on plateau, isochron and total gas ages include the error on the irradiation factor J. Atmospheric ^{40}Ar was estimated using a value of the initial $^{40}Ar/^{36}Ar$ of 295.5. A complete set of isotopic results is given in Table 3.DR1.

Table 3.DR1: Ar-Ar stepwise heating results.

	$^{40}Ar/^{39}Ar$	$^{37}Ar/^{39}Ar$	$^{36}Ar/^{39}Ar$	$\%^{40}Ar$ rad	$\%^{39}Ar$	Age	Error
GFD7 muscovite 1							
1	17,5325	0,1997	0,0504	15,05	4,01	20,24	1,64
2	5,5682	0,1787	0,0092	51,30	4,88	21,90	0,53
3	4,7275	0,6366	0,0062	61,88	2,51	22,43	0,84
4	3,3653	0,0343	0,0020	81,97	13,03	21,15	0,19
5	3,1606	0,0000	0,0014	86,30	22,11	20,91	0,13
6	2,9929	0,0236	0,0008	92,27	12,13	21,17	0,23
7	2,9642	0,2120	0,0007	93,46	4,93	21,24	0,45
8	2,8020	0,0000	0,0002	97,51	12,37	20,95	0,21
9	2,7646	0,0910	0,0001	99,21	8,69	21,03	0,23
10	2,7814	0,6522	0,0001	100,00	2,13	21,42	1,05
11	2,7512	0,1315	0,0000	100,00	4,75	21,16	0,48
12	2,7540	0,2407	0,0001	99,36	8,46	20,99	0,28
					Total age : 21.10 +/- 0.37		

ACKNOWLEDGMENTS

This work was funded by the European Union FP7 Marie Curie ITN “TOPOMOD”, contract 264517. Thanks to Alexandre Pichat and Hugo Humbert for the help in the field.

CHAPTER 4

Two successive events of crustal melting resulting from extensional exhumation and then thrusting of the Ronda Peridotites (South Spain)

The article composing this chapter has been submitted to Geology

Gianluca Frasca[1,2], Frédéric Gueydan[2], Marc Poujol[1], Jean-Pierre Brun[1], Fleurice Parat[2], Alexandre Pichat[2], and Sophie Mazier[1]

[1]*Géosciences Rennes, UMR 6118 CNRS/INSU, OSUR, Université Rennes 1, 35042 Rennes Cedex, France*

[2]*Géosciences Montpellier, Université Montpellier 2, UMR 5243 CNRS/INSU, Place E. Bataillon, CC60, 34093 Montpellier Cedex, France*

Abstract

The Alboran Domain, situated at the western end of the Mediterranean subduction system, is characterized by the world largest exposure of subcontinental mantle (the Ronda Peridotites) and by a Lower Miocene regional high-temperature thermal event, marked by crustal melting. Using U-Pb LA-ICP-MS dating, we identify two distinct episodes of crustal melting associated with two large-scale tectonic contacts that bound the Ronda Peridotites. The first episode of partial melting at ca. 22.5 Ma, associated to the regional foliation in the high-grade and strongly attenuated crustal section that overlies the Ronda Peridotites, is related to an extreme thinning of the continental crust and to mantle exhumation. The second episode of crustal melting at ca. 20 Ma, marked by leucocratic granite dikes that intrude both the peridotites and the overlying thinned crustal envelope, is related to the thrust emplacement of the section of thinned and hot continental lithosphere on top of crustal rocks. The crustal emplacement of the Ronda peridotites and the regional high-temperature thermal event of the western Alboran Domain therefore resulted from a fast switch from 1/ continental lithosphere extension in a back-arc setting, with local partial melting in the deep crust, and sub-continental mantle exhumation, to 2/ rift inversion by thrusting, triggered by shortening of the upper continental plate, with melting in the thrust footwall and dike intrusion in the hanging wall.

4.1 Introduction

The Mediterranean is characterized by the coexistence of orocline orogenic systems (Alps, Gibraltar), back-arc basins, and arcuate subduction zones (Calabria, Hellenic trench) caused by slab rollback (Wortel and Spakman, 2000). The Alboran-Gibraltar orocline (from the Betics in Spain to the Rif in Morocco) is characterized by the exhumation of large bodies of subcontinental mantle, the Ronda Peridotites, whose role in the Neogene geodynamics of the western Mediterranean is debated (Garrido et al., 2011; Van Hinsbergen et al., 2014). The initiation of the Appennines subduction occurred in late Oligocene and subsequent slab rollback leads to the successive opening of the Liguro-Provençal basin and the Tyrrhenian sea, with exhumation of the subcontinental mantle (e.g. Prada et al., 2014). In the Betic-Rif system the most recent tomographic images (e.g. Levander et al., 2014) display a very localized and subvertical slab below the Gibraltar arc that extend eastward over 600 km long below the Alboran domain, suggesting a significant amount of rollback during the last 30 Ma. However, the scarcity of data offshore, the complex and polyphase deformation history of the Alboran rocks onshore (e.g. Gueydan et al., 2015) and the wealth of scattered high temperature to low temperature ages between 22 and 16 Ma (e.g. Esteban et al., 2013) imply the lack of an unequivocal link between the rollback evolution and the subcontinental mantle exhumation.

In the western Betics, the peridotites bodies that preserved three typical metamorphic facies (Grt/Sp-peridotites, Granular Sp-peridotites, Pl-bearing peridotites; Obata, 1980), represent a tectonic sliver within the Alboran crust. The emplacement of the Ronda peridotites within the Alboran crust resulted from two successive deformation stages, marked by two major tectonic contacts (review in Précigout et al., 2013). First, extreme continental

lithosphere thinning, mostly accommodated in a crust-mantle extensional shear zone (white, Figs. 4.1B and 4.1C) controlled mantle exhumation from 75 km (Garrido et al., 2011; Précigout et al., 2013). The crustal envelope of the peridotites (Alpujarride) (Balanyá et al., 1997) shows a continuous Barrovian metamorphic zoning, in a coherent structural sequence from granulite facies rocks at mantle contact to un-metamorphosed rocks (in beige Fig. 4.1B) 4 km above, associated with decompression (Argles et al., 1999; Gueydan et al., 2015). Furthermore, the foliation development in the sheared granulites and migmatites is coeval and consistent with garnet-spinel mylonitization in the mantle (Platt et al., 2003, Précigout et al., 2013). The exhumation of the Ronda peridotite is thus primarily a consequence of an extreme crustal thinning, accommodated by a crust-mantle extensional shear zone (Afiri et al., 2011; Gueydan et al., 2015; Johanesen and Platt, 2015; Platt et al., 2003; Précigout et al., 2013). The occurrence of syn-tectonic partial melting (Marchesi et al., 2012) and locally of gabbro dikes within the mantle rocks (Hidas et al., 2015) testify to an extreme continental lithosphere thinning, which occurs in a back-arc setting, during the rollback of the Alboran slab (Précigout et al., 2013), as exemplified by the suprasubduction geochemical signature of magmatic intrusions in the Ronda peridotites (Marchesi et al., 2012).

Afterwards, shortening triggered the formation of the Ronda Peridotites thrust (Fig. 4.1) that accommodated the final crustal emplacement of the peridotites (review in Précigout et al., 2013). The basal sole of the Ronda Peridotites and the thrust footwall are characterized by partial melting in the underlying metamorphic rocks (Esteban et al., 2011 and ref. therein). The ages of in situ melting products and related granitic dikes intruding the peridotite yield a cluster between 22 and 19 Ma. Ar-Ar, Zircon and Apatites Fission Track also yield similar ages, between 24 and 15 Ma, implying a very fast cooling rate whose tectonic origin and relationship with mantle exhumation remain unknown. Finally, the complex polycyclic history of the mantle section, as suggested by the occurrence of pseudomorphs after diamond (Davies et al., 1993) and by Hercynian, Jurassic and Alpine ages (Sánchez-Rodriguez and Gebauer, 2000), allows for a certain degree of freedom in the interpretation of the ages of the continental lithosphere thinning and of the subsequent thrusting.

In order to unravel the tectonic history of the Ronda peridotites exhumation and thrust emplacement, we provide in this study, using U-Pb LA-ICP-MS dating, the precise timing of two different types of crustal melting associated with the Ronda Peridotites. Melting product from the crust-mantle extensional shear zone that accommodated the exhumation of the Ronda Peridotite is dated at ca. 22.5 Ma while the granitic dikes associated to the Ronda peridotites thrust emplacement onto the crust yield unequivocal ages at ca. 20 Ma.

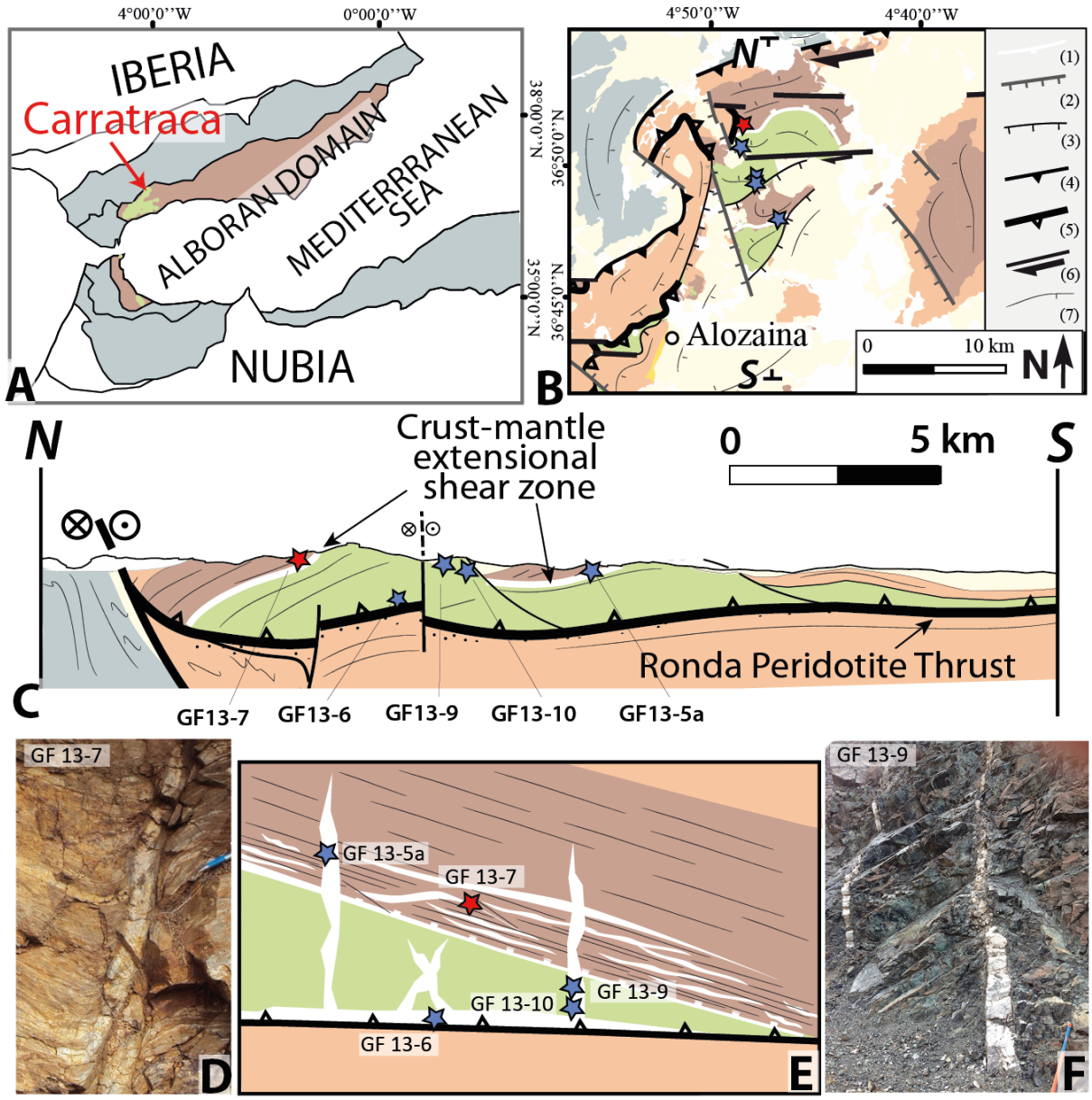

Figure 4.1. A/ Position of Alboran Domain between Nubia and Iberia plates, showing the location of subcontinental mantle and of the studied area (Carratraca). B/ Tectonic map of the Carratraca peridotite massif, with sampling locations. N and S are endpoints of cross-section line shown in C. C/ Simplified N-S regional cross-section. Stars indicate the position of the collected samples (Blue: rift-related sample; Red: thrust-related sample). D/ C'-type shear band in the lower crust with a synkinematic leucosome (GF13-7). E/ Schematic relationships between peridotites, overlying rocks, and metamorphic sole with location of the selected samples F/ Granite dikes within the peridotites (GF13-10).

4.2 Petrology, geochemistry and geochronology of the selected samples

Two types of leucogranitic dikes were sampled from the Ronda Peridotites and its crustal envelope: (1) a syn-deformational leucosome in the deepest part of the crust overlying the peridotites (granulites, around 20 m above the crust-mantle extensional shear zone, GF13-7), (2) two leucocratic dikes intruding the base of the Ronda Peridotites (GF13-9 and

GF13-10), and a leucocratic dike crosscutting the upper contact of the Ronda Peridotites (GF13-5a) (Fig. 4.1E). The syn-deformational sample (GF13-7) is associated with the extensional exhumation, as exemplified by the C'-type relationships between the shear zone and the regional foliation (Fig. 4.1D). Conversely, the leucogranites intruding the Ronda Peridotite and the crustal envelope (GF 13-5a, GF 13-9 and GF 13-10) are related to the hot thrust emplacement of the thinned lithosphere (Fig. 4.1F). U-Pb LA-ICP-MS dating and Sm-Nd and Sr isotope analyses were performed in Géosciences Rennes following the procedures described in Ballouard et al. (2015). The operating conditions for the LA-ICP-MS measurements during this study can be found in Table DR4.6, supplementary material[1].

The isotopic signature of the dikes is similar to the other Alboran Domain granites (Rossetti et al., 2013 and ref. therein). The high $^{87}Sr/^{86}Sr$ (0.715037, GF13-9, and 0.718605, GF13-7) and the low $^{143}Nd/^{144}Nd$ (0.512020, GF13-9, and 0.512026, GF13-7) values indicate a predominant crustal origin for both type of dikes, compatible with dehydratation melting of a metasedimentary source (Table DR4.1, supplementary material[1]). However, the different structural contexts (Fig. 4.1E) and large differences in their REE geochemistry (Fig. 4.2A) suggest different timing and different sources for the melt, as demonstrated by their respective TDM values of 1270 and 2600 Ma (Table DR4.1[1] and Fig. 4.2A).

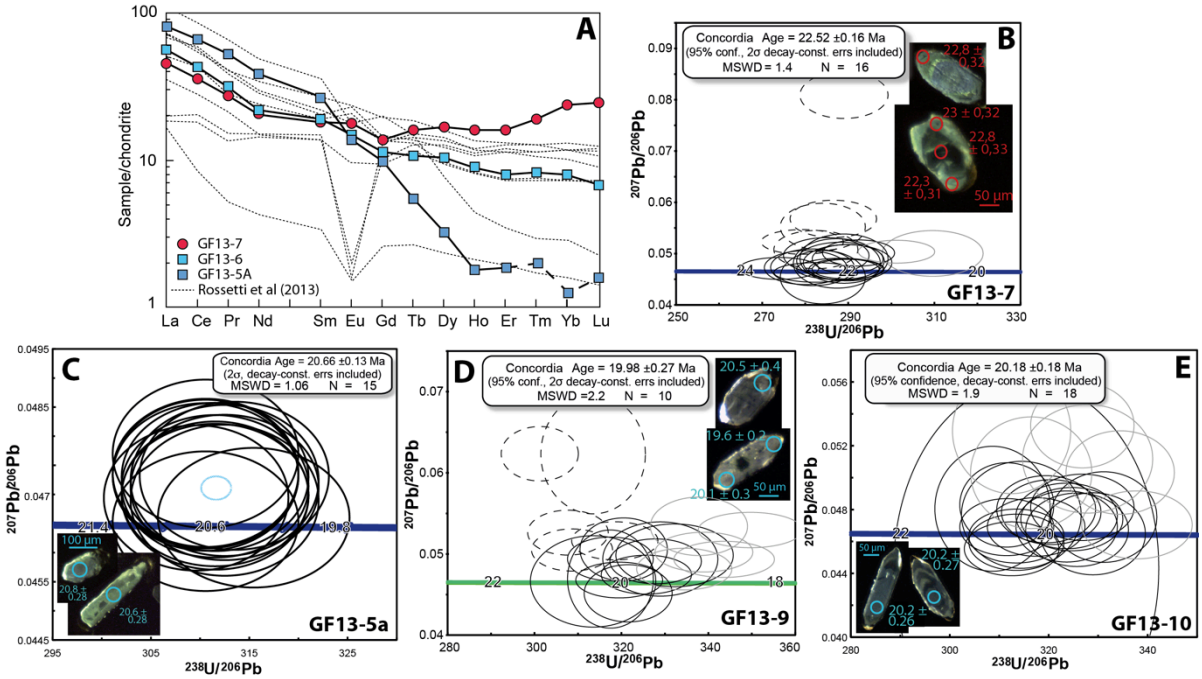

Figure 4.2. A/ Different chondrite-normalized patterns for the collected samples and those of Rossetti et al. 2013. B-E/ Concordia diagrams for the time interval between ca. 25–18 Ma, showing LA-ICP-MS U-Pb zircon analyses for samples GF13-7, GF13-9 and GF13-10. Error ellipses are at 2σ. Plain back ellipses: analyses used for Concordia age calculations; dashed ellipses: data with common Pb; light grey ellipses: data with slight Pb loss. Insets show CL pictures of some of the grains dated in this study together with the obtained $^{206}Pb/^{238}U$ dates. Data tables available in the supplementary material[1].

4.2.1 In situ melting in the lower crust above the peridotites at ca. 22.5 Ma

The leucosome in granulite (GF13-7) is peraluminous, mainly composed by K-feldspar, quartz plagioclase, with minor muscovite, and presents a concave REE pattern suggesting melting of the source rock with possible garnet melting and possible restitic plagioclase (Fig. 4.2A, and Table DR4.1[1]).

Zircon grains are subhedral to euhedral, ranging from 100 μm to 250 μm in size with an aspect ratio of 2:1. Cathodoluminescence (CL) images of the grains (Fig. 4.2A insets) show distinct core and rims for some of them although when euhedral, the grains present fairly homogeneous features in CL. The cores of the grains give apparent dates ranging from the Neoarchean to the Cretaceous (Table DR4.2[1]) in a good agreement with the TDM value for this sample (Table DR4.1[1]). The rims and the homogeneous grains give consistent Miocene apparent dates with Th/U ratios between 0.09-0.16. In a Terra-Wasserburg diagram, these Miocene data plot in a concordant to sub-concordant position (Fig. 4.2B). The concordant data allow to define a concordia age of 22.52 ± 0.16 Ma (MSWD=1.4, N=16) which is confirmed by a mean $^{206}Pb/^{238}U$ age of 22.52±0.18 (MSWD=1.6, N=20/22).

4.2.2 Melt extraction from the metamorphic sole below the Ronda peridotites at ca. 20 Ma

Granitic dikes intruding the peridotites and the overlying crustal rocks (GF13-6, GF13-5A and GF13-10) have a chondrite-normalized REE pattern enriched in LREE and depleted in HREE compared to the extensional-related sample (GF 13-7), suggesting, respectively, a lower degree of partial melting and different sources (Fig. 4.2A). Our samples present REE patterns similar to those of Rossetti et al. (2013) from the Rif (Fig. 4.2A). These metaluminous granites contain also slightly more plagioclase and biotite, and often titanite, than sample GF13-7.

In the leucogranite GF13-5a that intrudes the granulite, the zircon grains are often euhedral to subhedral with aspect ratios varying from 1:2 to 1:4 and sizes ranging from 100 to 400 μm: they commonly show low luminescence in CL images. Three inherited cores give a Paleozoic concordia age of 337.2 ± 0.13 Ma (MSWD=0.21) (table DR4.3[1]) while the remaining data give Miocene apparent dates. These Miocene zircon grains present Th/U values between 0.02 and 0.07. Plotted in a Terra Wasserburg concordia diagram, the 15 analyses plot in a concordant position (Fig. 4.2B) and allow to compute a concordia age of 20.66 ± 0.13 Ma (MSWD=1.06; N = 15). This age is confirmed by the mean $^{206}Pb/^{238}U$ age of 20.65 ± 0.13 Ma (MSWD=0.17; N = 15) (table DR4.3[1]). The inherited components are far less abundant than in the previous sample and, taking into account their similarities, suggests a common origin with GF13-10 but not with GF13-7. The base of the attenuated crustal section above the peridotites (granulite) therefore show two distinct crustal melting events: 1/ in-situ melting at 22.52 Ma, concordant with the HT foliation, and 2/ dike intrusion at 20.66

Ma that cross-cut the former HT foliation. The differences in geochemistry, age and structural setting unequivocaly separate these two different types of crustal melting.

The new ages for the dikes intruding the Ronda peridotites (GF13-9 and GF13-10) confirm these two distinct episodes of crustal melting. In the metaluminous granite GF13-9, the zircon grains are often euhedral to subhedral with an aspect ratio of 1:3 and sizes ranging from 100 to 300 μm: they commonly show distinct cores and rims. These inherited cores give apparent dates ranging from the Neoarchean to the Cretaceous while the remaining data give Miocene apparent dates. These Miocene zircon grains present Th/U values between 0.09 and 0.18. In a Terra Wasserburg concordia diagram, they plot in a concordant to discordant position depending on the degree of Pb loss and/or the presence of initial common Pb (Fig. 4.2D). A group of 10 concordant analyses allow to compute a concordia age of 19.98 ± 0.27 Ma (MSWD = 2.2; N = 10). This age is confirmed by the mean $^{206}Pb/^{238}U$ age of 20.14 ± 0.25 Ma (MSWD=2.4, N = 14) (table DR4.4[1]).

For sample GF13-10, zircon grains are often euhedral zircon with aspect ratios varying from 1:2 to 1:4, and sizes ranging between 100 μm and 400 μm. CL images show rare grains with distinct cores and rims. Only 3 such cores were dated and give Paleozoic apparent dates. The remaining data give Miocene apparent dates with Th/U values ranging from 0.17-0.25. These data plot in a concordant to sub-discordant position (Fig. 4.2E). The most concordant data define a concordia age of 20.18 ± 0.18 Ma (MSWD = 1.9; N = 18). This age is confirmed by the mean $^{206}Pb/^{238}U$ age of 20.08 ± 0.20 Ma (MSWD = 2.6; N=23) (table DR4.5[1], supplementary material). This age is therefore in full agreement with the previous age obtained in the same shear zone.

4.3 Discussion and conclusion

The coupling of geochronological and geochemical data with the regional structures permits to identify two distinct crustal melting events during the Lower Miocene.

The first episode of crustal melting, dated at 22.5 Ma and only located in the lowest levels of the continental crust overlying the Ronda peridotites, is associated to an extreme continental crust thinning that lead to regional high-temperature metamorphism with peak temperatures much higher than 650°C (Negro et al., 2006; Sánchez-Gómez et al., 1999). The supra-subduction environment of the continental rift (Garrido et al., 2011; Marchesi et al., 2012; Précigout et al., 2013) could likely be responsible for such a high geotherm (> 100°C/km). Previous dating of minerals in HT foliation yielded ages in good agreement with our results: 21.5 ± 1.8 Ma on garnet and clinopyroxene by Sm-Nd (Zindler et al., 1983), 22.9 ± 0.5 Ma from a zircon grain in the leucosome from the lower crust by U-Pb (Platt and Whitehouse, 1999) although this date was interpreted as the result of a Pb-loss, and 21.95 ± 0.11 Ma from a monazite grain in the migmatitic gneiss overlying the Beni Bousera peridotites (U-Th-Pb, Gueydan et al., 2015). The back-arc extension responsible for lithosphere thinning and mantle exhumation probably already started around 33 Ma ago, as indicated by the intrusion of tholeitic andesitic dikes between 33 and 28 Ma (Esteban et al.,

2013). Therefore, the age of 22.5 Ma found in the present study most probably reflects the onset of cooling in the back-arc rift, related to an extreme thinning of the continental crust. This cooling at the late stage of the thinning is also confirmed by the formation of the granular peridotites from cooling of a previously hot mantle (Lenoir et al., 2001). Furthermore, the interpretation of the age at 21 Ma in the granulite (Platt and Whitehouse, 1999; Whitehouse and Platt, 2002) as a cooling age of the high-temperture event is compatible with our tectonic interpretation.

The second episode of crustal melting marked the hot thrusting of the Ronda peridotites and its crustal envelope onto the continental crust, dated at ca. 20 Ma. This age is consistent with changes in sedimentation in the external domain (end of sedimentation in the Flysch Trough, Luján et al., 2006, onset of sedimentation in the Guadalquivir basin, Fernández et al., 1998) and in the internal domain (Serrano et al., 2007), and with an U-Pb age of 19.9 ± 1.7 Ma on zircon in the crustal rocks underlying the peridotites (Sánchez-Rodriguez and Gebauer, 2000). Note that ages around 22 Ma have been proposed for granitic dikes intruding the crust that overlies the peridotites (Esteban et al., 2011). However, these ages are either based on very few data (maximum 3 analyses per age) or on discordant analyses, while all our ages are based on more than 10 concordant points.

These two episodes of crustal melting are also well defined by the bimodal distribution of Ar-Ar, Zircon fission track (ZFT) and Apatite fission track ages (AFT) (Fig. 4.3), and thus suggest two distinct episodes of cooling. A first cooling event between 25 and 21 Ma, as already mentioned by Esteban et al. (2013), occurred at the late stage of continental rifting and yields the first peak of Ar-Ar, ZFT and AFT ages at respectively 21-22 Ma, 21-22 Ma and 20-21 Ma (Fig. 4.3). The limited amount of ages for this first cooling event most likely reflects the very high continental geotherm during rifting and hence a limited cooling of the continental crust. Subsequently, the majority of medium to low temperature ages are younger than 20 Ma, with a second peak of Ar-Ar, ZFT and AFT ages at respectively 19 Ma, 18-19 Ma and 18-16 Ma (Fig. 4.3). A general and fast cooling is therefore registered between 20 Ma and 16 Ma (Esteban et al., 2013, Monié et al., 1994) and is a consequence of the hot emplacement of the peridotites nappe on a colder crustal unit. Taking 10 km as the maximum thickness for the peridotites nappe (Balanyá et al., 1997) yields a duration of 4 Ma for the conductive cooling of the peridotites nappe (characteristic time=$\rho C d^2/k$). This sequence of events from hot rifting bewteen 30 and 20 Ma to thrusting at ca. 20 Ma and subsequent cooling between 20 and 16 Ma provides therefore a rather simple and convincing explanation for the entire set of geochronological data available in the area.

At a regional scale, our study confirms the geodynamical models of Duggen et al. (2004), based on geochemical tracers, for late Eocene to early Miocene of the Western Mediterranean: subduction processes (marked by the Malaga Dikes) followed by nappe emplacement (marked by crustal melting). Our work firstly identifies the crustal melting related to the strong crustal thinning during subduction rollback and, secondly, precisely dates the onset of the peridotites nappe emplacement at 20 Ma. A remaining key issue is to precisely locate the rift inversion, either to the North of the Algerian margin or close to the western termination of the system. These two hypotheses would imply, respectively, large

(e.g. Hidas et al., 2013; Frizon et al., 2009; Van Hinsbergen et al., 2014) or limited (e.g. Duggen et al., 2004; Frasca et al., 2015) amounts of rollback since 20 Ma.

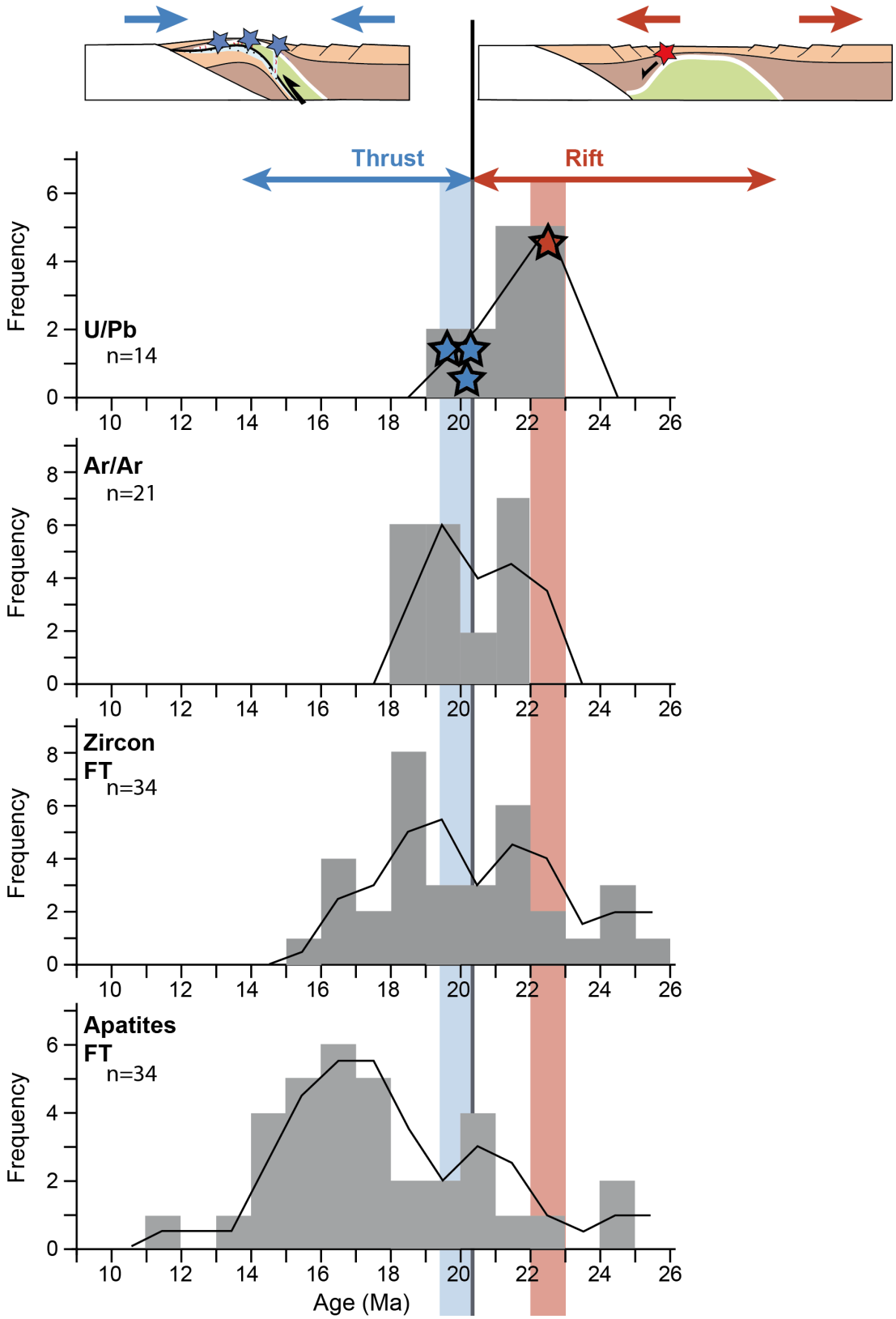

Figure 4.3. A/ Frequency distribution, from top to bottom, of U-Pb, Ar-Ar, Zircon and Apatite fission tracks (Esteban et al., 2013 and ref. therein; Monié et al., 1994; Platt et al., 2003) for the western Betics together with the ages obtained in our study (coloured dotted). The bimodal distribution of Ar/Ar, ZFT and AFT ages are well correlated with our two episodes of crustal melting (syn-rift in red, rift inversion in blue).

[1]GSA Data Repository item 2015/xxx, Tables DR1-DR6, Bulk rock geochemistry, U-Pb on zircons data and operating conditions for the LA-ICP-MS, is available online at www.geosociety.org/pubs/ft2015.htm, or on request from editing@geosociety.org or Documents Secretary, GSA, P.O. Box 9140, Boulder, CO 80301, USA.

ACKNOWLEDGMENTS

This work was funded by the European Union FP7 Marie Curie ITN "TOPOMOD", contract 264517. Thanks to Anne Delplanque for her help with drawing Figure 4.1.

ANNEXES

Table DR4.1: Major, trace element and isotopic compositions of leucogranitic dikes from the Ronda Peridotites and its crustal envelope

Sample	GF13-7	GF13-6	GF13-5A
SiO_2 (wt.%)	73.66	75.99	83.05
TiO_2	0.14	0.06	0.09
Al_2O_3	14.00	13.24	8.19
FeOt	1.81	0.68	0.72
MnO	0.02	0.01	0.01
MgO	0.36	0.48	0.18
CaO	1.33	1.95	0.61
Na_2O	3.61	4.80	1.51
K_2O	2.64	0.74	4.31
P_2O_5	0.14	0.05	0.03
LOI	1.57	0.87	0.93
Total	99.28	98.87	99.63
A/NK	1.59	1.52	1.15
A/2CNK	1.03	0.84	0.87
Be (ppm)	< 1	5	2
Sc	7	6	< 1
V	16	5	8
Cr	120	190	150
Co	4	3	2
Ni	< 20	< 20	< 20
Rb	96	20	144
Sr	405	204	82
Y	24	13	3
Zr	66	42	41
Nb	11	7	4
Sn	8	5	2
Cs	1.4	< 0.5	2
Ba	407	878	271
La	11.1	13.6	20.2
Ce	22.8	27.1	42.6
Pr	2.62	3.03	4.97
Nd	9.7	10.2	18.2
Sm	2.8	2.9	4.1
Eu	1.03	0.85	0.78

Gd	2.8	2.3	2
Tb	0.6	0.4	0.2
Dy	4.2	2.6	0.8
Ho	0.9	0.5	0.1
Er	2.6	1.3	0.3
Tm	0.48	0.21	0.05
Yb	3.9	1.3	0.2
Lu	0.62	0.17	0.04
Hf	1.9	1.8	1.5
Ta	2.1	1.8	0.3
W	13	< 1	< 1
Tl	0.3	< 0.1	0.5
Pb	23	12	32
Bi	< 0.4	< 0.4	< 0.4
Th	3.4	5.8	12.2
U	4.4	6.6	13.3
$^{87}Sr/^{86}Sr$	0.718652632	0.720878482	0.719916521
$\pm \sigma_2$	0.000013	0.000012	0.000012
$^{143}Nd/^{144}Nd$	0.512055388	0.512097033	0.512169131
$\pm \sigma_2$	0.000005	0.000004	0.000006
$^{147}Sm/^{144}Nd$	0.155281275	0.145694283	0.128046963
epsilonNd (t=20Ma)	-11.26	-10.99	-9.54

A/NK= $Al_2O_3/(Na_2O+K_2O)$, molar; A/2CNK=$Al_2O_3/(CaO+Na_2O+K_2O)$, molar.

Table DR4.2: Results of in-Situ U-Pb LA-ICP-MS Analyses of Zircon grains from sample GF13-7. In bold tha data used for the Concordia age. In italic data used for the mean $^{206}Pb/^{238}U$ age.

Grains	[Pb] ppm	[U] ppm	[Th] ppm	Th/U	$^{238}U/^{206}Pb$	Err σ_1, %	$^{207}Pb/^{206}Pb$	Err σ_1, %	Age $^{207}Pb/^{235}U$	Abs err	Age $^{206}Pb/^{238}U$	Abs err	Conc
Zr1-2	5.6	319.1	22.1	0.07	53.706	1.34	0.05534	1.34	134.8	2.0	118.9	1.6	88.2
Zr1-3	12.3	430.4	11.0	0.03	31.797	1.21	0.05243	1.14	208	2.5	199.6	2.4	96.0
Zr2-1	15.4	182.3	97.3	0.53	12.845	1.34	0.05597	1.09	477.7	5.3	483.3	6.2	101.2
Zr2-2	696.8	37.3	0.1	0.07	23.186	1.32	0.05351	1.03	280.5	3.3	272.2	3.6	97.0
Zr3	131.3	113.5	0.9	0.00	11.848	1.34	0.05699	1.12	516.5	5.7	522.3	6.7	101.1
Zr4-1	85.6	96.3	1.1	0.00	7.772	1.34	0.06412	1.09	771.2	7.5	780.3	9.8	101.2
Zr4-2	20.0	498.4	17.2	0.03	23.918	1.22	0.06270	1.08	313.3	3.4	264	3.1	84.3
Zr4-3	15.9	643.0	18.1	0.03	37.439	1.24	0.05617	1.37	190.9	2.6	169.9	2.1	89.0
Zr5	**1.0**	**298.7**	**38.3**	**0.13**	**282.486**	**1.41**	**0.05079**	**2.99**	**24.8**	**0.8**	**22.8**	**0.3**	**91.9**
Zr6	*0.9*	*266.3*	*28.2*	*0.11*	*279.330*	*1.40*	*0.05229*	*1.87*	*25.9*	*0.5*	*23*	*0.3*	*88.8*

Zr7	**1.3**	**393.2**	**59.2**	**0.15**	**288.184**	**1.44**	**0.04702**	**1.81**	**22.6**	**0.5**	**22.3**	**0.3**	**98.7**
Zr9	10.0	356.2	12.6	0.04	32.949	1.35	0.05260	1.18	202	2.7	192.7	2.6	95.4
Zr10	38.7	939.5	43.8	0.05	22.573	1.35	0.05431	1.05	290.9	3.5	279.4	3.7	96.0
Zr11	*1.0*	*292.6*	*33.1*	*0.11*	*286.533*	*1.43*	*0.05679*	*2.61*	*27.4*	*0.7*	*22.5*	*0.3*	*82.1*
Zr12-1	13.7	64.9	92.9	1.43	6.330	1.47	0.07071	2.29	946.5	14.9	945.6	12.9	99.9
Zr12-2	10.6	157.7	25.4	0.16	14.970	1.21	0.06066	1.30	450.6	5.3	416.8	4.9	92.5
Zr12-3	21.9	121.7	112.4	0.92	6.663	1.21	0.07285	1.14	933.4	8.0	901.5	10.2	92.4
Zr13	17.8	244.3	70.5	0.29	13.641	1.36	0.05748	1.10	465	5.3	456	6.0	98.1
Zr14	10.9	268.8	15.1	0.06	22.847	1.37	0.05293	1.13	281.4	3.6	276.1	3.7	98.1
Zr15-1	15.2	384.2	6.0	0.02	22.920	1.38	0.05218	1.09	277.2	3.4	275.3	3.7	99.3
Zr15-2	14.3	427.6	11.6	0.03	27.457	1.21	0.05297	1.25	239.5	3.0	230.6	2.8	96.3
Zr16	70.3	335.1	66.5	0.20	5.211	1.37	0.15886	1.03	1674.6	11.3	1131.7	14.2	68.5
Zr17	70.4	336.5	103.4	0.31	4.942	1.37	0.11666	1.04	1470.2	10.8	1187.8	14.9	77.1
Zr19	13.1	133.8	48.2	0.36	10.178	1.37	0.06173	1.10	617	6.6	604.2	8.0	97.9
Zr21	*0.8*	*267.0*	*33.5*	*0.13*	*309.598*	*1.55*	*0.05004*	*3.64*	*22.4*	*0.8*	*20.8*	*0.3*	*92.9*
Zr22-1	**1.0**	**301.8**	**33.7**	**0.11**	**281.690**	**1.41**	**0.04734**	**3.08**	**23.3**	**0.7**	**22.9**	**0.3**	**98.3**
Zr22-2	**1.1**	**342.3**	**41.9**	**0.12**	**284.900**	**1.42**	**0.04962**	**2.88**	**24.1**	**0.7**	**22.6**	**0.3**	**93.8**
Zr22-3	*1.0*	*299.2*	*37.2*	*0.12*	*284.091*	*1.42*	*0.05524*	*3.39*	*26.9*	*0.9*	*22.7*	*0.3*	*84.4*
Zr23	21.8	514.5	102.6	0.20	23.585	1.39	0.05461	1.17	281.3	3.7	267.7	3.6	95.2
Zr24-1	22.8	198.0	87.5	0.44	8.848	1.39	0.06237	1.07	689.4	7.2	690.3	9.1	100.1
Zr24-2	23.9	657.1	19.6	0.03	25.259	1.21	0.05307	1.19	258.3	3.1	250.3	3.0	96.9
Zr25-1	13.2	139.5	16.6	0.12	9.718	1.39	0.06072	1.12	630.9	6.9	631.4	8.4	100.1
Zr26-1	**1.6**	**500.5**	**45.9**	**0.09**	**282.486**	**1.41**	**0.04634**	**1.68**	**22.7**	**0.4**	**22.8**	**0.3**	**100.4**
Zr26-2	**1.4**	**444.9**	**50.0**	**0.11**	**289.855**	**1.45**	**0.04823**	**2.99**	**23.1**	**0.7**	**22.2**	**0.3**	**96.1**
Zr26-3	2.2	559.9	44.9	0.08	234.192	1.17	0.04664	1.76	27.5	0.5	27.5	0.3	100.0
Zr26-4	**2.3**	**671.5**	**73.2**	**0.11**	**273.973**	**1.37**	**0.04712**	**1.85**	**23.8**	**0.5**	**23.5**	**0.3**	**98.7**
Zr27	28.3	177.7	159.2	0.90	7.486	1.21	0.07213	1.10	858.2	7.4	808.3	9.2	94.2
Zr28	18.0	494.8	23.5	0.05	25.720	1.21	0.05624	1.14	267.5	3.1	245.9	2.9	91.9
Zr29-1	26.0	569.9	16.9	0.03	20.186	1.21	0.05617	1.09	329.7	3.6	311.7	3.7	94.5
Zr29-2	24.2	600.5	12.9	0.02	22.712	1.23	0.05620	1.28	298	3.7	277.7	3.3	93.2
Zr30-1	1.7	354.3	41.8	0.12	198.020	1.19	0.05195	1.87	36.1	0.7	32.5	0.4	90.0
Zr30-2	1.8	461.7	52.7	0.11	236.407	1.42	0.05190	2.83	30.2	0.9	27.2	0.4	90.1
Zr30-3	1.7	425.3	56.5	0.13	236.407	1.42	0.05042	3.03	29.4	0.9	27.2	0.4	92.5
Zr31	18.7	582.7	6.9	0.01	28.474	1.22	0.05242	1.37	229.7	3.1	222.5	2.7	96.9
Zr33	9.8	97.0	106.1	1.09	12.143	1.21	0.06165	1.28	538.7	5.9	510.1	6.0	94.7
Zr34	17.6	448.1	10.2	0.02	24.534	1.20	0.07198	1.22	344.9	4.0	257.5	3.1	74.7
Zr35	114.8	452.8	70.3	0.16	4.399	1.20	0.19129	1.04	1975.2	10.6	1320.5	14.3	71.7

Zr36-1	**1.9**	**561.9**	**72.8**	**0.13**	**289.855**	**1.16**	**0.04897**	**2.35**	**23.4**	**0.6**	**22.2**	**0.3**	**94.9**
Zr36-2	*1.2*	*335.2*	*52.8*	*0.16*	*289.017*	*1.45*	*0.08091*	*2.30*	*38.5*	*0.9*	*22.3*	*0.3*	*57.9*
Zr37-1	**0.9**	**270.7**	**30.4**	**0.11**	**280.112**	**1.40**	**0.04728**	**2.86**	**23.4**	**0.7**	**23**	**0.3**	**98.3**
Zr37-2	**0.9**	**282.5**	**37.4**	**0.13**	**284.091**	**1.42**	**0.04541**	**4.67**	**22.2**	**1.0**	**22.7**	**0.3**	**102.3**
Zr38	17.2	600.5	15.6	0.03	32.573	1.21	0.05523	1.18	213.3	2.6	194.9	2.3	91.4
Zr39-1	38.0	1101.3	174.4	0.16	28.043	1.21	0.05282	1.14	234.4	2.7	225.9	2.7	96.4
Zr39-2	23.7	757.6	7.8	0.01	29.386	1.20	0.05243	1.20	223.3	2.7	215.7	2.6	96.6
Zr40-1	13.5	445.9	7.9	0.02	30.618	1.19	0.05436	1.29	222.3	2.8	207.2	2.5	93.2
Zr41-1	**1.4**	**430.0**	**63.6**	**0.15**	**287.356**	**1.44**	**0.04810**	**4.10**	**23.2**	**0.9**	**22.4**	**0.3**	**96.6**
Zr41-2	**1.5**	**452.1**	**68.7**	**0.15**	**289.017**	**1.45**	**0.04903**	**4.00**	**23.5**	**0.9**	**22.2**	**0.3**	**94.5**
Zr41-3	**1.3**	**406.9**	**46.3**	**0.11**	**288.184**	**1.44**	**0.04858**	**3.07**	**23.3**	**0.7**	**22.3**	**0.3**	**95.7**
Zr42-1	42.8	835.0	180.1	0.22	20.096	1.21	0.05641	1.13	332.2	3.7	313.1	3.7	94.3
Zr43-1	**14.8**	**4695.2**	**26.0**	**0.01**	**289.855**	**1.16**	**0.04698**	**1.66**	**22.4**	**0.4**	**22.2**	**0.3**	**99.1**
Zr44	21.9	593.7	10.2	0.02	24.869	1.19	0.05286	1.15	260.9	3.0	254.1	3.0	97.4
Zr45	21.2	532.3	9.8	0.02	22.999	1.20	0.05578	1.13	292.9	3.3	274.4	3.2	93.7
Zr46	16.9	487.8	5.6	0.01	26.330	1.21	0.05252	1.18	246.6	2.9	240.3	2.8	97.4
Zr47	7.5	80.6	51.4	0.64	11.985	1.22	0.06116	1.36	540.9	6.2	516.6	6.0	95.5
Zr48-1	**2.4**	**738.9**	**34.4**	**0.05**	**289.017**	**1.16**	**0.04692**	**1.81**	**22.5**	**0.4**	**22.2**	**0.3**	**98.7**
Zr48-2	**2.1**	**637.2**	**88.0**	**0.14**	**292.398**	**1.17**	**0.05013**	**2.07**	**23.7**	**0.5**	**22**	**0.3**	**92.8**
Zr48-3	*2.3*	*737.0*	*40.4*	*0.05*	*301.205*	*1.20*	*0.05038*	*1.81*	*23.1*	*0.4*	*21.3*	*0.3*	*92.2*
Zr49	129.2	509.6	217.3	0.43	4.322	1.20	0.12691	1.06	1643.9	10.0	1341.6	14.5	80.0
Zr50	27.1	537.2	42.8	0.08	18.716	1.20	0.05809	1.10	361.7	3.9	335.6	3.9	92.8
Zr51	217.1	618.3	194.2	0.31	3.171	1.20	0.18197	1.05	2221	11.1	1767.1	18.5	79.6
Zr52	30.8	351.4	175.2	0.50	12.120	1.20	0.05902	1.14	521.6	5.3	511.1	5.9	98.0
Zr53	77.0	565.0	198.2	0.35	7.585	1.20	0.07412	1.08	866.4	7.3	798.3	9.0	82.9
Zr54-1	12.1	403.3	9.5	0.02	30.628	1.23	0.05306	1.39	217.5	3.0	207.1	2.5	95.2
Zr54-2	1.9	19.2	7.8	0.40	10.363	1.31	0.05992	2.40	595.2	11.0	593.8	7.4	99.8
Zr55	172.4	243.0	291.9	1.20	1.917	1.20	0.21766	1.07	2855.6	11.8	2705.6	26.5	96.4
Zr56	23.3	185.1	77.0	0.42	8.258	1.21	0.06382	1.16	736.5	6.9	736.8	8.4	100.0
Zr57	35.8	318.0	363.0	1.14	11.023	1.20	0.05909	1.17	561.8	5.7	559.8	6.5	99.6
Zr58	35.0	1157.7	15.2	0.01	30.157	1.21	0.05199	1.06	216.5	2.4	210.3	2.5	97.1

Table DR4.3: Results of in-Situ U-Pb LA-ICP-MS Analyses of Zircon grains from sample GF13-5a.

Grains	[U] ppm	[Pb] ppm	Th/U	$^{238}U/^{206}Pb$	Err σ_1, %	$^{207}Pb/^{206}Pb$	Err σ_1, %	Age $^{207}Pb/^{235}U$	Abs err	Age $^{206}Pb/^{238}U$	Abs err	Conc
Zr1-1	19.0	6349	0.05	310.559	1.2	0.04654	1.1	20.7	0.3	20.7	0.3	100.0
Zr1-2	19.5	6577	0.06	315.457	1.3	0.04660	1.1	20.5	0.3	20.4	0.3	99.5

Zr1-3	10.3	3443	0.07	313.480	1.3	0.04732	1.1	20.9	0.3	20.5	0.3	98.1
Zr2	10.8	3577	0.06	310.559	1.2	0.04733	1.1	21.1	0.3	20.8	0.3	98.6
Zr3	15.6	5232	0.06	312.500	1.3	0.04712	1.1	20.9	0.3	20.6	0.3	98.6
Zr4	*19.9*	*6635*	0.07	311.526	1.2	0.04699	1.1	20.9	0.3	20.7	0.3	99.0
Zr5	*17.3*	*5785*	0.06	311.526	1.2	0.04698	1.1	20.9	0.3	20.7	0.3	99.0
Zr6-1	24.7	8237	0.07	310.559	1.2	0.04732	1.1	21.1	0.3	20.8	0.3	98.6
Zr6-2	24.5	8213	0.07	311.526	1.2	0.04714	1.1	20.9	0.3	20.6	0.3	98.6
Zr7	8.4	2821	0.06	312.500	1.3	0.04690	1.1	20.8	0.3	20.6	0.3	99.0
Zr8	16.3	5481	0.06	310.559	1.2	0.04737	1.1	21.1	0.3	20.7	0.3	98.1
Zr9	11.1	3767	0.06	312.500	1.3	0.04724	1.1	20.9	0.3	20.6	0.3	98.6
Zr10	24.9	8386	0.06	310.559	1.2	0.04770	1.1	21.3	0.3	20.7	0.3	97.2
Zr11	37.2	854	0.49	24.143	1.4	0.05203	1.1	264.1	3.2	261.7	3.4	99.1
Zr13	39.6	865	0.57	23.552	1.3	0.05233	1.1	271.3	3.3	268	3.5	98.8
Zr14	24.8	8536	0.02	311.526	1.2	0.04730	1.1	21	0.3	20.6	0.3	98.1
Zr15	20.2	6843	0.06	309.598	1.2	0.04694	1.1	21	0.3	20.8	0.3	99.0

Table DR4.4: Results of in-Situ U-Pb LA-ICP-MS Analyses of Zircon grains from sample GF13-9. In bold tha data used for the Concordia age. In italic data used for the mean $^{206}Pb/^{238}U$ age.

Grains	[U] ppm	[Pb] ppm	Th/U	$^{238}U/^{206}Pb$	Err σ_1, %	$^{207}Pb/^{206}Pb$	Err σ_1, %	Age $^{207}Pb/^{235}U$	Abs err	Age $^{206}Pb/^{238}U$	Abs err	Conc
Zr1	444	4	0.15	110.011	1.32	0.05599	1.55	68.8	1.1	58.3	0.7	84.7
Zr2a	297	10	0.22	28.827	1.21	0.05279	1.25	228.6	2.8	219.9	2.6	96.2
Zr2b	432	20	0.13	20.803	1.21	0.05397	1.11	310.5	3.4	302.7	3.6	97.5
Zr3a	228	4	0.19	50.531	1.26	0.06372	1.43	162.7	2.3	126.3	1.6	77.6
Zr3b	*362*	*1*	*0.14*	*259.067*	*1.55*	*0.05101*	*2.45*	*27.2*	*0.7*	*24.9*	*0.4*	*91.5*
Zr4	*544*	*2*	*0.12*	*307.692*	*1.23*	*0.05263*	*2.15*	*23.6*	*0.5*	*20.9*	*0.3*	*88.6*
Zr5a	**551**	**2**	**0.12**	**319.489**	**1.28**	**0.04679**	**1.92**	**20.3**	**0.4**	**20.2**	**0.3**	**99.5**
Zr5b	798	61	0.61	14.579	1.20	0.05943	1.06	452.8	4.5	427.6	4.9	94.4
Zr7	*483*	*1*	*0.12*	*318.471*	*1.27*	*0.05162*	*1.86*	*22.5*	*0.4*	*20.2*	*0.3*	*89.8*
Zr8a	**456**	**1**	**0.09**	**332.226**	**1.66**	**0.04983**	**3.17**	**20.8**	**0.6**	**19.4**	**0.3**	**93.3**
Zr9	**353**	**1**	**0.12**	**313.480**	**1.88**	**0.04662**	**4.93**	**20.6**	**1.0**	**20.5**	**0.4**	**99.5**
Zr11	**399**	**1**	**0.12**	**328.947**	**1.64**	**0.04938**	**3.79**	**20.8**	**0.7**	**19.6**	**0.3**	**94.2**
Zr12	*507*	*1*	*0.12*	*334.448*	*1.34*	*0.04814*	*2.18*	*20.0*	*0.4*	*19.3*	*0.3*	*96.5*
Zr13	178	8	0.14	23.872	1.27	0.10669	1.36	487.5	5.5	264.6	3.3	54.3
Zr14	*516*	*1*	*0.11*	*338.983*	*1.36*	*0.05023*	*1.99*	*20.5*	*0.4*	*19.0*	*0.3*	*92.7*
Zr15	*593*	*2*	*0.11*	*349.650*	*1.40*	*0.05295*	*1.68*	*21.0*	*0.4*	*18.4*	*0.2*	*87.6*
Zr16	*477*	*1*	*0.19*	*343.643*	*1.37*	*0.04934*	*1.84*	*19.9*	*0.4*	*18.7*	*0.2*	*94.0*

Zr17	*408*	*6*	*0.14*	*337.838*	*1.35*	*0.05341*	*2.75*	*21.9*	*0.6*	*19.1*	*0.3*	*87.2*
Zr18	308	56	0.29	5.798	1.19	0.12426	1.04	1396.1	9.2	1025.8	11.3	73.5
Zr19	297	168	0.63	2.087	1.18	0.18836	1.02	2638.3	11.2	2523.3	24.7	95.6
Zr20	1023	74	0.38	14.140	1.19	0.05851	1.04	458.3	4.5	440.5	5.0	96.1
Zr21	**475**	**1**	**0.12**	**321.543**	**1.29**	**0.04515**	**3.19**	**19.5**	**0.6**	**20.0**	**0.3**	**102.6**
Zr22	122	12	0.78	11.476	1.19	0.05901	1.22	544.1	5.7	538.6	6.1	99.0
Zr23	*496*	*2*	*0.13*	*299.401*	*1.20*	*0.05048*	*2.30*	*23.3*	*0.5*	*21.5*	*0.3*	*92.3*
Zr24	244	25	0.46	10.031	1.18	0.06197	1.11	625.6	5.9	612.6	6.9	97.9
Zr26	*962*	*3*	*0.23*	*308.642*	*1.23*	*0.05049*	*2.10*	*22.6*	*0.5*	*20.8*	*0.3*	*92.0*
Zr27	728	187	0.27	4.272	1.17	0.15908	1.04	1841.6	10.2	1355.8	14.3	73.6
Zr29	*638*	*2*	*0.12*	*271.003*	*1.36*	*0.05489*	*2.30*	*27.9*	*0.6*	*23.7*	*0.3*	*84.9*
Zr8b	858	15	0.05	53.763	1.18	0.05719	1.33	138.9	1.9	118.8	1.4	85.5
Zr34	312	27	0.2	12.015	1.18	0.08734	1.18	704.9	6.6	515.4	5.8	73.1
Zr35	**684**	**2**	**0.18**	**325.733**	**1.30**	**0.04745**	**2.07**	**20.2**	**0.4**	**19.8**	**0.2**	**98.0**
Zr36	**387**	**1**	**0.14**	**317.460**	**1.27**	**0.04691**	**5.27**	**20.5**	**1.1**	**20.3**	**0.3**	**99.0**
Zr37a	**584**	**2**	**0.1**	**327.869**	**1.31**	**0.04909**	**2.30**	**20.7**	**0.5**	**19.6**	**0.2**	**94.7**
Zr37b	**435**	**1**	**0.12**	**320.513**	**1.28**	**0.05055**	**3.15**	**21.8**	**0.7**	**20.1**	**0.3**	**92.2**
Zr39	*968*	*3*	*0.27*	*301.205*	*1.20*	*0.06235*	*2.20*	*28.6*	*0.6*	*21.4*	*0.3*	*74.8*
Zr44	*495*	*2*	*0.11*	*313.480*	*1.57*	*0.06231*	*4.83*	*27.5*	*1.3*	*20.5*	*0.3*	*74.5*
Zr33	**578**	**2**	**0.12**	**317.460**	**1.27**	**0.04939**	**2.23**	**21.5**	**0.5**	**20.3**	**0.3**	**94.4**

Table DR4.5: Results of in-Situ U-Pb LA-ICP-MS Analyses of Zircon grains from sample GF13-10. In bold tha data used for the Concordia age. In italic data used for the mean $^{206}Pb/^{238}U$ age.

Grains	[U] ppm	[Pb] ppm	Th/U	$^{238}U/^{206}Pb$	Err σ_1, %	$^{207}Pb/^{206}Pb$	Err σ_1, %	Age $^{207}Pb/^{235}U$	Abs err	Age $^{206}Pb/^{238}U$	Abs err	Conc
Zr1	**849**	**3**	**0.20**	**313.480**	**1.25**	**0.04634**	**1.49**	**20.5**	**0.3**	**20.6**	**0.3**	**100.5**
Zr2	**679**	**2**	**0.17**	**317.460**	**1.27**	**0.04691**	**1.60**	**20.4**	**0.3**	**20.2**	**0.3**	**99.0**
Zr3	**780**	**2**	**0.21**	**312.500**	**1.25**	**0.04554**	**1.52**	**20.2**	**0.3**	**20.6**	**0.3**	**102.0**
Zr4	**514**	**2**	**0.18**	**320.513**	**1.28**	**0.04784**	**1.73**	**20.7**	**0.4**	**20.1**	**0.3**	**97.1**
Zr5	**394**	**1**	**0.15**	**325.733**	**1.30**	**0.04673**	**2.01**	**19.9**	**0.4**	**19.8**	**0.3**	**99.5**
Zr6	**652**	**2**	**0.19**	**323.625**	**1.29**	**0.0476**	**1.76**	**20.4**	**0.4**	**19.9**	**0.3**	**97.5**
Zr7	**719**	**2**	**0.20**	**323.625**	**1.29**	**0.04694**	**1.94**	**20.1**	**0.4**	**19.9**	**0.3**	**99.0**
Zr8	**804**	**2**	**0.19**	**313.480**	**1.25**	**0.04595**	**1.57**	**20.3**	**0.3**	**20.5**	**0.3**	**101.0**
Zr9	**838**	**3**	**0.22**	**311.526**	**1.25**	**0.0469**	**1.56**	**20.8**	**0.3**	**20.6**	**0.3**	**99.0**
Zr10	**643**	**2**	**0.25**	**319.489**	**1.28**	**0.04802**	**1.79**	**20.9**	**0.4**	**20.2**	**0.3**	**96.7**
Zr11	**1141**	**3**	**0.20**	**324.675**	**1.30**	**0.0474**	**1.71**	**20.2**	**0.4**	**19.8**	**0.3**	**98.0**
Zr12a	430	30	0.21	13.624	1.25	0.06028	1.14	483.5	5.1	456.6	5.5	94.4

Zr13	1225	4	0.21	326.797	1.31	0.05328	2.05	22.6	0.5	19.7	0.3	87.2
Zr14	474	1	0.17	327.869	1.64	0.05118	2.72	21.6	0.6	19.6	0.3	90.7
Zr15	**399**	**1**	**0.21**	**308.642**	**1.54**	**0.04805**	**3.33**	**21.5**	**0.7**	**20.8**	**0.3**	**96.7**
Zr16	**519**	**2**	**0.20**	**311.526**	**1.25**	**0.04829**	**2.24**	**21.5**	**0.5**	**20.7**	**0.3**	**96.3**
Zr17	386	1	0.18	312.500	1.56	0.05294	3.04	23.4	0.7	20.6	0.3	88.0
Zr18	850	3	0.25	316.456	1.58	0.05031	2.84	22.0	0.6	20.4	0.3	92.7
Zr19	**574**	**2**	**0.20**	**328.947**	**1.32**	**0.04648**	**2.26**	**19.6**	**0.4**	**19.6**	**0.3**	**100.0**
Zr20	**1247**	**4**	**0.21**	**326.797**	**1.31**	**0.04814**	**1.77**	**20.4**	**0.4**	**19.7**	**0.3**	**96.6**
Zr21a	1156	3	0.19	337.838	1.35	0.04704	1.85	19.3	0.4	19.0	0.3	98.4
Zr22a	**580**	**2**	**0.20**	**331.126**	**1.32**	**0.04753**	**2.44**	**19.9**	**0.5**	**19.5**	**0.3**	**98.0**
Zr22b	867	3	0.18	334.448	1.34	0.05032	2.13	20.8	0.4	19.2	0.3	92.3
Zr23	214	10	0.29	22.609	1.22	0.05352	1.36	286.8	3.6	279.0	3.3	97.3
Zr24	115	6	0.07	17.803	1.26	0.05773	1.59	375.2	5.1	352.3	4.3	93.9
Zr25	**562**	**2**	**0.16**	**314.465**	**1.57**	**0.04767**	**2.87**	**21.0**	**0.6**	**20.4**	**0.3**	**97.1**
Zr27	**364**	**1**	**0.15**	**315.457**	**3.47**	**0.04433**	**10.78**	**19.5**	**2.0**	**20.4**	**0.7**	**104.6**

Table DR4.6: Operating conditions for the LA-ICP-MS equipment

Laser-ablation system ESI NWR193UC	
Laser type/wavelength	Excimer 193 nm
Pulse duration	< 5 ns
Energy density on target	~ 7 J/cm^2
ThO^+/Th^+	< 0.5%
He gas flow	800 ml/min
N_2 gas flow	4 ml/min
Laser repetition rate	3 Hz
Laser spot size	30-40 μm
ICP-MS Agilent 7700x	
RF power	1350 W
Sampling depth	5.0-5.5 mm (optimised daily)
Carrier gas flow (Ar)	~ 0.85 l/min (optimized daily)
Coolant gas flow	16 l/min
Data acquisition protocol	Time-resolved analysis
Scanning mode	Peak hopping, one point per peak
Detector mode	Pulse counting, dead time correction applied, and analog mode when signal intensity > ~ 10^6 cps
Isotopes determined	^{204}(Hg + Pb), ^{206}Pb, ^{207}Pb, ^{208}Pb, ^{232}Th, ^{238}U
Dwell time per isotope	10-30 ms
Sampler, skimmer cones	Ni
Extraction lenses	X type

Table DR4.7: Geochronological data from the Western Betics

Sample	Paper	Long.	Lat.	Type	Mineral	RockType	Age, Ma	σ_2
AA9	Monie et al 1994	-4.860756156	36.53757323	Ar-Ar	Amph	amphibolite / sierra blanca	19.1	1.2
AA8	Monie et al 1994	-3.987663368	36.88827327	Ar-Ar	Amph	amphibolite / sierra tejeda	18.9	0.6
PB324	platt03	-4.438146217	36.80910444	Ar-Ar	Wmica	And phyllite (Malaguide lower unit)	18.6	1.6
PB375/CAR16	platt03	-4.7744384	36.89211693	Ar-Ar	Bi	And quartzite	21.3	0.3
PB375/CAR16	platt03	-4.773241187	36.89287879	Ar-Ar	Wmica	And quartzite	21.7	0.4
T316	Monie et al 1994	-3.952817263	36.76931587	Ar-Ar	Ms	banded gneiss / torrox	19.2	0.3
T316	Monie et al 1994	-3.952817263	36.76931587	Ar-Ar	K-feld	banded gneiss / torrox	19.8	0.4
PB376/CAR17	platt03	-4.769214197	36.89179042	Ar-Ar	Bi	Fibrolite schist	20	0.8
PB377	platt03	-4.750602974	36.88384527	Ar-Ar	Wmica	Fibrolite schist	21.5	1.5
PB377	platt03	-4.749623436	36.88297457	Ar-Ar	Bi	Fibrolite schist	21.2	0.6
AA21	Monie et al 1994	-5.218206739	36.53532935	Ar-Ar	Bi	gneiss / casares-los reales	21.1	0.2
AA15	Monie et al 1994	-4.936599406	36.73054718	Ar-Ar	Ms	gneiss / competa	18.9	0.4
AA3	Monie et al 1994	-3.989465753	36.85823352	Ar-Ar	Ms	gneiss / competa	18.9	0.4
AA10	Monie et al 1994	-4.830419701	36.57636131	Ar-Ar	Bi	granodiorite	19.3	0.2
AA11	Monie et al 1994	-4.827801837	36.57598733	Ar-Ar	Bi	granodiorite / ojen	19.3	0.2
AA22	Monie et al 1994	-5.205865382	36.52822372	Ar-Ar	Bi	granulite / casares-los reales	21.6	0.2
AA12	Monie et al 1994	-4.832707617	36.57796313	Ar-Ar	Bi	granulite/ ojen	19.1	0.3
VIN02	Monie et al 1994	-4.116634009	36.8923787	Ar-Ar	Bi	Graph schist / clast vinuela	21.7	0.6
T337	Monie et al 1994	-3.961228392	36.76991667	Ar-Ar	Bi	leucocratic augengneiss / torrox	20.2	0.3
T337	Monie et al 1994	-3.961228392	36.76991667	Ar-Ar	Ms	leucocratic augengneiss / torrox	19	0.7
T337	Monie et al 1994	-3.961228392	36.76991667	Ar-Ar	K-feld	leucocratic augengneiss / torrox	19.6	0.7
B20	Sosson98	-4.83149047	36.58039605	Ar-Ar	Wmica	los reales	18.9	0.5
B43	Sosson98	-4.819852688	36.5737332	Ar-Ar	Wmica	los reales	19	0.2
AA24	Monie et al 1994	-5.170337232	36.4728746	Ar-Ar	Phl	Marble / Sierra Blanca	20.2	0.3
AA5	Monie et al 1994	-3.996074497	36.88827327	Ar-Ar	Ms	metaquartzite / sierra tejeda	18.9	0.5
B7	Sosson98	-4.845171527	36.5774644	Ar-Ar	Wmica	ojen	18.9	0.4
T330	Monie et al 1994	-3.964232366	36.77712621	Ar-Ar	Bi	pelitic gneiss / torrox	18.8	0.6
T330	Monie et al 1994	-3.964232366	36.77712621	Ar-Ar	Ms	pelitic gneiss / torrox	19.1	0.8

PB374	platt03	-4.789893334	36.88939599	Ar-Ar	Wmica	Qtz-ky-Mu vein	19.9	0.8
PB378/CAR19	platt03	-4.753759263	36.88036247	Ar-Ar	Bi	Sill gneiss	20.9	0.4
CB21	Monie etal 1991	-3.73706013	36.73423576	Ar-Ar	Bi	Sill-gt-St-Ky alpujarride gneiss	19.3	0.4
CB22	Monie etal 1991	-3.731072306	36.72345768	Ar-Ar	Wmica	Sill-gt-St-Ky alpujarride gneiss	18.8	0.5
Az-1	Esteban et al 2005	-4.852920786	36.77730551	FT	apat	???? dove??	16.5	2.4
Az-1	Esteban et al 2005	-4.852894315	36.77759669	FT	zirc	???? dove??	18.7	2
Az-15	Esteban et al 2005	-4.852470776	36.77770258	FT	zirc	???? dove??	19.5	2.8
Az-15	Esteban et al 2005	-4.852391362	36.77770258	FT	apat	???? dove??	18.6	3.6
Ri112	Azdimousa et al 2014	-4.528971042	35.03657342	FT	zirc	albian-aptian	200	0
Ri112	Azdimousa et al 2014	-4.528971042	35.03657342	FT	apat	albian-aptian	17	1.9
PB375/CAR16	platt03	-4.774982588	36.89255228	FT	apat	And quartzite	19.2	4.6
92R-1	Hurford et al 1999 ODP	-4.308169578	36.20023968	FT	apat	calc-silicate	20.7	1.8
Tb-734	esteban 07-13	-5.235212178	36.46286384	FT	zirc	chlorite schist	18.8	2
Tb-733	esteban 07-13	-5.235212178	36.46286384	FT	zirc	chlorite schist	18.6	1.8
Tb-735	esteban 07-13	-5.235212178	36.46286384	FT	zirc	chlorite schist	20.1	1.8
MM19	platt03	-4.502720865	36.82515827	FT	zirc	Early Pal clastic rocks	278	42
MM19	platt03	-4.502720865	36.82554908	FT	apat	Early Pal clastic rocks	22.5	3.4
MM15	platt03	-4.331243603	36.74813635	FT	zirc	Early Pal clastic rocks	170	20
MM15	platt03	-4.331243603	36.74774553	FT	apat	Early Pal clastic rocks	15.7	1.6
MM12	platt03	-4.301831941	36.7971496	FT	apat	Early Pal clastic rocks	24.7	3
PB376/CAR17	platt03	-4.770955598	36.8914639	FT	apat	Fibrolite schist	17.8	2.4
PB376/CAR17	platt03	-4.76997606	6,89091971651 486546)	FT	zirc	Fibrolite schist	21	2
PB383	platt03	-4.750657392	36.86779173	FT	apat	garnet gneiss (shear zone)	19.2	8.4
PB383	platt03	-4.749061108	6,86953313520 039899)	FT	zirc	garnet gneiss (shear zone)	21.4	1.8
PB383	platt03	-4.74717459	36.86677592	FT	apat	garnet gneiss (shear zone)	15.9	3.8
96R-1	Hurford et al 1999 ODP	-4.310873832	36.19753543	FT	apat	gneiss	21.4	2.3
95R-2	Hurford et al 1999 ODP	-4.310332982	36.19537203	FT	apat	gneiss	21.5	2.2
97R-1	Hurford et al 1999 ODP	-4.309792131	36.19753543	FT	apat	gneiss	19.7	2.3
97R-2b	Hurford et al 1999 ODP	-4.307087876	36,1964537271 147293)	FT	apat	granite	19.4	1.6

DK6	esteban2013	-4.378113334	36,8031995483 454395)	FT	zirc	greywacke malaguide	24.3	2.2
DK7	esteban2013	-4,37252025018 2375 3	36.81088199	FT	zirc	greywacke malaguide	24.1	1.8
DK7	esteban2013	-4,37252025018 2375 3	36.81088199	FT	zirc	greywacke malaguide	24.1	1.8
NDA26	esteban04	-5.026333442	36.53617982	FT	apat	guadaiza	16.3	1.6
NDA26	esteban04	-5.026333442	36.53591735	FT	zirc	guadaiza	16.2	1.8
MM22	platt03	-4.528371714	36.83102048	FT	apat	Late Pal greywacke	150	36
MM22	platt03	-4.526951359	36.83102048	FT	zirc	Late Pal greywacke	355	50
MM18	platt03	-4.485999771	36.76663685	FT	zirc	Late Pal greywacke	315	39
MM18	platt03	-4.485608956	36.76741848	FT	apat	Late Pal greywacke	17.5	3.4
MM9	platt03	-4.269464835	36.71915555	FT	apat	Late Pal greywacke	15.1	1.8
PB380	platt03	-4.747319707	36.87200012	FT	apat	leucosome	20.4	2.4
102R-2	Hurford et al 1999 ODP	-4.310332982	36.19861713	FT	apat	leucosome	17.1	1.3
95R-2b	Hurford et al 1999 ODP	-4.309792131	36.19807628	FT	apat	leucosome	18.6	1.4
B20	Sosson98	-4.831653462	36.58206505	FT	apat	los reales	15.1	0.55
B43	Sosson98	-4.819174704	36.5735795	FT	apat	los reales	14.53	0.83
Az-14	esteban04	-4.808572649	36.81637901	FT	zirc	los reales	16.7	1.8
Az-14	esteban04	-4.806406811	36.81840949	FT	apat	los reales	16.9	3
Az-10	esteban04	-4.804917797	36.81313025	FT	zirc	los reales	19.8	2.4
Az-9	esteban04	-4.803293418	36.82003386	FT	zirc	los reales	16.8	1.8
Az-10	esteban04	-4.802887324	6,81461926835 184073)	FT	apat	los reales	17	2
Az-7	esteban04	-4.798284917	36.8171912	FT	apat	los reales	14.7	2
Az-7	esteban04	-4.795983714	36.81786803	FT	zirc	los reales	18.7	2.8
Az-13	esteban04	-4.793276417	36.79458526	FT	apat	los reales	15	2.2
Az-11	esteban04	-4.790975213	36.80595592	FT	apat	los reales	16.4	3
CARR1	esteban04	-4.750095017	36,8615908852 639933)	FT	zirc	los reales	17.2	2
CARR1	esteban04	-4.749801726	36.86197033	FT	apat	los reales	17.6	2
GF1	esteban04	-4.735625975	36,5555646626 048798)	FT	zirc	los reales	17.6	1.2
GF1	esteban04	-4.7356217	36.55544898	FT	apat	los reales	17.5	1.2
Az-2	esteban04	-4.709936859	36.5906783	FT	apat	los reales	18.1	3
Az-6	esteban04	-4.704612878	36.5901802	FT	zirc	los reales	18.9	2.4

98R-1	Hurford et al 1999 ODP	-4.310332982	36.19753543	FT	apat	migmatite	15.2	1.3
98R-2	Hurford et al 1999 ODP	-4.309792131	36.19807628	FT	apat	neosome	17.8	1.3
B7	Sosson98	-4.84562967	6,57807184831 65117)	FT	apat	ojen	15.06	1.06
RON10	esteban04	-4.842275814	6,59322247009 787787)	FT	apat	ojen	11.7	3.8
RON10	esteban04	-4.841539013	36.59414839	FT	zirc	ojen	16.6	2.4
NDA11	esteban04	-4.822501028	36.59626474	FT	zirc	ojen	15.9	1.8
Az-4	esteban04	-4.707655152	36.60615214	FT	zirc	ojen	19	2.8
MM21	platt03	-4.564035116	36.86827869	FT	apat	P-Tr Sandstone (Malaguide upper unit)	189	14
MM20	platt03	-4.526011826	36.85288398	FT	apat	P-Tr Sandstone (Malaguide upper unit)	185	24
MM10	platt03	-4.334370118	36.71873465	FT	apat	P-Tr Sandstone (Malaguide upper unit)	269	22
MM11	platt03	-4.290107508	36.80301182	FT	apat	P-Tr Sandstone (Malaguide upper unit)	20.9	3.8
CAR11	platt03	-4.8173204	36.89342298	FT	apat	Pal greywacke	22	4
MM14	platt03	-4.325230939	36.78800011	FT	zirc	Phyllite and quartzite	22.1	1.6
MM3	platt03	-4.236869394	36.75348769	FT	zirc	Phyllite and quartzite	22.7	1.8
MM3	platt03	-4.236478579	36.75309688	FT	apat	Phyllite and quartzite	13.4	2.2
MM16	platt03	-4.443432666	36.82094549	FT	zirc	Phyllite and quartzite (Malaguide lower unit)	21.9	2.8
DK3	esteban2013	-4.439340861	36.78489584	FT	zirc	phyllite malaguide	25.8	1.8
PB436	platt03	-4.814708299	36.88863413	FT	zirc	Psammite	18.9	3
CAR5	platt03	-4.814381786	6,88852529010 815573)	FT	zirc	Psammitic schist	19	4
CAR5	platt03	-4.813728761	36.88874297	FT	apat	Psammitic schist	18	6
CAR9	platt03	-4.814925974	36.89081088	FT	zirc	Pz greywacke	280	19
CAR9	platt03	-4.813946436	36,8902666911 312167)	FT	apat	Pz greywacke	25	4
CAR14	platt03	-4.789784497	36.88906948	FT	apat	quartzite	16.4	2.8
PB437	platt03	-4.789022634	36.89483787	FT	apat	quartzite	20.8	5.2
PB437	platt03	-4.789022634	36.89494671	FT	zirc	quartzite	21.1	4.4
DK1	esteban2013	-4.711969394	36.58761925	FT	zirc	schist los reales	20.9	2
DK1	esteban2013	-4.709936859	36.58941963	FT	zirc	schist los reales	19.8	1.6
DK5	esteban2013	-4.436734311	36.80596904	FT	zirc	schist malaguide	21.6	1.3
DK5	esteban2013	-4.436734311	36.80596904	FT	zirc	schist malaguide	23.1	1.3
DK2	esteban2013	-4.426744844	36.77879975	FT	zirc	schist malaguide	21.7	2.1

97R-2	Hurford et al 1999 ODP	-4.313037236	36.19861713	FT	apat	schist/gneiss	17.8	1.9
PB378/CAR19	platt03	-4.752453212	36.87949177	FT	zirc	Sill gneiss	22	4
PB378/CAR19	platt03	-4.751691349	36.87960061	FT	apat	Sill gneiss	14.9	2.2
Ri114	Azdimousa et al 2014	-4.582534435	34.86170469	FT	zirc		200	0
Tb-733	esteban 07	-5.236094612	36.46251854	U-Pb	zirc	chlorite schist	21.8	0.5
RDA21	Sanchez-Rodriguez&Gebauer99	-5.183227318	36.56441072	U-Pb	zirc	corundum-garnet pyroxenite	131	3
RDA24	Sanchez-Rodriguez&Gebauer99	-5.17507271	36,5625985861777778)	U-Pb	zirc core	corundum-garnet pyroxenite	178	6
RDA24	Sanchez-Rodriguez&Gebauer99	-5.174106685	36.56122539	U-Pb	zirc rim	corundum-garnet pyroxenite	22.8	1.8
tb-08-03 - NO inherited	esteban2013	-4.762178476	36.5337003	U-Pb	zirc core	dolerite dike	430	5
tb-06-833	esteban2013	-4.649525373	36.77509981	U-Pb	zirc	dolerite dike	33.1	0.7
Gu-35	esteban11aquitanian	-5.074191143	36.62323445	U-Pb	zirc	fine grained migmatite mylonite	22.3	0.7
PB383	platt03	-4.748915991	36.86721127	U-Pb	zirc	garnet gneiss (shear zone)	21.2	0.3
RDA19	Sanchez-Rodriguez&Gebauer99	-5.182901581	36.56509128	U-Pb	zirc rim	granite	21.8	4.7
RDA19	Sanchez-Rodriguez&Gebauer99	-5.181958824	36.56495436	U-Pb	zirc core	granite con U-Pb loss, quinid ercinico probabilmen	168	10
tb-06-838	esteban11aquitanian	-5.183526467	36.49042924	U-Pb	zirc	granite dyke	22.6	1.8
tb-06-842	esteban11aquitanian	-4.816022395	36.58545366	U-Pb	zirc	granite dyke	21.5	3.8
CA1	Sanchez-Rodriguez&Gebauer99	-5.202435953	36,4952052744 95369)	U-Pb	zirc	graphite-garnet pyroxenite	143	16
CA1	Sanchez-Rodriguez&Gebauer99	-5,20199401701 7598 3	,495649466970 39147)	U-Pb	zirc	graphite-garnet pyroxenite	286	5
PB384	Platt&Whitehouse99	-4.827279037	36.82004832	U-Pb	zirc rim	leucocratic gneiss	21.1	1.4
PB380	Platt&Whitehouse99	-4.747755057	36.871855	U-Pb	zirc rim	leucosome	22.9	0.5
#90Z84	Zeck & Whitehouse 1999	-3.958704336	36.77694176	U-Pb	zirc	metagranite	285	5
tb-06-835	esteban11yunquera	-4.619407612	36.62222143	U-Pb	zirc	metapelitic sequence few meters below marble	2310	0
tb-06-835	esteban11yunquera	-4.619407612	36.62222143	U-Pb	zirc	metapelitic sequence few meters below	622	17

						marble		
Yu-15	esteban11yunquera	-4.931774088	36.72772035	U-Pb	zirc	migmatitic gneiss	628	14
RON10	Sanchez-Rodriguez&Gebauer99	-4.828560673	36,6021393783506781)	U-Pb	zirc core	partially retrogressed eclogite	183	3
RON10	Sanchez-Rodriguez&Gebauer99	-4.828248135	36.60186756	U-Pb	zirc rim	partially retrogressed eclogite	19.9	1.7
#90Z84	Zeck & Whitehouse 2002	-3.957763398	36.7748717	U-Pb	zirc	Pl-Bt-schists	970	30
#90Z84	Zeck & Whitehouse 2002	-3.957412051	36.77615053	U-Pb	zirc	Pl-Bt-schists	313	6.7
#90Z84	Zeck & Whitehouse 2002	-3.957198836	36.7763772	U-Pb	zirc	Pl-Bt-schists	622	30
#90Z84	Zeck & Whitehouse 2002	-3.955693335	36.77618901	U-Pb	zirc rim	Pl-Bt-schists	20	2
tb-06-841	esteban11yunquera	-4.68707407	36.60697265	U-Pb	zirc	quartzite intercalation in marble cover	627	8

Conclusion

The PhD project aimed at advancing the understanding of the tectonics of the Western Betics, with particular emphasis on the relationships between Alboran domain displacement, subcontinental mantle exhumation and crustal emplacement. The results are mainly based on intensive fieldwork, geochronological studies and the critical analysis of the published literature on the Betic-Rif. The threefold question has required the interplay of three research challenges. Indeed, the comprehension of the structures related to the Alboran emplacement onto the Iberia margin (Chapter 2) has been necessary to a fruitful study of the rift-related structures (Chapter 3). Next, the gained understandings and new geochronological data have allowed the analysis of the crustal emplacement of the Ronda Peridotites (Chapter 4). We now summarize the main results, before turning to illustrate some research perspectives.

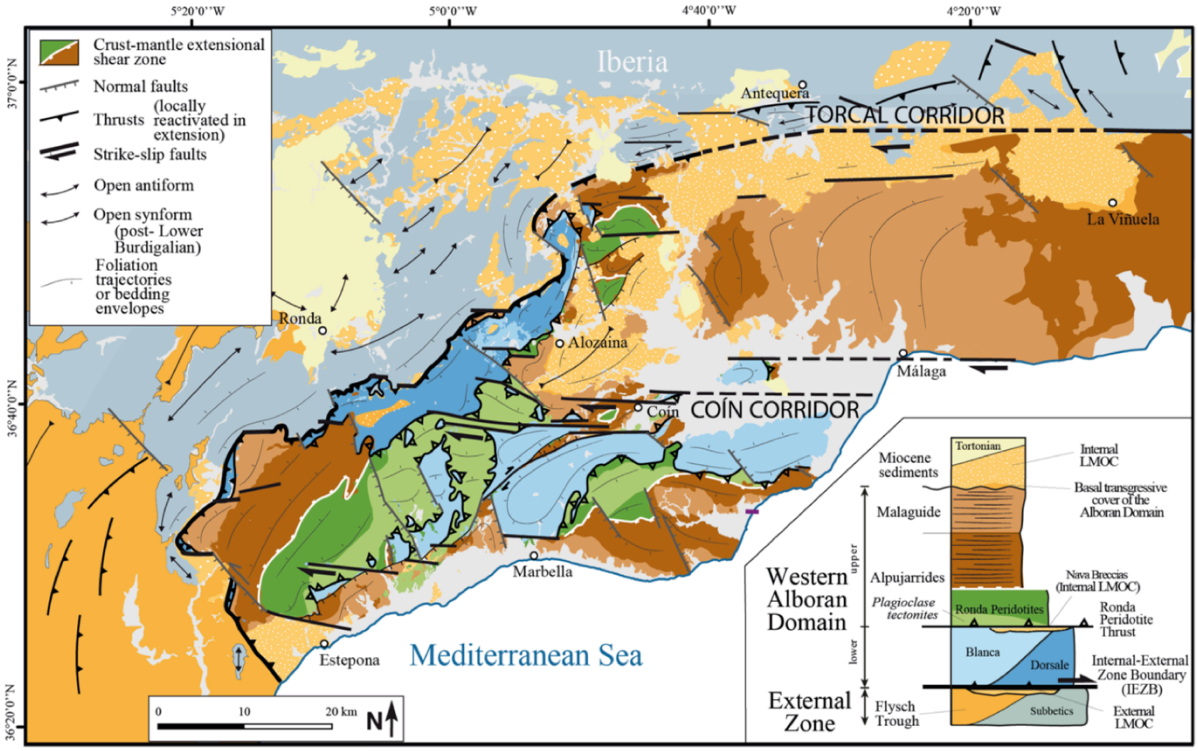

Figure C.1. Simplified structural map of the Western Betics (after Frasca et al., 2015). Inset: general vertical section, showing the two main tectonic contact (IEZB and Ronda Peridotites Thrust) and the main tectonic units, from bottom to top: Subbetics and Flysch through unit, Blanca and Dorsale, Ronda Peridotites, Alpujarride, Malaguide, Internal and External LMOC and Tortonian sediments.

First of all, we propose a new tectonic map of the Western Betics, which highlights the role of two major thrusts (Fig. C.1). The Internal/External Zone Boundary (IEZB) limits the metamorphic domain (Alboran Domain) from the fold-and-thrust belts in the External Zone, and the Ronda Peridotites Thrust allows the juxtaposition of a hyper-stretched lithosphere with large bodies of sub-continental mantle rocks on top of crustal rocks. New structural data (8734 measurements) has allowed to identify two E-W strike-slip corridors that played a major role in the deformation pattern of the Alboran Domain. E-W dextral strike-slip faults, N60° thrusts and N140° normal faults developed simultaneously during dextral strike-slip

simple shear (Fig. C.1). Using U-Pb LA-ICP-MS dating, we provide unequivocal data that constrain the age of the Ronda Peridotites Thrust and of the coeval leucocratic dikes at 20 Ma.

In addition to this intrusion event, we identify a second episode of crustal melting, associated with the crust-mantle extensional shear zone that bounds at the top the Ronda Peridotites. The extreme thinning of the continental crust and the mantle exhumation cause the formation of syn-kinematic leucosomes, coeval with the shearing along the regional high-temperature foliation, dated at 22.5 Ma. This succession of events from hot rifting between 30 and 20 Ma to thrusting at ca. 20 Ma and subsequent cooling between 20 and 16 Ma provides an effective explanation for the entire set of geochronological data available in the area (Fig. C.2).

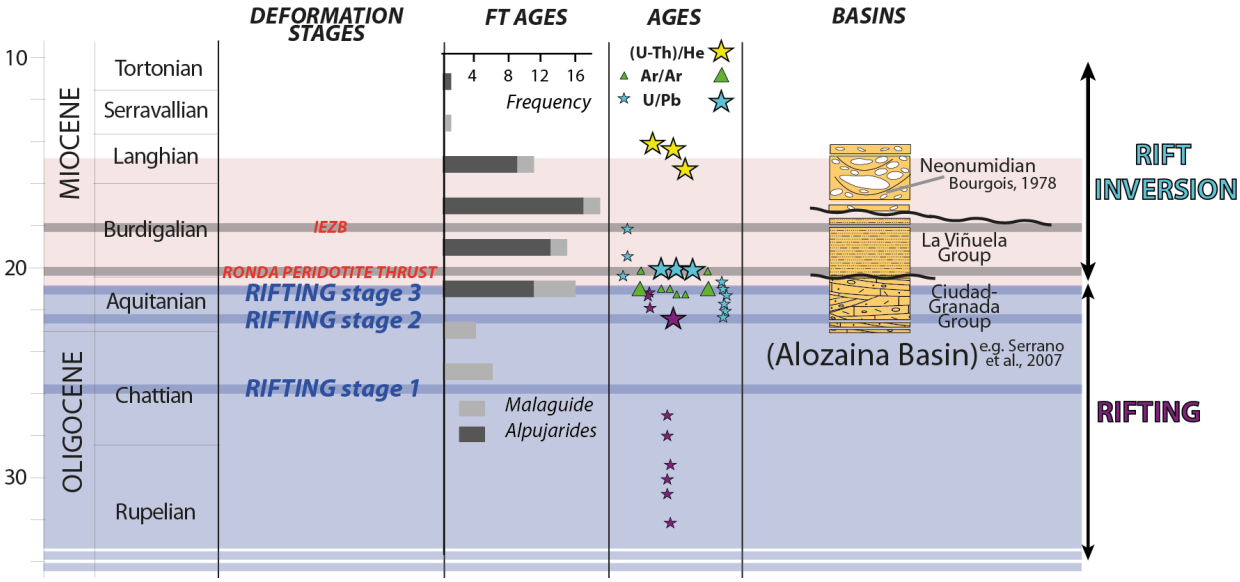

Figure C.2. The main Miocene tectonic events of the Western Betics with the new data and the interpretation furnished during the present thesis.

The Ronda Peridotites and their crustal envelopes are an exceptional exposure of hyper-stretched continental lithosphere, from which we obtained new structural data shading light on the kinematics during continental lithosphere necking. Based on 1406 foliation and lineations measurements in both crust and mantle rocks, we show, for the first time, the changes in deformation processes (ductile thinning and shearing, faulting) that accompany the progressive necking of the continental lithosphere (Fig. C.3). The observed variations in crustal thickness indicate amounts of stretching that locally reach values as high as 2400%, defining a stage of hyper-stretching.

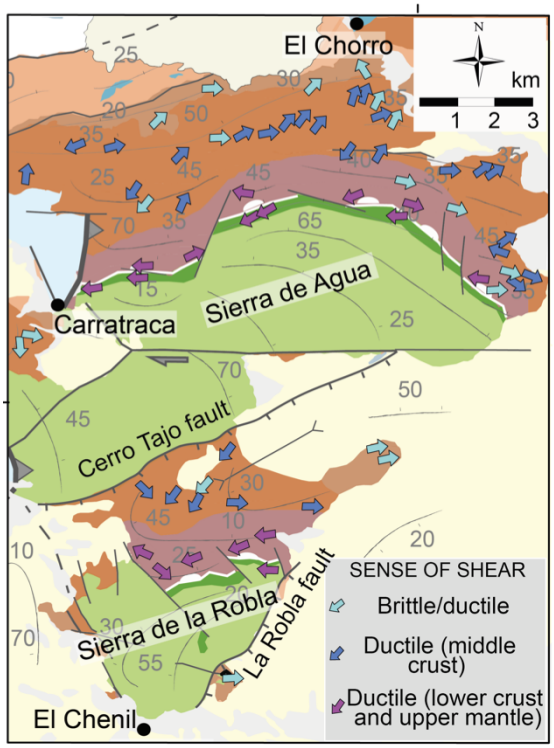

Figure C.3. Mean senses of shear in the Carratraca area. Ductile shear in the mantle and lower crust (violet arrows) and in the middle crust (blue arrows). Brittle/ductile shear, mainly observed in the upper crust (pale blue) (For the whole set of lineations and shear criteria see Chapter 3).

These geological observations are used to discuss and constrain the mechanics of the lithosphere necking process. In particular, three main successive steps characterized the lithosphere necking process (Fig. C.4). First, a mid-crustal shear zone and a crust-mantle shear zone, acting synchronously but with opposite senses of shear, accommodate the ductile crust thinning and the ascent of the sub-continental mantle. Second, hyper-stretching localizes in the neck, leading to an almost disappearance of the ductile crust and bringing the upper crust into contact with the subcontinental mantle, each of them endowed with their already acquired opposite senses of shear. Third, high-angle normal faulting, cutting through the Moho, and related block tilting end the full mantle exhumation in the domain of localized stretching.

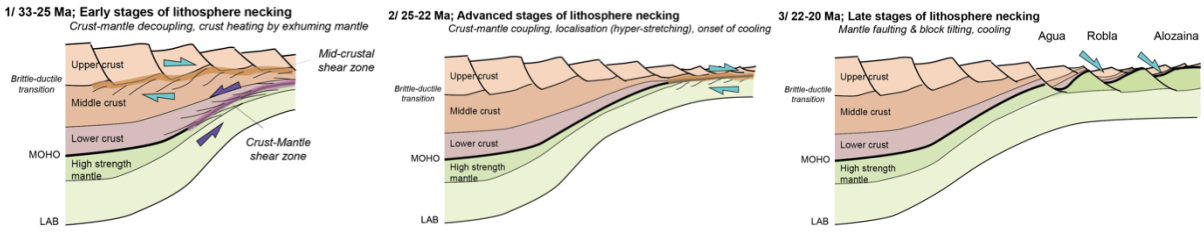

Figure C.4. Conceptual view of the lithosphere necking process in three main stages (See explanation in Chapter 3).

On these bases, we can propose the following tectonic evolution of the western Alboran domain, from rifting to thrusting. The crustal emplacement of the Ronda peridotites and the regional high-temperature thermal event of the western Alboran Domain therefore

resulted from a fast switch from 1) continental lithosphere extension in a back-arc setting, with local partial melting in the deep crust, and sub-continental mantle exhumation, to 2) rift inversion by thrusting, triggered by the shortening of the upper continental plate, with melting in the thrust footwall and dike intrusions in the hanging wall. The crustal emplacement of large bodies of sub-continental mantle has likely occurred at the onset of this westward thrusting. At lithosphere-scale, we interpret the observed deformation pattern as the subduction upper-plate expression of a lateral slab tear and its westward propagation since Lower Miocene (Fig. C.5).

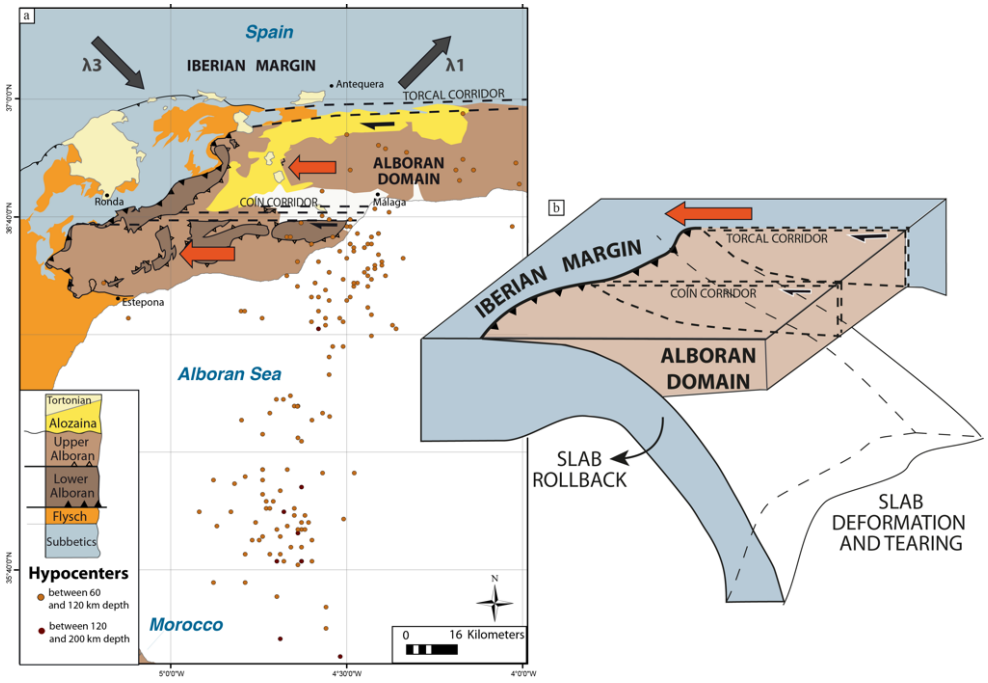

Figure C.5. (a) Synthetic scheme indicating the motion of Upper and Lower Western Alboran Units and the geometry of thrusts and strike-slip systems in the northern part of the Gibraltar arc. Present-day deep seismicity (epicenters between 60 and 200 km, from NEIC catalog, http://earthquake.usgs.gov/regional/neic/) is reported. (b) 3D sketch showing the tearing of the slab and its implication in the upper plate deformation (E-W strike-slip corridors).

RESEARCH PERSPECTIVE

Several future researches are stimulated by the findings of the present thesis. The possible works range from local studies, with application to the comprehension of the origin of the western Betics and of the Betic-Rif, to a general better comprehension of the mechanics of several tectonic processes, from rifting to thrusting. We divide these research perspectives into:

- local field studies coupled with geochronology, geochemistry, petrology, paleomagnetism and basin analysis;
- field studies at the level of the whole Betic-Rif accompanied by the same methods, but with a stronger need of large-scale geophysical input;
- modeling at local and large scale.

Local studies

We present a selection of local issues that all require an integrated multidisciplinary approach involving structural-driven geological studies.

First, we would like to investigate the relationships between distribution of high-temperature metamorphism and rifting-structures. To this aim, we first need geochronological studies concerning the age of the gabbros intrusion and of the high-temperature metamorphic event registered in the Blanca Group rocks, if possible also with data from the Blanca carbonatic rocks (Pb-Pb isochron). A ^{40}Ar-^{39}Ar dating from fault rocks can help then to constrain the timing of the extension observed along the coastline north of Estepona (chapter 2). Moreover, a petrological study is then necessary on the granulites at the base of the crust in order to investigate the thermal history of the rifted basement studied in the area. The comprehension of the link between high-temperature and rifting can have a general importance for **hydrocarbon exploration** in other rift-areas. The thermal evolution of the basements has, indeed, a strong influence on the subsidence history of the rifted basins and on the maturity of the organic matter present in the basin.

Second, the possible existence and the age of the high-pressure metamorphism in the crustal rocks need to be ascertained. After, the identification of possible fabrics that resisted to high-temperature transposition, the collection of samples with garnet from the upper and lower alboran unit could permit to use the Lu-Hf method. An effort should be done to find useful microfossils in tertiary sediments of the External Zone to couple the geochronological data with the stratigraphy. The lowermost levels of the basin in the western alboran domain should also be investigated to better constrain the timing of the high-temperature and of the rifting event.

Third, we need to reconstruct the whole rift geometry. The deformation patterns observed in the Carratraca massif and in the other Ronda peridotite massives (Balanyá et al., 1997; Tubía and Cuevas, 1986) (see section 1.4) need to be related to reconstruct the whole rift geometry. The shear direction in the Carratraca massif (chapter 3) and the peculiar normal faults trend suggest a strike-slip kinematics, most probably partly acquired during rift inversion. However, a possible original transtension during the rifting cannot be excluded and should be considered for the restoration of the system. For this restoration, an integration of paleomagnetic data could be necessary, avoiding sampling in metamorphic or metamorphosed rocks. Sampling leucocratic dikes at different distances from the strike-slip faults, Tortonian and younger sediments in good stratigraphic sections should be important to define the timing and the amount of the strike-slip movement.

Finally, we need to better characterize the thrust-emplacement of the mantle in the center of the Alboran Domain. To this goal, a careful study of the sense of shear in the metamorphic sole described at the base of the Sierra Alpujata peridotite (e.g. Tubía et al., 2013) and a coupling with petrological data (e.g. Bartoli et al., 2013) is necessary. The base of the mantle sliver, made of spinel-tectonite, is a petrological equivalent of the top of the

peridotite sliver (Hidas et al., 2015; Tubía et al., 2013) and thus the base could be the result of the reactivation of the crust-mantle extensional shear zone in an anomalous position.

Tectonic implications on the Betic-Rif

We present three large-scale tectonic lines of investigation, related to and arising from the local observations of the present thesis. The first one is identifying the possible lithosphere-scale signature of the rifting and thrusting, the second one is the relationship between western Betics and the rest of the Betic-Rif and the third one are the geodynamical implication on the Alboran system.

Lithosphere-scale signature of the rifting and thrusting

In the last 20 years the Ronda Peridotites have been considered as mantle slivers not attached to the Alboran subcontinental mantle for three main reason. 1) The mantle rocks most outcrop above crustal rocks; 2) the sense of shear at the base of the mantle is difficult to fit with the models that proposed the Ronda mantle as deeply rooted (Doblas and Oyarzun, 1989; Tubía and Cuevas, 1986); 3) some gravimetric models are consistent with the discontinuity of the mantle body (Torné et al., 1992) (Fig. C.6a). However, seismic refraction data (Barranco et al., 1990) indicate that the Ronda mantle continues at depth below the Alboran domain. Furthermore, Casas and Carbos (1990) model from gravity data a high-density body deeply rooted into the mantle (Fig. C.6b).

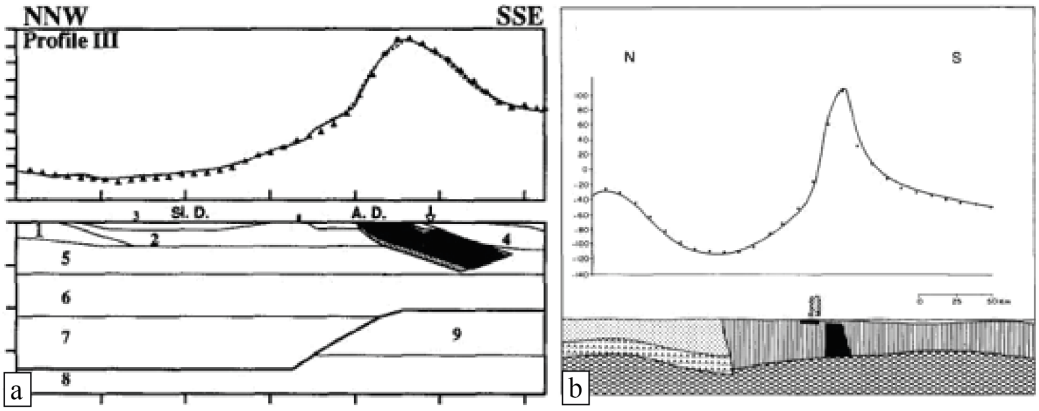

Figure C.6. Possible explanations for the anomaly observed close to the Sierra Alpujata peridotitic massif. On the left, data and model from Casas and Carbos (1990) and, on the right, data and model from Torné et al. (1992).

This controversy can be hopefully solved with a more precise description of the gravity anomaly. A sampling of gravity data has been recently conducted and the data are under process (INSU Project F. Gueydan). Moreover, the geophysical data from the Iberia array (http://iberarray.ictja.csic.es) and the PICASSO project (http://earth.usc.edu/picasso/home) will also help. Based on these data, El Moudnib et al. (2015) attribute an anomaly in the P-wave perturbation to the prolongation at depth of the

Ronda peridotite (Fig. C.7a). The most important result of El Moudnib et al. (2015) is that the Ronda Peridotite exhibits a large vertical continuity, extending from the surface to at least 24 km depth. This is clearly observed in the vertical cross-section of the model in which the Ronda body is merging into the Alboran subcontinental mantle (Fig. C.7b). These conclusions are consistent with the limited amount of the Alboran Domain displacement and with the hyper-stretching that led to mantle exhumation reported in this thesis.

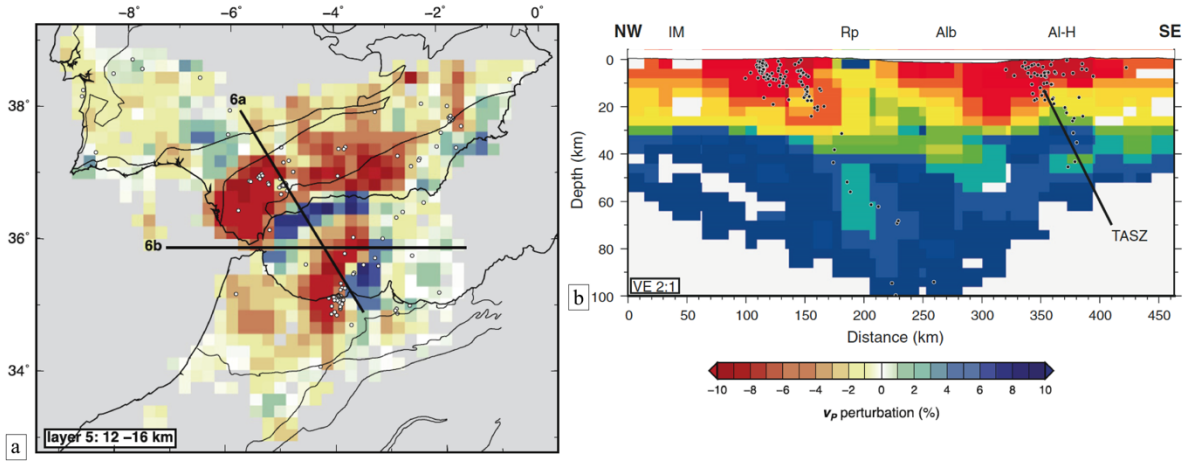

Figure C.7. P-wave velocity model from El Moudnib et al. (2015). (a) Horizontal slice of the obtained model with shown P-wave velocity perturbations (layer 5 of the model, between 12 and 16 km depth). White circles are earthquakes with focal depths (see El Moudnib et al., 2015, for details). Thin black lines indicate the boundaries between major structural units in Alboran. Thick lines indicate the location of the vertical cross sections shown in El Moudnib et al. (2015). (b) NW-SE -trending vertical cross section of the P-wave velocity model through the Iberian Massif (IM), Ronda peridotite (Rp), Alboran basin (Alb) and Al-Hoceima (Al-H). Earthquakes within 10 km of the cross section are plotted as circles. Vertical exaggeration is 2:1.

Relationship with the Betic-Rif

The P-wave anomaly proposed in El Moudnib et al. (2015) extends southward suggesting that the Ronda, Ceuta and Beni Bousera peridotites belong to the same continuous body at depth. This fact needs to be considered for the restoration of the geometry of the whole rift at the scale of the Gibraltar arc. The relationship between the slab imaged recently at depth (e.g. Levander et al., 2014), the Iberian and Maghrebian margins and these peridotitic body has to be investigated with new onshore and offshore data.

The eastward prolongation of the strike-slip faults in the western Betics into the strike-slip faults described in the eastern Betics has to be investigated with structural studies in the area between the Torcal Corridor, described in chapter 2, and the Alpujarra Corridor (Fig. C.8). Furthermore, an important tectonic group, the Nevado-Filabride is cropping out only in the central and eastern part of the chain. The reason of its absence in the Western Betics needs to be investigated with field studies coupled with geophysical investigation aiming at understanding its rooting at depth and lateral extension.

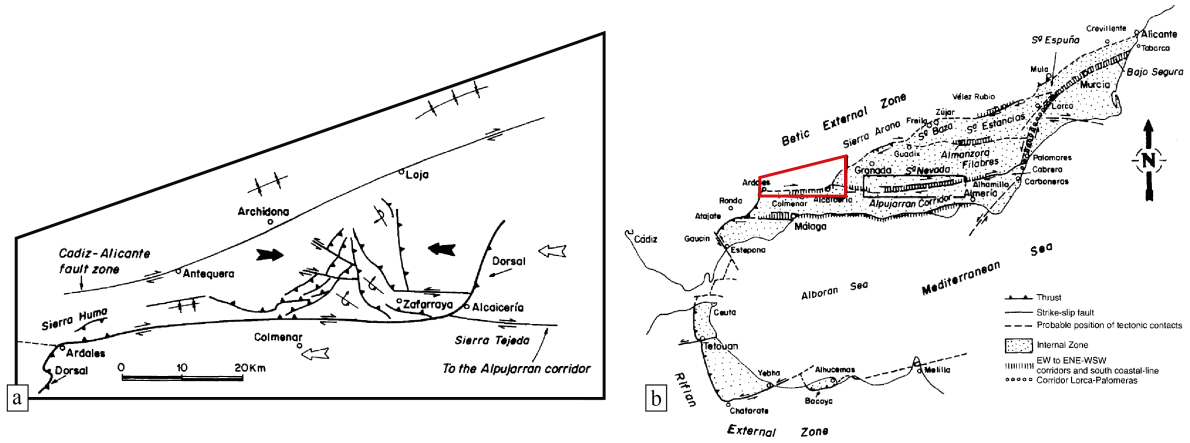

Figure C.8. (a) Simplified tectonic interpretation (from Sanz de Galdeano et al., 1996) of the External Zone to the north of the Torcal Corridor (Colmenar corridor in Sanz de Galdeano. The blank arrows indicate the direction of the displacement of the Internal Zone; the black arrows correspond to the direction of the principal compression undergone by the Subbetic in the sector between Archidona, Zafarraya and Loja. The thick line is the Internal-External Zone Boundary. The location of the area is reported on (b) with a red rectangle. Scheme of the contact between the Internal and External Zones in the Betic Cordillera and the corridors present in the latter. The polygon represent the position of the sketch map in a.

Geodynamical implications from the study of the Western Betics

The analyses of the gravity anomaly and of the surface geology in the rest of the Betic-Rif can help to identify the **position of the trench** at 20 Ma. Based on the results obtained, a discrimination between the geodynamic reconstructions of the Western Mediterranean proposed in figure C.9 would then be suggested. The present thesis suggests that the westward displacement between Alboran and Iberia is small compared to the displacement supposed by the majority of the models. Future geophysical investigations coupled with the data proposed in the thesis will help to put constraints on the timing of the trench displacement.

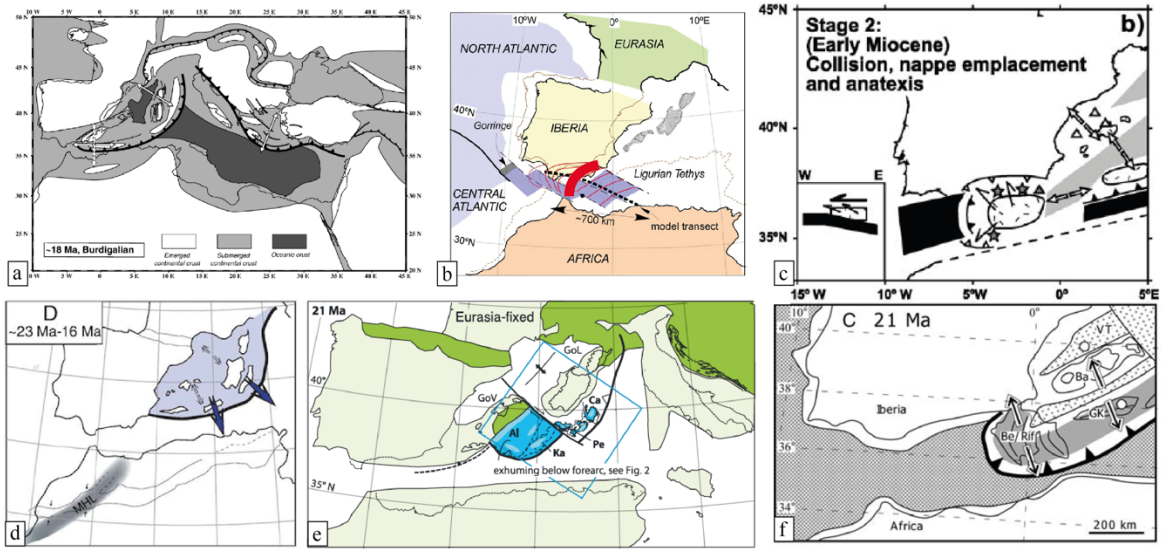

Figure C.9. Tectonic reconstruction proposed by different authors for the Lower Miocene. (a) Position of the trench at about 18 Ma from Jolivet et al. (2006); (b) whole reconstruction from Vergés and Fernández (2012),

the thick red line indicates the position of the slab; (c) position of the trench at about 20 Ma from Duggen et al. (2004); (d) at about 20 Ma from Frizon de Lamotte et al. (2009); (e) at 21 Ma from Van Hinsbergen et al. (2014); (f) at 21 Ma from Rosenbaum and Lister (2004).

Modeling at local and large scale

The results obtained from this study can be used to calibrate the initial and boundary conditions of future **models** and to test their response. For example, **numerical models** can give insights on the temporal and spatial evolution of the temperature during the thrusting event, as partly done already by Précigout et al. (2013) with a 1D model (Figs. C.10a and C.10b). In chapter 4, an extremely strong gradient of 100º to 200ºC/km is necessary to obtain partial melting (at least 650º C) along the Ronda Peridotite Thrust, while the top of the hyper-stretched section was already cooling down (below 400ºC, ^{40}Ar-^{39}Ar age at 21 Ma in a rift-related brittle fault breccia). This dynamical geological reconstruction cannot be captured in a 1D model, but needs both depth and a horizontal dimension.

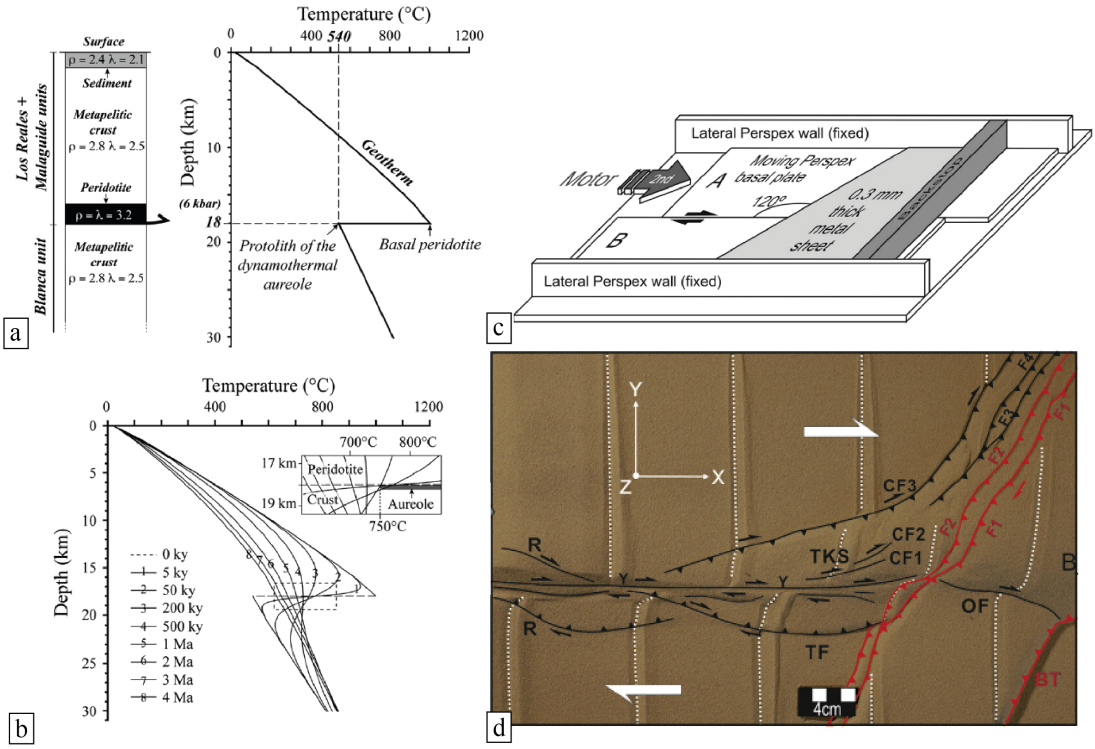

Figure C.10. Thermal modeling to constrain the timing of the Ronda Peridotite deformation (from Précigout et al., 2013). For details on the input parameters see Précigout et al. (2013). (a) Geotherm of the model before thermal balance. Based on the P-T data set from Esteban et al. (2008), the tectonic contact between the peridotite and the Blanca unit has been set at 18 km depth (6 kbar) with a temperature of 540°C for the top Blanca unit (protolith of the dynamothermal aureole) and a higher temperature for the basal peridotite. (b) Example of thermal balance over 4 million years with a starting temperature of 1000°C at the base of the peridotite. Analogue modeling reproducing the coeval development of thrusts and strike-slip faults (from Rosas et al., 2015). (c) Schematic illustration of the deformation rig used to simulate thrust-wrench fault interference for an angle of 120º. The orientation of the velocity discontinuity is 120º relatively to the strike of the basement strike-slip fault. (d) Obtained results for the thrust-wrench fault interference experiments: top view with interpretation of the structural output.

Analogue modeling can be also extremely useful to understand thrusts dynamics and their relationship with coeval strike-slip faults. A first step in this direction has been taken by Rosas et al. (2015). However, for a satisfying solution it would be necessary building an apparatus that is able to account for the rotation of the thrust sheets during the coeval action of the strike-slip faults, without resorting to imposed ad-hoc discontinuities in the boundary condition (Figs. C.10c and C.10d). These features are essential for the application to the natural case that we propose in Chapter 2.

REFERENCES

Acosta-Vigil, A., Rubatto, D., Bartoli, O., Cesare, B., Meli, S., Pedrera, A., Azor, A., and Tajcmanova, L. (2014). Age of anatexis in the crustal footwall of the Ronda Peridotites, S. Spain. Lithos, 210:147-167.

Afiri, A., Gueydan, F., Pitra, P., Essai, A., and Précigout, J. (2011). Oligo-miocene exhumation of the Beni-Bousera peridotite through a lithosphere-scale extensional shear zone. Geodinamica Acta, 24(1):49-60.

Aguado, R., Feinberg, H., Durand-Delga, M., Martín-Algarra, A., Esteras, M., and Didon, J. (1990). Nuevos datos sobre la edad de las formaciones miocenas transgresivas sobre las Zonas Internas Béticas: la Formación de San Pedro de Alcantara (Provincia de Málaga). Revista de la Sociedad Geológica de España, 3(1-2):79-85.

Alcalá, F. J., F. Guerrera, F. M. Martín-Martín, M., Raffaelli, G., and Serrano F. (2014). Geodynamic implications derived from Numidian-like distal turbidites deposited along the Internal–External Domain Boundary of the Betic Cordillera (S Spain). Terra Nova, 25:119-129.

Allerton, S., Reicherter, K. and Platt, J. (1994). A structural and palaeomagnetic study of a section through the eastern subbetic, southern Spain. Journal of the Geological Society, 151(4):659–668.

Andrieux, J., Fontboté, J., and Mattauer, M. (1971). Sur un modèle explicatif de l'arc de Gibraltar. Earth and Planetary Science Letters, 12:191-198.

Argles, T. and Platt, J. (1999). Stepped fibres in sillimanite-bearing veins: valid shear-sense indicators in high grade rocks?. Journal of Structural Geology, 21(2):153-159.

Argles, T., Platt, J., and Waters, D. (1999). Attenuation and excision of a crustal section during extensional exhumation: the Carratraca massif, Betic Cordillera, southern Spain. Journal of the Geological Society, 156(1):149-162.

Augier, R., Agard, P., Jolivet, L., Monié, P., Robin, C. and Booth-Rea, G. (2005a). P-T-D-t retrograde evolution of the Nevado–Filabride complex (SE Spain): new insights from in-situ 40Ar/39Ar ages and metamorphic petrology. J. Metamorph. Geol., 23:357-381.

Augier, R., Booth-Rea, G., Agard, P., Martínez-Martínez, J.M., Jolivet, L., Azañón, J.M. (2005b). Exhumation constraints for the lower Nevado-Filabride Complex (Betic Cordillera, SE Spain): a Raman thermometry and Tweequ multi-equilibrium thermobarometry. Bulletin de la Société Géologique de France, 176:403-416.

Augier, R., Jolivet, L., Robin, C. (2005c). Late Orogenic doming in the Eastern Betics: final exhumation of the Nevado–Filabride complex and its relation to basin genesis. Tectonics, 24, TC4003.

Azañón, J.-M. and Crespo-Blanc, A. (2000). Exhumation during a continental collision inferred from the tectonometamorphic evolution of the Alpujarride complex in the Central Betics (Alboran Domain, SE Spain). Tectonics, 19(3):549-565.

Azañon, J., Crespo-Blanc, A., García-Dueñas, V., and Sánchez-Gómez, M. (1996). Folding of metamorphic isograde in the Adra extensional unit (Alpujarride complex, central Betics). C. R. Acad. Sci. Paris, 323(11):949-956.

Azañón, J.-M., García-Dueñas, V., and Goffé, B. (1998). Exhumation of high-pressure metapelites and coeval crustal extension in the Alpujarride complex (Betic Cordillera). Tectonophysics, 285(3-4):231-252.

Azañón, J. M. and Goffé, B. (1997). Ferro- and magnesiocarpholite assemblages as record of high-P, low-T metamorphism in the Central Alpujarrides, Betic Cordillera (SE Spain). Eur. J. Mineral., 9: 1035-1051.

Azdimousa, A., Bourgois, J., Poupeau, G., Vázquez, M., Asebriy, L., Labrin, E. (2014). Fission track thermochronology of the Beni Bousera peridotite massif (Internal Rif, Morocco) and the exhumation of ultramafic rocks in the Gibraltar Arc. Arabian Journal of Geosciences, 7(5):1993-2005.

Bakker, H., Jong, K., Helmers, H., and Biermann, C. (1989). The geodynamic evolution of the Internal Zone of the Betic Cordilleras (south-east Spain): a model based on structural analysis and geothermobarometry. Journal of Metamorphic Geology, 7(3):359-381.

Balanyá, J. C. and García-Dueñas, V. (1987). Les directions structurales dans le domaine d'alborán de part et d'autre du détroit de Gibraltar. C. R. Acad. Sci. Paris, 304(15):929-932.

Balanyá, J. C., Crespo-Blanc, A., Díaz-Azpiroz, M., Exósito, I., and Luján, M. (2007). Structural trend line pattern and strain partitioning around the Gibraltar arc accretionary wedge: Insights as to the mode of orogenic arc building. Tectonics, 26(2):TC2005

Balanyá, J. C., Crespo-Blanc, A., Díaz-Azpiroz, M., Expósito, I., Torcal, F., Perez-Peña, V., and Booth-Rea, G. (2012). Arc-parallel vs. back-arc extension in the western Gibraltar arc: is the Gibraltar forearc still active? Geol. Acta, 10:249–263.

Balanyá, J. C., Crespo-Blanc, A., Díaz-Azpiroz, M., Expósito, I., and Luján, M. (2007). Structural trend line pattern and strain partitioning around the Gibraltar arc accretionary wedge: Insights as to the mode of orogenic arc building. Tectonics, 26(2):TC2005.

Balanyá, J. C., García-Dueñas, V., Azañón, J. M., and Sánchez-Gómez, M. (1997). Alternating contractional and extensional events in the Alpujarride nappes of the Alboran domain (Betics, Gibraltar arc). Tectonics, 16(2):226-238.

Balestro, G., Piana, F., De Donatis, M. and Bruciatelli, L. (2010). Representation and transfer of geological knowledge in ITsupported projects. Ital. J. Geosci. (Boll.Soc.Geol.It.). 129(3): 441-449.

Ballouard, C., Boulvais, P., Poujol, M., Gapais, D., Yamato, P., Tartèse, R., Cuney, M., 2015, Tectonic record, magmatic history and hydrothermal alteration in the Hercynian Guérande

leucogranite, Armorican Massif, France. Lithos, v. 220-223, p. 1-22.

Barcos, L., Díaz-Azpiroz, M., Balanyá, J., and Expósito, I. (2011). Dominios estructurales y reparto de la deformación en zonas transpresivas de corteza superior (Torcal de Antequera, Cadena Bética). Geogaceta, 50:31-34.

Barcos, L., Jiménez-Bonilla, A., Expósito, I., Balanyá, J. C. and Díaz-Azpiroz, M. (2014) Reparto de la deformación en la terminación oriental de la Zona de Cizalla del Torcal (Béticas, S España). Geogaceta, 56:23-26.

Barich A., Acosta-Vigil A., Garrido C.J., Cesare B., Tajčmanová L., Bartoli O. (2014) Microstructures and petrology of melt inclusions in the anatectic sequence of Jubrique (Betic Cordillera, S Spain): Implications for crustal anatexis. Lithos, 206-207:303-320.

Barranco, L. M., Ansorge, J., Banda, E. (1990). Seismic refraction constraints on the geometry of the Ronda peridotitic massif (Betic Cordillera, Spain). Tectonophysics, 184:379-392.

Bartoli, O., Tajcmanová, L., Cesare, B., and Acosta-Vigil, A. (2013). Phase equilibria constraints on melting of stromatic migmatites from Ronda (S. Spain): insights on the formation of peritectic garnet. Journal of Metamorphic Geology, 31(7):775-789.

Behr, W.M . and Platt, J., (2012). Kinematic and thermal evolution during two-stage exhumation of a Mediterranean subduction complex Tectonics, 31:TC4025

Berástegui, X., Banks, C., Puig, C., Taberner, C., Waltham, D., and Fernández, M. (1998). Lateral diapiric emplacement of Triassic evaporites at the southern margin of the Guadalquivir Basin, Spain. Geological Society, London, Special Publications, 134(1):49-68.

Berndt, T., Ruiz-Martínez, V. C., Chalouan, A. (2015). New constraints on the evolution of the Gibraltar Arc from palaeomagnetic data of the Ceuta and Beni Bousera peridotites (Rif, northern Africa). Journal of Geodynamics, 84:19-39.

Beslier, M.-O., Girardeau, J., and Boillot, G. (1990). Kinematics of peridotite emplacement during north Atlantic continental rifting, Galicia, northwestern Spain. Tectonophysics, 184(3): 321-343.

Bezada, M., Humphreys, E., Toomey, D., Harna, M., Dávila, J., and Gallart, J. (2013). Evidence for slab rollback in westernmost Mediterranean from improved upper mantle imaging. Earth and Planetary Science Letters, 368:51-60.

Biju-Duval, B., Dercourt, J., and Le Pichon, X. (1977). From the Tethys ocean to the Mediterranean seas: a plate tectonic model of the evolution of the western alpine system. Histoire structurale des bassins méditerranéens, pages 143.

Blanco, M. and Spackman, W. (1993). The P-wave velocity structure of the mantle below the iberian peninsula: Evidence for a subducted lithosphere below southern Spain. Tectonophysics, 221 (1):13-34.

Blichert-Toft, J., Albarède, F., and Kornprobst, J. (1999). Lu-Hf isotope systematics of garnet

pyroxenites from Beni Bousera, Morocco: Implications for basalt origin. Science, 283:1303-1306.

Boillot, G., Grimaud, S., Mauffret, A., Mougenot, D. Kornprobst, J., Mergoil, D. J., and Torrent, G. (1980). Ocean continent boundary of the Iberian margin: A serpentinite diapir west of the Galicia Bank. Earth and Planetary Science Letters, 48:23-34.

Boillot, G., Recq, M, Winterer, E.L., Meyer, A.W., Applegate, J., Baltuck, M., Bergen, J.A., Comas, M.C., Davies, T.A., Dunham, K., Evans, C.A., Girardeau, J., Goldberg, G., Haggerty, J., Jansa, L.F., Johnson, J.A., Kasahara, J., Loreau, J.P., Luna-Sierra, E., Mollade, M., Ogg, J., Sarti, M., Thurow, J., and Williamson M. (1987). Tectonic Denudation Of The Upper Mantle Along Passive Margin: A Model Based On Drilling Results (Odp Leg 103, Western Galicia Margin, Spain). Tectonophysics, 132:335-342.

Bonini, W.E., Loomis,T.P. and Robertson, J.D. (1973). Gravity anomalies, ultramaphic intrusions and the tectonic of the region around the Strait of Gibraltar. Geophys. Res., 78:1372-1382.

Bonnin, M., Nolet, G., Villaseñor, A., Gallart, J., and Thomas, C. (2014). Multiple-frequency tomography of the upper mantle beneath the african/iberian collision zone. Geophysical Journal International, 198(3):1458-1473.

Booth-Rea, G., Ranero, C.R., Martínez-Martínez, C. R., Grevemeyer, J. M. I. (2007) Crustal types and Tertiary tectonic evolution of the Alborán sea, western Mediterranean. Geochemistry, Geophysics, Geosystems, 8(10): Q10005.

Booth-Rea, G., Azañón, J. M., García-Dueñas, V., Augier, R., and Sánchez-Gómez, M. (2003). A « core-complex-like structure » formed by superimposed extension, folding and high-angle normal faulting. The Santi Petri dome (Western Betics, Spain). Comptes Rendus Geoscience, 335(2):265-274.

Booth-Rea, G., Azañon, J.M., Martinez-Martinez, J.M., Vidal, O. and Garcia-Dueñas, V. (2005). Contrasting structural and P-T evolution of tectonic units in the southeastern Betics: Key for understanding the exhumation of the Alboran Domain HP/LT crustal rocks (western Mediterranean). Tectonics, 24:TC2009.

Booth-Rea, G., Ranero, C.R., Martinez-Martinez, J.M., Grevemeyer, I. (2007). Crustal types and Tertiary tectonic evolution of the Alborán sea, western Mediterranean. Geochemistry, Geophysics, Geosystems, 8(10):Q10005.

Bourgois, J. (1978). La transversale de Ronda (Cordillères Bétiques, Espagne). Données géologiques pour un modèle d'évolution de l'Arc de Gibraltar. Annales Scientifiques de l'Université de Besançon (France), 30:1-445.

Bourgois, J., Chauve, P., Lorenz, C., Monnot, J., Peyre, Y., Rigo, E. and Rivière, M. (1972). La formation d'Alozaina. Série d'âge oligocène et aquitanien transgressive sur le Bétique de Malaga. C. R. Acad. Sci. Paris, 275(D):531-534.

Bourgois, J., Chauve, P., Magne, J., Monnot, J., Peyre, Y., Rigo, E. and Rivière, M. (1972). La formation de Las Millanas. Série burdigalienne transgressive, sur les zones internes des

cordillères bétiques occidentales (région d'Alozaina-Tolox, province de Malaga, Espagne). C. R. Acad. Sci. Paris, 275(D):169-172.

Bousquet, J.-C. (1979). Quaternary strike-slip faults in southeastern Spain. Tectonophysics, 52(1-4):277-286.

Boyer, S. E. and Elliott, D. (1982). Thrust systems. AAPG Bulletin, 66(9):1196–1230.

Braga, J.C., Martín, J.M. and Quesada, C. (2003). Patterns and average rates of late Neogene - Recent uplift of the Betic Cordillera, SE Spain. Geomorphology 50:3-26.

Brun, J.-P. and Beslier, M.O. (1996). Mantle exhumation at passive margins. Earth and Planetary Science Letters 142:161-173.

Brun, J.-P. and Sokoutis, D. (2010). 45 m.y. of aegean crust and mantle flow driven by trench retreat. Geology, 38(9):815-818.

Buforn, E., Bezzeghoud, M., Udías, A., and Pro, C. (2004). Seismic sources on the Iberia-African plate boundary and their tectonic implications. Pure appl. geophys., 161(3):623-646.

Calvert, A., Sandvol, E., Seber, D., Barazangi, M., Roecker, S. Mourabit, T., Vidal, F., Alguacil, G., and Jabour, N. (2000) Geodynamic evolution of the lithosphere and upper mantle beneath the Alboran region of the western Mediterranean: Constraints from travel time tomography. J. Geophys. Res., 105(10):871–898.

Calvo, M., Cuevas, J., Tubía, J. (2001). Preliminary palaeomagnetic results on Oligocene-Early Miocene mafic dykes from southern Spain. Tectonophysics 332(3):333-345.

Calvo, M., Osete, M.L., Vegas, R. (1994). Palaeomagnetic rotations in opposite senses in southeastern Spain. Geophys. Res. Lett. 21 (9):761-764.

Cano Medina, F. (1990). Sheet Olvera, 1036. Geological map scale 1:50000, Instituto Geológico y Minero de España, Madrid.

Cano Medina, F. and Ruiz Reig, P. (1990). Sheet Ardales, 1051. Geological map scale 1:50000, Instituto Geológico y Minero de España, Madrid.

Casas, A. and Carbo, A. (1990). Deep structure of the Betic Cordillera derived from the inter-pretation of a complete bouguer anomaly map. Journal of Geodynamics, 12(2–4):137-147. Geophysics of the Mediterranean Basin.

Célérier, B. (2013). FSA: Fault & Stress Analysis software, version 35.1, http://www.pages-perso-bernard-celerier.univ-montp2.fr/software/dcmt/fsa/fsa.html.

Chalouan, A. and Michard, A. (1990). The Ghomarides nappes, Rif coastal range, Morocco: A variscan chip in the alpine belt. Tectonics, 9(6):1565-1583.

Chalouan, A., Michard, A., El Kadiri, K., Frizon de Lamotte, D., Negro, F., Soto, J., and Saddiqi, O. (2008). The Rif belt, in Michard, A., Saddiqi, O., Chalouan, A., de Lamotte, D.F., editors, Continental Evolution: The Geology of Morocco: Structure, Stratigraphy, and Tectonics of the Africa–Atlantic–Mediterranean Triple Junction. Springer: 203-302.

Chamón Cobos, C., Quinquer Agut, R., Crespo, V., Aguilar, M., and Reyes, J.L. (1972). Sheet Alora, 1052. Geological map scale 1:50000, Instituto Geológico y Minero de España, Madrid.

Chertova, M. V., Spakman, W., Geenen, T., Van den Berg, A. P., and Van Hinsbergen, D. J. J. (2014). Underpinning tectonic reconstructions of the western Mediterranean region with dynamic slab evolution from 3-D numerical modeling. J. Geophys. Res., Solid Earth, 119:5876–5902.

Cifelli, F., Mattei, M., and Porreca, M. (2008). New paleomagnetic data from Oligocene-Upper Miocene sediments in the Rif chain (northern Morocco): Insights on the neogene tectonic evolution of the Gibraltar arc. Journal of Geophysical Research: Solid Earth, 113(B2):B02104.

Clark S. J. P. and Dempster T. J. (2009). The record of tectonic denudation and erosion in an emerging orogen: an apatite fission-track study of the Sierra Nevada, southern Spain. Journal of the Geological Society, London, 166: 87-100.

Cochran, J.R., and Karner, G.D. (2007). Constraints on the deformation and rupturing of continental lithosphere of the Red Sea: The transition from rifting to drifting, in Karner, G. D., Manatschal, G., Pinheiro, L. M., editors, Imaging, Mapping and Modelling Continental Lithosphere Extension and Breakup. Geological Society, London, Special Publications, 282:265-289.

Comas, M. C., García-Dueñas, V., and Jurado, M. (1992). Neogene tectonic evolution of the Alboran Sea from MCS data. Geo-Marine Letters, 12(2-3):157-164.

Comas, M. C., Platt, J. P., Soto, J. I., and Watts, A. B. (1999). The origin and tectonic history of the Alboran basin: Insights from LEG 161 results. In Zahn, R., Comas, M. C. and Klaus, A., editors, Proceedings of the Ocean Drilling Program, Scientific Results:555-580

Contrucci, I., Matias, L., Moulin, M., Geli, L., Klingelhofer, F., Nouze, H., Aslanian, D., Olivet, J.L., Rehault, J.P., and Sibuet, J.C. (2004). Deep structure of theWest African continental margin (Congo, Zaire, Angola), between 5°S and 8°S, from reflection/refraction seismics and gravity data: Geophysical Journal International, 158:529-553.

Crespo-Blanc, A. (2007). Superimposed folding and oblique structures in the palaeomargin-derived units of the Central Betics (SW Spain). Journal of the Geological Society, London, 164: 621-636.

Crespo-Blanc, A. and Campos, J. (2001). Structure and kinematics of the south iberian paleomargin and its relationship with the Flysch Trough Units: extensional tectonics within the Gibraltar arc fold-and-thrust belt (Western Betics). Journal of Structural Geology, 23(10):1615-1630.

Crespo-Blanc, A. and Frizon de Lamotte, D. (2006). Structural evolution of the external zones derived from the Flysch Trough and the south iberian and maghrebian paleomargins around the Gibraltar arc: a comparative study. Bulletin de la Societé Géologique de France, 177(5):267-282.

Crespo-Blanc, A., Balanyá, J. C., Expósito, I., Luján, M., and Suades, E. (2012) Crescent-like large-scale structures in the external zones of the western Gibraltar Arc (Betic–Rif orogenic wedge). Journal of the Geological Society, London, 169: 667-679.

Cruz San Julían, J. (1990). Sheet Teba, 1037. Geological map scale 1:50000, Instituto Geológico y Minero de España, Madrid.

Cuevas, J., Esteban, J., and Tubía, J. (2006). Tectonic implications of the granite dike swarm in the Ronda Peridotites (Betic Cordilleras, southern Spain). Journal of the Geological Society, 163(4):631-640.

Cuevas, J., Navarro-Vilá, F., and Tubía, J. (2001). Evolución estructural poliorogénica del complejo Maláguide (Cordilleras béticas). Boletín Geológico y Minero, 112(3):47-58.

Dahlstrom, C. (1969). Balanced cross sections. Canadian Journal of Earth Sciences, 6(4):743-757.

Darot, M. (1974). Cinematique de l'extrusion, a partir du manteau, des peridotites de la Sierra Bermeja (Serrania de Ronda, Espagne). C. R. Acad. Sci., 278: 1673-1675.

Davies, G. R., Nixon, P. H., Pearson, D. G., and Obata, M. (1993). Tectonic implications of graphitized diamonds from the Ronda, peridotite massif, southern Spain. Geology, 21(5):471-474.

Davis, M. and Kusznir, N. (2004). Depth-dependent lithospheric stretching at rifted continental margins. Proceedings of NSF Rifted Margins Theoretical Institute, 136:1-92.

De Larouziére, F. D., Bolze, J., Bordet, P., Hernandez, J., Montenat, C., and d'Estevou, P. O. (1988). The Betic segment of the lithospheric trans-Alboran shear zone during the Late Miocene. Tectonophysics, 152(1-2):41-52.

De Smet, M.E.M. (1984). Wrenching in the external zone of the Betic Cordilleras, southern Spain. Tectonophysics, 107:57-79.

Del Olmo Sanz, A., Macía de Pablo, J.G., Aldaya Valverde, F., Campos Fernández, J., Chacón Montero, J., García Rosell, V., Sanz de Galdeano, C., Orozco Fernández, M., Torres-Roldán, R. (1984). Sheet Cortes de la Frontera, 1064. Geological map scale 1:50000, Instituto Geológico y Minero de España, Madrid.

Del Olmo Sanz, A., Moreno Serrano, F., Campos Fernández, J., Estévez, A., García-Dueñas, V., García-Rossell, L., Martín-Algarra, A., Orozco Fernández, M., and Sanz de Galdeano, C. (1990). Sheet Ronda, 1051. Geological map scale 1:50000, Instituto Geológico y Minero de España, Madrid.

Dercourt, J., Zonenshain, L. P., Ricou, L. E., Karmin, V. C., Le Pichon, X., Knipper, A. L., Grandjacquet, C., Sburtshickov, I. M., Geyssant, J., Lepvrier, C., Pechersky, D. A., Boulin, J., Sibuet, J. C., Savostin, L. A., Sorokhtin, O., Westphal, M., Bazhenov, M. L., Laver, J. P., and Biju-Duval, B. (1986). Geological evolution of the Tethys belt from the Atlantic to the Pamir since the Lias. Tectonophysics, 123(1-4):241-315.

Dewey, J. F., Helman, M. L., Turco, E., Hutton, D. H. W., and Knot, S. D. (1989). Kinematics of the western Mediterranean. In Coward, M. P., Dietrich, D., and Park, R. G., editors, Conference on Alpine tectonics, Volume 45 of Geol. Soc. Lond. Spec. Pubs. Geological Society of London, London: 265-283.

Díaz-Azpiroz, M., Barcos, L., Balanyá, J. C., Fernández, C., Expósito, I., and Czeck, D. (2014). Applying a general triclinic transpression model to highly partitioned brittle-ductile shear zones: A case study from the Torcal de Antequera massif, external Betics, southern Spain. Journal of Structural Geology, 68, (B):316-336.

Díaz, J., Gallart, J. (2014) Seismic anisotropy from the Variscan core of Iberia to the Western African Craton: New constrains on upper mantle flow at regional scales, Earth and Planetary Science Letters, 394: 48-57

Didon, J., Durand-Delga, M., and Kornprobst, J. (1973). Homologies géologiques entre les deux rives du détroit de Gibraltar. Bulletin de la Societé Géologique de France, 15(2):77-105.

Doblas, M. and Oyarzun, R. (1989). Neogene extensional collapse in the Western Mediterranean (Betic-Rif alpine orogenic belt): Implications for the genesis of the Gibraltar arc and magmatic activity. Geology, 17(5):430-433.

Docherty, C. and Banda, E. (1995). Evidence for the eastward migration of the Alboran Sea based on regional subsidence analysis: A case for basin formation by delamination of the subcrustal lithosphere. Tectonics, 14 (4):804-818.

Doré, T. and Lundin, E. (2015). Research focus: Hyperextended continental margins_-knowns and unknowns. Geology, 43(1):95–96.

Duggen, S., Hoernle, K., van den Bogaard, P., and Harris, C. (2004). Magmatic evolution of the Alboran region: The role of subduction in forming the Western Mediterranean and causing the messinian salinity crisis. Earth and Planetary Science Letters, 218(1-2):91-108.

Duggen, S., Hoernle, K., van den Bogaard, P., Rupke, L., and Phipps Morgan, J. (2003). Deep roots of the Messinian salinity crisis. Nature, 422:602-606.

Durand-Delga, M. (1963). Essai sur la structure des domaines émergés autour de la méditerranée occidentale. Geol. Rundschau, 53:534-535.

Durand-Delga, M. (1980). La Méditerranée Occidentale: étapes de sa genèse et problème structuraux liés à celle-ci. Mémoire hors série de la Société Géologique de France, 10:203-224.

Egeler, C. and Simon, O. (1969). Orogenic evolution of the Betic zone (Betic Cordilleras, Spain), with emphasis on the nappe structures. Geologie en Mijnbouw, 48(3):296-305.

El Moudnib, L., Villaseñor, A., Harnafi, M., Gallart, J., Pazos, A., Serrano, I., Córdoba, D., Pulgar, J. A., Ibarra, P., Himmi, M. M. and Chourak, M. (2015). Crustal structure of the Betic-Rif system, western Mediterranean, from local earthquake tomography. Tectonophysics, 643: 94-105.

Esteban, J. J., Cuevas, J., Tubía, J., Sergeev, S., and Larionov, A. (2011). A revised Aquitanian age for the emplacement of the Ronda Peridotites (Betic Cordilleras, southern Spain). Geological Magazine, 148(01):183-187.

Esteban, J. J., Cuevas, J., Vegas, N., and Tubía, J. M. (2008). Deformation and kinematics in a melt-bearing shear zone from the Western Betic Cordilleras (southern Spain). Journal of Structural Geology, 30(3):380-393.

Esteban, J. J., Sánchez-Rodríguez, L., Seward, D., Cuevas, J., and Tubía, J. M. (2004). The late thermal history of the Ronda area, southern Spain. Tectonophysics, 389(1-2):81-92.

Esteban, J. J., Tubía, J. M., Cuevas, J., Seward, D., Larionov, A., Sergeev, S., and Navarro-Vilá, F. (2013). Insights into extensional events in the Betic Cordilleras, southern Spain: New fission-track and U-Pb SHRIMP analyses. Tectonophysics, 603:179-188.

Esteban, J.J., Cuevas, J, Tubía, J.M., Gil Ibarguchi, J.I. and Seward, D. (2005). Metamorfismo, exhumación y termocronología de la Unidad de Yunquera (Alpujárrides occidentales, Cordilleras Béticas). Revista de la Sociedad Geológica de España, 18(1-2):61-74.

Expósito, I., Balanyá, J. C., Crespo-Blanc, A., Díaz-Azpiroz, M., and Lujan, M. (2012). Overthrust shear folding and contrasting deformation styles in a multiple decollement setting, Gibraltar arc external wedge. Tectonophysics, 576-577:86-98.

Faccenna, C., Mattei, M., Funiciello, R., and Jolivet, L. (1997). Styles of back-arc extension in the Central Mediterranean. Terra Nova, 9:126-130.

Faccenna, C., Piromallo, C., Crespo Blanc, A., Jolivet, L., and Rossetti, F. (2004). Lateral slab deformation and the origin of the arcs of the western Mediterranean. Tectonics, 23: TC1012

Fadil, A., Vernant, P., McClusky, S., Reilinger, R., Gomez, F., Ben Sari, D., Mourabit, T., Feigl, K., and Barazangi, M. (2006). Active tectonics of the western mediterranean: Geodetic evidence for rollback of a delaminated subcontinental lithospheric slab beneath the Rif mountains, morocco. Geology, 34(7):529–532.

Farley, K.A., Wolf, R.A., and Silver, L.T. (1996). The effect of long alpha-stopping distances on (U-Th)/He ages. Geochimica et Cosmochimica Acta, 60: 4223-4229.

Feinberg, H., Saddiqi, O., and Michard, A. (1996). New constraints on the bending of the Gibraltar arc from paleomagnetism of the ronda peridotite (betic cordilleras, Spain). In Morris A., T. D., editor, Paleomagnetism and Tectonics of the Mediterranean Region, volume 105 of Geol. Soc. Lond. Spec. Pubs, pages 43-52. The Geological Society, London.

Felder, T.E. (1980). Geologic Evolution of the Westernmost Part of the Internal Betic Zone (Betic Cordilleras, Southern Spain). Geologische Rundschau, 69(1): 131-148

Fernández-Fernández, E.M., Jabaloy-Sánchez, A., Nieto, F., González-Lodeiro, F. (2007). Structure of the Maláguide Complex near Vélez Rubio (Eastern Betic Cordillera, SE Spain). Tectonics, 26:TC4008.

Fernández-Ibañez, F. and Soto, J. I. (2008). Crustal rheology and seismicity in the Gibraltar arc (western Mediterranean). Tectonics, 27(2):TC2007.

Fernández, M., Berástegui, X., Puig, C., García-Castellanos, D., Jurado, M. J., Torné, M., and Banks, C.(1998). Geophysical and geological constraints on the evolution of the Guadalquivir foreland basin, Spain. Geological Society, London, Special Publications, 134(1):29-48.

Flinch J.F. (1993). Tectonic evolution of the Gibraltar Arc. PhD thesis, Rice University, Houston, Texas.

Frasca, G., Gueydan, F., and Brun, J. P. (2015). Structural record of Lower Miocene westward Alboran Domain motion in the Western betics (southern Spain): Tectonophysics, (in press).

Frets, E. C., Tommasi, A., Garrido, C. J., Vauchez, A., Mainprice, D., Targuisti, K., and Amri, I. (2014). The Beni-Bousera peridotite (Rif belt, Morocco): an oblique-slip low-angle shear zone thinning the subcontinental mantle lithosphere. Journal of Petrology, 55(2):283-313.

Frizon de Lamotte, D. F., Leturmy, P., Missenard, Y., Khomsi, S., Ruiz, G., Saddiqi, O., Guillocheau, F., and Michard, A. (2009). Mesozoic and cenozoic vertical movements in the atlas system (Algeria, Morocco, Tunisia): An overview. Tectonophysics, 475(1):9-28.

Frizon de Lamotte, D., Andrieux, J., Guezou, J.-C. (1991). Cinématique des chevauchements néogènes dans l'Arc bético–rifain; discussion sur les modèles géodynamiques. Bull. Soc. Geol. France, 162(4):611-626.

García de Domingo, A., Hernaiz Huerta, P., Balanyá, J. C., and García-Dueñas, V. (1994). Sheet Algeciras, 87. Geological map scale 1:200000, Instituto Geológico y Minero de España, Madrid.

García-Castellanos, D. and Villaseñor, A. (2011). Messinian salinity crisis regulated by competing tectonics and erosion at the Gibraltar arc. Nature, 480: 359-363.

García-Castellanos, D., Fernández, M., Torné, M. (2002). Modeling the evolution of the Guadalquivir foreland basin (southern Spain). Tectonics, 21(3): 1018.

García-Dueñas, V., Balanyá, J. C., and Martínez-Martínez, J. (1992). Miocene extensional detachments in the outcropping basement of the northern Alboran basin (Betics) and their tectonic implications. Geo-Marine Letters, 12:88-95.

García-Dueñas, V., Martínez-Martínez, J., Orozco, M., and Soto, J. (1988). Plis-nappes, cisillements syn- à post-métamorphiques et cisaillements ductiles-fragiles en distension dans les Nevado-Filabrides (Cordillères Bétiques, Espagne). C. R. Acad. Sci. Paris, 307(2):1389-1395.

García-Hernández M., López-Garrido A.C., Rivas P., Sanz de Galdeano C., Vera, J.A. (1980). Mesozoic palaeogeographic evolution of the external zones of the Betic Cordillera. Geol. Mijnb. 59:155–68.

Garrido, C. J. and Bodinier, J.-L. (1999). Diversity of mafic rocks in the Ronda Peridotite: Evidence for pervasive melt–rock reaction during heating of subcontinental lithosphere by upwelling asthenosphere. Journal of Petrology, 40(5): 729-754.

Garrido, C. J., Gueydan, F., Booth-Rea, G., Précigout, J., Hidas, K., Padrón-Navarta, J. A., and Marchesi, C. (2011). Garnet lherzolite and garnet-spinel mylonite in the Ronda peridotite: Vestiges of Oligocene backarc mantle lithospheric extension in the Western Mediterranean. Geology, 39(10):927-930.

Gautheron, C., Tassan-Got, L., Barbarand, J., Pagel, M., 2009. Effect of alpha-damageannealing on apatite (U–Th)/He thermochronology. Chemical Geology, 266(3):157-170.

Goffé, B., Michard, A., García-Dueñas, V., Gonzalez-Lodeiro, F., Monié, P., Campos, J., Galindo-Zaldívar, J., Jabaloy, A., Martínez-Martínez, J. M., and Simancas, J. F. (1989). First evidence of high-pressure, low-temperature metamorphism in the Alpujárride nappes, Betic Cordilleras (SE Spain). European Journal of Mineralogy, 1(1): 139–142.

Gonzalez-Castillo, L., Galindo-Zaldivar, J., de Lacy, M., Borque, M., Martinez-Moreno, F., García-Armenteros, J., and Gil, A. (2015). Active rollback in the Gibraltar arc: Evidences from CGPS data in the western Betic Cordillera. Tectonophysics, (in press).

Gueguen, E., Doglioni, C., and Fernández, M. (1998). On the post-25 Ma geodynamic evolution of the Western Mediterranean. Tectonophysics, 298(1-3):259-269.

Guerrera, F., Martín-Algarra, A., and Martín-Martín, M. (2012). Tectono-sedimentary evolution of the 'numidian formation' and lateral facies (southern branch of the Western Tethys): constraints for Central-Western Mediterranean geodynamics. Terra Nova, 24(1):34-41.

Gueydan, F. and Précigout, J. (2014). Modes of continental rifting as a function of ductile strain localization in the lithospheric mantle. Tectonophysics, 612-613:18-25.

Gueydan, F., Morency, C., and Brun, J.-P. (2008). Continental rifting as a function of lithosphere mantle strength. Tectonophysics, 460(1-4):83-93.

Gueydan, F., Pitra P., Afiri, A., Poujol, M., Essaifi, A., and Paquette, J.-L. (2015). Oligo-Miocene thinning of the Beni Bousera peridotites and their Variscan crustal host rocks, Internal Rif, Morocco: Tectonics, (in press).

Gutscher, M.-A., Dominguez, S., Westbrook, G., Roy, P. L., Rosas, F., Duarte, J., Terrinha, P., Miranda, J., Graindorge, D., Gailler, A., Sallares, V., and Bartolome, R. (2012). The Gibraltar subduction: A decade of new geophysical data. Tectonophysics, 574-575:72-91.

Gutscher, M.-A., Malod, J., Rehault, J.-P., Contrucci, I., Klingelhoefer, F., Mendes-Victor, L., and Spakman, W. (2002). Evidence for active subduction beneath Gibraltar. Geology,30:1071-1074.

Handy, M.R., Schmid, S.M., Bousquet, R., Kissling, E., Bernoulli, D. (2010): Reconciling

plate-tectonic reconstructions with the geological-geophysical record of spreading and subduction in the Alps. Earth Science Reviews, 102, 121-158.

Hebeda, E., Boelrijk, N., Priem, H., Verdurmen, E., Verschure, R., and Simon, O. (1980). Excess radiogenic Ar and undisturbed Rb-Sr systems in basic intrusives subjected to alpine metamorphism in southeastern Spain. Earth and Planetary Science Letters, 47(1):81-90.

Hidas, K., Booth-Rea, G., Garrido, C. J., Martínez-Martínez, J. M., Padrón-Navarta, J. A., Konc, Z., Giaconia, F., Frets, E., and Marchesi, C. (2013). Backarc basin inversion and subcontinental mantle emplacement in the crust: kilometre-scale folding and shearing at the base of the proto-Alborán lithospheric mantle (Betic Cordillera, southern Spain). Journal of the Geological Society, 170(1):47-55.

Hidas, K., Varas-Reus, M. I., Garrido, C. J., Marchesi, C., Acosta-Vigil, A., Padrón-Navarta, J. A., Targuisti, K., and Konc, Z. (2015). Hyperextension of continental to oceanic-like lithosphere: The record of late gabbros in the shallow subcontinental lithospheric mantle of the westernmost Mediterranean. Tectonophysics, 650:65-79.

Houseman, G. A. and Molnar, P. (1997). Gravitational (Rayleigh-Taylor) instability of a layer with non-linear viscosity and convective thinning of continental lithosphere. Geophys. J. Int., 128:125-150.

Hurford, A. J., Platt, J. P. and Carter, A. (1999). Fission-track analysis of samples from the Alboran Sea basement. In Zahn, R., Comas, M. C. and Klaus, A., editors, Proceedings of the Ocean Drilling Program, Scientific Results, 161:295-300.

Insua-Arévalo, J.M., Martínez-Díaz, J.J., García-Mayordomo, J. and Martín-González, F. (2012). Active tectonics in the Malaga Basin: evidences from morphotectonic markers (Western Betic Cordillera, Spain). Journal of Iberian Geology, 38(1):175-190.

Iribarren, L., Vergés, J., and Fernández, M. (2009). Sediment supply from the Betic-Rif orogen to basins through Neogene. Tectonophysics, 475(1):68-84.

Jackson, S.E., Pearson, N.J., Griffin, W.L., Belousova, E.A., 2004. The application of laser ablation–inductively coupled plasma-mass spectrometry to in situ U–Pb zircon geochronology. Chemical Geology 211: 47–69.

Jiménez-Bonilla, A., Balanyá, J. C., Expósito, I., and Díaz-Azpiroz, M. (2011). Superposición de estructuras y controles tectónicos en el desarrollo del límite SW de la depresión de Ronda (Subbético y Complejo de Flyschs, Béticas). Geogaceta, 50(1):23-26.

Johanesen, K. E. and Platt, J. P. (2015). Rheology, microstructure, and fabric in a large scale mantle shear zone, Ronda Peridotite, Southern Spain. Journal of Structural Geology, 73:1-17.

Johanesen, K., Platt, J. P., Kaplan, M. S., and Ianno, A. J. (2014). A revised thermal history of the Ronda Peridotite, S. Spain: New evidence for excision during exhumation. Earth and Planetary Science Letters, 393:187-199.

Johnson, C. (1997). Resolving denudational histories in orogenic belts with apatite fission-track thermochronology and structural data: an example from southern Spain. Geology, 25(7):

623-629.

Johnson, C., Harbury, N., and Hurford, A. J. (1997). The role of extension in the Miocene denudation of the Nevado-Filábride complex, Betic Cordillera (SE Spain). Tectonics, 16(2):189-204.

Jolivet L., Faccenna, C. and Piromallo, C. (2009). From mantle to crust: Stretching the Mediterranean. Earth Planet. Sci. Lett., 285:198-209.

Jolivet, L., and Brun, J.-P. (2008). Cenozoic geodynamic evolution of the Aegean. International Journal of Earth Sciences, 99:109-138.

Jolivet, L., Augier, R., Robin, C., Suc, J.-P., and Rouchy, J. M. (2006). Lithospheric-scale geodynamic context of the Messinian salinity crisis. Sedimentary Geology, 188–189:9–33.

Jolivet, L. and Faccenna, C. (2000). Mediterranean extension and the Africa-Eurasia collision. Tectonics, 19:1095-1106.

Jolivet, L., Faccenna, C., Huet, B., Labrousse, L., Pourhiet, L. L., Lacombe, O., Lecomte, E., Burov, E., Denéle, Y., Brun, J.-P., Philippon, M., Paul, A., Salaün, G., Karabulut, H., Piromallo, C., Monié, P., Gueydan, F., Okay, A. I., Oberhänsli, R., Pourteau, A., Augier, R., Gadenne, L., and Driussi, O. (2013). Aegean tectonics: Strain localisation, slab tearing and trench retreat. Tectonophysics, 597-598:1-33.

Kirker, A. and Platt, J. P. (1998). Unidirectional slip vectors in the Western Betic Cordillera: implications for the formation of the Gibraltar arc. Journal of the Geological Society, 155(1):193-207.

Kornprobst, J. (1974). Contribution à l'étude pétrographique et structurale de la Zone Interne du Rif (Maroc septentrional). Geological Service of Morocco. 251:1-256.

Kornprobst, J. (1976). Signification structurale des péridotites dans l'orogéne Bético-Rifain: arguments tirés de l'étude des détritus observés dans les sédiments Paléozoïque. Bulletin de la Societé Géologique de France, 3:607-618.

Koulali, A., Ouazara, D., Tahayt, A., King, R. W., Vernant, P., Reilinger, R., McClusky, S., Mourabit, T., Davila, J. M., and Amraouih, N. (2011). New GPS constraints on active deformation along the Africa-Iberia plate boundary. Earth Planet. Sci. Lett., 308:211-217.

Lavier, L. L. and Manatschal, G. (2006). A mechanism to thin the continental lithosphere at magma-poor margins. Nature, 440(7082):324–328.

Lavier, L. L., Roger Buck, W., and Poliakov, A. N. B. (1999). Self-consistent rolling-hinge model for the evolution of large-offset low-angle normal faults. Geology, 27(12):1127-1130.

Le Pichon, X. and Angelier, J. (1981). The Aegean Sea. Philos. Trans. R. Soc. Lond, 300(A):357-372.

Leblanc, D. (1990). Tectonic adaptation of the external zones around the curved core of an orogen: the Gibraltar arc. Journal of Structural Geology, 12(8):1013-1018.

Lenoir, X., Garrido, C.J., Bodinier, J.L., Dautria, J.M., and Gervilla, F. (2001). The recrystallization front of the Ronda peridotite: Evidence for melting and thermal erosion of subcontinental lithospheric mantle beneath the Alboran basin: Journal of Petrology, 42:141-158.

Levander, A., Bezada, M. J., Niu, F., Humphreys, E. D., Palomeras, I., Thurner, S. M., Masy, J., Schmitz, M., Gallart, J., Carbonell, R., and Miller, M. S. (2014). Subduction-driven recycling of continental margin lithosphere. Nature. 515(7526):253-256.

Lister, G., Etheridge, M., and Symonds, P. (1986). Detachment faulting and the evolution of passive continental margins. Geology, 14(3):246-250.

Lonergan, L. and Platt, J. P. (1995). The Malaguide-Alpujarride boundary: a major extensional contact in the Internal Zone of the eastern Betic Cordillera, SE Spain. J. Struct. Geol. 17:1655-1671

Lonergan, L. and White, N. (1997). Origin of the Betic-Rif mountain belt. Tectonics, 16:504-522.

Loomis, T.P. (1972). Contact metamorphism of pelitic rock by the Ronda ultramafic intrusion, southern Spain. Geological Society of America Bulletin, 83:2449-2474.

López-Garrido, A. C. and Sanz de Galdeano, C. (1999). Neogene sedimentation and tectonic-eustatic control of the Malaga basin, south Spain. Journal of Petroleum Geology, 22(1):81-96.

Ludwig, K.R. (2001). Isoplot/Ex rev. 2.49: Berkeley. California, Berkeley Geochronology Center, Special Publication A, 1: 56.

Luján, M., Crespo-Blanc, A., and Balanyá, J. (2006). The Flysch Trough thrust imbricate (Betic Cordillera): a key element of the Gibraltar arc orogenic wedge. Tectonics, 25:TC6001.

Lundeen, M. (1978). Emplacement of the ronda peridotite, Sierra Bermeja, Spain. GeologicalSociety of America Bulletin, 89:172-180.

Malinverno, A. and W. Ryan (1986). Extension in the Tyrrhenian Sea and shortening in the Apennines as result of arc migration driven by sinking of the lithosphere. Tectonics, 5:227-245.

Manatschal, G. (2004). New models for evolution of magma-poor rifted margins based on a reviewof data and concepts from West Iberia and the Alps. International Journal of Earth Sciences. 93:432-466.

Manatschal, G., Froitzheim, N., Rubenach, M., and Turrin, B. (2001). The role of detachment faulting in the formation of an ocean-continent transition: insights from the iberia abyssal plain. Geological Society, London, Special Publications, 187(1):405-428.

Marchesi, C., Garrido, C. J., Bosch, D., Bodinier, J.-L., Hidas, K., Padrón-Navarta, J.A., and Gervilla, F. (2012) A Late Oligocene Suprasubduction Setting in the Westernmost Mediterranean Revealed by Intrusive Pyroxenite Dikes in the Ronda Peridotite (southern

Spain). The Journal of Geology, 120, (2): 237-247.

Marrett, R. and Allmendinger, R. W. (1990). Kinematic analysis of fault-slip data. Journal of structural geology, 12(8):973–986.

Martín-Algarra, A. (1987). Evolución geológica alpina del contacto entre las Zonas Internas y las Zonas Externas de la Cordillera Bética. PhD thesis, Universidad de Granada.

Martín-Algarra, A. and Checa, A. (1990). Rellenos pelágicos Jurásicos en el interior del Permotrías de la Unidad de Montecorto (Cordillera Bética, provincia de Cádiz y Málaga)

Martín-Algarra, A. and Vera, J. A. (2004). El Subbético del sector occidental. In Vera, J.A., editor, Geología de España, Capítulo IV: 375–377. SGE-IGME, Madrid.

Martín-Algarra, A. and Estévez, A. (1984). La brèche de la Nava: dépôt continental synchrone de la structuration pendant le Miocène inférieur des Zones Internes de l'ouest des Cordillères Bétiques. C. R. Acad. Sci. Paris, 299: 463-466.

Martín-Algarra, A., Andreo, B., Balanyá, J. C., Estévez, A. C., López-Garrido, A. C., O'Dogherty, L., and García-Dueñas, V. (2004a) Unidades Frontales de las Zonas Internas. . In Vera, J.A., editor, Geología de España, Capítulo IV: 396-401. SGE-IGME, Madrid.

Martín-Algarra, A., Balanyá, J. C., Crespo-Blanc, A., Esteras, M., Luján M., Martín-Algarra A., Martín-Martín (2004b). Complejo del Campo de Gibraltar. In Vera, J.A., editor, Geología de España, Capítulo IV: 389–395. SGE-IGME, Madrid.

Martín-Algarra, A., Mazzoli, S., Perrone, V., Rodríguez-Cañero, R., and Navas-Parejo, P. (2009). Variscan tectonics in the Malaguide complex (Betic Cordillera, southern Spain): stratigraphic and structural alpine vs. pre-alpine constraints from the Ardales area (province of Malaga). Part I: Stratigraphy. Journal of Geology, 117:241-262.

Martin-Rojas, I., Somma, R., Delgado, F., Estévez, A., Iannace, A., Perrone, V., and Zamparelli, V. (2009). Triassic continental rifting of pangaea: direct evidence from the Alpujarride carbonates, Betic Cordillera, SE Spain. Journal of the Geological Society, 166(3):447-458.

Martin-Rojas, I., Somma, R., Estévez, A., Delgado, F., and Zamparelli, V. (2014). La plataforma Triásica Alpujárride (Zonas Internas de la Cordillera bética, españa). Revista de la Sociedad Geológica de España, 27(1):63-78.

Martín, J. M., Braga, J. C., and Betzler, C. (2001). The messinian Guadalhorce corridor: the last northern, Atlantic-Mediterranean gateway. Terra Nova, 13(6): 418-424.

Martínez-García, P., Comas, M., Soto, J. I., Lonergan, L., and Watts, A. B. (2013). Strike-slip tectonics and basin inversion in the Western Mediterranean: the post-Messinian evolution of the Alboran Sea. Basin Research, 25:1-27.

Martínez-Martínez, J. M., Booth-Rea, G., Azañón, J. M., Torcal F. (2006). Active transfer fault zone linking a segmented extensional system (Betics, southern Spain): insight into heterogeneous extension driven by edge delamination. Tectonophysics, 422:159-173.

Martínez-Martínez, J. M., Soto, J.I. and Balanyá, J.C. (2002). Orthogonal folding of extensional detachments: structure and origin of the Sierra Nevada elongated dome (Betics, SE Spain). Tectonics, 21: TC1012.

Martínez-Martínez, J. M., Torres-Ruiz, J., Pesquera, A., and Gil-Crespo, P. (2010). Geological relationships and U-Pb zircon and 40Ar/39Ar tourmaline geochronology of gneisses and tourmalinites from the Nevado-Filabride complex (western Sierra Nevada, Spain): Tectonic implications. Lithos, 119(3-4):238-250.

Mattei, M., Cifelli, F., Martín Rojas, I., Crespo Blanc, A., Comas, M., Faccenna, C., and Porreca, M. (2006). Neogene tectonic evolution of the Gibraltar arc: new paleomagnetic constrains from the Betic chain. Earth Planet. Sci. Lett., 250:522-540.

Mazzoli, S. and Helman, M. L. (1994). Neogene patterns of relative plate motion for Africa-Europe: some implications for recent central Mediterranean tectonics. Geol. Rundsch., 83:464-468.

Mazzoli, S. and Martín-Algarra, A. (2011). Deformation partitioning during transpressional emplacement of a 'mantle extrusion wedge': the Ronda peridotites, Western Betic Cordillera, Spain. Journal of the Geological Society of London, 168:373-382.

Mazzoli, S., Martín-Algarra, A., Reddy, S., Sánchez-Vizcaíno, V. L., Fedele, L., and Noviello, A. (2013). The evolution of the footwall to the ronda subcontinental mantle peridotites: insights from the Nieves Unit (Western Betic Cordillera). Journal of the Geological Society of London, 170:385-402.

McClay, K.R. (1987). In: Cox, K. (ed.) The Mapping of Geological Structures. Geological Society, London, Professional Handbook Series, 1572.

Meijninger, B.M.L. and Vissers, R.L.M. (2006). Miocene extensional basin development in the Betic Cordillera, SE Spain revealed through analysis of the Alhama de Murcia and Crevillente Faults. Basin Res., 18:547-571.

Michard, A., Mokhtari, A., Chalouan, A., Saddiqi, O., Rossi, P., and Rjimati, E.-C. (2014). New ophiolite slivers in the External Rif belt, and tentative restoration of a dual Tethyan suture in the western Maghrebides. Bulletin de la Societe Geologique de France, 185(5):313-28.

Mohn G., Manatschal G., Müntener O., Beltrando M., Masini E. (2010). Unravelling The Interaction Between Tectonic And Sedimentary Processes During Lithospheric Thinning In The Alpine Tethys Margins. Int. J. Earth Sci., 99:75-101.

Mohn, G., Manatschal, G., Beltrando, M., Masini, E., Kusznir, N. (2012). Necking of continental crust in magma-poor rifted margins: evidence from the fossil Alpine Tethys margins. Tectonics, 31.

Monié, P., Galindo-Zaldívar, J., Lodeiro, F. G., Goffé, B., and Jabaloy, A. (1991). 40Ar/39Ar geochronology of alpine tectonism in the Betic Cordilleras (southern Spain). Journal of the Geological Society, 148(2):289-297.

Monié, P., Torres-Roldán, R., and García-Casco, A. (1994). Cooling and exhumation of the Western Betic Cordillera, 40Ar/39Ar thermochronological constraints on a collapsed terrane. Tectonophysics, 238(1-4):353-379.

Montel, J.-M., Kornprobst, J., and Vielzeuf, D. (2000). Preservation of old U-Th-Pb ages in shielded monazite: example from the Beni-Bousera hercynian kinzigites (Morocco). Journal of Metamorphic Geology, 18(3):335-342.

Montenat, C. and Ott d'Estevou, P. (1999). The diversity of Late Neogene sedimentary basins generated by wrench faulting in the Eastern Betic Cordillera, SE Spain. Journal of Petroleum Geology, 22:61-80.

Morel, J.L. and Meghraoui, M. (1996). Goringe–Alboran–Tell tectonic zone; a transpression system along the Africa–Eurasia plate boundary. Geology 24 (8): 755–758.

Moreno Serrano, F., Campos Fernández, J., García Rosell, V., Orozco Fernández, M., Sanz de Galdeano, C. (1991). Sheet Ubrique, 1050. Geological map scale 1:50000, Instituto Geológico y Minero de España, Madrid.

Moulin M., Aslanian D., Olivet J.L., Klingelhoefer F., Nouzé H., Rehault J.P., Unterneuhr P. (2005). Geological constraints on the evolution of the angolan margin based on reflection and refraction seismic data (Zaïango Project). Geophys. J. Int., 162:793-810.

Nagel, T. J. and Buck, W. R. (2004). Symmetric alternative to asymmetric rifting models. Geology, 32(11):937-940.

Navarro-Vilá, F. and Tubía, J. (1983). Essai d'une nouvelle différenciation des nappes Alpujarrídes dans le secteur occidental des Cordilléres Bétiques (Andalousie, Espagne). C. R. Acad. Sci. Paris, 296:111-114.

Negro, F., Beyssac, O., Goffé, B., Saddiqi, O., and Bouybaouéne, M. L. (2006). Thermal structure of the Alboran Domain in the Rif (northern Morocco) and the Western Betics (southern Spain). Constraints from Raman spectroscopy of carbonaceous material. Journal of Metamorphic Geology, 24 (4):309-327.

O'Dogherty, L., Martín-Algarra, A., Gursky, H., and Aguado, R. (2001). The Middle Jurassic radiolarites and pelagic limestones of the Nieves Unit (Rondaide complex, Betic Cordillera): basin starvation in a rifted marginal slope of the Western Tethys. Geologische Rundschau, 90:831-846.

Obata, M. (1980). The Ronda peridotite: garnet-, spinel-, and plagioclase-lherzolite facies and the P-T trajectories of a high-temprature mantle intrusion. Journal of Petrology, 21(3):533-572.

Olivier, P. (1981). L'accident de Jebha-Chrafate (Rif, Maroc). Revue de Géographie Physique et Géologie Dynamique, 23:27-106.

Olivier, P. (1984). Evolution de la limite entre Zones Internes et Zones Externes dans l'arc de Gibraltar (Maroc, Espagne). PhD thesis, Université de Toulouse.

Olivier, P. and Leblanc, D. (1984). The role of strike-slip faults in the Betic-Rifian orogeny. Tectonophysics, 101:345-355.

Orozco, M. and Alonso-Chaves, F. (2012). Kilometre-scale sheath folds in the western Betics (south of Spain). Geologische Rundschau, 101:505-519.

Osete, M., Freeman, R., Vegas, R. (1988). Preliminary palaeomagnetic results from the Subbetic zone (Betic Cordillera, Southern Spain): kinematic and structural implications. Phys. Earth Planet. Inter. 52(3):283-300.

Osete, M., Villalaín, J., Palencia, A., Osete, C., Sandoval, J., García-Dueñas, V. (2004). New palaeomagnetic data from the Betic Cordillera: constraints on the timing and the geographical distribution of tectonic rotations in southern Spain. In: Geodynamics of Azores–Tunisia. Springer: 701-722.

Osmundsen, P. T., and Ebbing, J. (2008). Styles of extension offshore mid-Norway and implications for mechanisms of crustal thinning at passive margins. Tectonics, 27:TC6016.

Pacquet, J. (1969). Étude géologique de l'ouest de la province de Murcie (Espagne). Mém. Soc. Géol. Fr., 48(111):1-270.

Padrón-Navarta, J., López Sánchez-Vizcaíno, V., Garrido, C., Gómez-Pugnaire, M., Jabaloy, A., Capitani, G., and Mellini, M. (2008). Highly ordered antigorite from Cerro del Almirez HP-HT serpentinites, SE Spain. Contributions to Mineralogy and Petrology, 156(5):679-688.

Palano, M., González, P. J., and Fernández, J. (2013). Strain and stress fields along the Gibraltar orogenic arc: Constraints on active geodynamics. Gondwana Research, 23(3):1071-1088.

Palomeras, I., Thurner, S., Levander, A., Liu, K., Villasenor, A., Carbonell, R., and Harnafi, M. (2014). Finite-frequency Rayleigh wave tomography of the western Mediterranean: Mapping its lithospheric structure. Geochemistry, Geophysics, Geosystems, 15(1):140-160.

Pearson, D.G. and Nowell, G.M. (2004). Re-Os and Lu-Hf isotope constraints on the origin and age of pyroxenites from the Beni Bousera peridotite massif implications for mixed peridotite pyroxenite mantle sources. Journal of Petrology, 45: 439-455.

Pearson, D.G., Davies, G.R., Nixon, P.H., and Milledge, H.J. (1989). Graphitized diamonds from a peridotite massif in Morocco and implications for anomalous diamond occurrences: Nature, 335:60-63.

Pedrera, A., Marín-Lechado, C., Martos-Rosillo, S. and Roldán, F.J. (2012). Curved fold-and-thrust accretion during the extrusion of a synorogenic viscous allochthonous sheet: The Estepa Range (External Zones, Western Betic Cordillera, Spain). Tectonics, 31 : TC4013.

Pedrera, A., Ruiz-Constán, A., Galindo-Zaldívar, J., Chalouan, A., Sanz de Galdeano, C., Martín-Lechado, C., Ruano, P., Benmakhlouf, M., Akil, M., López-Garrido, A., Chabli, A., Ahmamou, M., and González-Castillo, L. (2011). Is there an active subduction beneath the Gibraltar orogenic arc? Constraints from Pliocene to present-day stress field. Journal of

Geodynamics, 52(2):83-96.

Pérez-Valera, L. A., Rosenbaum, G., Sánchez-Gómez, M., Azor, A., Fernández-Soler, J. M., Pérez-Valera, F. and Vasconcelos P. M. (2013). Age distribution of lamproites along the Socovos Fault (southern Spain) and lithospheric scale tearing. Lithos, 180-181: 252-263.

Péron-Pinvidic, G. and Manatschal, G. (2009). The Final Rifting Evolution At Deep Magma-Poor Passive Margins From Iberia-Newfoundland: A New Point Of View. Int. J. Earth Sci., 98:1581-1597.

Péron-Pinvidic, G., Manatschal, G., Minshull, T. A. and Sawyer, D. S. (2007). Tectonosedimentary evolution of the deep Iberia-Newfoundland margins: Evidence for a complex breakup history. Tectonics, 26:1-29.

Pérouse, E., Vernant, P., Chéry, J., Reilinger, R., and McClusky, S. (2010). Active surface deformation and sub-lithospheric processes in the Western Mediterranean constrained by numerical models. Geology, 38(9):823–826.

Perri, F., Critelli, S., Martín-Algarra, A., Martín-Martín, M., Perrone, V., Mongelli, G., and Zattin, M. (2013). Triassic redbeds in the Malaguide complex (Betic Cordillera, Spain): Petrography, geochemistry and geodynamic implications. Earth-Science Reviews, 117:1-28.

Peyre, Y. (1974). Géologie d'Antequera et de la région Cordillères Bétiques (Espagne). PhD thesis, University of Paris, France. 528 pp.

Piles Mateo, E., Chamón Cobos, C., Estevéz González, C., Crespo, V., Aguilar, M., and Reyes, J.L. (1972a). Sheet Marbella, 1065. Geological map scale 1:50000, Instituto Geológico y Minero de España, Madrid.

Piles Mateo, E., Estevéz González, C., Barba Martín, A. (1972b). Sheet Coín, 1066. Geological map scale 1:50000, Instituto Geológico y Minero de España, Madrid.
Pineda, A. (1983). Sheet Archidona, 1024. Geological map scale 1:50000, Instituto Geológico y Minero de España, Madrid.

Piromallo C., and A. Morelli (2003), P-wave tomography of the mantle under the Alpine-Mediterranean area, J. Geophys. Res., 108, B2, 2065

Platt, J. P. (1998). Comment on "Alternating contractional and extensional events in the Alpujarride nappes of the Alboran Domain (Betics, Gibraltar arc)" by J.C. Balanyá et al. Tectonics, 17(6):973-976.

Platt, J. P. and Vissers, R. L. M. (1989). Extensional collapse of thickened continental lithosphere: A working hypothesis for the Alboran Sea and Gibraltar arc. Geology, 17:540-543.

Platt, J. P., Allerton, S., Kirker, A., Mandeville, C., Mayfield, A., Platzman, E., and Rimi, A. (2003a). The ultimate arc: Differential displacement, oroclinal bending, and vertical axis rotation in the External Betic-Rif arc. Tectonics, 22(3):1017. doi: 10.1029/2001TC001321

Platt, J. P., Anczkiewicz, R., Soto, J.-I., Kelley, S. P., and Thirlwall, M. (2006). Early

Miocene continental subduction and rapid exhumation in the western Mediterranean. Geology, 34(11):981-984.

Platt, J. P., and Whitehouse, M. (1999). Early Miocene high-temperature metamorphism and rapid exhumation in the Betic Cordillera (Spain): evidence from U-Pb zircon ages. Earth and Planetary Science Letters, 171(4):591-605.

Platt, J. P., Argles, T., Carter, A., Kelley, S., Whitehouse, M., and Lonergan, L. (2003a). Exhumation of the Ronda peridotite and its crustal envelope: constraints from thermal modelling of a P-T-time array. Journal of the Geological Society, 160(5):655-676.

Platt, J. P., Behr, W. M., Johanesen, K., and Williams, J. R. (2013). The Betic-Rif arc and its orogenic hinterland: A review. Annual Review of Earth and Planetary Sciences, 41(1):313-357.

Platt, J. P., Behrmann, J., Martínez, J.-M., and Vissers, R. L. M. (1984). A zone of mylonite and related ductile deformation beneath the Alpujarride nappe complex, Betic Cordilleras, S. Spain. Geologische Rundschau, 73(2):773-785.

Platt, J. P., Houseman, G., Gutscher, M.-A., Malod, J., Rehault, J.-P., Contrucci, I., Klingelhoefer, F., Mendes-Victor, L., and Spakman, W. (2003c). Evidence for active subduction beneath Gibraltar: Comment and Reply. Geology, 31(1): 22-23.

Platt, J. P., Kelley, S., Carter, A., and Orozco, M. (2005). Timing of tectonic events in the Alpujárride complex, Betic Cordillera, southern Spain. Journal of the Geological Society, 162(3):451-462.

Platt, J. P., Whitehouse, M., Kelley, S., Carter, A., and Hollick, L. (2003b). Simultaneous extensional exhumation across the Alboran Basin: implications for the causes of late orogenic extension. Geology, 31(3):251-254.

Platt, J., Allerton, S., Kirker, A., and Platzman, E. (1995). Origin of the western subbetic arc (south Spain): palaeomagnetic and structural evidence. Journal of Structural Geology, 17(6):765–775.

Platt, J., Kelley, S., Carter, A., and Orozco, M. (2005). Timing of tectonic events in the alpuj´arride complex, betic cordillera, southern Spain. Journal of the Geological Society, 162(3):451-462.

Platt, J.P. (2007). From orogenic hinterlands to Mediterranean-style back-arc basins: A comparative analysis. Journal of the Geological Society of London, 164

Platzman, E. (1992). Paleomagnetic rotations and the kinematics of the Gibraltar Arc. Geology 20 (4):311-314.

Platzman, E. and Lowrie, W. (1992). Paleomagnetic evidence for rotation of the Iberian peninsula and the External Betic Cordillera, southern Spain. Earth and Planetary Science Letters, 108(1-3):45-60.

Platzman, E. and Platt, J. P. (2004). Kinematics of a twisted core complex: Oblique axis

rotation in an extended terrane (betic cordillera, southern Spain). Tectonics, 23(6): TC6010.

Platzman, E. S., Platt, J., Kelley, S., and Allerton, S. (2000). Large clockwise rotations in an extensional allochthon, Alboran domain (southern Spain). Journal of the Geological Society, 157(6):1187-1197.

Platzman, E., Platt, J., Olivier, P. (1993). Palaeomagnetic rotations and fault kinematics in the Rif Arc of Morocco. J. Geol. Soc. 150 (4):707-718.

Prada, M., Sallares, V., Ranero, C. R., Vendrell, M. G., Grevemeyer, I., Zitellini, N., and de Franco, R. (2014). Seismic structure of the central Tyrrhenian basin: Geophysical constraints on the nature of the main crustal domains. Journal of Geophysical Research: Solid Earth, 119(1): 52-70.

Précigout, J., Gueydan, F., Gapais, D., Garrido, C., and Essaifi, A. (2007). Strain localisation in the subcontinental mantle - a ductile alternative to the brittle mantle. Tectonophysics, 445(3-4):318-336.

Précigout, J., Gueydan, F., Garrido, C. J., Cogné, N., and Booth-Rea, G. (2013). Deformation and exhumation of the Ronda peridotite (Spain). Tectonics, 32(4):1011-1025.

Priem, H. N. A., Boelrijk, N. A. I. M.,Hebeda, E. H., Oen, I. S., Verdurmen, E. A. Th. and Verschure, R.H. (1979). Isotopic dating of the emplacement of the ultramafic masses in the Serrania de Ronda. Contributions to Mineralogy and Petrology, 70:103-9.

Puga, E., de Federico, A. D., and Demant, A. (1995). The eclogitized pillows of the betic ophiolitic association: relics of the tethys ocean floor incorporated in the alpine chain after subduction. Terra Nova, 7(1):31–43.

Puga, E., Fanning, M., de Federico, A. D., Nieto, J. M., Beccaluva, L., Bianchini, G., and Puga, M. A. D. (2011). Petrology, geochemistry and U-Pb geochronology of the Betic ophiolites: Inferences for Pangaea break-up and birth of the westernmost Tethys ocean. Lithos, 124(3-4):255-272.

Puga, E., Nieto, J., Díaz de Federico, A., Bodinier, J., and Morten, L. (1999). Petrology and metamorphic evolution of ultramafic rocks and dolerite dikes of the Betic ophiolite association (Mulhacen complex, SE Spain): evidence of eo-alpine subduction following an ocean- floor metasomatic process. Lithos, 49:23-56.

Ranero, C., and Pérez-Gussinyé, M. (2010). Sequential faulting explains the asymmetry and extension discrepancy of conjugate margins. Nature, 468(7321): 294-299.

Rebai, S., Philip,H., Taboada, A. (1992). Modern tectonic stress field in theMediterranean region: evidence for variation in stress directions at different scales. Geophysical Journal International 110:106–140.

Rehault, J.-P., Boillot, G., and Mauffret, A. (1985). The western Mediterranean Basin. In Stanley, D.J., and Wezel, F.C., editors, Geological evolution of the Mediterranean Basin, Berlin/Heidelberg, Springer: 101-129.

Reston, T.J. (2007). The extension discrepancy at North Atlantic non-volcanic rifted margins: depth-dependent stretching or unrecognised faulting?. Geology, 35 :367-370.

Reuber, I., Michard, A., Chalouan, A., Juteau, T., Jermoumi, B. (1982). Structure and emplacement of the alpine-type peridotites from Beni Bousera, Rif, Morocco: a polyphase tectonic interpretation. Tectonophysics, 82(3), 231-251.

Romagny, A., Münch, Ph., Cornée, J.-J., Corsini, M., Azdimousa, A., Melinte-Dobrinescu, M.C., Drinia, H., Bonno, M., Arnaud, N., Monié, P., Quillévéré, F. and Ben Moussa, A. (2014). Late Miocene to present-day exhumation and uplift of the Internal Zone of the Rif chain: Insights from low temperature thermochronometry and basin analysis. Journal of Geodynamics, 77:39-55.

Rosas, F., Duarte, J., Schellart, W., Tomás, R., Grigorova, V., and Terrinha, P. (2015). Analogue modelling of different angle thrust-wrench fault interference in a brittle medium. Journal of Structural Geology, 74:81-104.

Rosenbaum, G. (2014). Geodynamics of oroclinal bending: Insights from the Mediterranean. Journal of Geodynamics, 82:5-15.

Rosenbaum, G. and Lister, G. S. (2004). Formation of arcuate orogenic belts in the western Mediterranean region. Geological Society of America Special Papers, 383:41-56.

Rosenbaum, G., Lister, G. S., Duboz, C., et al. (2002). Reconstruction of the tectonic evolution of the Western Mediterranean since the Oligocene. Journal of the Virtual Explorer, 8:107-130.

Rossetti, F., Dini, A., Lucci, F., Bouybaouenne, M., and Faccenna, C. (2013). Early Miocene strike-slip tectonics and granite emplacement in the Alboran Domain (Rif chain, Morocco): significance for the geodynamic evolution of Western Mediterranean. Tectonophysics, 608: 774-791.

Rossetti, F., Faccenna, C., and Crespo-Blanc, A. (2005). Structural and kinematic constraints of the Alpujarride complex (central Betic Cordillera, Spain). J. Struct. Geol., 27:199-216.

Rossetti, F., Theye, T., Lucci, F., Bouybaouene, M. L., Dini, A., Gerdes, A., Phillips, D., and Cozzupoli, D. (2010). Timing and modes of granite magmatism in the core of the Alboran domain, Rif chain, Northern Morocco: Implications for the alpine evolution of the western Mediterranean. Tectonics, 29(2):TC6011.

Royden, L. H. (1993). Evolution of retreating subduction boundaries formed during continental collision. Tectonics, 12:629-638.

Ruiz Cruz, M. D. and Sanz de Galdeano, C. (2014). Garnet variety and zircon ages in UHP meta-sedimentary rocks from the Jubrique Zone (Alpujárride complex, Betic Cordillera, Spain): evidence for a pre-alpine emplacement of the Ronda Peridotites. International Geology Review, 56(7):845-868.

Ruiz-Constán, A., Galindo-Zaldívar, J., Pedrera, A., and Sanz de Galdeano, C. (2009). Gravity anomalies and orthogonal box fold development on heterogeneous basement in the

neogene Ronda depression (Western Betic Cordillera). Journal of Geodynamics, 47(4):210-217.

Ruiz-Constán, A., Pedrera, A., Galindo-Zaldívar, J., Pous, J., Arzate, J., Roldán-García, F., Marin-Lechado, C., and Anahnah, F. (2012a). Constraints on the frontal crustal structure of a continental collision from an integrated geophysical research: The central-Western Betic Cordillera (SW Spain). Geochemistry, Geophysics, Geosystems, 13(8): Q08012.

Ruiz-Constán, A., Pedrera, A., Galindo-Zaldívar, J., Stich, D., Morales, J. (2012b). Recent and active tectonics in the western part of the Betic Cordillera. Journal of Iberian Geology, 38(1):161-174.

Rutter, E., Faulkner, D., and Burgess, R. (2012). Structure and geological history of the Carboneras fault zone, SE Spain: Part of a stretching transform fault system. Journal of Structural Geology, 45:68-86.

Sánchez-Gómez, M., Azañón, J. M., García-Dueñas, V. and Sanz de Galdeano, C. (2004). Geología de Ceuta y Melilla (y áreas adyacentes). In Vera, J.A., editor, Geología de España, Capítulo IV (4.6): 444-449. SGE-IGME, Madrid.

Sánchez-Gómez, M., Azañón, J. M., García-Dueñas, V., and Soto, J. I. (1999). Correlation between metamorphic rocks recovered from site 976 and the Alpujárride rocks of the Western Betics. In Zahn, R., Comas, M. C. and Klaus, A., editors, Proceedings of the Ocean Drilling Program, Scientific Results, 307-317.

Sánchez-Gómez, M., Balanyá, J. C., García-Dueñas, V., and Azañón, J. M. (2002). Intracrustal tectonic evolution of large lithosphere mantle slabs in the western end of the Mediterranean orogen (Gibraltar arc). Journal of the Virtual Explorer, 8:23-34.

Sánchez-Gómez, M., García-Dueñas, V., and Muñoz, M. (1995). Relations structurales entre les Péridotites de la Sierra Bermeja et les unités alpujarrides sous-jacentes (Benahavís, Ronda, Espagne). C. R. Acad. Sci., 321(2):885-892.

Sánchez-Navas, A., García-Casco, A. and Martín-Algarra, A. (2014). Pre-Alpine discordant granitic dikes in the metamorphic core of the Betic Cordillera: tectonic implications. Terra Nova, 26(6):477-486.

Sánchez-Rodríguez, L. (1998). Pre-Alpine and Alpine evolution of the Ronda Ultramafic Complex and its country-rocks (Betic chain, southern Spain): U-Pb SHRIMP zircon and fission-track dating. PhD thesis, Swiss Federal Institute of Technology Zürich.

Sánchez-Rodríguez, L. and Gebauer, D. (2000). Mesozoic formation of pyroxenites and gabbros in the Ronda area (southern Spain), followed by Early Miocene subduction metamorphism and emplacement into the middle crust: U-Pb sensitive high-resolution ion microprobe dating of zircon. Tectonophysics, 316(1-2):19-44.

Sanz de Galdeano, C. (1990). Geologic evolution of the Betic Cordilleras in the Western Mediterranean, Miocene to the present. Tectonophysics, 172(1-2):107-119.

Sanz De Galdeano, C. (1996). The E-W segments of the contact between the External and

Internal Zones of the Betic and Rif Cordillera and the E-W corridors of the Internal Zone (a combined explanation). Estudios Geológicos, 52:123-136.

Sanz De Galdeano, C. (2012). Génesis de la estructura arqueada de la Sierra de las Cabras al Gibalto (Subbético, provincias de Málaga y Granada, España). Estudios Geológicos, 68(2):179-187.

Sanz de Galdeano, C. and Andreo, B. (1995). Structure of Sierra Blanca (Alpujarride complex, west of the Betic Cordillera). Estudios Geológicos, 51:43-55.

Sanz de Galdeano, C. and López-Garrido, A.C. (2012a). Tectónica de las sierras penibéticas de Abdalajís y de Huma (provincia de Málaga, España). Su relación con el contacto con la Zona Interna. Estudios Geológicos, 69(2):133-147.

Sanz de Galdeano, C. and López-Garrido, A.C. (2012b). The Torcal de Antequera, an example of a structure formed by a large scale dextral transcurrent system. Estudios Geológicos, 68(2):189-202.

Sanz de Galdeano, C., Andreo, B., and López-Garrido, A.-C. (2001a). Comment on the paper "Late exhumation stages of the Alpujarride complex (Western Betic Cordilleras, Spain): new thermochronological and structural data on Los Reales and Ojen nappes" by Marc Sosson, Anne-Claire Morillon, Jacques Bourgois, Gilbert Féraud, Gérard Poupeau, Pierre Saint-Marc. Tectonophysics, 331(4):413-417.

Sanz de Galdeano, C., Andreo, B., García-Tortosa, F., and López-Garrido, A. C. (2001b). The Triassic paleogeographic transition between the Alpujarride and Malaguide complexes, Betic-Rif Internal Zone (S Spain, N Morocco). Palaeogeography, Palaeoclimatology, Palaeoecology, 167:157-173.

Sanz de Galdeano, C., López-Garrido, A. C., and Andreo, B. (1998). The stratigraphic and tectonic relationships of the Alpujarride and Malaguide complexes in the Western Betic Cordillera (Casares, prov. of Malaga, southern Spain). C. R. Acad. Sci. Paris, 328(2):113-119.

Sanz de Galdeano, C., Lozano, J. A., and Puga, E. (2008). El "Trías de Antequera"" naturaleza, origen y estructura. Revista de la Sociedad Geológica de España, 21(3-4):111-124.
Sanz de Galdeano, C., Serrano, F., López-Garrido, A. C. and Martín-Pérez, J. A. (1993). Paleogeography of the Late Aquitanian-Early Burdigalian Basin in the Western Betic internal zone. Geobios, 26(1):43-55.

Schettino, A. and Turco, E. (2011). Tectonic history of the Western Tethys since the late Triassic. Geological Society of America Bulletin, 123(1-2):89-105.

Seber, D., M. Barazangi, A. Ibenbrahimt, and B. Ahmed (1996), Geophysical evidence for lithospheric delamination beneath the Alboran Sea and Rif-Betic mountains. Nature, 379: 785–790.

Serrano, F., Guerra-Merchán, A., Kadiri, K. E., Sanz de Galdeano, C., López-Garrido, A. C., Martín-Martín, M., and Hlila, R. (2007). Tectono-sedimentary setting of the Oligocene-Early Miocene deposits on the Betic-Rifian Internal Zone (Spain and Morocco). Geobios, 40(2):191-205.

Shuster, D. M., Flowers, R. M. and Farley, K. A. (2006). The influence of natural radiation damage on Helium diffusion kinetics in apatite. Earth and Planetary Science Letters, 249: 148-161.

Simancas, J. F. and Campos, J. (1993). Compresión NNW-SSE tardi a postmetámorfica y extension subordinada en el Complejo Alpujárride (Dominio de Alborán, Orógeno Bético). Revista de la Sociedad Geológica de España, 6(1-2):23-35.

Soria, J. M. (1994). Rocas volcanoclasticas submarinas de edad Burdigaliense Inferior en el sector del Mencal (Zona Subbetica, Cordillera Betica central). Contexto sedimentario y tectonico. Estudios Geológicos, SO:169-178.

Sosson, M., Morrillon, A.-C., Bourgois, J., Féraud, G., Poupeau, G., and Saint-Marc, P. (1998). Late exhumation stages of the Alpujarride complex (western Betic Cordilleras, Spain): new thermochronological and structural data on Los Reales and Ojen nappes. Tectonophysics, 285(3-4):253-273.

Soto, J. I. and Gervilla, F. (1991). Los macizos ultramáficos de Sierra de las Aguas y Sierra de la Robla como una ventana extensional (Béticas occidentales). Geogaceta, 9, 21-23.

Soustelle, V., Tommasi, A., Bodinier, J.L., Garrido, C.J., Vauchez, A. (2009). Deformation and reactive melt transport in the mantle lithosphere above a large-scale partial melting domain: the Ronda Peridotite Massif, southern Spain. J. Petrol. 50:1235–1266.

Spakman, W. and Wortel, R. (2004). A tomographic view on the Western Mediterranean geodynamics. In Cavazza, W., Roure, F., Spakman, W., Stampfli, G., and Ziegler, P., editors, The TRANSMED Atlas. The Mediterranean Region from Crust to Mantle, Berlin/Heidelberg. Springer:31-52.

Stromberg, S. G. and Bluck, B. (1998). Turbidite facies, fluid-escape structures and mechanisms of emplacement of the oligo-miocene Aljibe Flysch, Gibraltar arc, betics, southern Spain. Sedimentary Geology, 115(1-4):267-288.

Suades, E., Comas, M. and Crespo-Blanc, A. (2013). Tectonic evolution of the Malaga Basin (Alboran Sea): insights from its sedimentary infill. Geogaceta, 54:87-90.

Suades, E. and Crespo-Blanc, A. (2013). Gravitational dismantling of the Miocene mountain front of the Gibraltar Arc system deduced from the analysis of an olistostromic complex. Geologica Acta, 11(2):215-229.

Thurner, S., Palomeras, I., Levander, A., Carbonell, R., and Lee, C.-T. (2014). Ongoing lithospheric removal in the western Mediterranean: Evidence from Ps receiver functions and thermobarometry of Neogene basalts (PICASSO Project). Geochemistry, Geophysics, Geosystems, 15(4):1113–1127.

Thurow, J. and Kuhnt, W. (1986). Mid-Cretaceous of the Gibraltar arc area. Geological Society, London, Special Publications, 21(1):423-445.

Torné, M., Banda, E., García-Dueñas, V., and Balanyá, J. (1992). Mantle-lithospheric bodies

in the Alboran crustal domain (Ronda peridotites, Betic-Rif orogenic belt). Earth Planet. Sci. Lett., 110:163-171.

Torné, M., Fernández, M., Comas, M. and Soto, J. (2000). Lithospheric structure beneath the Alborán Basin: results from 3D gravity modeling and tectonic relevance. J. Geophys. Res. 105:3209-3228.

Torres-Roldán, R. L. (1979). The tectonic subdivision of the Betic Zone (Betic Cordilleras, southern Spain); its significance and one possible geotectonic scenario for the westernmost alpine belt. American Journal of Science, 279(1):19–51.

Torres-Roldán, R.L., Poli, G., Peccerillo, A. (1986). An Early Miocene arc-tholeiitic magmatic dike event from the Alboran Sea - Evidence for precollisional subduction and back-arc crustal extension in the westernmost Mediterranean. Geologische Rundschau, 75:219–234.

Trümpy, R. (2001). Why Plate tectonics was not invented in the Alps. Int. J. Earth Sciences, 90:477-483.

Tubía, J., Cuevas, J., and Esteban, J. (2004). Tectonic evidence in the Ronda Peridotites, Spain, for mantle diapirism related to delamination. Geology, 32(11):941-944.

Tubía, J., Cuevas, J., and Esteban, J. (2013). Localization of deformation and kinematic shift during the hot emplacement of the ronda peridotites (Betic Cordilleras, southern Spain). Journal of Structural Geology, 50:148-160.

Tubía, J., Cuevas, J., and Ibarguchi, J. G. (1997). Sequential development of the metamorphic aureole beneath the Ronda Peridotites and its bearing on the tectonic evolution of the Betic Cordillera. Tectonophysics, 279(1):227-252.

Tubía, J., Cuevas, J., Esteban, J., and Ibarguchi, J. G. (2009). Remnants of a Mesozoic rift in a subducted terrane of the Alpujarride complex (Betic Cordilleras, southern Spain). The Journal of Geology, 117(1):71-87.

Tubía, J., Cuevas, J., Navarro-Vilá, F., Alvarez, F., and Aldaya, F. (1992). Tectonic evolution of the Alpujárride complex (Betic Cordillera, southern Spain). Journal of structural geology, 14(2):193-203.

Tubía, J.M. (1994). The Ronda peridotites (Los Reales nappe): an example of the relationship between lithospheric thickening by oblique tectonics and extensional deformation within the Betic Cordillera (Spain). Tectonophysics, 283: 381-398.

Tubía, J.M. and Cuevas, J. (1986). High-temperature emplacement of the Los Reales peridotite nappe (Betic Cordillera, Spain). Journal of Structural Geology 8:473-482.

Tubía, J.M. and Gil Ibarguchi, J.I. (1991). Eclogites of the Ojen nappe: a record of subduction in the Alpujárride complex (Betic Cordilleras, southern Spain). Journal of the Geological Society, London, 148:801-804.

Turner, S., Platt, J., George, R., Kelley, S., Pearson, D., and Nowell, G. (1999). Magmatism associated with orogenic collapse of the betic–alboran domain, se Spain. Journal of Petrology,

40(6):1011-1036.

Van Bemmelen, R.W. (1969). Origin of the Western Mediterranean Sea. Geol. Mijnbouw, 26:13-52.

Van der Wal, D. and Vissers, R. L. (1993). Uplift and emplacement of upper mantle rocks in the Western Mediterranean. Geology, 21(12):1119-1122.

Van der Wal, D. And Vissers, R. L. M. (1996). Structural petrology of the Ronda Peridotite, SW Spain: Deformation history. Journal of Petrology, 37(1):23–43.

Van Hinsbergen, D. J. J., Vissers, R. L. M., and Spakman, W. (2014). Origin and consequences of Western Mediterranean subduction, rollback, and slab segmentation. Tectonics, 33(4):393-419.

Vauchez, A. and Nicolas, A. (1991). Mountain building: strike-parallel motion and mantle anisotropy. Tectonophysics, 185(3):183-201.

Vázquez, M., Jabaloy, A., Barbero, L., and Stuart, F. M. (2011). Deciphering tectonic- and erosion-driven exhumation of the nevado–filábride complex (Betic Cordillera, southern Spain) by low temperature thermochronology. Terra Nova, 23(4):257-263.

Vera, J. A., Arias, C., García-Hernández, M., López-Garrido, A., Martín-Algarra, A., Martín-Chivelet, J., Molina, J., Rivas, P., Ruiz-Ortiz, P., Sanz de Galdeano, C., and Vilas, L. (2004). Las Zonas Externas Béticas y el Paleomargen Sudibérico. In Vera, J.A., editor, Geología de España, Capítulo IV: 3543-61. SGE-IGME, Madrid.

Vergés, J. and Fernández, M. (2012). Tethys-Atlantic interaction along the Iberia-Africa plate boundary: The Betic-Rif orogenic system. Tectonophysics, 579(5):144-172.

Vernant, P., Fadil, A., Mourabit, T., Ouazar, D., Koulali, A., Davila, J.M., Garate, J., McClusky, S., Reilinger, R.E. (2010). Geodetic constraints on active tectonics of the Western Mediterranean: implications for the kinematics and dynamics of the Nubia–Eurasia plate boundary zone. Journal of Geodynamics, 49: 123–129.

Villalaín, J., Osete, M., Vegas, R., García-Dueñas, V., and Heller, F. (1994). Widespread neogene remagnetization in Jurassic limestones of the south-iberian palaeomargin (Western Betics, Gibraltar arc). Physics of the Earth and Planetary Interiors, 85(1-2):15-33.

Villalaín, J., Osete, M., Vegas, R., García-Dueñas, V., Heller, F. (1994). Widespread neo-gene remagnetization in Jurassic limestones of the South-Iberian Palaeomargin (Western Betics, Gibraltar Arc). Phys. Earth Planet. Inter., 85 (1):15-33.

Villasante-Marcos, V., Osete, M., Gervilla, F., García-Dueñas, V. (2003). Palaeomagnetic study of the Ronda peridotites (Betic Cordillera, Southern Spain). Tectonophysics, 377(1): 119-141.

Vissers, R. L. M. and Meijer, P. (2012). Iberian plate kinematics and alpine collision in the pyrenees. Earth-Science Reviews, 114(1-2):61-83.

Vissers, R. L. M., Platt, J. P. and van der Wal, D. (1995). Late orogenic extension of the Betic Cordillera and the Alboran domain: A lithospheric view. Tectonics, 14:786-803.

Vissers, R.L.M. (2012). Extension in a convergent tectonic setting: a lithospheric view on the Alboran system of SW Europe. Geologica Belgica, 15(1-2): 53-7.

Vitale, S., Zaghloul, M. N., Tramparulo, F. D., and Ouaragli, B. E. (2014a). Deformation characterization of a regional thrust zone in the northern Rif (Chefchaouen, Morocco). Journal of Geodynamics, 77:22-38.

Vitale, S., Zaghloul, M. N., Tramparulo, F. D., Ouaragli, B. E., and Ciarcia, S. (2014b). From Jurassic extension to Miocene shortening: An example of polyphasic deformation in the external Dorsale Calcaire unit (Chefchaouen, Morocco). Tectonophysics, 633:63-76.

Watts, A., Platt, J., and Buhl, P. (1993). Tectonic evolution of the Alboran sea basin. Basin Research, 5:153-177.

Westerhof, A.G. (1977). On the contact relations of high temperature peridotite in the Serranía de Ronda, southern Spain. Tectonophysics, 39:579-591.

Whitehouse, M. and Platt, J. (2003). Dating high-grade metamorphism - constraints from rare-earth elements in zircon and garnet. Contributions to Mineralogy and Petrology, 145(1):61-74.

Whitmarsh, R. B. and Miles, P. R. (1995). Models of the development of the west Iberia rifted continental margin at 40º30'N deduced from surface and deep-tow magnetic anomalies. Journal of Geophysical Research: Solid Earth, 100(B3):3789-3806.

Whitmarsh, R. B., Manatschal, G., Minshull, T. A. (2001). Evolution of magma-poor continental margins from rifting to seafloor spreading. Nature 413:150-154.

Wildi, W., Nold, M., and Uttinger, J. (1977) La Dorsale Calcaire entre Tétouan et Asifane (Rif Interne, Maroc). Eclogae geol. Helv., 770:371-416.

Wortel, M. J. R. and Spakman, W. (2000). Subduction and slab detachment in the Mediterranean-Carpathian region. Science, 209:1910-1917.

Zeck, H. P. (1999). Alpine plate kinematics in the western Mediterranean: a westward directed subduction regime followed by slab roll-back and slab detachment. Geol. Soc. London, Spec. Publ. 156:109-120.

Zeck, H. P. and Whitehouse, M. J. (2002). Repeated age resetting in zircons from Hercynian-Alpine polymetamorphic schists (Betic – Rif tectonic belt, S. Spain) – a U-Th-Pb ion microprobe study. Chemical geology, 182:275-292.

Zeck, H. P. and Williams, I. S. (2001). Hercynian metamorphism in Nappe Core Complexes of the Alpine Betic-Rif belt, western Mediterranean - a SHRIMP Zircon study. Journal of Petrology, 42(7):1373-1385.

Zeitler, P.K., Herczeg, A.L., Mcdougall, I. and Honda, M. (1987). (U-Th)/He dating of

apatite: A potential thermochronometer. Geochimica et Cosmochimica Acta, 51:2865-2868.

Zindler, A., Staudigel, H., Hart, S.R., Endres, R., and Goldstein, S. (1983). Nd and Sm isotopic study of a mafic layer from Ronda ultramafic complex. Nature, 304:226-230.

VU :

Le Directeur de Thèse
(Nom et Prénom)

VU :

Le Responsable de l'École Doctorale

VU pour autorisation de soutenance

Rennes, le

Le Président de l'Université de Rennes 1

Guy CATHELINEAU

VU après soutenance pour autorisation de publication :

Le Président de Jury,
(Nom et Prénom)

Abstract

In the frame of the Africa-Europe convergence, the Mediterranean tectonic system presents a complex interaction between subduction rollback and upper-plate deformation during the Tertiary. The western Mediterranean is characterized by the *exhumation* of the largest *subcontinental mantle* massif worldwide (the *Ronda Peridotite*) and a narrow *arcuate geometry* across the Gibraltar arc within the Betic-Rif belt, where the relationship between slab dynamics and surface tectonics is not well understood. The thesis focuses on the Western Betics, which is characterized by two major thrusts: 1/ the *Internal/External Zone Boundary* limits the internal metamorphic domain (Alboran Domain) from the fold-and-thrust belts in the External Zone, and 2/ the *Ronda Peridotites Thrust* allows the juxtaposition of a hyper-stretched lithosphere with large bodies of sub-continental mantle rocks on top of upper crustal rocks.

First part: New structural data are presented and used to argue for two Lower Miocene E-W-trending strike-slip corridors played a major role in the deformation pattern of the Alboran Domain, in which E-W dextral strike-slip faults, N60°-trending thrusts and N140°-trending normal faults developed simultaneously during dextral strike-slip simple shear. The inferred continuous westward translation of the Alboran Domain is accommodated by a major E-W-trending lateral ramp (strike-slip) and a N60°-trending frontal thrust. At lithosphere-scale, we interpret the observed deformation pattern as the upper-plate expression of a lateral slab tear and of its westward propagation since Lower Miocene. The crustal emplacement of the Ronda Peridotites occurred at the onset of this westward motion.

Second part: New structural data together with Ar-Ar ages serve to document the changes in deformation processes that accommodate the progressive necking of a continental lithosphere. We identify three main successive steps. First, a mid-crustal shear zone and a crust-mantle shear zone accommodate ductile crust thinning and ascent of the sub-continental mantle. The shear zones act synchronously but with opposite senses of shear, top-to-W and top-to-E respectively in the crust-mantle extensional shear zone, and at the brittle-ductile transition in the crust. Second, hyper-stretching localizes in the neck, leading to an almost disappearance of the ductile crust and to crustal stretching values larger than 2000%, and bringing the upper crust into contact with the subcontinental mantle, each of them with their already acquired opposite senses of shear. Finally, high-angle normal faulting, dated by ^{40}Ar-^{39}Ar step-heating method on muscovite at ca. 21 Ma, cut through the Moho, where the ductile crust almost disappear and related block tilting ends the full exhumation of mantle in the zone of localized stretching.

Third part: New geochronological data precisely constrain the transition from rifting to thrusting. Using U-Pb LA-ICP-MS dating, we identify two distinct episodes of crustal melting associated with two large-scale tectonic contacts that bound the Ronda Peridotites. The first episode of partial melting within the HT foliation at ca. 22.5 Ma is related to the extreme thinning of the continental crust and to mantle exhumation. The second episode of crustal melting at ca. 20 Ma, marked by leucocratic granite dikes that intrude both the peridotites and the overlying thinned crustal envelope, is related to the thrust emplacement of the section of thinned and hot continental lithosphere on top of crustal rocks.

In summary, the Miocene tectonics of the western Betics is marked by the inversion of a continental rift, triggered by shortening of the upper continental plate and accommodated by E-W dextral strike-slip corridors. During thrusting and westward displacement of the Alboran domain with respect to Iberia, the hot upper plate, which involved the previously exhumed sub-continental mantle, underwent fast cooling.